Defining and Controlling the Subtype Identity of Human Stem Cell-Derived Motor Neurons

Gist F. Croft

Submitted in partial fulfillment of the

requirements for the degree of

Doctor of Philosophy

under the Executive Committee

of the Graduate School of Arts and Sciences

COLUMBIA UNIVERSITY
2012

© 2012
Gist F. Croft
All rights reserved

ABSTRACT

Defining and controlling the subtype identity of human stem cell-derived motor neurons

Gist F. Croft

One cardinal promise of stem cell research is that many intractable, common, and poorly understood diseases may be studied in an entirely new way: in vitro in the specific human cell types affected in vivo. Embryonic stem (ES) cells have the pluripotency to generate all somatic cells types, and the invention of somatic cell reprogramming techniques has allowed the creation of cell lines with both ES-cell grade pluripotency—induced pluripotent stem (iPS) cells—and the genetic determinants of diseases. If iPS cells derived from patients with genetic disease are to enable studying the affected human cell types in vitro then it is necessary to: first, precisely define the appropriate cellular phenotypes in vivo; second, selectively generate those cell types in vitro; and third, demonstrate that iPS cells retain similarly predictable and tractable cellular potential as ES cells. In the motor neuron degenerative disease Amyotrophic Lateral Sclerosis (ALS) spinal motor neurons innervating different types of muscles and individual muscle groups show selective vulnerability or resistance to disease. We therefore set out to define the subtypes of human motor neurons in vivo and to generate these in vitro. Here we report that human motor neurons in vivo share with mouse the molecular markers of motor neuron column, division, and pool organization, as well as positional expression of HOX proteins which regulate this diversity in chick and mouse. We then used combinations of these markers to classify motor neuron subtypes derived from human ES cells in vitro under standard differentiation conditions. These human ES cell-derived motor neurons expressed marker combinations appropriate to each motor

column, but were strongly biased to cervical phenotypes. In order to access a greater diversity of motor neuron subtypes, including some with differential responses to ALS in vivo, we defined a developmental strategy to generate more caudal ES-cell derived motor neurons. We show that FGF treatment, in a patterning window we defined, generated human ES-cell derived motor neurons with more caudal (brachial, thoracic, and lumbar) phenotypes. We then participated in a long term collaboration to generate iPS cell lines from donors with ALS-genotypes (familial ALS), and no clinical motor dysfunction (controls). We first showed that ALS and control iPS cells from patients of advanced age could generate motor neurons in vitro (Dimos, Rodolfa et al. 2008). To address questions about the variability of iPS cells, and their comparability to ES cells for making defined neuronal subtypes, we generated a panel of iPS lines from donors of varying demography, thoroughly characterized these cells by standard assays for pluripotent cells, and assessed their ability to generate functional motor neurons in comparison to a panel of ES cell lines. We showed that iPS cells were equivalent to ES cells, and that human genetic diversity may influence the efficiency of motor neuron generation (Boulting, Kiskinis et al. 2011). Next, we used these lines to show that iPS cells could generate the same diversity of motor neurons in vitro, and that the rostrocaudal output of this diversity was rationally manipulable. Finally, since ALS is an adult onset disease, we anticipated that if ES and iPS cell-derived motor neurons could reach significant landmarks of functional maturation in vitro, then the chances of manifesting disease phenotypes would be increased. Therefore we developed methods for long term cultures in which ES and iPS cell-derived motor neurons showed progressive molecular, morphological, and electrophysiological maturation. Together these results enable future studies to ask if ALS-patient iPS cell-derived motor neurons will show pan-motor neuron or subtype-specific ALS

phenotypes in vitro. In turn these which may help elucidate mechanisms of disease resistance and vulnerability and identify novel therapeutic targets.

Table of Contents

Chapter 1. General Introduction 1

Part I. Introduction 1

Part II. Spinal motor neuron diversity and ontogeny in vertebrates 5

Part III. Mouse embryonic stem cell-derived motor neurons 21

Part IV. Human embryonic stem cell-derived motor neurons 28

Part V. Induced pluripotent stem cell derived motor neurons 35

Chapter 2. Molecular description of human motor neuron diversity: rostrocaudal regions, columns, divisions, and pools 62

Chapter 3. Motor neuron differentiation from human embryonic stem cells: optimization, characterization of subtype diversity, and analysis of maturation 104

Chapter 4. Motor neuron differentiation from human induced pluripotent stem cells: comparison to embryonic stem cells, sources of variability and motor neuron subtype diversity 173

Chapter 5. Controlling the rostrocaudal subtype diversity of human stem cell-derived motor neurons 236

Chapter 6. General Discussion: Conclusion and Perspectives 273

Chapter 7. Experimental Procedures 285

Chapter 8. References 295

Figure List

Figure 1.1. Neuronal subtype diversity in the central nervous system

Figure 1.2. Motor columns, divisions, and pools: anatomy, targets, and molecular markers

Figure 1.3. HB9 is expressed by motor neurons in the human embryo

Figure 1.4. Histological analysis of the developing human spinal cord

Figure 1.5. Histological analysis of the period of motor neurogenesis in the human spinal cord

Figure 1.6. Sonic hedgehog protein patterns the ventral neural tube producing neuronal diversity

Figure 1.7. Wnt and FGF induce *CDX* gene expression which encodes caudal neural identity

Figure 1.8. FGF and RA subdivide caudal neural pattern through *HOXC* genes

Figure 1.9. FOXP1 dose-dependently marks LMC and PGC motor neurons

Figure 1.10. Xenotransplanted mouse ES-MNs integrate into chick motor system

Table 2.1. Summary of motor neuron rostrocaudal, columnar and divisional subtype marker expression in chick and mouse

Figure 2.1. Documentation of human spinal cord samples and linear length of limb-innervating and thoracic regions

Table 2.2. Human embryonic spinal cord resource

Figure 2.2. Human spinal motor neurons share column markers and organization with mouse

Figure 2.3. pSMAD and low level FOXP1 identify human PGC at thoracic levels

Figure 2.4. Human MNs express markers of LMC divisional identities

Figure 2.5. HB9 and ISL1 expression levels in motor neuron columns, division, and control cells

Figure 2.6. Some rostral brachial LMC pools identified by combinatorial expression of LIM HD and column marker proteins

Figure 2.7. PEA3 marks brachial and lumbar LMC pools.

Figure 2.8. Human motor neurons in vivo express HOX proteins in rostrocaudal collinear sequence

Table 2.3. Summary of motor neuron rostrocaudal, columnar and divisional subtype marker expression in human

Figure 3.1. Establishing a Standard Protocol for ES-MN differentiation

Figure 3.2. ES-MNs are defined by expression of HB9 and or ISL1 at varying ratios

Figure 3.3. Optimization of Standard Protocol for ES-MN differentiation

Figure 3.4. Defining an Accelerated Protocol for high efficiency differentiation of ES-MNs

Figure 3.5. ES-MNs progressively acquire action potential firing capacity

Figure 3.6. Progressive maturation in passive and active ES-MN membrane properties

Figure 3.7. ES-MNs display two characteristic features of in vivo motor neuron firing

Figure 3.8. EdU inhibits motor neurogenesis

Figure 3.9. Progressive morphological maturation of ES-MNs

Figure 3.10. ES-MNs rapidly acquire mature NF-H expression profile

Figure 3.11. ES-MNs express marker combinations matching all in vivo motor columns

Figure 3.12. ES-MNs express predominantly HOXA5 and exclude HOX protein coexpression

Figure 3.13. ES-MNs can be cryopreserved with limited effect on subtype identity

Figure 3.14. ES-MN in matured cultures are predominantly $FOXP1^{+}$

Figure 3.15. FOXP1^{+} ES-MNs show a subtype-specific morphological phenotype

Figure 3.16. ES-MNs respond to in vivo cues in xenotransplant to chick spinal cord

Figure 4.1. iPS cells can be established from ALS-patient fibroblasts after biopsy

Figure 4.2. Patient-specific iPS cells are pluripotent

Figure 4.3. ALS iPSC lines can be differentiated to motor neurons

Figure 4.4. ALS iPSC lines generate cells with astrocyte-like phenotypes

Table 4.1. iPSC and ESC lines used for comparative studies

Figure 4.5. All test set iPSC lines pass standard assays of pluripotency

Figure 4.6. iPSC lines show characteristic motor neuron differentiation efficiencies, but no global difference from ESC lines

Table 4.2. Statistical analysis of categorical variables on %ISL1 differentiation efficiency

Table 4.3. %ISL1^{+} cells varies by cell line

Figure 4.7. iPS-MNs cultures show phenotypes consistent with motor neuron identity

Figure 4.8. iPS- and ES-MNs exhibit the same coherent cervical HOX phenotypes

Figure 4.9. iPSC- and ESC-derived neurons are physiologically active.

Figure 4.10. iPSC and ESC-derived neurons show voltage gated sodium channels and fire action potentials

Figure 4.11. Persistent transgene expression in some iPSC lines does not affect MN differentiation.

Table 4.5 Statistical analysis of mean total cells numbers per line after dissociated cell seeding identifies two defective iPSC lines

Figure 4.12. 2 of 16 iPSC lines display a defective EB and total cell number phenotype during motor neuron differentiation

Figure 4.13. 1 of 14 non-defective iPSC lines shows a neuronal defect after standard motor neuron differentiation

Table 4.6. ANOVA for %TuJ1 shows line 11b had a significantly different phenotype

Figure 4.14. Pharmacological neuralization completely rescues all three defective-phenotype iPSC lines

Figure 4.15. Sources of variability in motor neuron differentiation between iPSC lines

Table 4.7. ANOVAs on %ISL1 show signficant effects of donor identity and sex

Figure 4.16. Southern blots show multiple lines from the same donor are independent lines

Figure 4.17. Empirical measures of cell-line-specific motor neuron efficiency correlate with lineage scorecard predictions for germ layer and neuronal differentiation proclivity

Figure 5.1. Comparison of chick and human embryos during the period of caudal neural patterning

Figure 5.2. Transition to Pax6 marks the beginning, and Sox1 the end of inferred patterning window

Figure 5.3. In vivo markers of human neural plate to neural tube stages define cognate developmental stages in vitro

Figure 5.4. Design of caudal patterning ES-MN differentiation experiments

Figure 5.5. FGF induces a caudal shift in HOX expression

Figure 5.6. FGF treatment reduces the percent of neurons and motor neurons, without affecting their phenotype

Figure 5.7. FGF induces caudal motor neuron subtypes at the expense of rostral

Figure 5.8. HOX protein expression is mutually exclusive in caudalized ES-MNs

Figure 5.9. Motor column diversity preserved in caudal ES-MNs

Figure 5.10. HOX proteins and column markers together more precisely classify ES-MN subtypes

Figure 5.11. FGF induces more caudal motor neuron subtypes from iPS and ES cells

Acknowledgements

I thank my mentors Chris Henderson and Hynek Wichterle. They have taught me far more than I bargained for: how to think about real science and how to actually do it. They have been generous with their time, patience, knowledge and wisdom and have allowed me to play on a dream of a scientific stage and to learn from two different thinkers and stylists: the Titian and Kandinsky of motor neuron biology. They will always have my gratitude and I hope to make them proud on the journey they have done so much to launch me on. I'll miss their insight and humour, but I will *always* be able to summon their voices in my head giving constructive feedback.

I thank my committee members: Serge Przedborski for years of thoughtful commentary and collegiality, and Tom Jessell for his insight and support, and especially for, with one paragraph-long oral suggestion, "why don't you go back to early patterning events…..etc" at my qualifying exam, turning my work immediately and perhaps permanently in a developmental direction which has been extremely salutary and satisfying to my inclinations, and the perspicacity of which accounts for at least half of the experimental successes I have had. I also thank Lorenz Studer for agreeing to sit as my outside examiner and for his generosity of time and expertise—along with his postdoc Yechiel Elkabetz—which greatly aided my fledgling efforts at the outset of my PhD in working human stem cells, neural rosettes, and motor neuron differentiation.

I thank Project ALS, the Estess Sisters, and especially Valerie. Her force of will and determination has been an inspiration to me as surely as her organization's funding made all of my work possible in a field, and at a time when few had the courage and vision to fight for what

they believed could make a better future. I also thank the anonymous fibroblast and embryo donors who made possible the iPS and human expression studies.

I thank my scientific mentors beyond my current colleagues: beginning with my father, a true empiricist and humanitarian. Next, my high school chemistry teacher Sandra Krupinski and a man called The Dude (Dr. Ed O'Neill) who first inspired me to study biology. For the care and tutelage each of these individuals invested in me they deserve a share of my accomplishments, such as they are.

I thank Mackenzie W. Amoroso, with whom for a time I formed a scientific force known as The Warriors. She provided excellent technical and moral support for many years and I have had the good fortune to become her friend and scientific mentor. I also thank Susan Morton whose antibodies will live on after we are all gone, and who I always enjoyed stopping to chat with, even as she dropped pearls of wisdom about antigen reactivity or drops of antiserum, without which these endeavors would have been far less than they are. I also thank Su Chun Zhang who generously shared his excellent and detailed protocol for motor neuron generation on which mine was almost completely based.

I thank my wonderful colleagues in the Henderson, Project ALS, and Wichterle Labs, especially Kevin Kanning who taught me how to be a graduate student and Mirza Peljto—may he always be holding tickets to that next Dylan show—and all the others who have made it a pleasure to work here. Kevin Eggan and his lab were an extreme pleasure to work with and added tremendously to my scientific horizons.

And I thank my mother and my father and my grandmother Claire, for their love and support, believing in me and giving me the confidence to think independently. I especially thank my wife

for endless understanding of years of late nights at the lab and the computer, and amazing help and support in the last days of this work and figuring out how to drop my figures into a word document. I especially thank my sister in-law Cecilia, and my daughters' six wonderful grandparents, without whose help I could not have finished my work here. And smallest but not least my two beautiful daughters, Claire and Cassandra, whose smiles, snorts, and running commentary make everything better.

Statement of Contributions

Specific contributions in the case of collaborative work are detailed at the beginning of each chapter.

For electrophysiology experiments presented in Chapter 3 and results text for electrophysiological experiments is adapted with modifications, and figure legends are reproduced with very minor modifications from an article in preparation on which I will share an authorship and Tomonori Takazawa (Amy B. MacDermott Laboratory, Columbia University). Figure legends for Chapter

All data are the result of my experiments with the following exceptions. All electrophysiology recordings and data analysis in Chapter 3 were performed exclusively by Tomonori Takazawa on cultures I prepared; these experiments were planned collaboratively. Most of the data in Chapter 4 were the result of collaborative experiments, some I did not contribute to, and some were performed independently by me. Contributions to all experiments, planning and data analysis are listed in the Statement of Contributions for that chapter.

Mackenzie W. Amoroso provided technical support, and insight for all experiments.

Chapter 1. General Introduction

Part I. INTRODUCTION

The function of the central nervous system is predicated on the specific connectivity of billions of distinct neuronal subtypes that form trillions of plastic synapses. At the founding of the modern discipline of neuroscience Ramon y Cajal described thousands of these distinct neuronal types by their morphologies (Fig. 1.1). Thus even at the beginning Cajal's studies clearly articulated two fundamental questions for understanding brain function, although this was highly controversial at the time. First, distinctive morphologies suggested distinct neuronal subtypes. Second, the axonal and dendritic morphologies that distinguished neuronal subtypes, as Cajal argued, were themselves the myriad specific connections formed from one neuron to another. As molecular and genetic methods have replaced silver staining and camera lucida our appreciation for neuronal diversity and our knowledge of the circuits formed by specific connections between them have expanded like the Purkinje cell arbors Cajal depicted. From a reductionist standpoint however his basic questions remain: What are the different neuronal actors and what makes them distinct? And how do they connect to each other in functional circuits to produce behavior?

Because of its concrete behavioral output, the motor system has been an attractive target for studies seeking to define specific neuronal subtypes and the logic and development of functional circuit connections between them. We now understand a great deal about the hierarchy of motor neuron subtypes at the molecular, genetic, and circuit levels. A distinct group of motor neurons in the ventral horn of the spinal cord, termed a motor pool, innervates and controls the

contractions of each of several hundred skeletal muscles. Motor pools in turn are organized in rostrocaudal columns, termed motor columns, according to the type of target muscle they innervate (Fig. 1.2). During development motor columns and their constituent motor pools are generated in rostrocaudal register with their target muscle by pattering factors and genes which articulate the rostrocaudal body plan of the embryo.

The result is that individual motor neurons possess distinct transcriptional identities, accumulated from rostrocaudal and columnar identities, and finally specific to the individual motor pools to which they belong. Functional identities are downstream of these transcriptional identities. For example, the axons of a leg muscle innervating motor neurons must make a series of directional choices in order to arrive successfully at the muscle that they are destined to control. Centrally they must also choose to participate in forming hundreds or thousands of specific synapses with sensory afferents, descending cortical inputs and local interneurons, and spinal central pattern generators in order to mediate motor behavior.

The human motor system conforms to of the same basic functional and anatomic categories that have been described in vertebrate model systems. However, almost all of the genetic and molecular information about of the development of the motor system and motor neuron subtypes is based on studies in animal models, since human motor neurons were available only in postmortem samples. This scarcity, and the lack of living motor neurons for experimental studies, was compounded by the diversity of motor neuron subtypes and pools requiring study. With the establishment of human embryonic stem (ES) cells as a research tool, and the demonstration that they could be directed to differentiate into spinal motor neurons, this inaccessibility has changed. Now the field is in a position to study human spinal motor neurons

directly, and attempt to understand the development and function of human motor neuron subtypes.

Spinal motor neurons are of intellectual interest, but they are also the target of several diseases. The motor neuron disease Amyotrophic Lateral Sclerosis (ALS) becomes symptomatic as the spinal motor neurons which innervate muscles die, leading to progressive paralysis and ultimately death. The mechanisms of motor neuron-selective degeneration are not well understood and there are no effective therapies. The derivation of induced pluripotent stem (iPS) cells from ALS-patients brings together the genotypes which determine familial forms of the disease with the pluripotency to generate the affected cells in vitro. However, reproducing degenerative cellular phenotypes in vitro will be a major challenge using ES/iPS-derived cells. While ALS is not believed to have a developmental component, developmental biology could provide leverage on this problem in two ways. First, motor neurons show differential susceptibility depending on their motor column or motor pool subtypes, therefore these subtypes may offer novel and specific ways to understand the mechanisms of motor neuron degeneration in ALS. However, human motor neuron subtypes have not been molecularly defined in vivo, and rational means to generate them in vitro have not been described. Second, it is likely that in order to model an adult-onset neurodegenerative disease like ALS, ES/iPS cell-derived motor neurons should at the minimum adopt coherent in vivo-like identities and progress to states of maturity as indicated by changes at the molecular, morphological, and electrophysiological levels, however maturational strategies and assays to monitor maturation need to be defined.

Aims

The aim of the this thesis was to lay the groundwork for the study of ALS using motor neurons, and their specific subtypes, derived from ALS-patient iPS cell lines. First, we needed to establish that the molecular markers of vertebrate motor neurons and their subtypes were conserved in humans in vivo. Second, we sought to characterize the subtype diversity of motor neurons differentiated from ES cells (ES-MNs) and to develop assays under which to test the maturation of motor neurons. Third, in order to generate ALS-motor neurons, we participated in collaborative efforts to generate iPS cell lines from familial ALS patients and control donors, and to compare these lines to each other and to ES cells for their capacity to generate motor neurons and the functional phenotypes of those cells. Fourth, we designed a strategy, based on developmental mechanisms, to control the rostrocaudal subtype of ES and iPS cell-derived motor neurons, and asked if coherent subtype identities could be rationally orchestrated.

Summary of research background

In order to set the stage for the studies described in Chapters 2-5, it is necessary to review the literature which forms the background for this work. First, we review the molecular markers that distinguish motor column subtypes as defined in vertebrate models. Then we review the developmental mechanisms which generate motor column subtype identity (Part II). Next, we review the evidence that motor neurons can be differentiated from mouse ES cells, and describe the molecular and functional diversity of mouse ES cell-derived motor neurons (ES-MNs) (Part III). Then, we describe the generation of human ES cells, their differentiation to motor neurons, and the evidence for in vitro subtype diversity in human ES-MNs (Part IV). Finally we review

the development of iPS cells which allow patient-specific ALS-genotypes to be captured in cells with the properties of ES cells (Part V).

Part II. SPINAL MOTOR NEURON DIVERSITY AND ONTOGENY IN VERTEBRATES

Categories of motor neuron diversity: motor columns, divisions, and pools

Motor neurons control muscle contraction and motor behavior

Motor neurons are the sole means of behavioral output from the nervous system. Their cell bodies are located in rostrocaudal columns in the ventral horns of the spinal cord and in the dorsal hindbrain, and their axons synapse on muscles controlling contractions. Central control of motor neuron/muscle activity is governed by descending cortical inputs which synapse on local interneurons and on some motor neurons directly as well as on central pattern generators. Motor neurons are also integrated into spinal reflex circuits which modulate the activity of motor neurons based on sensory feedback from homonymous and antagonistic muscles. Finally, central pattern generators are complex local circuits which coordinate the activity of many muscle groups acting in concert to effect locomotion and other stereotyped motor behaviors.

Motor neurons with similar muscle targets are grouped into motor columns

The organization of spinal motor neurons is described by a series of hierarchical categories which are defined by their peripheral targets, and these are reflected by characteristic anatomical positions in the spinal cord and the expression of definitive molecular markers (Fig. 1.2A-C) (Jessell 2000). First, motor neurons can be divided into two classes: by far the most abundant

are somatic motor neurons, which project directly to muscle targets, and second are visceral preganglionic motor neurons, which synapse on sympathetic ganglia. The visceral preganglionic motor neurons are grouped into a dorsal column termed the preganglionic motor column (PGC, or Column of Terni in chick) and are found at thoracic levels (Prasad and Hollyday 1991). Somatic motor neurons can then be subdivided into three columnar categories. First, median motor column (MMC) cells constitute a continuous column in a medial and ventral position throughout the rostrocaudal length of the spinal cord, and innervate dorsal epaxial muscles of the back (Fetcho 1987; Gutman, Ajmera et al. 1993). Second, hypaxial motor column (HMC) motor neurons, which are restricted primarily to the thoracic spinal cord, are located just lateral to the MMC, and innervate intercostal and abdominal muscles (Gutman, Ajmera et al. 1993). Third, the lateral motor columns (LMCs), which are located dorsal and lateral to the MMC, are found only at the level of the fore- and hind-limbs that contain their muscle targets. The LMC is further subdivided into medial and lateral divisions which innervate muscles derived from the ventral or dorsal primordial muscle masses of the limb (Landmesser 1978).

Molecular markers of motor column subtype identity

At the molecular level all motor neurons can all be identified by expression of the acetylcholine synthetic enzyme choline acetyltransferase (ChAT), since this is the neurotransmitter by which they communicate with muscles, and the transcription factors HB9 (Arber, Han et al. 1999) and or ISLET1 (ISL1) (Ericson, Thor et al. 1992). Motor column and division subtypes can be identified by their combinatorial expression of specific molecular markers (Fig. 1.2D). The MMC expresses transcription factor LHX3, which is initially expressed by all nascent motor neurons but rapidly downregulated in all motor columns except the MMC. At brachial and lumbar levels LMC motor neurons express either HB9 or ISL1, the forkhead box protein

FOXP1, and the retinoid synthetic enzyme RALDH2, which serve as specific molecular markers of LMC identity among motor neurons (Dasen, De Camilli et al. 2008). The LMC divisions can be identified based on their combinatorial expression of LIM homeodomain proteins and HB9: medial division (LMC_M: ISL1 and ISLET2 (ISL2)) and lateral division (LMC_L: HB9 and LIM1, ISL2). At thoracic levels, the HMC is marked by expression of HB9 and ISL1/2, the absence of both FOXP1 and LHX3 and the expression of ER81 (Dasen, Liu et al. 2003), while PGC motor neurons express ISL1, low levels of FOXP1, nNOS, and phosphorylated SMAD (pSMAD) proteins (Dasen and Jessell 2009).

Motor pools innervate individual muscles

The last level of specificity is the motor pool: the group of motor neurons which are dedicated to synapse on one specific muscle (Romanes 1942). Axonal retrograde transport of horse radish peroxidase, and later fluorescent dyes, allowed the nerves innervating individual muscle to be traced to their origin at spinal motor neurons. This allowed a one-to-one map to be established between individual limb muscles and the motor pools which innervate them (Romanes 1964; Landmesser 1978; Landmesser 1978; Hollyday 1980).

While motor pool identity is defined by muscle target, many pools can be identified centrally by a distinct profile of transcription factor expression. For example, in the rostral brachial chick LMC_L the *deltoid* (DL) motor pool expresses high level ISL2 and LIM1, the *extensor metacarpi radialis/ulnaris* (EMR) motor pool expresses low levels of ISL2 and LIM1, and the *rhomboideus* (RB) motor pool, not part of the LMC, expresses ISL1, ISL2, and LHX3 (Ensini, Tsuchida et al. 1998). Additionally, dozens of HOX genes and HOX cofactors (MEIS and PBX proteins) are expressed in the brachial LMC where their cross-repressive activities determine the location

identity of many motor pools (Dasen, Tice et al. 2005). Some motor pools can be identified by expression of specific transcription factors (PEA3, ER81, RUNX1, SCIP, and Nkx6 proteins) which can serve as pool markers (Lin, Saito et al. 1998; Arber, Ladle et al. 2000; Haase, Dessaud et al. 2002; Livet, Sigrist et al. 2002; Dasen, Tice et al. 2005).

In some cases pool markers have been shown to respond to peripheral signals and drive motor pool specific connectivity phenotypes. For example, intermediate target- and muscle-derived GDNF induces the expression of the ETS protein PEA3 in *cutaneous maximus* (CM) and *latissumus dorsi* (LD) motor pools (Haase, Dessaud et al. 2002). PEA3 and GDNF knockout mice showed defects in cell body settling position and terminal arborization pattern of these motor pools pools (Haase, Dessaud et al. 2002; Livet, Sigrist et al. 2002). Thus selective expression of transcription factors not only marks motor pool identities, but can result from interaction with muscle targets and determine functional motor pool phenotypes.

Anatomy and molecular markers of human motor neurons and their subtypes

Human spinal motor neurons are arranged in the same broad categories as mouse, medial motor neurons (MMC, HMC), intermediolateral motor neurons (PGC),and lateral column motor neurons ($LMC_{M/L}$) as described by histological criteria (Rath, Gopinath et al. 1982; Altman and Bayer 2001; Bayer and Altman 2002). However, molecular tools and tracing studies have not been used to definitively establish a distinction between the MMC and HMC, the divisions of the LMC, or specific motor pools. At the molecular level, *in situ* probes for the motor neuron marker *HB9* identified motor neurons in the anterior horn of the spinal cord at Carnegie stage (CS) 15 (35-38 days of development) (Ross, Ruiz-Perez et al. 1998; Hagan, Ross et al. 2000), (Fig. 1.3A). Cells in the subventricular zone also showed hybridization beginning at CS14 (not

shown), however by CS19 (day 48-51) only more caudal regions showed subventricular staining (Fig. 1.4C, D) and by CS21 (day 53-54, data not shown in publication, the sacral subventricular signal was no longer detected). The authors also report but do not show that anterior horn and subventricular signal was seen at CS14 (31-35 days) but not at CS12 (26-30 days). These data validate the use of HB9 as a selective marker for embryonic human motor neurons and they appear at day 35-38 and perhaps as early as day 31-35.

If the subventricular expression pattern is interpreted as *HB9* expression in motor neuron progenitors, this suggests that human motor neurons initiate HB9 at an earlier stage than do chick (Tanabe, William et al. 1998) but similar to mouse (Arber, Han et al. 1999). Whether HB9 is expressed in motor neuron progenitors or in immediately post-mitotic motor neurons, the rostrocaudal progression of signal loss strongly suggests it is correlated with motor neurogenesis. The period of human motor neurogenesis is thus likely to occur in vivo over a period of almost 3 weeks: embryonic days 31 to 51.

Histological analysis offers another perspective on the period of motor neurogenesis, suggesting essentially the same start but perhaps an earlier conclusion. Incipient motor neurons were recognized by Ramon y Cajal in the human spinal cord at "week 4" as early as 1909 (Fig 1.4A) (Altman and Bayer 2001). More recently a detailed analysis of dozens of archival embryos was used to construct a comprehensive histological account of spinal development from GW 4 to gestational month 4 (Bayer and Altman 2002) of which the first trimester data is most relevant here (Fig. 1.4A). These authors clearly identify motor neurons which have migrated out of the subventricular germinal zone by GW 4.5, and interpret a subsequent thinning of the subventricualr neuroepithelium at GW 5.5—the presumed human motor neuron progenitor domain—as indication of largely completed motor nuerogenesis (Fig 1.5A, B). This particular

estimate however, derives from the cervical spinal cord only, and is only a few days in advance of the loss of subventricualr HB9 expression described above, and they do not present a full rostrocaudal account of spinal cords samples before GW 8.5. In summary the period of human motor neurogenesis cannot be definitively established with these tools alone, but the histological and molecular evidence supports the idea that human motor neurons are born between about embryonic day 30 and 50.

Motor columns begin to separate from a histologically undifferentiated mass of motor neurons by GW 6.5 and are quite well segregated into columns by GW 7, however cell group movements and further separation of motor columns and pools occurs well into the second trimester (Bayer and Altman 2002). Between GW7.5 and GW17 motor neurons express increasingly distinctive levels of non-phosphorylated neurofilaments relative to immediately surrounding cells, and at late embryonic stages (GW10-14) they express EphA4 with relative uniformity (Clowry, Moss et al. 2005). Chromatolytic reactions in the cell bodies of motor neurons degenerated through injury or disease (poliomyelitis) allowed identification of some motor pools, although in the absence of tracing studies in human, the current hypotheses about motor pool-muscle maps are based mostly on analogy to precise retrograde tracing in experimental vertebrates (Sharrard 1955; Romanes 1964; Altman and Bayer 2001; Bayer and Altman 2002).

None of the molecular markers which delineate specific columnar or motor pool subtypes in chick or mouse have been investigated in human, with the exception of ER81. ER81 expression was not associated with the HMC in this study, but the timepoint of analysis was long after the period of columnar diversification (Clowry, Moss et al. 2005). ER81 was, however, observed in some unidentified LMC pools at GW14, suggesting that it functions in human as a pool marker. ER81 was also observed in dorsal root gangli as it has been in mouse (Arber, Ladle et al. 2000).

Since these reports numerous new antibodies against proteins expressed in a motor neuron subtype-specific manner were generated. Therefore, new, detailed studies of the molecular markers and determinants of motor column, division, and pool identities in first trimester human embryos are needed to confirm the relevance of the markers of rostrocaudal and columnar identity, and validate their use in assigning in vitro derived cells to cognate in vivo categories.

Rostrocaudal patterning generates motor column diversity

Motor neurons are grouped into columns, divisions and pools, and many of these subtypes can be identified by transcriptional codes. We next ask how generic motor neurons acquire these subtype identities in vivo. A detailed understanding of the processes governing motor neuron diversification has been adduced in chick and mouse. These mechanisms can be reduced to the idea that the embryo deploys developmental morphogens along the dorsoventral and rostrocaudal axes, to generate unique positional identities defined by the concentration, timing and combination of these cues. Interactive genetic mechanisms then interpret these positional identities, resolving a series of unique cellular motor neuron columnar identities. A classic example of this principle is found in the dorsoventral patterning which generates cellular diversity, including pan-motor neuron identity, in the ventral spinal cord.

Dorso-ventral patterning and the specification of motor neuron progenitors

Motor neuron progenitors (pMNs) are induced in a specific ventral domain of the spinal cord by high levels of sonic hedgehog (SHH) protein and are then marked by the expression of OLIG2 (Roelink, Porter et al. 1995). The most ventral neural tube cells, floorplate cells secrete that then diffuses dorsally generating a concentration gradient in the ventral half of the spinal cord. SHH

induces expression of Class II homeodomain (HD) proteins Nkx2.2 and Nkx6.1, and represses expression of Class I HD proteins Pax7, Dbx1, Dbx2, Irx3, and Pax6 at staggered threshold concentrations (Fig. 1.6). Cross repressive interactions between Class I and II HD proteins then resolve the SHH gradient into a set of 5 unique progenitor cell identities—(p0, p1, p2, pMN, and p3) located in serial dorsoventral domains in the spinal cord. In this fashion, a morphogen gradient is interpreted by cross repressive genetic mechanisms, and positional information is translated into a array of unique cellular identities

HOXC genes determine motor column subtype identities

Since all motor neurons arise from a single dorsoventral progenitor domain, generated by high levels of SHH signaling, how is the columnar diversity of motor neurons orchestrated? The interaction of HOX genes underpins the diversification of generic motor neurons into columnar subtypes and links their diversity to rostrocaudal topography in register with their muscle targets. HOX genes are induced in the neural tube, and later are expressed by postmitotic motor neurons in a rostrocaudal sequence which is collinear to their 3'-5' position in *HOX* clusters in the genome (Deschamps and van Nes 2005). Cross repressive activity of many HOXC genes helps resolve initial graded expression patterns into sequential regions where cells express unique combinations of HOX genes. The result is that motor neurons at brachial limb-innervating levels express HOXC6, those at thoracic non-limb innervating levels express HOXC9, and those at lumbar limb-innervating levels express HOXC10 (Liu, Laufer et al. 2001) (Fig. 1.2). In these domains HOXC genes determine the elaboration of level appropriate columnar identities: HOXC6 and HOXC10 are required for the specification of the LMCs and repress thoracic motor columns, whereas HOXC9 suppresses LMC fate in thoracic spinal cord and supports the elaboration of HMC and PGC column subtypes (Dasen, Liu et al. 2003; Jung, Lacombe et al.

2010). Finally dozens of HOX genes, including HOXA5 and HOXC8, work in combination to generate the diversity of forelimb innervating motor pools (Dasen, Tice et al. 2005). HOX genes are thus both instrumental in the diversification of motor neurons and serve as specific markers of motor neuron rostrocaudal subtype identity.

Wnt and FGF induce CDX genes to determine caudal neural identity in primitive streak and neural plate stage embryos

While *HOXC* genes appear to control the columnar identity of postmitotic motor neurons, in order to manipulate these identities it is necessary to work backwards in development to understand how *HOXC* genes are induced in this pattern in the spinal cord in the first place. The emerging model for this process again conforms to the principle of developmental morphogens inducing positional identities interpreted by interactive gene expression programs. However, in this case the axis is rostrocaudal, the process unfolds in several temporal waves, each sculpting more refined positional zones, and progenitor cells must integrate information from several overlapped morphogen signaling pathways. Caudal neural identity is first induced in chick in vivo in response to morphogens secreted from two anatomical sources. First, at the beginning of gastrulation through the 1-4 somite stage (Hamburger and Hamilton (HH) stage 3^{+}-8) gradients of Wnt, from the paraxial mesoderm, and FGFs from the primitive streak induce caudal neural identity in cells which will form the spinal cord (Bel-Vialar, Itasaki et al. 2002; Nordstrom, Jessell et al. 2002; Nordstrom, Maier et al. 2006). This primitive caudal identity is encoded by the expression of *CDX* genes in the caudal neural plate by the 1-4 somite stage (HH 8) (Fig. 1.7). This first caudal determining period of Wnt and FGF signaling begins coincident with primary neural induction and gastrulation. At this timepoint the prospective neural plate has been

specified—as shown by fate mapping studies—however it does not yet express the first identified definitive marker of neural plate identity in chick and mouse (SOX1).

Spinal identity is subdivided and diversified by FGF and RA in neural plate and neural tube: HOXB genes

Next, from the 4-17 somite stages (HH8-12) FGF from the regressing Hensen's node exposes progressively more caudal spinal regions to higher levels of FGF for longer time periods: it is adjacent to the presumptive cervical region at HH8, brachial region at HH10, and lumbar region at HH15 (Liu, Laufer et al. 2001). Meanwhile the somites are formed from paraxial mesoderm in the anterior wake of the node, and expose brachial progenitors to a rostral to caudal gradient of Retinoic Acid (RA) (Fig. 1.8). The generic caudal identity of prospective spinal cord cells, encoded by *CDX* genes, is then refined into rostral and caudal zones by the activity of RA, acting directly on 3' *HOX* genes (*HOXB1*, *HOXB3-5*), and FGF acting through *CDX* genes as well as on 5' *HOX* genes (*HOXB6-9*) more directly (Bel-Vialar, Itasaki et al. 2002). These morphogens refine *HOX* expression such that by HH stage 17 the hindbrain and spinal cord can be subdivided into three progenitor zones based upon their expression of *HOXB/C* genes: caudal hindbrain, rostral and caudal spinal cord can be prospectively identified by their combinatorial expression of *HOXB4*, *HOXB8*, and *HOXC9* (Nordstrom, Maier et al. 2006). Importantly, these authors showed that this entire spectrum of specific regional identities, at the *CDX* and then *HOX* levels, can be rationally reconstructed by exposing prospective forebrain explants to combination of Wnt, FGF, and RA signals. As described previously, by the time motor neurons have exited the cell cycle (~HH24), they have been imbued with positional identities marked by HOXC6 (Brachial), HOXC9 (thoracic), and HOXC10 (lumbar) (Liu, Laufer et al. 2001; Dasen, Liu et al.

2003). Finally the most caudal identities—lumbar: *HOXC10*—depend on additional node-derived GDF signals (Liu, Laufer et al. 2001) (Fig. 1.8).

Many HOX genes interact to diversify limb innervating motor pools

After specifying columnar identities, many other *HOX* genes act at a tertiary level to diversify the generic identity of forelimb innervating LMC motor neurons into the multiple pool identities required for targeted innervation of limb muscles (Dasen, Tice et al. 2005). HOXA5 is expressed in the rostral, and HOXC8 in the caudal brachial LMC and the respective motor pools therein. HOXA5 is required for the *scapulohumeralis posterior* (SCA) which is marked by RUNX1 expression, and HOXC8 is required for the specification of the *flexor carpi ulnaris* (FCU, SCIP^{+}), *pectoralis* (PEC, PEA3^{+}), and *anterior latissimus dorsi* (ALD, PEA3^{+}) motor pools. Cross-repressive actions between *HOXA5* and *HOXC8*, with *HOXC8* in a dominant position, establish the boundary of *HOX* expression and pool location, and positive or negative perturbations of *HOXC8* expression result in shifts in pool identity as measured by molecular profile of motor pools and axonal target selection. A second tier of interactions between other *HOX* genes and the HOX-cofactor MEIS1 sculpts a series of motor pool identities at the same intrasegmental (HOXC8^{+}) level. These include MEIS repression of *HOX4*, *HOX7* repression of *HOX4*, and *HOX4* activation of Pec-, ALD-, and FCU-motor pool-specific expression of their respective pool-markers PEA3 and SCIP.

FOXP1 gates limb level HOX diversification of motor pools

FOXP1, as previously described, is a marker for LMC motor neurons, however it is also a required determinant of LMC functional identity. The FOXP1 knockout mouse showed a loss of functional motor pool identities leading to random limb innervation and complete absence of

coordinated limb muscle control (Dasen, De Camilli et al. 2008). All motor neurons reverted to an axial innervating character (MMC/HMC), an atavistic phenotype characteristic of evolutionarily basal aquatic vertebrates without limbs or sympathetic nervous systems, relying on axial, sinusoidal locomotion: which was the striking locomotor phenotype of these animals. In limbed vertebrates, high-level FOXP1 expression, in the context of HOXC6 or HOXC10, directs limb-level LMC motor neuron diversification by enabling the productive interaction of the dozens of HOX genes to determine motor pool identities. At thoracic levels however, in the context of HOXC9 expression, low-level FOXP1 expression direct motor neurons to adopt PGC motor neuron identities (Fig. 1.9).

Relationship to human development

No direct evidence is available on the expression of any of the rostrocaudal morphogens, *CDX* or *HOX* genes in the human spinal cord. However the human embryo generates the same anatomical structures—primitive streak, node and somites—that produce these morphogens in the chick and mouse. While molecular studies on human or primate embryos would be extremely useful in this regard, it is unlikely that relevant staged samples could be procured at all and if so intact at an early enough timepoint in development to be useful. Moreover, an experimental system in which perturbations could be introduced and their effects tested is not conceivable in human. Therefore it would be highly desirable to develop the ability to investigate these mechanisms and markers in human in the one available system: human ES cell in vitro differentiation.

Motor neuron degeneration in ALS

ALS is an adult onset neurodegenerative disease that was first described by Jean-Martin Charcot (Charcot and Joffroy 1869) and is characterized by the selective death of spinal motor neurons and upper motor neurons of the motor cortex. Axonal degeneration and cell loss spreads, from an from an initiating motor pool, to nearly all others causing muscle weakness, spasticity and paralysis leading to death within a few years of diagnosis (Ravits and La Spada 2009). 90% of ALS is sporadic—without known genetic cause—however 10% is familial. Mutations in several genes have been linked to ALS: beginning with SOD1 (Rosen, Siddique et al. 1993), and now including many others (Boillee, Vande Velde et al. 2006). Most recent and exciting was the identification of TDP-43 in several reports in both familial (Gitcho, Baloh et al. 2008; Van Deerlin, Leverenz et al. 2008) and sporadic (Kabashi, Valdmanis et al. 2008; Sreedharan, Blair et al. 2008) ALS, which therefore links the familial and sporadic and by implicating a new molecule may give new clues to mechanisms. Mutations in the SOD1 gene have formed the basis for rodent models which have provided important insights into the sequence and specifics of pathology—axonal dieback, misfolded SOD1 and protein aggregation, axonal transport defects, mitochondrial dysfunction, and glutamate excitoxicity, for example—pointing towards key players but not identifying upstream mechanisms which could serve as therapeutic targets. Animal models have also generated some groundbreaking insights, for example, the importance of non motor neurons to disease progression: astrocytes and microglia (Clement, Nguyen et al. 2003; Boillee, Yamanaka et al. 2006). Despite this progress disease mechanism are not well understood and there are no effective therapies.

Motor neuron subtype-selective disease phenotypes

The motor neuron selectivity of cell loss in ALS has historically, and with good reason, occupied much attention. However, while almost all motor neurons degenerate in ALS, certain classes and motor pools show enhanced susceptibility or resistance to degeneration (Kanning, Kaplan et al. 2010).

Distal limb projecting, or facial motor muscles in bulbar forms, are typically affected first, compared to thoracic muscles (Ravits, Paul et al. 2007). These clinical findings suggest that limb innervating motor neurons of the LMC are more susceptible to the onset or triggers of ALS than are the axial muscle innervating MMC or HMC motor neurons of the trunk. Whether this susceptibility is due to intrinsic properties of these motor neurons, their interactions with glia, or circuit and activity characteristics is not known. Sympathetic motor function and motor neurons may be relatively less affected in ALS, suggesting that PGC motor neurons are resistant to degeneration. This strength of this subtype-phenotype is less clear and is complicated by a less direct understanding of the neural substrates of sympathetic nervous system function and less direct measures. Bunina bodies, characteristic of degenerating motor neurons in ALS, have been identified in PGC (intermediolateral column) motor neurons suggesting that they are affected, although depending on the spinal level the density of deposits was less than compared to somatic motor neurons (Takahashi, Oyanagi et al. 1993). The number of PGC motor neurons with NF-H accumulations was higher in ALS patients compared to controls, but not as frequent as in ALS-patient ventral motor column (MMC/HMC/LMC) motor neurons (Itoh, Sobue et al. 1992). To address this controversy a series of functional tests on human patients determined that sympathetic nervous system function was somewhat tonically increased in ALS patients, although there was a wide variety of patient responses and the authors concluded that there was

subtle involvement of the sympathetic nervous system in ALS (Oey, Vos et al. 2002). In conclusion it seems clear that PGC motor neurons are affected in ALS, but perhaps less pervasively than somatic muscle motor neurons. If LMC and PGC motor neurons can be studied in vitro, it will be intriguing to determine if they indeed are relatively susceptible and relatively resistant, respectively.

One clear subtype-selective phenotype in ALS is the relative order of degeneration of fast fatigable (FF), followed by fatigue-resistant (FR), and finally slow (S) motor units (Kanning, Kaplan et al. 2010). This sequence is evident in the muscle morphology of mutant-SOD1 mice (Frey, Schneider et al. 2000; Pun, Santos et al. 2006), early loss of large diameter (FF) axons in ventral roots (Fischer, Culver et al. 2004), and calcitonin gene related peptide^{+} (FF) cell bodies in the spinal cord (Kong and Xu 1998). Loss of FF and FR motor units may be compensated for by sprouting from FR and S motor units with resulting EMG and fiber type changes (Kanning, Kaplan et al. 2010). Data from human patients supports this sequence of events: early signs of deinnervation in muscles, electromyelograms consistent with deinnervation/reinnervation, and twitch force studies (Dengler, Konstanzer et al. 1990; Fischer, Culver et al. 2004; de Carvalho, Pinto et al. 2008). Despite these intriguing differences, the developmental mechanisms leading to FF, FR, or S motor unit motor neurons are not known. Furthermore these motor neurons can be distinguished in situ by differences in cell soma size and axon caliber, but are not unambiguously distinguished by any molecular or any genetic markers.

Two motor pools however show remarkable resilience even at end stages of disease. In ALS patients' eyes muscle and pelvic sphincter functions are well preserved even at end stages (Mitsumoto, Przedborski et al. 2006). ALS patient autopsy samples showed significance preservation of both the oculomotor (Gizzi, DiRocco et al. 1992; Kaminski, Richmonds et al.

2002) and Onuf's nuclei (Mannen, Iwata et al. 1977; Schroder and Reske-Nielsen 1984; Mannen 2000). Furthermore these phenotypes translate robustly to ALS mice, where several eye muscle-innervating nuclei, including the oculomotor (Ferrucci, Spalloni et al. 2010), as well as Onuf's (Artem Kaplan and Christopher E. Henderson, unpublished results) are also robustly preserved. These strong motor pool-specific ALS-resistance phenotypes suggest that studying these motor pools could identify mechanisms of cellular resistance or vulnerability by comparison with other motor neurons.

Summary

Chick and mouse motor neuron subtypes are defined at the level of motor column, division, and pool, and can be identified by molecular markers. These functional subtypes are conserved in human, but will these molecular markers be conserved as well? The developmental mechanisms which produce the diversity of motor neuron subtypes in chick are early embryonic rostrocaudal patterning, initiated by morphogens secreted from discrete embryological structures over several developmental time periods. We know that the human embryo generates the same structures as the chick and mouse (see Chapter 6) but we do not know if the same cues are deployed. In models systems these morphogenetic cues are translated into positional identity and motor neuron subtype diversity by *CDX* and *HOX* genes. While human embryonic stem cells can respond to two of these morphogens, RA and SHH (see Chapter 1, Part IV), will Wnt, FGF, and RA in combination have similar activities as in model systems?

ALS is a disease with poorly understood mechanism which selectively targets motor neurons, but we have observed that this response is not uniform among motor neuron subtypes. If human

motor neuron subtypes can be defined at the molecular level in vivo, and developmental mechanisms controlled in vitro, it may be possible to generate motor neurons from human stem cells with identifiable subtype identities which match those showing differential responses to ALS in vivo. Comparing the disease-response phenotype of these outlying subtypes to more classically affected, or especially to more susceptible motor neurons may reduce the noise of gene expression, cell-biological, or phenotypic changes which distinguish ALS motor neurons from non-motor neurons, and produce a novel range of mechanistic insights.

Part III. MOUSE EMBRYONIC STEM CELL-DERIVED MOTOR NEURONS

Introduction

The development of the mouse embryonic stem (ES) cells in the 1980s revolutionized mouse genetics but also opened several possible avenues for in vitro investigation. Because of the pluripotency of stem cells developmental biologists could imagine studying lineage development in a highly reduced but highly tractable system. Those interested in diseases could also imagine generating the affected cell types in vitro and using these to build new models to understand disease mechanisms. Finally, many were excited by the prospect of generating differentiated cells in vitro to be used in transplantation approaches to replace damaged or dead cells. Since research on mouse ES cells and ES-derived motor neurons frame much of the work on the human system, it is important to review these precedents. Here we review the origins and defining characteristics of mouse stem cells and their application to the problem of mouse motor neuron differentiation and diversity.

Mouse embryonic stem cells

In 1981 mouse ES cells were derived from the blastocysts of the preimplantation mouse embryo (Evans and Kaufman 1981; Martin 1981). These cells provided the functional in vitro definition of ES cells: unlimited proliferation (self-renewal) with retention of the ability to differentiate into cells from each of the three embryonic germ layers: ectoderm, mesoderm, and endoderm (pluripotency). 25 years of concerted effort have defined a core network of transcription factors (OCT4, SOX2, NANOG, TCF3) that determine the self-renewing pluripotent state and maintain it through mutual transcriptional positive feedback (Loh, Wu et al. 2006). Not least this work provided the groundwork for reprogramming approaches to induce the state of pluripotency (iPS, see below) using defined genetic factors.

In vivo tests of pluripotency

The formal test of ES cell pluripotency was provided by the ability to contribute significantly to all tissues in the morula aggregation assay (Bradley, Evans et al. 1984). This advance provided a technical means to manipulate the mouse germline, and formally demonstrated that ES cells, in the context of implantation development, were able to give rise to all cells of the embryo . A more direct test of pluripotency is the tetraploid embryo complementation assay (Eggan and Jaenisch 2003). In this assay a fertilized egg at the two-cell stage is fused to create a tetraploid cell. The result is normal development only up to the morula stage, and a normal trophoblast, but a complete failure of embryonic development. If diploid ES cells are inserted into this blastocyst, only these cells contribute to development of the embryo. Therefore when embryos do develop, they are constituted of cells differentiated exclusively from the ES cells inserted, thus providing formal proof of the pluripotency of the ES cells used in the experiment.

In vitro and in situ tests of pluripotency

Several in vitro or transplantation assays are commonly used shortcuts to the more complete demonstrations of pluripotency described above. First, ES cells can be allowed to undergo spontaneous differentiation by removing the factors (leukemia inhibitory factor (LIF) and or fibroblast conditioned medium) which actively maintain an undifferentiated state in vitro (Smith, Heath et al. 1988). Transcriptional or protein endpoints can then be used to look for the elaboration of cellular identities characteristic of the 3 embryonic germ layers. Alternatively the teratoma formation assay is interpreted as slightly stronger evidence of pluripotency. In this assay, spontaneous differentiation occurs when ES cells are transplanted into immune deficient (SCID) mouse kidney capsule, where pluripotent cells elaborate not only cellular and molecular markers of 3 germ layers, but develop tissue patterns characteristic of the 3 germ layers.

ES-cell derived motor neurons

Motor neurons can be generated from stem cells in vitro using developmental mechanisms

Pluripotency implies than any given somatic cell can be generated from ES cells. A new subfield of motor neuron and stem cell biology was inaugurated by the finding that developmental mechanisms could be used to robustly direct mouse ES cells to differentiate to a specific post-mitotic fate: the spinal motor neuron (Wichterle, Lieberam et al. 2002). Mouse ES cells were removed from pluripotency-maintaining culture conditions, cultured as free floating aggregates termed embryoid bodies (EBs) and allowed to differentiate spontaneously for several days. Then, since RA is synthesized by anterior (cervical) somites in early somite stage embryos and activates rostral spinal *HOX* gene expression in the neural tube (Muhr, Graziano et al. 1999;

Liu, Laufer et al. 2001) it was used to impose a caudal, spinal identity on neuroectodermal cells with a default anterior identity. Again following developmental principles SHH was used to induce the ventral identity and gene expression programs required for motor neuron specification. The resulting population of neurons was composed of almost 50% $HB9^{+}$, ISL^{+}, ChAT-expressing cells which met the molecular characteristics of spinal motor neurons and were defined as ES-derived motor neurons (ES-MNs). When transplanted to chick embryonic neural tube these ES-MNs were able to settle in the ventral horn and projects axons to muscle targets (Fig. 1.10). It is important to note that the timecourse of motor neuron lineage elaboration in these experiments precisely paralleled that found in vivo, and this allowed the morphogenetic cues RA and SHH to be presented in a logical and defined temporal window in vitro.

ES-MN diversity in mouse

The subtype diversity of ES-MN was later found to be almost exclusively of a rostral, cervical phenotype under these RA-based differentiation conditions, as assessed by expression of HOXA5 (Wichterle, Lieberam et al. 2002; Soundararajan, Miles et al. 2006; Peljto, Dasen et al. 2010). Most mouse ES-MNs however express the MMC marker LHX3(Wichterle, Lieberam et al. 2002; Soundararajan, Miles et al. 2006; Peljto, Dasen et al. 2010).

Controlling subtype diversity of mouse ES-MNs

Subsequent research identified a differentiation strategy which was able to generate motor neurons expressing more caudal *HOX* genes (*HOXC6*, *HOXC8*) which, following in vivo developmental rules, resulted in the emergence of more caudal columnar identities including FOXP1-expressing LMC motor neurons (Peljto, Dasen et al. 2010). This differentiation strategy did not use exogenous morphogens, but the authors showed that elaboration of caudal identities

and subsequent brachial LMC fates were dependent on FGF and Wnt signaling endogenous to the cultured EBs, and operated through *CDX*-dependent mechanisms, as in vivo. Further work is needed to generate more caudal motor neuron identities, to specify them by rational addition of salient patterning factors, and to increase the efficiency of differentiation.

Elaboration of motor pool identities in ES-MNs in vitro

Once these caudalizing conditions were defined it was possible to ask if the motor neurons with LMC phenotypes— expressing HOXC6 and FOXP1—were able to generate identified molecular phenotypes of motor pools characterized within the brachial LMC. Caudalized ES-MNs expressed several LMC motor pool markers (SCIP, expressed by the FCU and PEA3, expressed by the CM) consistent with their HOX and LMC divisional profiles (Peljto, Dasen et al. 2010). Furthermore PEA3 expression was dependent on exogenous application of the growth factor GDNF, which is required for its expression in vivo. These results suggest that if the appropriate HOX profile is established in ES-MNs, then coherent column identities will follow, and that if required growth factors are present, then motor pool identities will crystallize.

Functional phenotypes of ES-MNs

Electrophysiology

Perhaps the most functional property of a mature neuron is its ability to integrate chemical synaptic activity into coherent and stereotyped electrophysiological responses. It was therefore important to ask if ES-MNs were capable of developing mature electrophysiological characteristics. ES-MNs have been shown to develop a physiological profile appropriate to

developing motor neurons (Miles, Yohn et al. 2004): they respond to salient neurotransmitters (GABA, glycine, glutamate), fire repetitive action potentials, and form synapses with myotubes in co-culture. Impressively, when ES-MNs were transplanted into the mouse tibial nerve (distal to nerve sectioning) they were able to send projections to the *gastrocnemius* muscle, form synapses and drive muscle contractions, and ameliorate functional deficits (Yohn, Miles et al. 2008). Together these results demonstrate that ES-MNs have a significant capacity for functional maturation.

Motor neuron subtype-specific phenotypes

A series of xenotransplantation experiments supports the idea that ES-MNs can become functional, but that they exhibit phenotypes specific to their transcriptionally defined motor column subtype. ES-MNs expressing the MMC marker LHX3 showed a strong preference for axial, MMC axonal trajectories upon transplantation to developing chick neural tube, thus confirming the functional nature of MMC identity for in vitro derived cells (Soundararajan, Miles et al. 2006; Peljto, Dasen et al. 2010). When $FOXP1^+$ ES-MNs were generated along with $LHX3^+$ MMC ES-MNs, their relative functional phenotypes could be addressed even more clearly. $LHX3^+$ or $FOXP1^+$ ES-MNs showed significant preferences for medial or lateral settling positions in accord with their endogenous MMC and LMC counterparts (Peljto, Dasen et al. 2010). Furthermore $LHX3^+$ or $FOXP1^+$ ES-MNs preferentially selected appropriate axonal trajectories through axial or limb innervating nerves respectively, as confirmed by retrograde labeling of axons of transplanted ES-MNs. These findings demonstrated that ES-MNs with appropriate HOX and column marker profiles were competent to interpret endogenous cues for cell body positioning and axon guidance. This suggests that if HOX and motor column markers are coherently specified, then not only molecular but correct functional phenotypes will follow.

Using ES-MNs to model ALS

Several reports point toward the specific utility of ES-derived motor neurons for modeling ALS. Mouse ES-MNs were able to recapitulate the selective sensitivity to mutant SOD1 rodent primary astrocytes (Di Giorgio, Carrasco et al. 2007; Nagai, Re et al. 2007) shown by primary motor neurons. These data point to a significant role for non-cell-autonomous mechanisms in animal models of familial ALS. In one report there were indications of a potentially cell-autonomous protein aggregation and survival phenotype for mutant-SOD1 ES-MNs (Di Giorgio, Carrasco et al. 2007), although these findings have not been confirmed by subsequent reports.

Conclusions

The promise of ES cell pluripotency was confirmed in the mouse system by the selective generation of motor neurons in vitro. We have seen that in vivo developmental principles can guide successful differentiation strategies and that these need to be timed appropriately to parallel in vivo development. The motor neuron subtypes generated showed specific combinatorial molecular profiles that matched in vivo categories. Importantly when the HOX and column marker profiles were successively induced in ES-MNs then appropriate motor column and pool identities and functional phenotypes precipitated. These results engendered the question of whether similar approaches and results could be taken in the human ES system, and they establish a required context for the studies presented in this work.

Part IV. HUMAN EMBRYONIC STEM CELL-DERIVED MOTOR NEURONS

Introduction

The rapid adoption of mouse ES cell technology as a productive system for biological investigation made the establishment of human ES cell lines doubly exciting. Human ES cells potentially made human specific aspects of neural development and disease available for study for the first time, as well as representing a potential allogeneic substrate for cell transplantation strategies. Here we review the derivation of human ES cell lines and their utilization to generate spinal motor neurons.

Human ES cells are pluripotent

In 1989 human embryonic stem cells were first derived from surplus human blastocysts (Thomson, Itskovitz-Eldor et al. 1998). These ES cell lines demonstrated the hallmark characteristics of self-renewal and pluripotency. While the gold standard pluripotency assays of morula aggregation or tetraploid embryo complementation are ethically impossible using human cells, human ES cells passed all the standard in vitro tests for mouse ES cells. They expressed similar markers to mouse ES cells, and were competent to generate 3 germ layers by spontaneous differentiation or teratoma formation. Despite domestic and international political limitations many ES lines have subsequently been derived by similar methods, contributing to a moderate diversity of ES lines and an enriched understanding of the core transcriptional and functional phenotype of human ES cells (Cowan, Klimanskaya et al. 2004).

Motor neurons can be differentiated from human ES cells using developmental mechanisms

The demonstration that mouse ES cells could be efficiently directed to motor neuron fate then raised the question of whether the same approach could be used with human. Several groups initially reported the differentiation of motor neurons from human ES cells (Li, Du et al. 2005; Shin, Dalton et al. 2005; Lee, Shamy et al. 2007). While protocols varied slightly, especially regarding timing and means of neural induction, specification of the motor neurons in each system was based on the same developmental mechanisms used in mouse: caudalization of default anterior identity with RA and ventralization with SHH. These cues were delayed and prolonged compared to mouse to adjust for the slower tempo of human development in vivo.

Subsequent work has made advances in the efficiencies of motor neuron differentiation by several means. First, the efficiency of neural induction could be increased by initiating small EBs by starting from single cell suspensions, utilizing an inhibitor of Rho kinase (ROCK) which permitted survival of isolated single ES cells (Watanabe, Ueno et al. 2007). These conditions potentiated the effects of in-vivo inhibitors of non-neural differentiation like Noggin, and promoted homogenous differentiation by limiting EB size and thus the stochastic formation of uncontrolled signaling centers in large EBs. More recently pharmacological means were found to increase the efficiency of neural induction to nearly 100% (Chambers, Fasano et al. 2009). When an inhibitor of TGF-beta superfamily Type I signaling (SB-431542, Activin Receptor Like Kinases (ALK)-4, -5, -7 inhibitor (Inman, Nicolas et al. 2002)) was used in combination with Noggin, nearly uniform neural induction was achieved at 7-10 days in advance of the average timing in previous protocols. Finally, a pharmacological substitute for Noggin (LDN-193189, and inhibitor of ALK-2 and -3 (Yu, Deng et al. 2008) was shown to have equivalent if not more penetrant effect to Noggin in combination with SB-431542 (Boulting, Kiskinis et al.).

Analysis of generic ES-MN identity and differentiation efficiency

Many other groups have now reported human ES-MN differentiation from ES cells and all have used either HB9 or ISL1 to identify motor neurons (Di Giorgio, Boulting et al. 2008; Li, Hu et al. 2008; Marchetto, Muotri et al. 2008; Karumbayaram, Kelly et al. 2009; Wada, Honda et al. 2009; Patani, Hollins et al. 2011). HB9 is the more selective of these markers in rodent, because of the relative abundance of ISL^+ interneurons in the spinal cord and dorsal root ganglia. Finally, because other somatic cell types, particularly in the pancreas and esophagus (Ross, Ruiz-Perez et al. 1998; Hagan, Ross et al. 2000) also express HB9 or ISL, it is important to confirm the neuronal character of $HB9^+$ or ISL^+ cells in vitro as well. The efficiencies of differentiation vary widely, from 8% (Di Giorgio, Boulting et al. 2008) 80% (Erceg, Lainez et al. 2008), however HB9 staining was as intense in cytoplasm of every cell shown as in nuclei. Most groups show nuclear staining for HB9 and report efficiencies around 20-30%.

Reported efficiencies are based on immunostaining nuclei using an HB9-specific antibody (Table 7.1, #1) and are completely dependent on the methods used seed cells, pick fields, and count $HB9^+$ cells. For example only one group has reported strictly dissociated EBs which were subsequently quantitated for %HB9 out of all cells in the resulting re-seeded homogenous mixture, 8% (Di Giorgio, Boulting et al. 2008). Most groups attach undissociated rosette clusters or EBs to polyamino acid/laminin substrata and immunostain heterogeneous and partly-three dimensional cultures. This method is not amenable to accurate quantitation with respect to total differentiated cell numbers because heterogeneous fields must be hand-picked in the immediate environment of attached EBs. Furthermore, many groups culture human ES-MN cultures for 3 weeks (Wada, Honda et al. 2009; Patani, Hollins et al. 2011) before analysis of differentiation

efficiency (30% and 17% respectively). These authors do not report how fields are selected for analysis.

In order to further confirm motor neuron identity only one group has tested coexpression of HB9 and ISL1 ~80% of $HB9^+$ cells expressed ISL1 (Li, Du et al. 2005), but as discussed above, field selection in these cultures means this value must be interpreted with caution. Therefore this aspect of motor neuron transcription factor expression needs a rigorous quantitative treatment. Most groups have also shown ChAT expression by some $HB9^+$ cells at mostly later (6-8 weeks) timepoints in culture, consistent with maturing motor neuron identity (Li, Du et al. 2005; Lee, Shamy et al. 2007; Di Giorgio, Boulting et al. 2008; Placantonakis, Tomishima et al. 2009; Wada, Honda et al. 2009; Boulting, Kiskinis et al. 2011).

Maturation of ES-MNs in vitro

Since human ES-MNs are born in vitro (above reports) about the same time as in vivo (30-50 days of development (Hagan, Ross et al. 2000; Altman and Bayer 2001; Bayer and Altman 2002)) they are presumably immature. The utility of ES-MNs as a tool to study functional physiology or disease phenotypes may depend on their ability to attain significant maturation in vitro.

Since the most fundamental functional property of motor neurons is their ability to integrate synaptic input and generate action potentials to trigger muscle contraction, their electrophysiological status and activity are a the key indicator of maturity. Almost every group reporting ES-MN differentiation has shown a that some ES-MNs acquire electrical activity at later timepoints (day 30-90), including single or repeated action potentials, response to glutamate, voltage gated sodium channels, delayed inward rectifier channels (Li, Du et al. 2005;

Singh Roy, Nakano et al. 2005; Lee, Shamy et al. 2007; Wada, Honda et al. 2009; Patani, Hollins et al. 2011). In one instance depolarization of motor neuron (RA and SHH induced) but not parallel control cultures released Acetylcholine, providing the only evidence thus far, beyond ChAT staining, for ES-MNs able to functionally secrete their characteristic neurotransmitter (Lee, Shamy et al. 2007). However a detailed timecourse of the transition from recently-born ES-MNs to spike-train competent motor neurons or an analysis of the efficiency has not been reported. Since no MN-selective electrophysiological properties have yet been investigated for hES-MNs, it would be useful to both describe the timecourse and character of ES-MN electrophysiological maturation, and to determine the extent to which this functional physiology mirrors in vivo MN-selective phenotypes.

Another approach to assaying motor neuron-specific phenotypes is to study their behavior when transplanted in vivo. In these conditions, hES-MNs were found to survive in the spinal cord, showed some evidence of ventral migration, projected axons to the periphery over long distances >3.5mm in pursuit of mostly axial and body wall targets (Lee, Shamy et al. 2007). Transplantation approaches to examine the phenotypic behavior of hES-MNs have shown basic proof of principle and may in the future be able test motor neuron subtype-selective phenotypes.

ES-MN diversity

One principal category of functional and molecular diversity among motor neurons in vivo is the division into one of 4 motor columns. There is evidence that the MMC marker LHX3 is expressed by some post-mitotic ES-MNs. When HB9-enhancer lentivirus labeled presumed ES-MNs were FACS sorted for GFP, *LHX3* mRNA was coenriched (Singh Roy, Nakano et al. 2005). A BAC:HB9:GFP reporter line also showed that some GFP cells stained for LHX3

(Placantonakis, Tomishima et al. 2009). Another report showed $LHX3^+$ and $FOXP1^+$ cells in cultures that also contained some $HB9^+$ cells, but none of these cells was tested for either HB9 or ISL1 (Patani, Hollins et al. 2011). In conclusion, although evidence from several reports suggests that some ES-MNs show a $LHX3^+$ MMC-like columnar subtype identity no systematic analysis of column marker expression by $HB9^+$ or ISL^+ cells has yet been performed. Since motor column subtypes have different developmental, survival, and disease related properties it is critical to systematically define the diversity of subtypes present in hES-MN differentiations.

As we have seen from in vivo studies in mouse and chick, motor neuron columnar and pool subtypes are strongly dependent on rostrocaudal identity as encoded by HOX gene expression. It is therefore of principal interest to characterize the rostrocaudal/HOX diversity of human ES-MNs. Several reports have addressed this aspect of subtype identity at the level of gene expression, by microarray or PCR, and also at the level of protein expression in single cells. HOXA5, HOXC6, HOXC8, HOXC9 and HOXC10 protein have been reported in hESMN-containing cultures. Only in the case of HOXC6 was this gated on a MN-selective marker (HB9), though HOXC8 was expressed by NKX6.1 cells, and HOXC6 and HOXC8 were coexpressed in some cells as well (Lee, Shamy et al. 2007). Many $HOXC8^+TuJ1^+$ cells have been shown as examples from a group which routinely produces some of the most robust and most believable ES-MN cultures, however these HOXC8 cells have never been formally shown to express either HB9 or ISL1 (Li, Du et al. 2005). Another group reporting $HOXC8^+$ human ES-MNs showed $HOXC8^+$ $ChAT^+$ staining in which, the HOXC8 stain was as cytoplasmic as the HB9 and accounted apparently for 80% of total cells (Erceg, Lainez et al. 2008). Finally one group reported HOXC9 and HOXC10 expressing cells but these were not stained with HB9 or ISL1, HOXC9 was not shown, and one of the HOXC10 antibodies which was used is known to

work on chick but not mouse, therefore these data must also be interpreted cautiously (Patani, Hollins et al. 2011). Gene expression studies of ES-MN cultures or FACS purified HB9:GFP^{+} cells have shown enrichment for anterior HOX1-6 genes indicative of hindbrain to brachial spinal positional HOX identities (Lee, Shamy et al. 2007; Placantonakis, Tomishima et al. 2009). In aggregate these data suggest that human RA-dependent ES-MNs may be biased towards rostral spinal fates, but there are some reliable examples of more brachial expression (HOXC6 and HOXC8). However, a quantitative profile of HOX protein-expression has yet to be established at the level of individual human ES-MNs. Since columnar and motor pool identities emerge in the context of rostrocaudal identities, in order to begin studying these subtypes it is important to determine the rostrocaudal diversity and any biases present in ES-MNs. Furthermore if strategies to control motor neuron diversity are to be devised, it is critical to establish the rostrocaudal starting points.

Conclusion

Human ES cells have been used to generate cells with many of the molecular characteristics of motor neurons, importantly including the basic transcription factors HB9 and ISL and expression of appropriate neurotransmitter synthetic enzyme ChAT. These ES-MNs appear to be rostrally biased and at least contain some LHX3-expressing cohort. However a systematic characterization has not been undertaken and in most cases direct confirmation of pan-MN markers was lacking. Human ES-MNs can acquire mature characteristics including active electrophysiology, and axonal pathfinding on transplant to chick embryo, which are consistent with maturing motor neuron identity. However it will be important to understand the timecourse

and extent of maturation at a quantitative and systematic level. Assays which are more definitive for motor neuronal identity, rather than pan-neuronal, and functional assays that can discriminate between motor neuron subtypes are also needed. Finally, most publications on hES-MNs do not employ methods of quantitation that can reliably represent the population of ES-MNs generated. It is therefore not possible to draw strong conclusions about overall differentiation efficiency or the relative contribution of motor neuron subtypes. In order to measure the outcome of strategies aimed at controlling subtype diversity, it is important to be able to quantitatively account for the population representatively. qPCR is one such approach, but it lacks the single cell resolution which can definitively assign, for example, HOXC8 expression to a cell also expressing a validated motor neuron marker, like HB9. A homogeneous culture approach could allow for quantitative description of ES-MN diversity, and would additionally be well-suited for high-throughput assays for of phenotype or drug screening. Therefore unbiased and homogeneous methods of culture and quantitation are needed to address developmental questions, characterize subtype diversity, and lay the groundwork for screening assays.

Part V. INDUCED PLURIPOTENT STEM CELL-DERIVED MOTOR NEURONS

Motivation

Two of the major goals of translational stem cell biology are cell replacement strategies and modeling diseases using disease-specific stem cells. Because of graft vs. host rejection of even immunomatched allogeneic transplants, a syngeneic alternative is obviously the ideal. If replacement cells could be generated from the same individual this serious complication might be avoided. One strategy to generate replacement cells is to generate syngeneic stem cells, and

then differentiate the transplant cells from these. Another broad goal for the field is to use the disease genotype of patients suffering from genetic diseases to generate disease-allele bearing stem cells, and then produce the affected cell types from them for study in vitro. Notably, this strategy provides a unique opportunity to generate disease models from patients where no known etiologic alleles have been identified. For both of these aims it was thus important to generate patient-specific stem cell lines.

Approaches to patient-specific and disease-model stem cell lines.

Transgenesis, gene targeting, and somatic cell nuclear transplantation

One approach to modeling ALS in human stem cell-derived motor neurons would be to differentiate these from stem cells bearing ALS causing alleles. Since no extant ES cell lines harbor alleles linked to ALS, this goal required the insertion of pathological alleles as transgenes, via gene targeting, or the through the derivation of pluripotent cell lines natively harboring these disease-associated alleles. While both transgenesis and gene targeting are routine tools in mouse genetics, they have been problematic to accomplish in human ES cells. Human ES cells have a particularly vigilant and robust host defense mechanism which silences transgenic DNA. In addition, if transgenic lines could be made they might be limited to alleles which show toxic gain of function phenotypes. While a subset of ALS-causing alleles fits this description, notably the well studied SOD1 gene, other alleles (TDP43, FUS, PON) may not. Furthermore, even if gene silencing can be overcome, the gene regulation and dosage achieved may vary greatly from the genetic setting of affected patients, and lead to an exaggerated model which may be less faithful to the in vivo conditions. Another goal of genetic modification would be to rescue loss-of-

function alleles in patient-specific lines. To this end, a recent study identified the location of genomic "safe harbors" showing limited silencing and unregulated expression which may offer an attractive alternative approach for therapeutic transgenes as well as disease modeling (Papapetrou, Lee et al. 2011).

Gene targeting on the other hand, offers precise control of gene dosage and endogenous regulation of gene expression. Unfortunately this strategy has proven even more difficult than transgenesis in human ES cells, having been successful only twice (Zwaka and Thomson 2003; Urbach, Schuldiner et al. 2004) and its success is potentially dependent on the targeted allele. Recently zinc finger nuclease-mediated gene-editing has been developed as a much higher efficiency method to induce or rescue pathogenic lesions (Lombardo, Genovese et al. 2007).

Another strategy for developing patient-specific pluripotent cell lines is to convert somatic cells from affected patients into pluripotent cells. In other species this has been achieved by enucleation of fertilized eggs and insertion of donor cell nucleus or DNA, a procedure known as somatic cell nuclear transplantation (SCNT), which was used to clone the much heralded sheep Dolly (Wilmut, Schnieke et al. 1997) thereby demonstrating the ultimate developmental competence of a reprogrammed somatic cell: the generation of an entire animal. While this approach is very promising, it is for now blocked by tactical and technical obstacles in human cells. First, procuring human oocytes is extremely difficult, hazardous to donors, and not scaleable. More importantly, while this process has relatively high efficiency in mouse and many other species, even if it is extremely labor intensive, and it has recently been demonstrated in primates (Byrne, Pedersen et al. 2007), SCNT reprogramming has yet to be accomplished using human cells.

Somatic cell reprogramming with defined factors: induced pluripotent stem cells

Mouse induced pluripotent stem cells (iPS) cells

SCNT experiments in many species did however prove a critical principal: factors in the ooplasm are capable of reprogramming a terminally differentiated somatic cell to a state of pluripotency. This insight, combined with emerging consensus descriptions of ES cell and core pluripotency networks described above, became the foundation of a search to define these factors. In a technical tour de force, a combinatorial approach was used to test highly expressed stem cell genes for their ability to reprogram somatic cells to pluripotency. This study identified 4 genes that, when delivered by viral vectors, were sufficient to reprogram mouse somatic cells to a fully pluripotent state (Takahashi and Yamanaka 2006). These cells, termed induced pluripotent stem (iPS) cells, derived from mouse, demonstrated equivalent pluripotency to mouse ES cells and were subsequently shown to contribute to germline in chimeras and then to pass the tetraploid embryo complementation assay of pluripotency (Wernig, Meissner et al. 2007).

Human iPS cells

Because of the understanding of the core pluripotency transcription factor network in human ES cells (Boyer, Lee et al. 2005), and its fundamental similarity to mouse, the rapid same viral reprogramming approach was subsequently used to reprogram human somatic cells (Yu, Vodyanik et al. 2007; Nakagawa, Koyanagi et al. 2008; Park, Zhao et al. 2008). These reprogrammed cells were similar to ES cells and met all in vitro tests of ES cell pluripotency and the teratoma assay. For ethical reasons, the formal proof of pluripotency, the ability to clone an entire human, including germ cells, must never be done.

Technical innovations

Subsequent work has technically improved on the basic iPSC methodology. Early reprogramming cocktails used the oncogene c-MYC, and this was later shown not to be necessary (Nakagawa, Koyanagi et al. 2008; Wernig, Meissner et al. 2008). Other groups have found small molecules which could replace one or more reprogramming genes or increase efficiency. Others have used removable cassettes (Soldner, Hockemeyer et al. 2009), or non integrating vectors, to avoid genetic lesions at integrations sites (Okita, Nakagawa et al. 2008). More recently attempt to use synthetic RNA reprogramming has been successful (Warren, Manos et al. 2010).

Assessing the quality of human iPS cells

General equivalence of iPS and ES cells and concerns

Many concerns remain over the general comparability of first- or subsequent-generation iPS to ES cells as well as their utility in disease modeling or especially in cell transplantation approaches. First there is widespread and legitimate concern that multiple genomic lesions viral integration sites creates the risk of seriously perturbing genetic function and cellular phenotype. However given the rapid advances in non-integrating reprogramming described above it is likely that these concerns will soon be historical.

Persistent cellular memory of somatic cell identities in iPS cells may be a more difficult issue to resolve. Failure to reset DNA methylation marks appears to result in misexpression of proteins (Ohi, Qin et al. 2011) and chromatin modifications may also not be reset to an embryonic state.

Indeed it was recently shown that misexpressed proteins lead to immune rejection even in highly inbred syngeneic mice (Zhao, Zhang et al. 2011). These are serious concerns for those contemplating cell replacement with iPS cells. However, while these issues should serve as an important caveat to consider and variable to control in disease modeling studies they do not present a strong argument against the utility of iPS cells for these purposes.

Indeed, even if first- or later-generation iPS cells are genetically damaged, or maintain epigenetic and or gene expression signatures of the somatic cells from which they were induced, it is possible that they could still be very useful tools for modeling disease. As long as iPS cells can give rise to disease-relevant cell types whose function is relatively unperturbed by these defects, and if these cell types can manifest disease phenotypes in vitro, then they may still offer a unique and valuable resource for studying disease.

Motor neuron lineage equivalence of iPS and ES cells

Proof of principle

Once iPS cells were derived from human somatic cells, the technical stage was set to ask if somatic cells from patients with genetic diseases, like ALS, could also be reprogrammed to pluripotency and if so whether this capacity would include the ability to generate cell types highly relevant to ALS: motor neurons and astrocytes. To answer this question we participated in a collaboration with the Eggan Laboratory at Harvard University, clinicians at the Eleanor and Lou Gehrig ALS clinic at Columbia University Medical Center, and colleagues here in the basic sciences. We were the first to demonstrate that iPS cells derived from ALS patient and control somatic cells could be differentiated to motor neurons (Dimos, Rodolfa et al. 2008).

Mixed data on iPS MN-lineage differentiation efficiency

While our data provided the proof of principle that ALS iPS cells could differentiate to disease relevant cell types, and others reported similar results for lines from a variety of diseases, a subsequent report showed consistently compromised neural differentiation efficiency, and most problematic, high variability in the motor neuron lineage differentiation when compared with one ES cell line controls (Hu, Weick et al. 2010). Since the crucial step in using iPS cells to study disease will be to define disease phenotypes in vitro, the Hu study raised the worrisome possibility that large variability between iPS-MNs from different donors or reprogramming events, and in general between iPS and ES cells, might obscure disease phenotypes, making them technically ill-suited for disease modeling. To address the utility of virally reprogrammed iPS cells for disease modeling, it was therefore necessary to test their ability to generate motor neurons, and compare the variability and efficiency in comparison to ES cells. To this end we undertook a large comparative study of iPS and ES cell motor neuron differentiation described in Chapter 3.

Ability of iPS cells to recapitulate disease phenotypes

Several proof of principle demonstrations of the ability of iPS cells to model developmental or early onset diseases have been published, including Familial Dysautonomia (FDA) (Lee, Papapetrou et al. 2009), Long Q-T syndrome (Moretti, Bellin et al. 2010), and SMA (Ebert, Yu et al. 2009). The phenotype described for FDA-iPS cells was particularly interesting because it faithfully reproduced the sensory neuron-selective IKBAP splicing defects seen in vivo as well as functional neuronal phenotypes, and was amenable pharmacological rescue in vitro. The phenotype for SMA-iPS cells on the other hand, was determined in relation to a motor neuron

marker—a reduced number of ISL^+ cells—but it is not clear how this phenotype is related to the in vivo disease, and it was not rescued. Importantly, while iPS cells have now been generated for a wide variety of late onset neurodegenerative diseases—ALS, Alzheimer's, and Parkinson's—no phenotypes have yet been reported and this remains the major challenge for the field.

Another hope for the field of disease modeling is that human cells will be able to reproduce human-specific phenotypes not accurately reproduced in rodent models. This potential remains to be tested. Whether the disease phenotypes are specific to human cells or redundant to current mouse models, using human cell types as a screening platform may offer another significant advantage: the potential to eliminate at the outset false positives from drug screens where activity is limited to model systems but fails in the human genetic context.

Cell transplantation

A startling proof of principle experiment has also demonstrated the potential utility of IPS cells for cell replacement gene therapy approaches. iPS cells were derived from humanized sickle cell mice, the sickle allele was then corrected by gene targeting. Gene corrected iPS clones were then differentiation into hematopoietic progenitors and transplanted back to the sickle cell donors, which generated a profound rescue of the sickle phenotype (Hanna, Wernig et al. 2007).

Conclusions

We have seen that iPS cells can be generated from mouse and human somatic cells and that these can reproduce the cardinal functional characteristics of embryonic stem cells. Importantly they

can generate the cell types affected in many diseases and have already been used to generate highly relevant new model systems for a variety of developmental disorders and diseases. Several challenges and question remain from a disease modeling perspective however. Most generally, will iPS-derived neurons, with presumably an embryonic "age" like ES-derived neurons be able to mature sufficiently to reproduce disease relevant phenotypes which take decades to develop in vitro. It also remains to be shown that the genetic constellation driving or permitting ALS or other neurodegenerative diseases will be powerful enough to effect this pathological transition in vitro. Finally, do human iPS cells regain the *tabula rasa* of embryonic cells which will allow them navigate in vitro the normal course of development to generate extremely specific differentiated derivatives? Specifically, in the context of ALS and motor neurons, will iPS cells demonstrate responsivity to multiple patterning cues to enact programs of diversification into dozens of specific and coherent motor neuron subtypes?

Summary of outstanding questions and results

We have reviewed the categories of vertebrate motor neuron diversity and their ontogeny. In order to address the open question of how relevant these molecular categories are to human motor neurons in vivo we present in Chapter 2 an analysis of the molecular markers of human motor neurons in vivo. This study shows that the human spinal cord is remarkably similar in molecular organization to the mouse at the level of HOX protein, pan motor neuron, column and divisional marker expression. In addition several motor pools familiar from chick and mouse and potentially one novel profile not found in those species could be putatively identified in

human cords. Most important for our purposes these findings validate a set of markers which can be used to assess human motor neuron subtypes in vitro.

We have seen that mouse ES cells can be used to model motor neuron development and generate a spectrum of motor neuron subtypes which adhere to coherent in vivo categories and display appropriate functional phenotypes. We have learned that human ES and iPS cells can also generate motor neurons with perhaps a larger variety that mouse ES cells. However there is limited evidence regarding the subtypes of motor neurons generated from human stem cells. Furthermore the maturation of human ES-derived motor neurons has not been systematically addressed in vitro. We therefore present in Chapter 3 a detailed description of the diversity of motor neuron subtypes generated from human ES cells at the level of rostrocaudal and columnar identity, and analyses of their morphological and electrophysiological maturation in vitro. These studies show that human ES-MNs include cells matching the molecular profiles of all identified in vivo motor columns and divisions, but are restricted predominantly to rostral spinal levels. I also present evidence of the temporal sequence of ES-MN maturation in vitro at the level of molecules, morphology, and electrophysiology.

We have reviewed the exciting advances in the field of iPS cell reprogramming, but the capacity of these cells to generate ALS relevant cell types has been called into question. In Chapter 4 I therefore present the collaborative derivation of a test set of human iPS cell lines and analysis of these lines for their ability to generate functional motor neurons, in comparison to human ES cell lines. The results of these studies demonstrated a fundamental equivalence of iPS and ES cells in their ability to generate motor neurons with coherent identities and functional electrophysiology. We also identify potential demographic sources of variability which could explain previous reports.

Finally, we reviewed the developmental mechanisms which control the diversification of spinal motor neurons from generic progenitors into a diverse array of columnar, divisional, and pool identities. However these mechanisms have not been rationally deployed to generate specific subsets of motor neurons. I therefore present in Chapter 5 the design of a developmentally based strategy to generate rostral vs. caudal spinal motor neurons. These studies show that both ES and iPS cells can be manipulated developmental cues presented in a defined in vitro developmental time window to generate rostral or more caudal motor neuron subtypes, together representing most of the molecular diversity of coherent spinal motor neurons subtypes down to the level of divisional identity.

Together these studies lay the groundwork for asking if specific motor pool subtypes can be generated from human stem cells. They also establish the conditions to test whether specific motor neuron columnar or motor pool subtypes will show differential responses to ALS in vitro, with the hope that these future studies will illuminate the mechanism of degeneration and facilitate the development of new therapies.

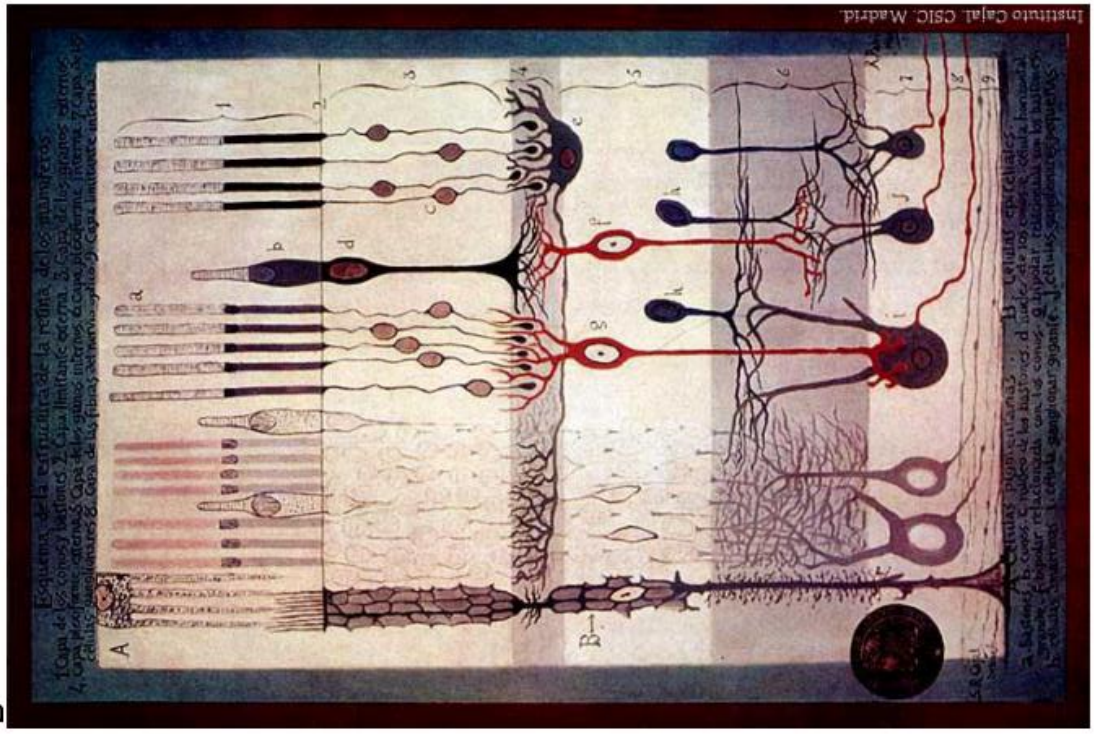

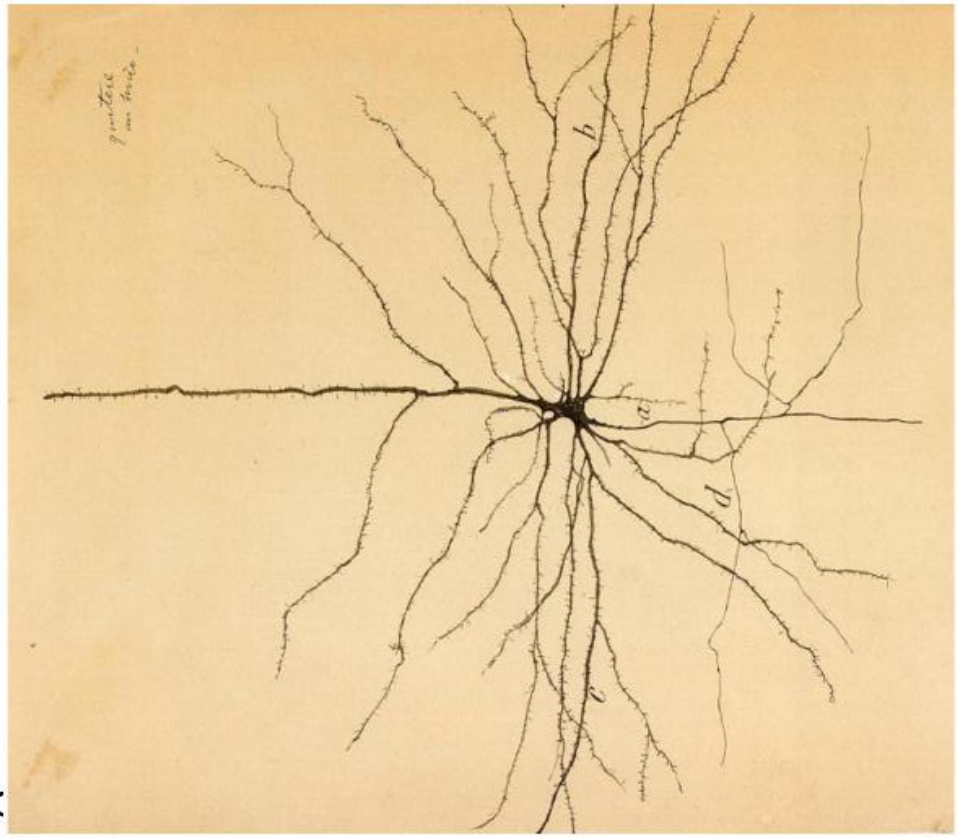

Figure 1.1

Figure 1.1. Neuronal subtype diversity in the central nervous system.

(A) Cortical pyramidal neuron, Ramon y Cajal (B) Cells of the neural retina, Ramon y Cajal.

Figure 1.2

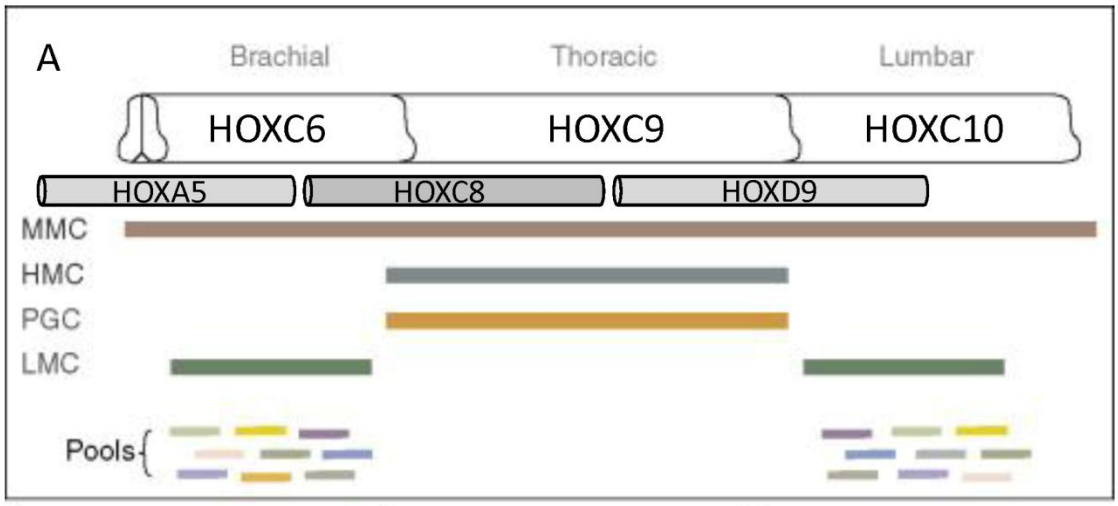

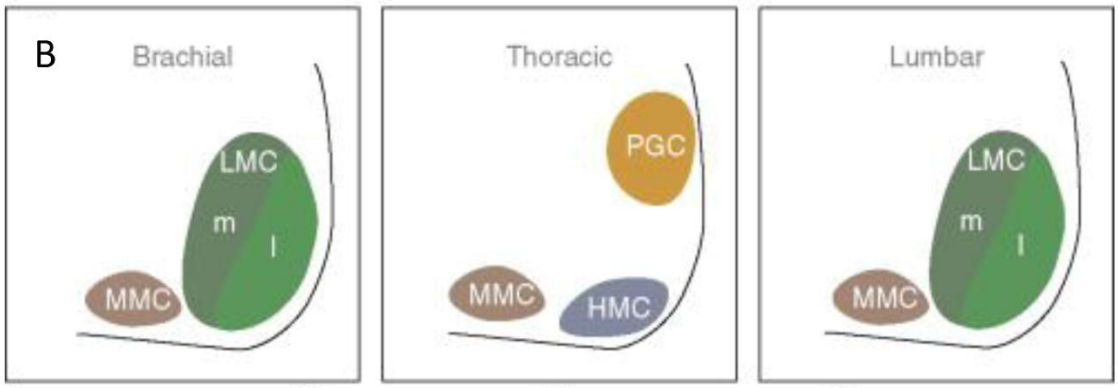

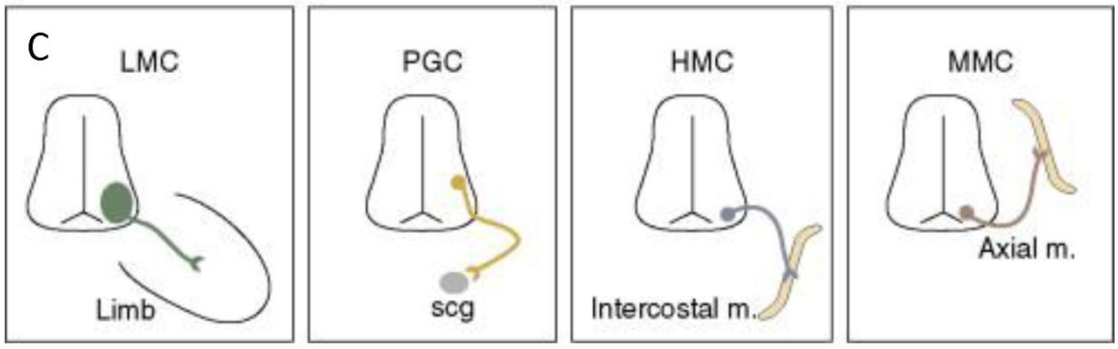

D

MMC	HB9	ISL1	ISL2	LHX3					
HMC	HB9	ISL1	ISL2				ER81		
PGC		ISL1	ISL2		FOXP1			pSMAD	nNOS
LMC_M	HB9	ISL1	ISL2		FOXP1				
LMC_L	HB9	ISL1	ISL2		FOXP1	LHX1			

Figure 1.2. Motor columns, divisions, and pools: anatomy, targets, and molecular markers

Motor neurons are grouped into 4 columns in the spinal cord: media motor column (MMC), hypaxial motor column (HMC), preganglionic motor column (PGC), and lateral motor column (LMC). (A) the MMC is continuous, while LMC is restricted to limb-levels, and HMC and PGC are restricted to thoracic. HOXC6, HOXC9, HOXC10 are expressed in brachial, thoracic, and lumbar spinal cord and determine column identities appropriate to level. HOXA5, HOXC8, and HOXD9 expression spans limb and non-limb levels. HOXA5 and HOXC8 participate in motor pool diversification in the brachial LMC. (B) Cross section at limb and non-limb levels showing columns present. The LMC is partitioned into a medial and lateral division. (C) Motor column muscle targets: LMC, limb muscles; PGC, sympathetic ganglia; HMC; hypaxial muscles: intercostals and abdominals; MMC, epaxial muscles. (D) Combinatorial gene expression uniquely identifies motor columns and divisions; black type, high expression; grey type, low level or no expression; no type, no expression. Adapted from (Dasen and Jessell 2009).

Figure 1.3

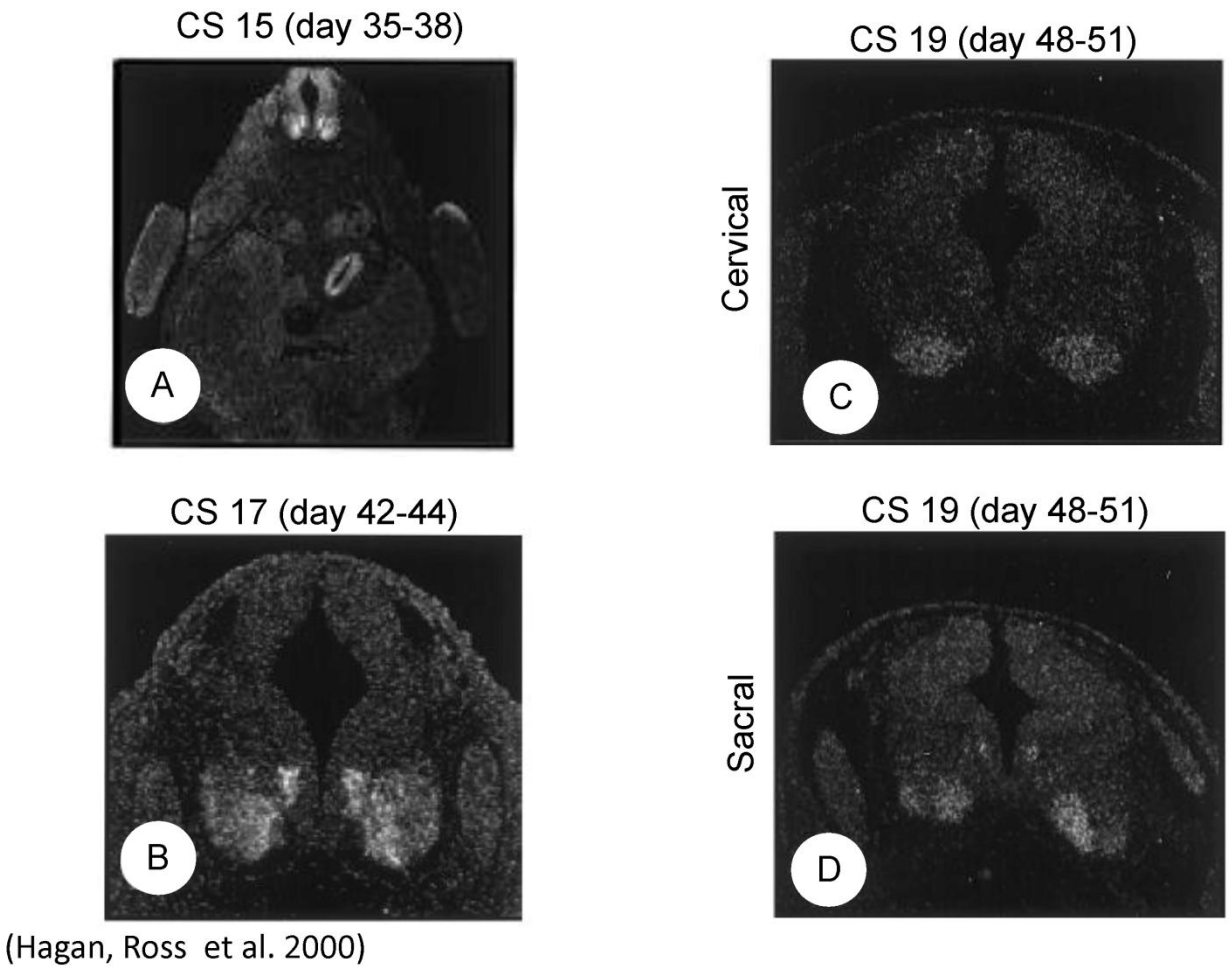

Figure 1.3. HB9 is expressed by motor neurons in the human embryo

Adapted from (Hagan, Ross et al. 2000) (A) Autoradiographic image of *HB9* in situ on Carnegie stage (CS)15 (day 35-38) human embryo section at the cervical level shows motor neurons in the lateral ventral horn, subventricular *HB9* expressing cells (presumptive progenitors), and stomach. (B) Motor neurons and presumptive progenitors at cervical level CS 17 (day 42-44). (C-D) CS 19 (day 48-51) sections(Bayer and Altman 2002) at cervical (C) and sacral (D) levels show subventricular HB9 expression is lost at cervical and maintained at sacral levels at this timepoint.

Figure 1.4

A

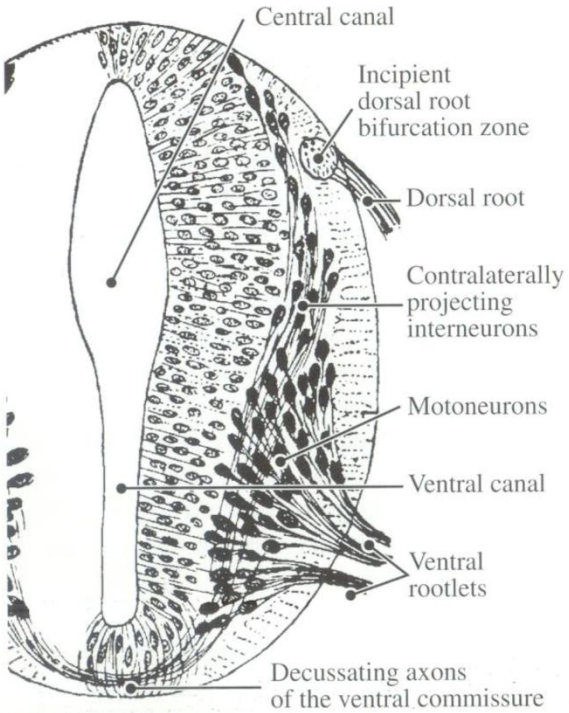

Figure 5-9. Ramón y Cajal's (1909) drawing (after His) of the cytological organization of the spinal cord of a "4-week-old" human embryo. The accumulation of the earliest complement of motoneurons is associated with the outgrowth of motor fibers and the formation ventral rootlets. Some of the original labels have been modified.

Ramon y Cajal, 1909. reprinted in (Bayer and Altman 2002)

B

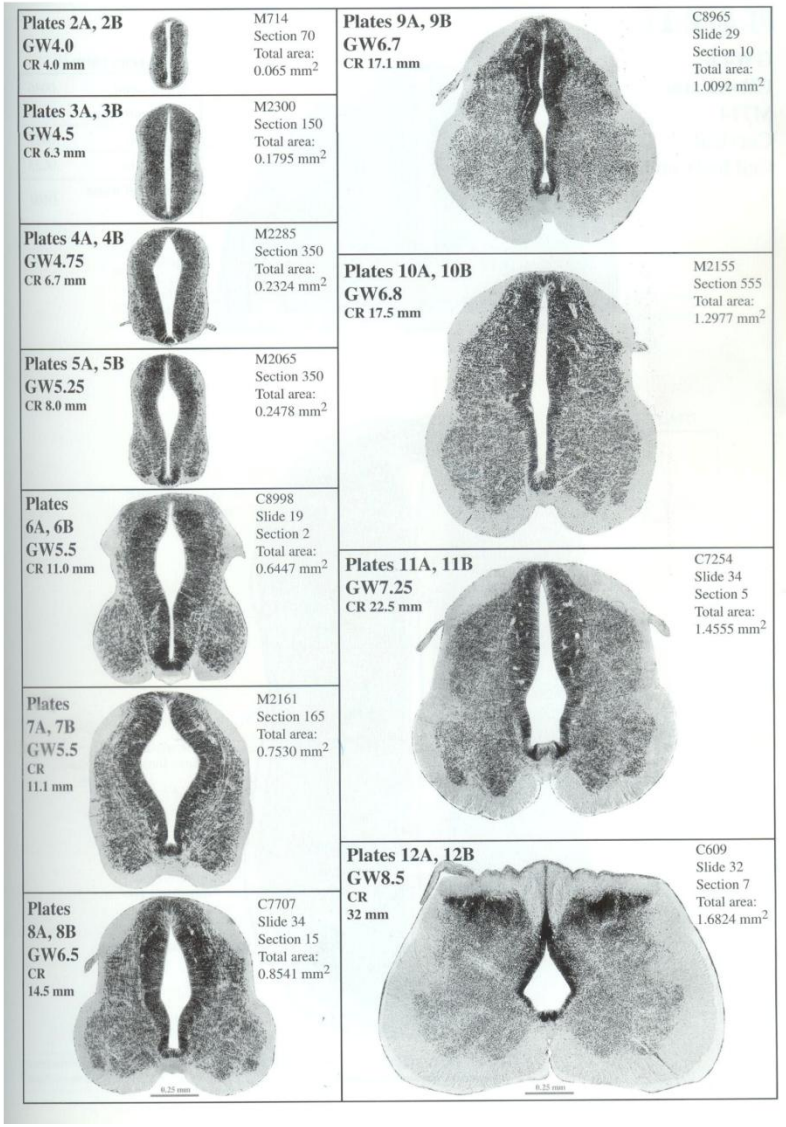

Figure 1.4. Histological analysis of the developing human spinal cord.

(A) “4 week embryo” showing newborn motor neurons extending axons through the ventral root, Ramon y Cajal 1909 (B) Gestational week (GW) 4-14 human embryo time series shows the period of motor neurogenesis and motor column segregation at the cervical level. From (Altman and Bayer 2001; Bayer and Altman 2002)

Figure 1.5

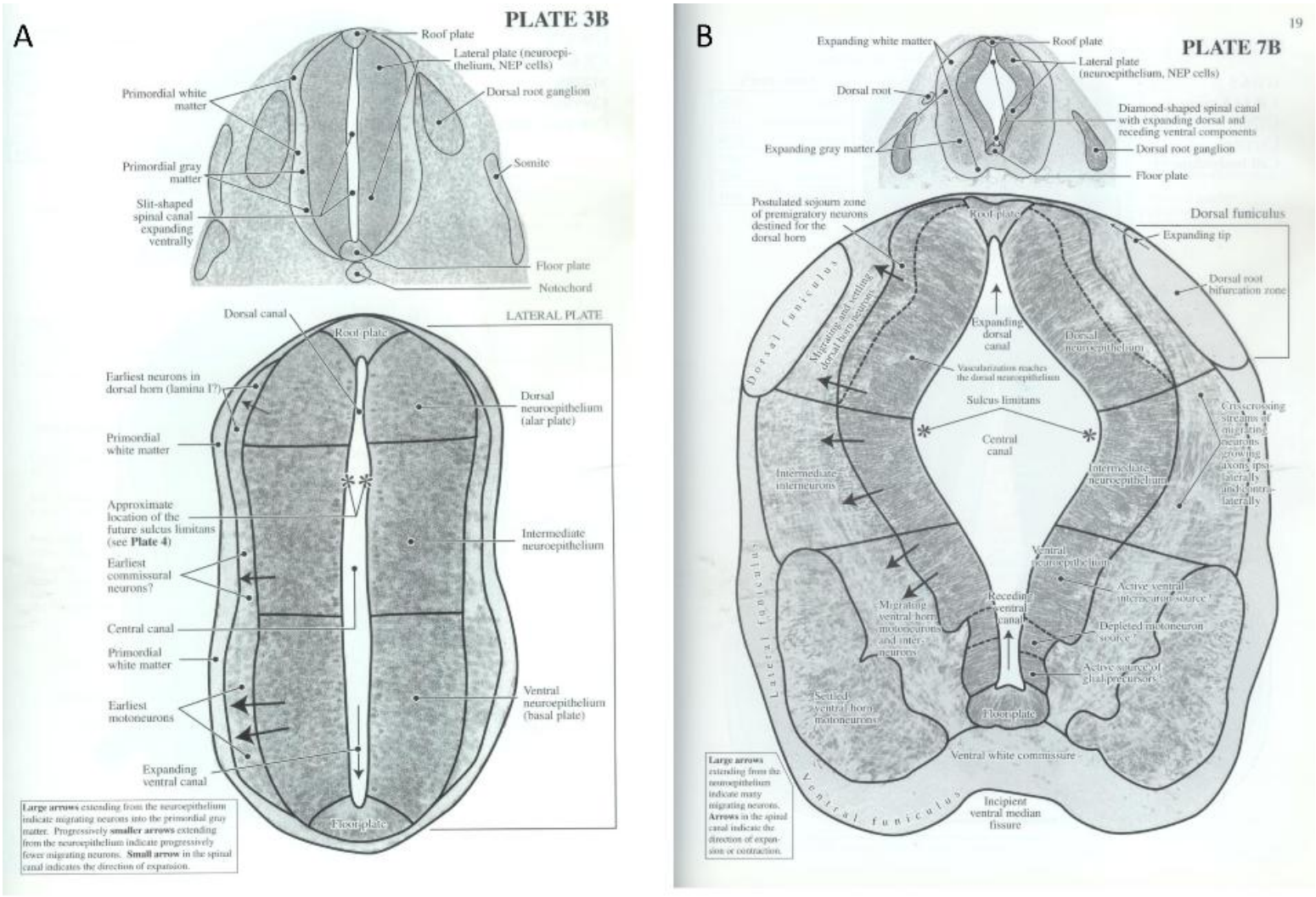

(Bayer and Altman 2002)

Figure 1.5. Histological analysis of the period of motor neurogenesis in the human spinal cord

(A) Gestational week (GW) 4.5 embryo section from cervical level shows the first motor neurons have migrated laterally. (B) GW 5.5 embryo at cervical level has large contingent of motor neurons in ventral horns and a thinned, potentially depleted ventral subventricular neuroepithelium suggesting the end of motor neurogenesis. From (Bayer and Altman 2002).

Figure 1.6

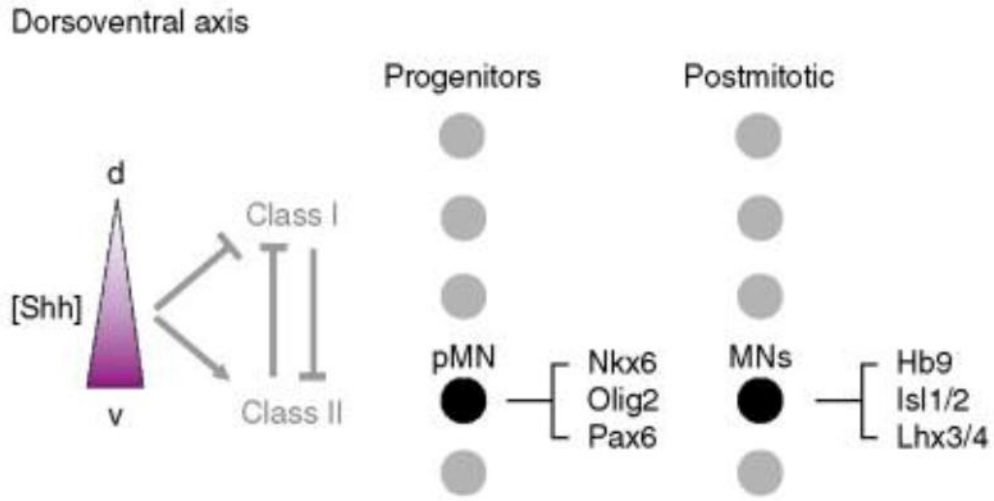

Figure 1.6. Sonic hedgehog protein patterns the ventral neural producing neuronal diversity

Sonic hedgehog (Shh) protein is secreted by the notochord and forms a ventral to dorsal concentration gradient in the ventral half of the neural tube. Class I and Class II HD transcription factors are induced and inhibited at staggered Shh concentration thresholds. Cross repressive interactions between Class I and Class II HD proteins resolve a series of 5 progenitor cell identities in specific dorsoventral domains. Motor neuron progenitors (pMN)s express Nkx6, Olig2, and Pax6. pMNs give rise to postmitotic motor neurons which express HB9, ISL1/2, and LHX3/4. From (Dasen and Jessell 2009).

Figure 1.7

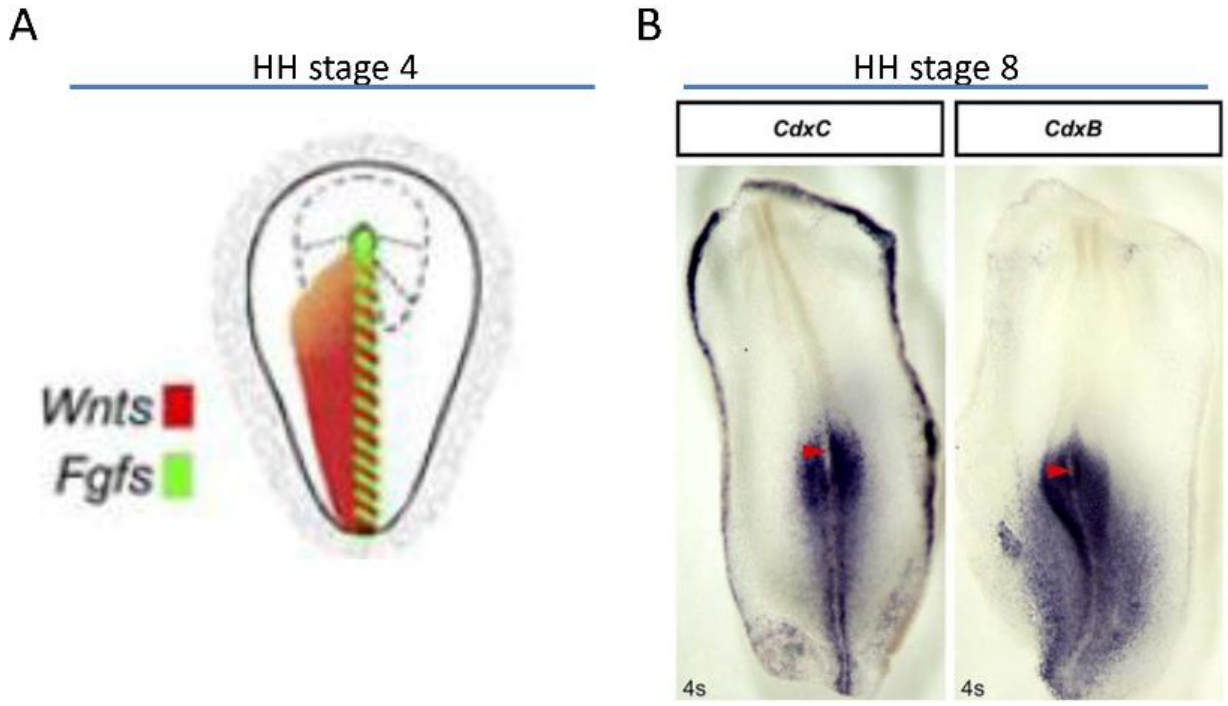

Figure 1.7. Wnt and FGF induce *CDX* gene expression which encodes caudal neural identity

(A) Wnt is secreted from paraxial mesoderm and FGF from the primitive streak in Hamburger and Hamilton (HH) stage 3^{+}/4 chick embryos leading to (B) expression of *CDX* genes by HH8 (4 somite stage) in prospective caudal neural tissue (hindbrain and spinal cord). Adapted from (Nordstrom, Maier et al. 2006).

Figure 1.8

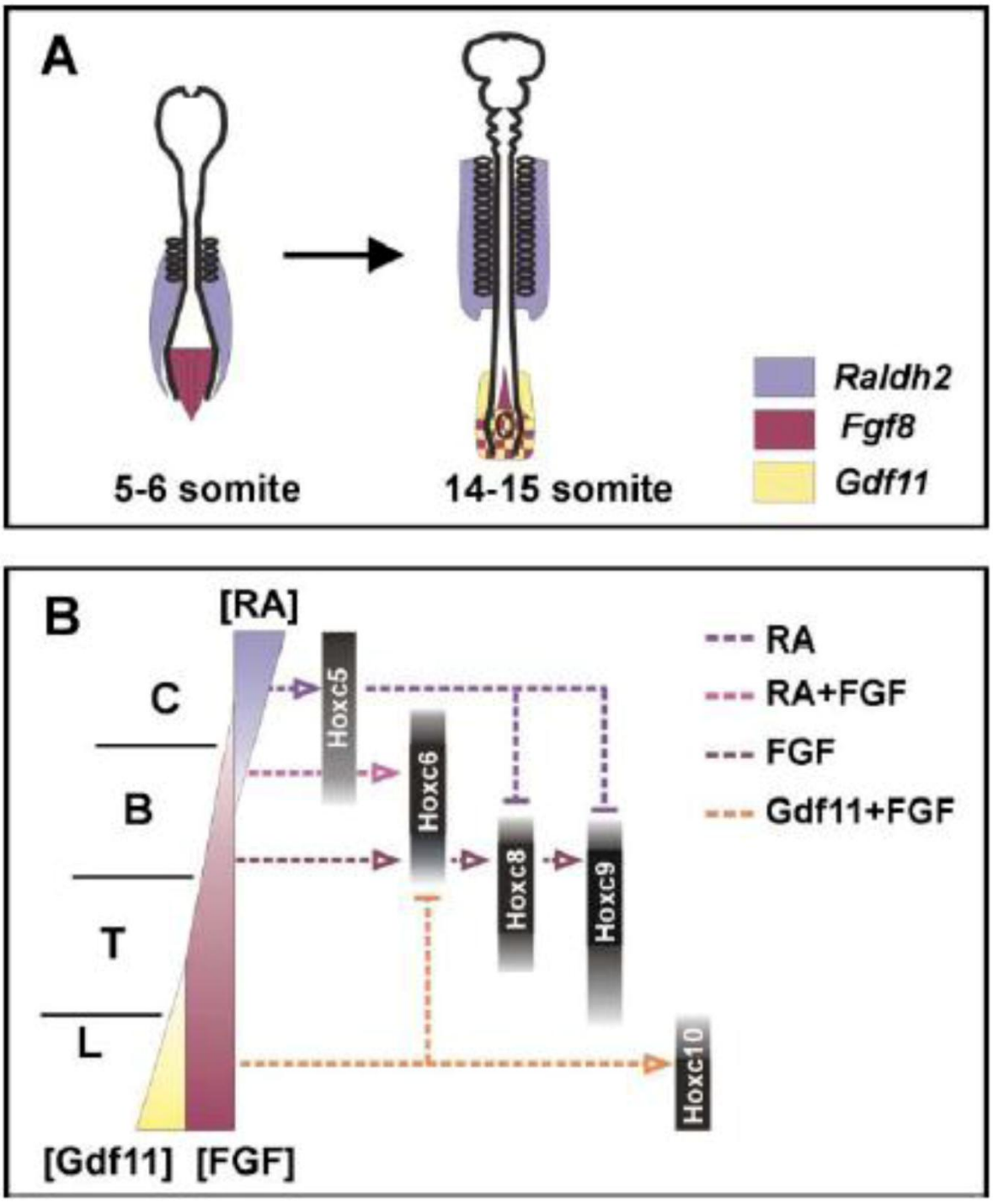
A
5-6 somite
14-15 somite
Raldh2
Fgf8
Gdf11
B
[RA]
C
B
T
L
Hoxc5
Hoxc6
Hoxc8
Hoxc9
Hoxc10
RA
RA+FGF
FGF
Gdf11+FGF
[Gdf11]
[FGF]

Figure 1.8. FGF and RA subdivide caudal neural pattern through *HOXC* genes

(A) Between the 4- and 15-somite stages retinoic acid (RA) produced by rostral somites, and FGF secreted by the node generate (B) the pattern of spinal cord and motor neuron *HOXC* gene expression which controls motor column identity. Node derived GDFs are required for expression of the lumbar determinant *HOXC10*. From (Liu, Laufer et al. 2001).

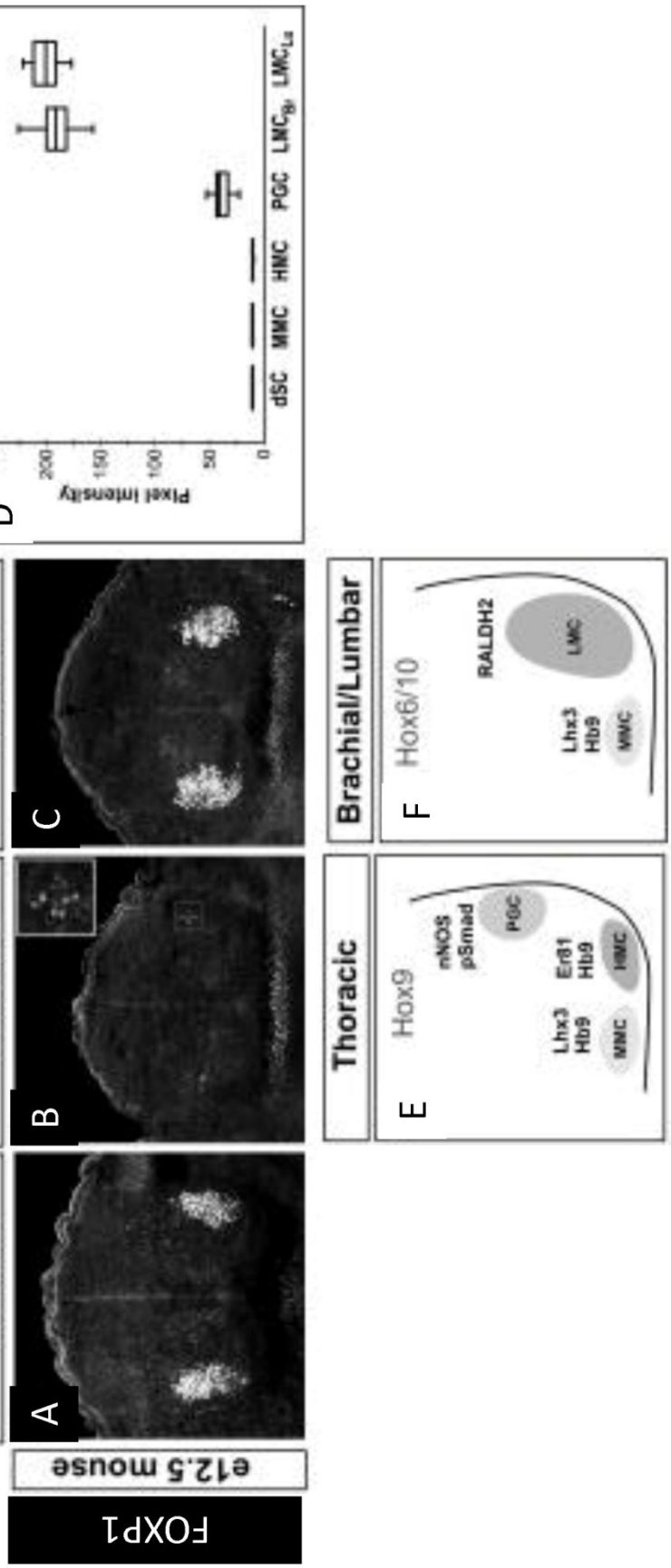
FOXP1
e12.5 mouse
Brachial
Thoracic
Lumbar
A
B
C
D
Pixel Intensity
250
200
150
100
50
0
dSC
MMC
HNC
PGC
LMC
LMC
Thoracic
Brachial/Lumbar
E
Hox9
nNOS
pSmad
PGC
Lhx3
Hb9
Er81
Hb9
MMC
HMC
F
Hox6/10
RALDH2
LMC
Lhx3
Hb9
MMC

Figure 1.9

Figure 1.9. FOXP1 dose-dependently marks LMC and PGC motor neurons

(A-D). FOXP1 is expressed at high levels by (A) brachial and (C) lumbar LMC motor neurons, and low levels by thoracic PGC motor neurons. (D) FOXP1 pixel intensity for dorsal spinal cord (dSC), HMC, MMC, brachial and lumbar LMC, and PGC shows ~5 fold lower level expression in PGC vs LMC motor neurons. (E-F) partial molecular profile of motor columns present at (E) thoracic and (F) brachial or lumbar levels. Adapted from (Dasen, De Camilli et al. 2008).

Figure 1.10

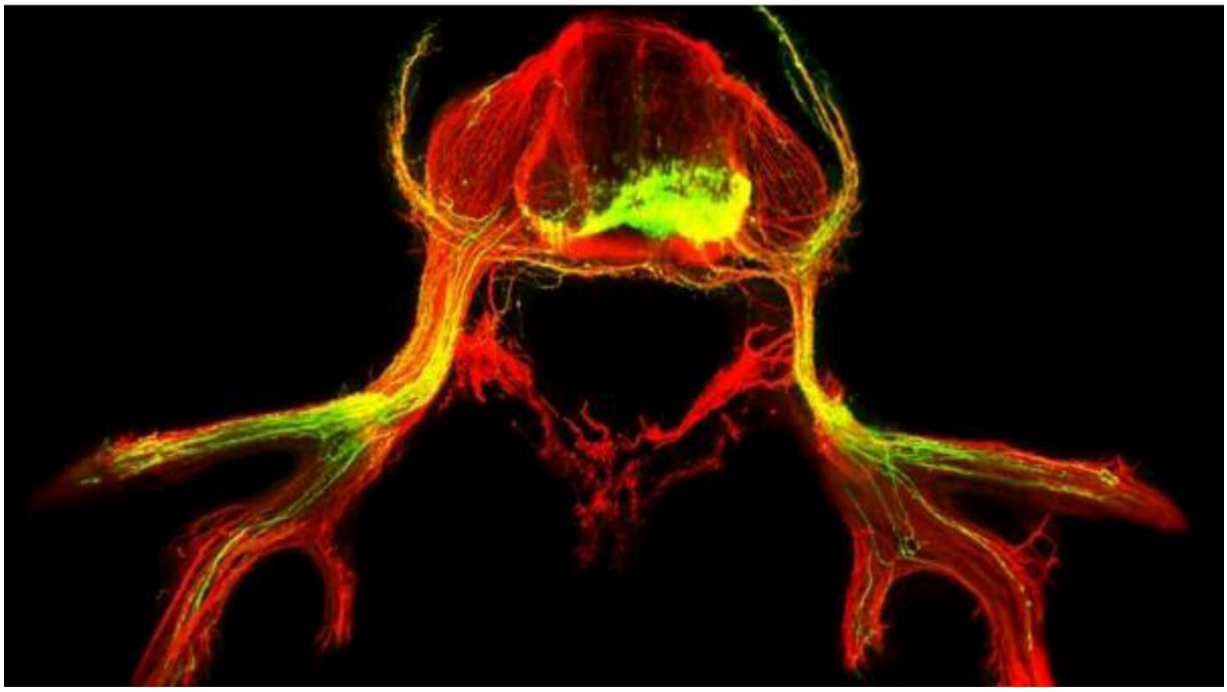

Figure 1.10. Xenotransplanted mouse ES-MNs integrate into chick motor system

Mouse HB9:GFP ES-MNs (green) were xenotransplanted to brachial spinal cord of HH 15/16 chick neural tube and the host was allowed to develop for 2-3 days. Mouse ES-MNs settled in ventral horns and projected along endogenous muscle nerves (neurofilament-red) towards hypaxial, epaxial, and limb muscles, but not towards sympathetic chain ganglia. Mouse ES-MNs formed neuromuscular junctions with host muscles (not shown). From (Wichterle, Lieberam et al. 2002).

Chapter 2. Molecular description of human motor neuron diversity: rostrocaudal regions, columns, divisions, and pools

Introduction

Since the experimental work in this thesis was to be focused on identification of human motor neuron subtypes, we first reviewed the published data on motor neurons in the fetal human spinal cord. Human spinal motor neurons are arranged in rostrocaudal columns in the ventral horns of the spinal cord (Altman and Bayer 2001; Bayer and Altman 2002). These are anatomically divided into a medial group, innervating axial muscles and found throughout the cord, a lateral group, innervating limb muscles, found only at cervical and lumbar levels, and a dorsolateral group found predominantly at thoracic levels which innervates sympathetic ganglia (Altman and Bayer 2001; Bayer and Altman 2002). In vertebrate model systems the molecular determinants and markers of the subtypes of motor neurons have been well defined at the ontological and molecular levels and were reviewed above. Taken together these markers form a combinatorial code that links expression of a set of markers to in vivo subtype identities at the level of motor column and division (Table 2.1). If similar correlations could be established for human motor neurons in vivo, this would provide important tools for developmental studies.

While a wealth of histological information is available regarding the development of the human spinal cord (Altman and Bayer 2001; Bayer and Altman 2002), few molecular tools have been brought to bear on these samples. Of the classical markers of motor neuron identity only HB9 (Ross, Ruiz-Perez et al. 1998; Hagan, Ross et al. 2000) has been investigated at the level of mRNA. However, this study did not address motor neuron columnar or rostrocaudal diversity. Another study showed that subsets of LMC motor neurons, presumably motor pools stained for

ER81 at GW 13, but did not find HMC-specific expression as expected (Clowry, Moss et al. 2005). These findings suggest that human motor neurons do express some of the markers characterized in other vertebrate models but leave the question of human motor neuron rostrocaudal and columnar diversity completely open.

We have discussed the determinant role that *HOX* genes play motor neuron diversification. We have also discussed the expression pattern and subsequent role that HOXA5 and HOXC8 play in diversifying the brachial lumbar LMC into a series of motor pools. Other HOX proteins are also expressed throughout the rostrocaudal length of the spinal cord as well and serve as markers of rostrocaudal identity and appear to have significant functions in determining motor neuron diversity. The expression profile of HOXD9 in mouse, for example, like HOXA5 and HOXC8, spans the border between thoracic and limb-innervating (lumbar) regions (Jung, Lacombe et al. 2010), summarized in Table 2.1. Furthermore, functional experiments show that HOXD9 over-expression in thoracic spinal cord was able to ectopically drive LMC identity. Additionally, because of surfeit of HOX paralogs and possible redundancies, their modular and shifting activities across evolution, and the action of multiple interacting co-factors, it will be important to test for the expression of proteins like HOXA5, HOXC8, and HOXD9, in addition to HOXC genes and other HOX proteins in human cords.

Our overall goal was to determine which markers of motor neuron diversity at the level of rostrocaudal HOX protein expression and markers of motor column, division, and pools are conserved in the human system. We hoped this effort would generate molecular markers and validated reagents that could be used to analyze the subtypes of motor neurons generated in vitro from human stem cells. To this end we first defined the expression pattern of the classical motor neuron markers HB9 and ISL1 in early human spinal cord with respect to the mouse. Next we

sought to determine the presence and expression pattern of the molecular markers of motor column identity (FOXP1, LHX3, pSMAD, ISL2, and LHX1). We then addressed whether the combinatorial expression of LIM homeodomain proteins and pan-MN markers could distinguish the medial and lateral divisions of the LMC. We then searched for the molecular signature of specific motor pools in the brachial LMC, first by examining LIM homeodomain combinations in the context of column markers, and second by addressing expression of motor pool specific markers. Finally, since HOX proteins are markers of rostrocaudal identity in vertebrate motor neurons, and some HOX proteins are determinant for columnar and many pool identities, we tested a series of HOX antibodies to determine the characteristic expression of HOX proteins along the rostrocaudal length of the spinal cord.

Results

Description of human embryonic spinal cord samples

In order to compare the molecular profile of human motor neurons to the model established for chick and mouse, we collaborated with clinicians at CUMC to obtain first-trimester human embryos from voluntary terminations. The developmental stage of samples was estimated by clinicians by patient oral history by subtracting 2 weeks from the date of the last menstrual period (LMP) to yield an estimated gestational week (GW) age of development. In some cases this was supplemented by intrauterine ultrasound to measure crown-rump length. Following informed consent and termination procedure, products of conception were evaluated for the presence of intact spinal tissues within 10 minutes. Samples were photographed, dissected free of vertebrae and attached tissue, and fixed. These were subsequently cryoprotected, sub-

dissected into ~5-mm segments for embedding, measured and photographed again (Fig. 2.1). Ten spinal cord samples from reported GW 6-10+ were collected, processed and embedded (Table 2.2). The remaining sections (of three embryos, see below) and un-sectioned tissue blocks (seven embryos) will remain at the Project ALS lab as an open resource for the investigation of protein expression in early human spinal cords. Three almost fully intact spinal cords were examined in this study in detail: one GW 8 and two GW 7 cords. All samples initially showed a full complement of dorsal root ganglia, however many of these were removed during sub-dissection from the vertebral column. Both GW7 cords showed thin ventral rootlets, while the GW8 sample showed thicker ventral roots.

In GW7 sample 1 (Fig. 2.1A) the spinal cord was intact from the cauda equina, which was embedded in the pelvis, to the level of the clavicle whereas all more rostral neural structures had been lost. The linear length of the cord was 17 mm (all measurements post-fixation). GW 7 sample 2 (Fig. 2.1B) was largely intact from the pelvic cauda equina through most of the hindbrain, however several lesions were present including a large one at the juncture of the spinal cord and hindbrain. The linear length of this cord, including hindbrain, was 25 mm. The GW 8 sample (Fig. 2.1C) was intact from cauda equina to mid-lumbar level where a lesion had sectioned the cord, and then intact again up to the level of the clavicle. The GW 8 spinal cord was thicker and whiter, suggesting more advanced neurogenesis and development of white matter tracts, and showed obvious enlargements in the lumbar and cervical areas. Both GW 7 week cords were dissected into three, and the GW8 cord into four, ~6-mm segments, embedded, and then sectioned through their entire length into 12 µm serial sections deposited serially on 59-112 slides per cord with 6-7 sections per slide. This allowed observation of 18-24 sections per cord per slide representing all rostrocaudal levels. We concluded from this collaboration that

human spinal cord samples are readily available following scheduled terminations, and that the vertebral column often protected this tissue from significant intra-operative physical damage even while most other neural and somatic tissues were lost or destroyed.

Expression of pan-motor neuron and motor column markers

We first sought to determine the rostral and caudal limits of the brachial and lumbar limb-innervating LMCs using both histochemical and morphometric approaches. Using antibodies that recognize the classical pan-motor neuron markers HB9 and ISL1, and another selective for the LMC (FOXP1) we identified groups of ventral horn cells positive for all combinations of these markers (Fig. 2.2A). In order to align the two GW 7 cords we computed the rostrocaudal length of spinal cord in which we found lateral lying populations of $HB9^+$ or $ISL1^+$ cells which were also $FOXP1^+$ (putative LMC MNs) by multiplying the number sections with LMC by the section thickness (12 µm). The mean length of the rostral LMC-containing region was 3.3 mm (range=0.3 mm), and of the caudal LMC-containing region was 4.5 mm (range=0.4 mm), and these were designated as brachial and lumbar fore- and hind-limb innervating levels respectively. The length of spinal cord in between LMC-containing sections was designated as thoracic and measured 5.1 mm (range=0.3 mm) (Fig. 2.1D). In these GW 7 cords the brachial and lumbar LMC were not visible as enlargements under the dissecting scope. In the older, GW8 embryo however, both brachial and lumbar enlargements could be appreciated and corresponded to the rostrocaudal location of LMCs as identified later by immunohistochemistry (Fig. 2.1C). In all subsequent experiments this allowed the coordinates of a given spinal section to be determined relative to these reference points and to total linear position as indexed by serial section number.

In order to determine whether human motor neurons shared the molecular markers of motor column identity as defined in chick and mouse, we analyzed the expression of the LMC and PGC marker FOXP1, and the MMC marker LHX3, among HB9 and ISL1-expressing cells in the ventral horns. All observations were made on at least 4 sections per spinal level (limb/non-limb) and were consistent between both GW 7 and the GW 8 embryo, unless otherwise noted. At all non-limb innervating levels, two continuous columns of motor neurons ($HB9^{+}/ISL1^{+}$) were observed in a ventromedial position (Fig. 2.2A). These cells could be clearly delineated into two columns on the basis of strong LHX3 expression in the more medial group and the absence of LHX3 in the more lateral group. These molecular profiles are consistent with MMC and HMC identity in mouse and chick. ISL1 expression was generally higher in the HMC than MMC, and HB9 expression generally higher in the MMC, although there was substantial variation in expression levels of each marker in both columns (Fig. 2.5). We next sought to confirm the identity of the HMC using antibodies that detect the ETS protein ER81, which serves as a specific maker for the HMC (Dasen, Liu et al. 2003) (Table 2.2). However, none of the ER81 antibodies showed specific reactivity with any cells in human samples. Finally, a small population of $ISL1^{+}$ cells was observed in a dorsolateral position corresponding to the PGC (Bayer and Altman 2002) and these co-expressed low levels of FOXP1, corresponding to the molecular profile of PGC MNs in chick and mouse (Fig. 2.3; see below).

At limb-innervating levels the HMC was absent, while the MMC was retained. Putative LMC MNs ($FOXP1^{+}/LHX3^{-}$) could be subdivided into a dorsomedial group with higher ISL1 and lower HB9 expression levels and a ventrolateral group with lower ISL1 and higher HB9 expression. These molecular profiles match those of the medial and lateral divisions, respectively, of the mouse LMC. Notably the imbalance of ISL1 and HB9 expression for cells of

the medial or lateral divisions was more pronounced in the lumbar LMC (Fig 2.2 and see Fig 2.5 for quantitation).

In summary the motor columns of the human spinal cord show characteristic molecular profiles that correspond to those defined in mouse (summarized in cartoon, Fig. 2.2B, C). At limb levels the MMC is marked by LHX3 and expresses HB9 and ISL1. At non-limb levels LMCs are absent and the MMC is joined by the HMC and the PGC. For ease of reference data from subsequent figures has been incorporated into the summary diagrams of Fig. 2.2.

PGC MNs express pSMAD and low levels of FOXP1

In order to substantiate the identity of the putative PGC cells, we tested antibodies for other PGC markers (Fig 2.3). First, cords were stained with an antibody specific for the phosphorylated forms of SMAD proteins 1,5 and 8, which act as a selective marker for chick and mouse PGC MNs (Dasen, De Camilli et al. 2008). This antibody selectively distinguishes the dorsolateral population of putative PGC neurons found at thoracic levels, and was not co-expressed by MNs in other columns or spinal levels (Fig. 2.3B). In addition we tested an antibody to neuronal nitric oxide synthase (nNOS) which is a specific marker for PGC cells in mouse. However this antibody showed no reactivity on human samples.

Next, since PGC cells are known to express low levels of FOXP1 (Dasen, De Camilli et al. 2008) we analyzed the expression level of FOXP1 in LMC vs. PGC cells. All images were captured at the same non-saturating exposure time in order to directly compare staining intensity. In order to compare FOXP1 expression levels between these columns in one representative GW 7 embryo, we first restricted intensity analysis to the region including only the $ISL1^+$ LMC_m, at 2 representative levels of the brachial, and 3 of the lumbar cord, and the region defined by $ISL1^+$

$pSMAD^+$ cells at 4 representative levels of the thoracic cord. We used Metamorph to measure the FOXP1 staining intensity for $ISL1^+$ nuclei in each of these regions showed that FOXP1 intensity was significantly different between PGC, brachial and lumbar LMC_M (Shapiro-Wilk normality test failed, $p<0.05$, ANOVA, Kruskal Wallis ANOVA on RANKS , H=206.650, DF=2, P=<0.001). PGC cells (n=235) showed significantly lower FOXP1 intensity compared brachial LMC_M (n=269, Dunn's pairwise comparison, Diff. of ranks= 201.709, Q=10.801, $p<0.05$), or lumbar LMC_m (n=220, Dunn's pairwise comparison, Diff. of ranks=267.972, Q=13.658, $p<0.05$). Interestingly the brachial LMC_M expresses significantly higher levels of FOXP1 than the lumbar LMC_m (Dunn's pairwise comparison, Diff. of ranks=66.264, Q=3.485, $p<0.05$) (Fig. 2.3C). Finally, when grouped together LMC cells showed significantly higher FOXP1 staining than PGC motor neurons (Shapiro-Wilk normality test failed, $p<0.05$, Mann Whitney Rank Sum Test, T=48440.000 n(small)= 235 n(big)= 489 (P = <0.001)). We concluded from these data that this population represented human PGC MNs since there is a match for the anatomical location and appropriate combination of markers: $ISL1^+$ $HB9^-$ $LHX3^-$ $pSMAD^+$ and a quantitatively low level FOXP1 expression.

We therefore established that all mouse motor columns (MMC, HMC, LMC, and PGC) are present in human at the same relative rostrocaudal levels as in mouse, and are unambiguously delineated by a combination of pan-MN (HB9 and ISL1) and motor column (FOXP1, LHX3, pSMAD) markers. We next revisited the marked difference we had observed in HB9 and ISL1 expression between lateral and medial LMC cells, in order to determine if the medial and lateral divisions of the LMC were molecularly distinct in the human. To do this we used two approaches: first we examined the combinatorial profile of LIM homeodomain proteins which

can distinguish these divisions in mouse and chick, and second we performed a quantitative analysis on the expression levels of HB9 and ISL1 in these divisions and in control cells.

Molecular characterization of the medial and lateral divisions of the human LMC

To determine how closely human LMC medial and lateral divisions resemble mouse LMC divisions we profiled the expression of ISL2 and LHX1 in human LMC in the context of HB9/ISL1/FOXP1 expression (Fig. 2.4). We found that LHX1 was excluded from the MMC and the LMC_M but was expressed at high levels in the $HB9^+FOXP1^+$ LMC_L. LHX1 was also expressed at moderate levels by many non-motor neurons in the spinal cord. ISL1, as shown previously, is expressed in both MMC and LMC_M, but only weakly in the LMC_L. ISL2 however was expressed in LMC_L as well as the MMC and the LMC_M. This pattern of expression mirrors that in mouse and chick and is summarized in Figure 2.4. We concluded that human LMC divisions express combinations of LIM homeodomain proteins and column markers conforming to the established vertebrate models of divisional identity.

HB9 and ISL1 expression levels vary from cell to cell but are correlated with motor column identity

Because we had observed an obvious qualitative difference in average expression level of HB9 and ISL1 between different LMC divisions, and variation in relative expression levels in HMC and MMC columns, we sought to describe this phenotype quantitatively. We hoped these analyses would clarify the utility and limits of these widely used "pan"-MN marker proteins by reference to in vivo expression patterns, and that this should have direct implications for the use of these markers in vitro.

We therefore quantified the qualitative expression pattern of HB9 and ISL1 that was consistent across all 3 embryos, by examining one representative GW 7 embryo in greater detail. We first drew boundaries closely around the cell groups as defined by the foregoing combinatorial analysis of motor column and division markers (regions shown in thin lines labeled by column Fig. 2.5A) and then used Metamorph Multiwavelength Cell Scoring module to identify all $DAPI^+$ nuclei, as well as nuclei which expressed high levels of either HB9 or ISL1 (Fig. 2.5A). This analysis quantitated the number of motor neurons (as defined by high level expression of either HB9 or ISL1 and within the boundaries of motor columns defined here and consistent with previous histological studies (Altman and Bayer 2001; Bayer and Altman 2002) in 2-3 representative sections per spinal level (as defined by limb or non-limb innervating (Fig. 2.5B, D, E) as well as the expression level of each protein in each cell, as judged by immunofluorescence intensity, which allowed us to describe the mean intensity of expression for each marker in each column (Fig. 2.5C).

To define the specificity of these markers in human spinal cord we first analyzed their expression in non-motor neuron populations. A population of dorsal cells, presumptive interneurons, found at all spinal levels (DOR IN, Fig. 2.5A, C), showed ISL1 levels comparable to those in the MMC or HMC but expressed only background levels of HB9. Dorsal root ganglia (DRG) sensory neurons expressed variable but very high levels of ISL1 but showed only background signal for HB9. Finally we observed at all spinal levels that a population of columnar epithelial cells composing the ventral floorplate (FP) (Bayer and Altman 2002) showed only background level ISL1 staining, but stained for HB9 at levels comparable to those in the HMC. We concluded from these analyses that coexpression of HB9 and ISL1 is restricted to MNs, but that HB9 and ISl1 are expressed singly in several other—albeit minor—neuronal populations in the human

spinal cord at GW 7. With the exception of sub-floorplate expression, these expression patterns match those described in mouse literature.

To determine if relative expression patterns of HB9 and ISL1 differed according to columnar identity, we next examined for each motor column the percentage of cells that scored positively for either marker, as well as the mean expression level per column (Fig. 2.5B-F). All motor columns contained cells that expressed each combination ($HB9^+ISL^-$, $HB9^+ISL^+$, or $HB9^-ISL1^+$). The extremes were constituted by the LMC_L, where very few $ISL1^+$ cells did not co-express HB9 and the brachial and lumbar LMC_M, where many MNs expressed ISL1 but not HB9 (Fig. 2.5B,D). At both brachial and lumbar levels, the mean intensity of HB9 expression was greater in the LMC_L than the LMC_M, and the mean intensity for ISL1 was the reverse. The range of expression levels however was relatively large compared to the mean difference, especially at brachial levels (Fig. 2C). We concluded from these analyses that ISL1>HB9 is characteristic for LMC_M MNs and HB9>ISL1 is characteristic for LMC_L MNs in vivo. However due to the presence of many co-expressing cells in both divisions, the presence of robust numbers of individual divisional MNs which violate this rule, and a wide range of expression values, HB9/ISL1 co-expression levels are insufficient to predict the divisional identity of individual cells. Importantly, the presence of many LMC MNs expressing low or background levels of one motor neuron marker indicates that either marker in isolation is insufficient to capture the breadth of motor neuron diversity. Analyses based on HB9 alone will miss much of the LMC_M and those based on ISL1 alone will exclude much of the LMC_L, for example.

Finally, to determine if there was a distinctive pattern of HB9 and ISL1 expression in MMC vs. HMC motor columns we performed the same analyses on these populations. We observed that a majority of MNs in both columns expressed high levels of HB9 and ISL1 together, although

some cells expressed only one or the other marker at high levels. (Fig. 2.5B, D). We concluded that a more balanced level of HB9 and ISL1 co-expression is characteristic of both the MMC and HMC, when compared to the LMCs. Again HB9 and ISL1 expression status alone could not alone distinguish columnar identity.

In order to facilitate comparisons to ES-derived motor neurons in vivo, we also grouped these data together in several other ways. Since ES-derived motor neurons may well include motor neurons from multiple columns at the same level, we asked what the overall distribution of HB9 and ISL1 cells was if we grouped all columns together at a given level, grouped all levels of a given column together, or analyzed all motor neurons at once (Fig. 2.5E, F). These could then be compared to similar profiles for ES- and iPS-derived motor neurons discussed in Chapter 3 and Chapter 5.

In summary these analyses show that the ratio of HB9/ISL1 expression varied continuously from 1:0 to 0:1. This means that not all $HB9^+$ MNs express ISL1 and vice versa. Strong ISL1 expression was characteristic of LMC_M, strong HB9 expression characteristic of LMC_L, and strong co-expression is characteristic for MMC and HMC. However, wide variation between individual cells means that these markers alone are not sufficient to ascertain columnar or divisional identity and, outside the embryo, will need to be used in combination with other columnar or subtype markers.

Molecular characterization of putative motor pools

Having established that human motor neurons express the canonical markers delineating vertebrate motor neuron subtype identities at the level of motor neuron, column and division, we next asked if individual motor pools could be identified in the human spinal cord by matching

marker expression patterns to those of the mouse and chick. We first looked at the rostral brachial LMC, a region in which in mouse and chicken motor pools have been mapped by retrograde tracing studies and correlated with a combinatorial code of LIM homeodomain protein expression (Ensini, Tsuchida et al. 1998) (Fig. 2.6). First we established that MMC and LMC MNs at this level express HOXA5, thereby anchoring this region in the rostral brachial LMC (see below for HOX expression patterns).

We first observed a more lateral-lying ventral population not found at other levels of the human cord which was positive for HB9, ISL1, ISL2, and LHX3 but not LHX1. This distinctive molecular profile and lateral location are consistent with those of the chick *rhomboideus* (RB) motor pool, and we therefore concluded that this population is likely the human RB motor pool.

We also observed a population of LMC_L cells dorsal to the putative RB pool that expressed the combination of markers found in the chick *deltoid* (DL) motor pool: high ISL2, but not ISL1, and high LHX1, suggesting that this may be the human DL motor pool. In the chick another LMC_L pool is distinguishable at this level by its low level expression of ISL1 and LIM1, the *extensor metacarpi radialis/ulnaris* (EMR). We did not see a clear indication of this molecular profile in our samples, however since it is based on a subtle reduction in staining intensity of ISL2 and LHX1 other markers may be required. We did however observe another, more unusual combination of markers situated in a motor pool-size group of motor neurons situated within the boundary of the $ISL1^+$ LMC_M. These cells expressed high levels of ISL1, ISL2, and FOXP1, but not LHX1, consistent with LMC_M identity. However, these cells also expressed high HB9, which as we have seen is not completely inconsistent with LMC_M identity, especially at brachial levels. However such a concentrated group of strongly $HB9^+$ cells in the LMC_M was not seen at any other spinal level. More intriguingly still this group expressed LHX3. This expression

pattern was found in all three embryos examined. There is no reported cognate for this expression pattern in mouse or chick, raising the possibility that this novel molecular profile corresponds to one or more motor pools that may be human- or primate-specific. Although formal confirmation by retrograde labeling is clearly not feasible, this analysis therefore potentially confirms the presence in human of one motor pool, the RB, already identified in chick, provides evidence consistent with another, the DL, but fails to find clear evidence for the EMR motor pool. Interestingly we provide evidence for a novel species-specific motor pool with atypical molecular characteristics, which may be linked to evolutionarily new motor functions.

Another approach to identifying human motor pools was to use motor pool-specific genes found in chick and mouse. We tested several antisera used to identify chick and mouse motor pools including: ER81, SCIP, PEA3, and RUNX1. Of these only one, the anti-PEA3 antiserum, showed reactivity on human samples. A subset of motor neurons within the rostral end first 200 µm of the HOXC8 domain (see below) of the rostral brachial LMC_L (Fig. 2.7) stained for PEA3. Just caudal to these LMC_L cells, a $PEA3^+$, LMC_M population was also observed (not shown) to express PEA3 (Fig. 2.7). The rostrocaudal position and divisional identity of the more rostral LMC_L and more caudal LMC_M putative motor pools match the anterior *latissimus dorsi* (ALD) motor pool in the chick/ the LD motor pool in the mouse and the *cutaneous maximus* (CM) motor pool in the mouse respectively (Dasen, Tice et al. 2005; Vrieseling and Arber 2006). In the lumbar region we lack the precise rostrocaudal information conveyed by the HOXA5/HOXC8 boundary in the brachial LMC. However since the $PEA3^+$ cells were in the LMC_L we can infer that they belong to the human cognate of one of three identified $PEA3^+$ chick LCM_L motor pools: the *iliotrochanterici* (at chick LS1-3), the anterior *iliotibialis* (LS3-5), or the *caudilioflexorius* (LS6-7) (Lin, Saito et al. 1998) or one of two identified mouse lumbar LMC_L

motor pools: *rectus femoris* (L1-L2) or the *gluteus* (L2-L5) (Arber, Ladle et al. 2000). Because of the caudal location of this human PEA3^{+} LMC$_{L}$ putative pool (3.1 mm caudal to the rostral aspect of the 5.5 mm LMC region) it is more likely to correspond to the mouse *gluteus*, the chicken *iliotibialis* or *caudilioflexorius* muscles, the latter of which does not have a clear cognate in human. More definitive assignment of any of these pools would require retrograde tracing studies or additional markers.

We have therefore shown evidence by combinatorial expression of LIM-HD proteins as well as the specific ETS protein marker PEA3, that the some of the molecular categories down to the level of motor pool are conserved in human. In the process we identified a novel species-divergent motor pool potentially associated with evolved hand/wrist motor functions.

HOX gene expression defines rostrocaudal motor neuron domains

We next asked if HOX proteins were expressed in the stereotyped collinear array which controls chick and mouse motor neuron diversification (Dasen, Liu et al. 2003; Dasen, Tice et al. 2005). We first screened a panel of 15 commercial and academic anti-HOX antibodies for their reactivity with human antigens present in our spinal cord samples and found that antibodies against HOXA5, HOXC8 and HOXD9 (Table 7.1) exhibited strong and stereotypical staining of human spinal cords (Fig 2.8). HOXA5 expression began in the cervical region and penetrated to the mid-brachial LMC; HOXC8 expression began in the mid brachial LMC and continued about halfway into the thoracic region; and HOXD9 expression was initiated caudal to thoracic HOXC8 expression, and continued caudally through the rostral third of the lumbar LMC. This expression pattern is identical to that described in chick (Liu, Laufer et al. 2001; Dasen, Liu et al. 2003) for HOXA5 and HOXC8 and mouse (Jung, Lacombe et al. 2010) for HOXD9. We

concluded that human motor neurons conserved the same pattern of HOX protein expression for these family members.

We also noted several other aspects of HOX expression which conform to expectations based on other vertebrate models. First, the rostral onset of each HOX gene began in the dorsal, non-motor neuron spinal cord, and gradually, within a few 100 µm caudal, penetrated ventrally to encompass all MNs at a given level. Second, we noted that the HOX genes analyzed were almost never co-expressed by individual cells in any section examined. This was especially important for the case of HOXA5 and HOXC8 whose expression zones in mouse and chick, and now in human, are immediately adjacent, and indeed slightly overlapped such that for several hundred µm some LMC groups at the same level are $HOXA5^{+}$ and some are $HOXC8^{+}$. Even at these levels however, individual cells coexpressing these HOX genes were exceptionally rare. We concluded from these data that these HOX genes were expressed mutually exclusively in human samples.

Finally, as this thesis was being written, several HOX antibodies were reported to define the rostrocaudal subtype of human ES-derived motor neurons in vitro (Patani, Hollins et al. 2011) We therefore tested these in order to gain a more complete picture of HOX expression in the spinal cord. One HOXC10 monoclonal antibody used in the Patani study showed no staining on any cells at any level in the spinal cord in our hands, and is reported to detect only chick and not mouse protein (Susan Morton and Jeremy Dasen personal communication, and DSHB data sheet). Additionally, one HOXC9 antibody (#25 Table 7.1) stained every spinal cell at every location and dilution tested where any cells were stained. These data suggest that the in vitro results of the Patani study should be interpreted with caution.

Discussion

Together these studies provide a global map of human spinal motor neuron diversity that correlates the combinatorial expression of two classical motor neuron markers (HB9 and ISL1) with selective markers of motor column identity (FOXP1, LHX3), three accessory markers of columnar identity (ISL2, LHX1, pSMAD), and three HOX proteins (HOXA5, HOXC8, HOXD9) (Table 2.3). We conclude that the molecular diversity of motor neurons at this early developmental stage is exquisitely conserved from mouse and chick to human, with the exception of one putative human-specific motor pool. Importantly, these findings validate a set of antibodies that will be instrumental for characterization of in vitro derived human MNs.

Human motor neurons show conserved molecular organization with vertebrate models

We have provided evidence that human MNs in vivo are grouped into the same molecular categories as chick and mouse MNs. This includes selective markers for the MMC (LHX3), LMC (FOXP1), and PGC ($FOXP1^{LOW}$, pSMAD). The medial and lateral divisions of the LMC ($LMC_{M/L}$) also exhibited canonical distinguishing markers: the LMC_L showed dominant ISL1 expression, and the LMC_L showed dominant HB9 expression, and also the combination of ISL2 and LHX1. Human motor neurons also exhibited the conserved molecular signature of several individual motor pools. At the brachial level, motor neuron groups matching the profile of the *rhomboideus* and deltoid motor pools were identified. At both the brachial and lumbar levels restricted groups of $LMC_{M/L}$ motor neurons expressed PEA3, which matched the profile of anterior *latissimus dorsi* and *cutaneous maximus* pools at the brachial, and a likely match for the *caudilioflexorius* or *gluteus* motor pool at the lumbar levels. Finally the pattern of expression of

those HOX proteins which we were able to detect, precisely matches that in chick and mouse, where HOXA5 is expressed in cervical to mid-brachial, HOXC8 in mid brachial to mid thoracic, and HOXC9 in mid thoracic to mid-lumbar.

Implications for developmental mechanisms

The remarkable conservation of markers for these key aspects of motor neuron organization suggests that the a very durable and flexible logic for motor neuron diversification and integration with an evolving body plan was achieved early in vertebrate evolution and has not significantly changed since. Importantly this conservation implies that many of the mechanisms orchestrate the developmental elaboration of this diversity may also be strongly conserved. In support of this idea are the known functional roles for several of the marker proteins used. FOXP1 in particular plays a decisive role in directing the organization of limb-innervating motor neurons, as shown by the atavistic phenotype of knockouts (Dasen, De Camilli et al. 2008). HOXA5 and HOXC8 also play strong functional roles, although downstream of both HOXC6 and FOXP1, in controlling the elaboration of brachial motor pool identities (Dasen, Tice et al. 2005). And HOXD9 can drive lumbar LMC identity when over-expressed in thoracic MNs, although at endogenous levels this function is kept at bay by the LMC-repressive activity of HOXC9 (Jung, Lacombe et al. 2010).

None of the HOX proteins we were able to study exclusively determine motor column identity in chick or mouse. This is clear since in model systems and now in human each of their expression domains crosses a boundary between limb and non-limb levels and they are expressed in both LMC cells at limb-levels and MMC and HMC cells at limb and non limb levels. It will thus be critical in future studies to develop reagents—antibodies or in situ probes—to assess the

expression of the HOXC genes (6, 9, 10) which have been shown to determine columnar identity. This would add stronger evidence that the mechanisms underpinning motor column diversification are conserved in human, and also provide the most direct upstream markers by which to test ES-cell directed differentiation approaches aimed at controlling rostrocaudal and column specific identities. Nevertheless the strong conservation of markers like FOXP1 and LHX3, known to be functional determinants of subtype identity, provides strong evidence supporting the idea that consensus vertebrate model mechanisms could be used as the basis for ES-cell directed differentiation approaches seeking to control the subtype output of motor neurons.

Identification of a novel molecular profile and putative motor pool

The one significant difference identified between human and other vertebrates was the identification of putative motor pool with novel characteristics in the rostral brachial LMC_M. This pool expressed markers appropriate to the LMC_M but also expressed LMC_L markers, but more interestingly it expressed both LMC_L and MMC marker proteins (FOXP1 and LHX3). There is no known cognate for this molecular profile in chicken or mouse. In the most definitive study of human developmental spinal motor anatomy, which included inferences based on comparison to retrograde tracing studies in rat, cat, and other species, these authors speculate that motor neurons in this rostral cervical and most dorsal position were likely to innervate hand or wrist muscles (Altman and Bayer 2001). It is tempting to speculate that this novel motor pool innervates a muscle with novel function in humans or primates, and one obvious choice would be thumb or hand muscles. On the other hand, the presence of axial and limb muscle determinants may point toward an intermediate function, once involved perhaps in species or primate specific shoulder movements. It will be interesting to examine primate spinal cords to determine if this

derived characteristic is shared with primates or if it is human specific. In a general sense, we should expect more specific differences with mouse to emerge in future studies, particularly at the level of individual motor pools.

Interpretation of negative results

Most of the antibodies and antisera tested for HOX genes, column, and pool markers showed no reactivity on human samples. We did not interpret these results as positive evidence that these factors were not expressed in human for the following reasons. First, none of the reagents that failed to show staining in our hands have been validated by others to work on human tissues, with the exception of ER81, and we did not confirm the precise antiserum used in that study (Clowry, Moss et al. 2005). Second, in most cases these reagents were designed based on chick or mouse protein sequences. Protein sequence analysis where proteins or peptides were used for immunization, showed variable and incomplete similarity between human and mouse or chick sequences. Even where differences concern only several amino acids, this could easily explain the inability to detect human proteins. This points to the need to develop validated human-reactive reagents for many marker proteins of interest, most importantly the HOXC proteins 6, 9, and 10 since these are determinant for columnar identities, and other motor pool markers. In parallel, in situ hybridization approaches should be attempted to directly assess expression of human genes for which there are no antibodies.

Interpretation of in vitro motor neuron phenotypes

The map of marker expression detailed here can now be used as a strong basis from which to interpret in vitro molecular phenotypes (Table 2.2). Based on this map, specific molecular profiles found in human ES-derived motor neurons can be assigned to one or several in vivo

identities. Since some marker combinations were not observed in vivo—HOXA5^{+}HOXC8^{+} cells for example—this map can also indicate where potential in vitro expression patterns do not match any in vivo cell type. This map can therefore be used to evaluate the effect of differentiation strategies on subtype or rostrocaudal identities and to confirm that these subtypes match coherent molecular identities.

Acknowledgements

Anne Davis, MD and her fellows were generous and enthusiastic collaborators who providing access to embryos which made this entire enterprise possible; Tom Jessell generously provided numerous monoclonal antibodies and antisera and Susan Morton provided antisera and monoclonal antibodies for HOX genes, pan-MN antibodies, and pool markers, and generously provided years of consultation on mouse expression patterns and antigen sequences, designed peptides and oversaw immunization projects and screened antisera to generate new immunoreagents (Table 7.1, PALS antibodies): rabbit and gpHB9, and gpFOXP1; Jeremy Dasen generously providing several HOX antisera he generated; and Mackenzie W. Amoroso helped coordinate and drive the collaboration to procure embryos, assisted in initial specimen collection and helped image and organize data.

Table 2.1

		ISL1	HB9	FOXP1	LHX3	HOXC6	HOXC9	HOXC10	HOXA5	HOXC8	HOXD9	ISL2	LHX1	pSMAD	nNOS	RALDH2	ER81
	MMC											?					?
	HMC											?					?
cervical non-limb	PGC											?		?	?		?
	MMC																
	LMCm																
rostral brachial	LMCl																
	MMC																
	LMCm																
caudal brachial	LMCl																
	MMC																
	HMC																
rostral thoracic	PGC											?					
	MMC																
	HMC																
caudal thoracic	PGC											?					
	MMC																
	LMCm																
rostral lumbar	LMCl																
	MMC																
	LMCm																
caudal lumbar	LMCl																
	MMC																
	HMC																?
sacral	PGC?											?					

Table 2.1. Summary of motor neuron rostrocaudal, columnar, and divisional subtype marker expression in chick and mouse

Compiled from chick and mouse primary references reviewed in Chapter 1, rostral/caudal subdivisions of brachial, thoracic, and lumbar are defined by expression of HOXA5, HOXC8 (Liu et al. 2003) in chick and HOXD9 (Jung, Lacombe et al.) in mouse. Black boxes indicate high level expression, grey boxes indicate low level or no expression, and white boxes indicate no expression. Question marks indicate lack of strong supporting evidence for marker expression in indicated motor columns at indicated levels.

Figure 2.1

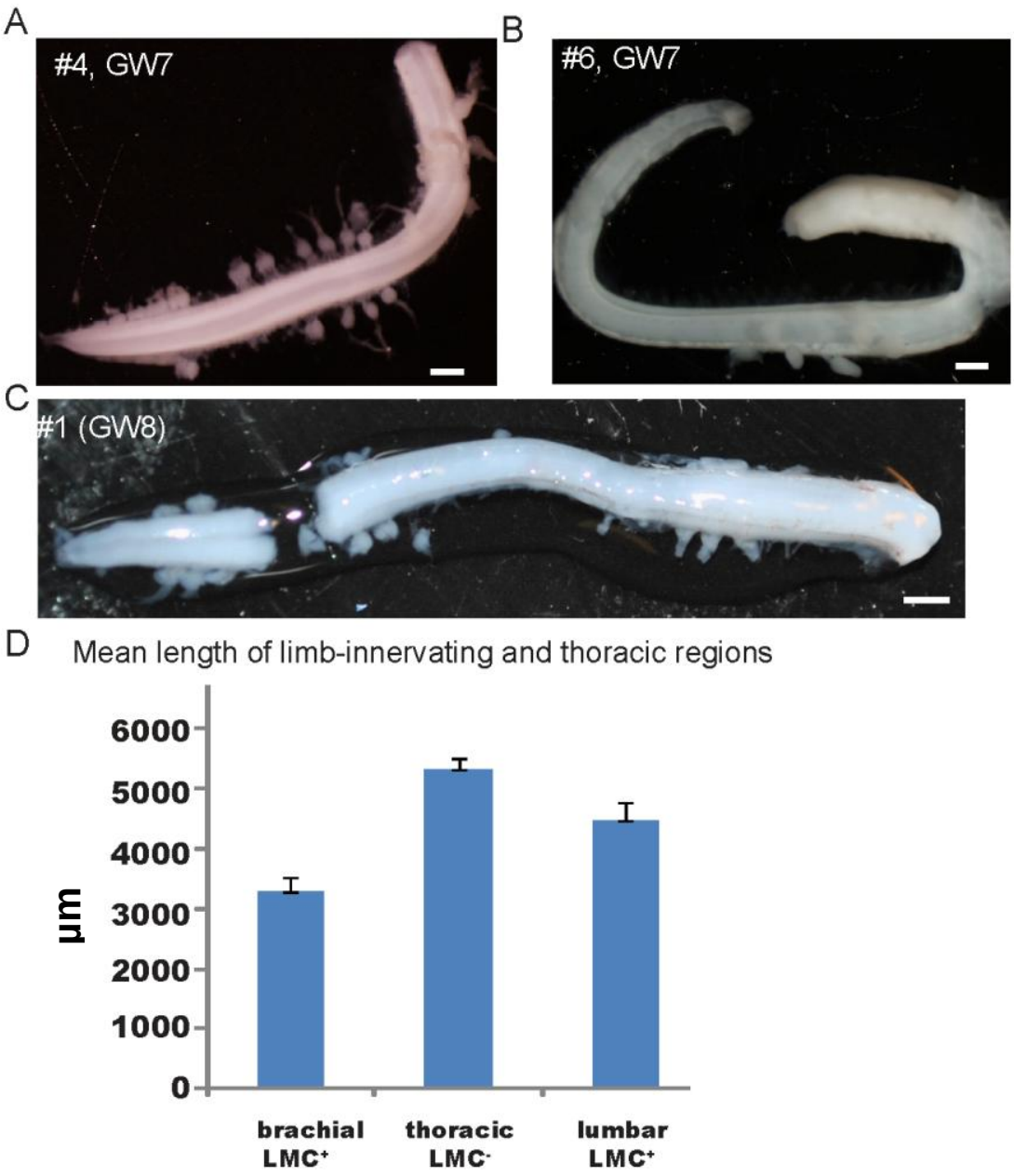
A
#4, GW7
B
#6, GW7
C
#1 (GW8)
D
Mean length of limb-innervating and thoracic regions
µm
6000
5000
4000
3000
2000
1000
0
brachial
LMC+
thoracic
LMC-
lumbar
LMC+

Figure 2.1. Documentation of human spinal cord samples and linear length of limb-innervating and thoracic regions

(A-C) embryonic human spinal cords from gestational week (GW) 7 and 8 used in this study. Scale bars 1 mm (D) Mean post-fixation linear length (μm) + range of regions in GW 7 samples (n=2) staining for $FOXP1^{+}$ LMC in the brachial and lumbar regions, where thoracic was defined as the region between LMC^{+} segments.

Table 2.2

#	Reported age (GW)	Adjusted age	Spinal regions intact	Photog embed	Section	Stain analyze	Notes on staging/fixation	Collection date (2010)	Collection day #
1	8	8	cervical to sacral	Y	Y	Y	overfixed (almost 3 hours RT); HEIR unmasks epitopes effectively	10/23	1
2	6	6	thoracic fragment	Y				11/20	3
3	6-10	6	hindbrain to sacral	Y			likely ~6wks development	11/20	5
4	7	7-	hindbrain to sacral	Y	Y	Y	smallest most intact embryo, looked more like mouse e10.5-11.5, 35-40 days by CS	11/20	13
5	6.7	7-	part of spinal cord	Y				11/20	14
6	7	7	cervical to sacral	Y	Y	Y		11/20	6
7	7	7+	thoracic to sacral	Y			larger embryo than other 7wk sampels	11/20	8
8	10	10-	hindbrain to sacral	Y			smaller than other "10wk" sampels, lumbosacral lesion, some folding of cord	11/20	15
9	"10"	10	cervical to sacral	Y			reported age ambiguous, very large, developed/old embryo	11/20	12
10	10	10+	hindbrain and brachial	Y			largest, oldest/most developed looking sample collected	11/20	11

Table 2.2. Human embryonic spinal cord resource

Catalogue of human embryos collected for spinal cord staining. Reported age in gestational weeks (GW) was determined by clinicians by patient reported last menstrual period and was sometimes informed by pre-operative crown-rump length ultrasound measurement. Reported age was adjusted if embryonic development appeared to be out of phase with reported age. All 10 specimens were fixed, cryoprotected, dissected free from any attached tissue, photographed, subsectioned and embedded in OCT for cryosectioning. Spinal cords in grey were fully sectioned (serially) and deposited on slides; unsectioned embryos were embedded in OCT and stored for future sectioned, along with unstained slides, at -80°C at the Project A.L.S. Laboratory. Slides and tissue blocks are available as an open resource for studies of early human spinal cord development. Sample #1 was overfixed but Tris-EDTA heat induced epitope retrieval unmasked antigen and revealed staining which matched other analyzed samples as described in Chapter 7: Experimental Procedures.

Figure 2.2

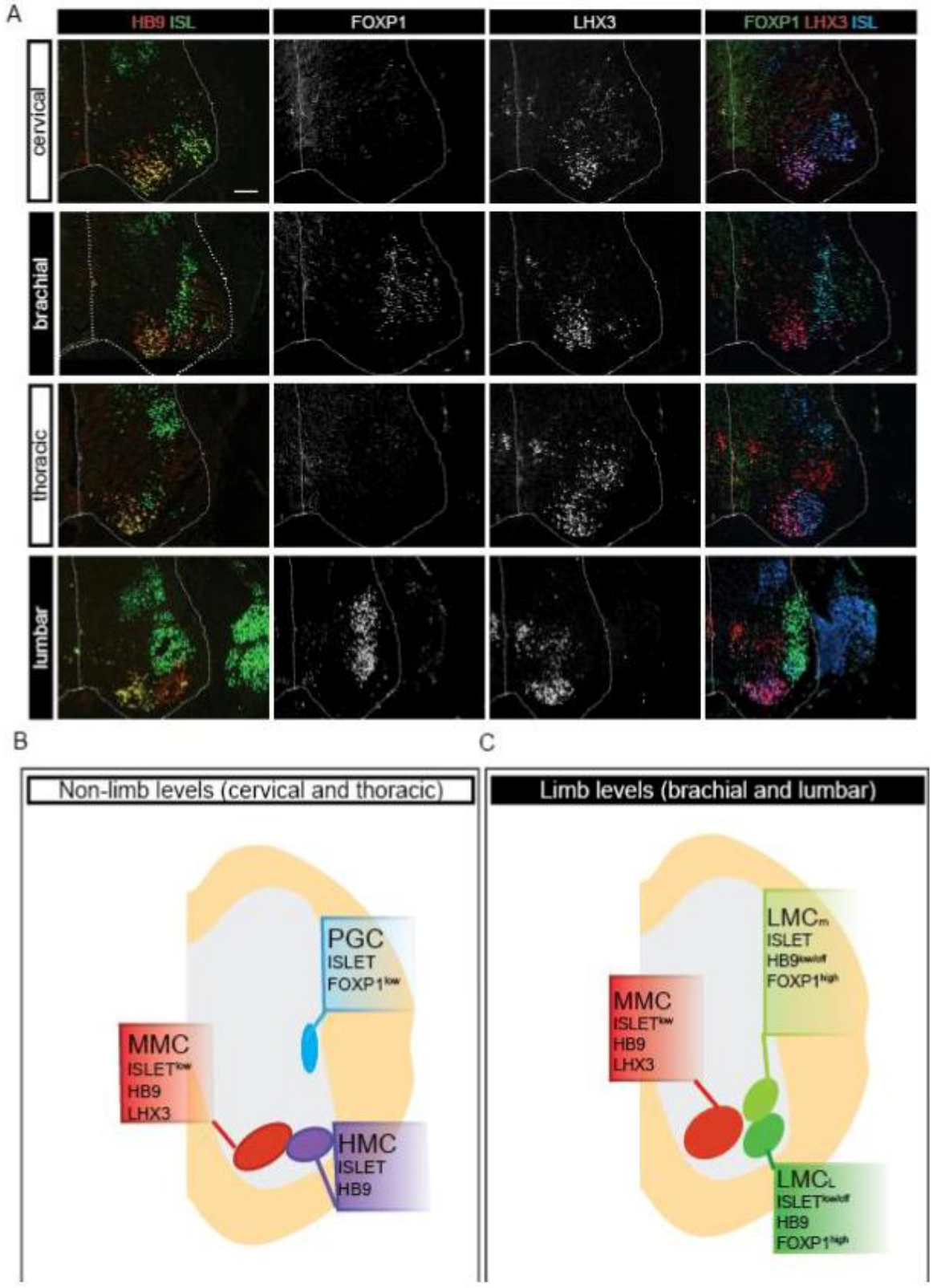
A
HB9 ISL
FOXP1
LHX3
FOXP1 LHX3 ISL
cervical
brachial
thoracic
lumbar
B
Non-limb levels (cervical and thoracic)
PGC
ISLET
FOXP1kw
MMC
ISLETkw
HB9
LHX3
HMC
ISLET
HB9
C
Limb levels (brachial and lumbar)
LMCm
ISLET
HB9kw/off
FOXP1high
MMC
ISLETkw
HB9
LHX3
LMCL
ISLETkw/off
HB9
FOXP1high

Figure 2.2. Human spinal motor neurons share column markers and organization with mouse

(A) Human spinal cords were found to contain populations of cells matching the molecular and anatomic characteristics of motor columns defined in chick and mouse. MMC cells were located ventro-dorsally and expressed LHX3, HB9, and ISL1. At non limb levels HMC motor neurons expressed neither LHX3 nor FOXP1. At limb levels LMC cells expressed high level FOXP1. The LMC was subdivided into a lateral predominantly $HB9^{high}$ and $ISL^{low/off}$ LMC_L and a medial $HB9^{low/off}$ $ISL1^{high}$ LMC_M. Sections representative of all non-limb (cervical and thoracic) and limb (brachial and lumbar) spinal levels are shown. n=3 embryos. Scale bar 100 µm. (B-C) Summary diagrams of non-limb level and limb level human motor columns expression profiles.

Figure 2.3

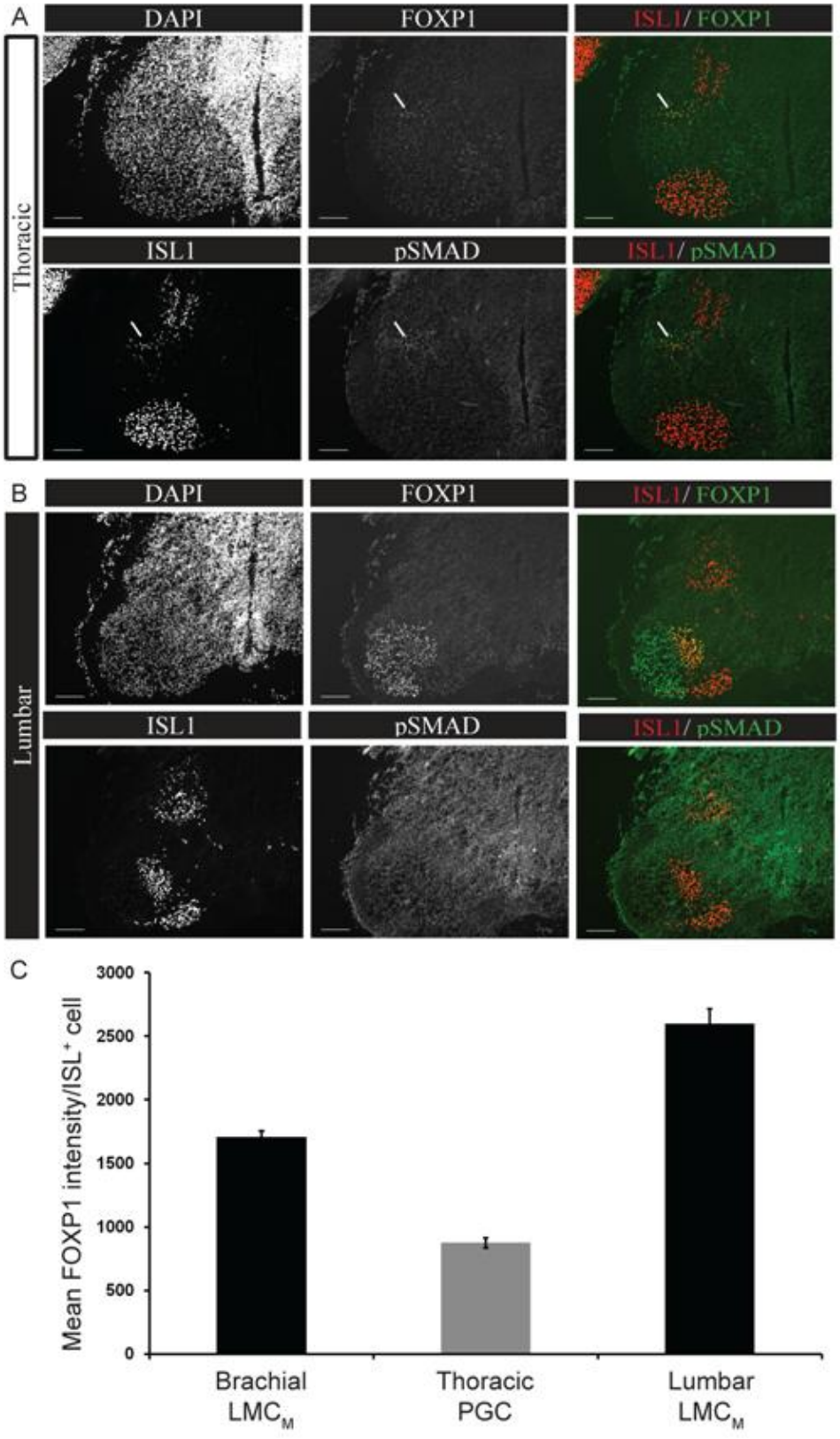
A
DAPI
FOXP1
ISL1/ FOXP1
Thoracic
ISL1
pSMAD
ISL1/ pSMAD
B
DAPI
FOXP1
ISL1/ FOXP1
Lumbar
ISL1
pSMAD
ISL1/ pSMAD
C
Mean FOXP1 intensity/ISL+ cell
3000
2500
2000
1500
1000
500
0
Brachial LMCM
Thoracic PGC
Lumbar LMCM

Figure 2.3. pSMAD and low level FOXP1 identify human PGC at thoracic levels

Human PGC motor neurons were located dorso-laterally at thoracic (A) but not at (B) limb levels. PGC motor neurons were identified by staining for ISL1, FOXP1 and pSMAD. Scale bar 100 um. >3 sections/spinal level (thoracic vs. limb) were examined from n=2 GW 7 embryos. (C) PGC motor neuron FOXP1 expression is quantitatively lower than in either brachial or lumbar LMC; mean+/-SEM FOXP1 intensity/$ISL1^{+}$ cell in the brachial LMC_M, (n=270 cells from 2 representative hemi-sections), thoracic PGC (n= 236 cells from 4 representative hemisections), and lumbar LMC_M (n=221 cells from 2 representative hemi-sections) from one GW 7 embryo.

Figure 2.4

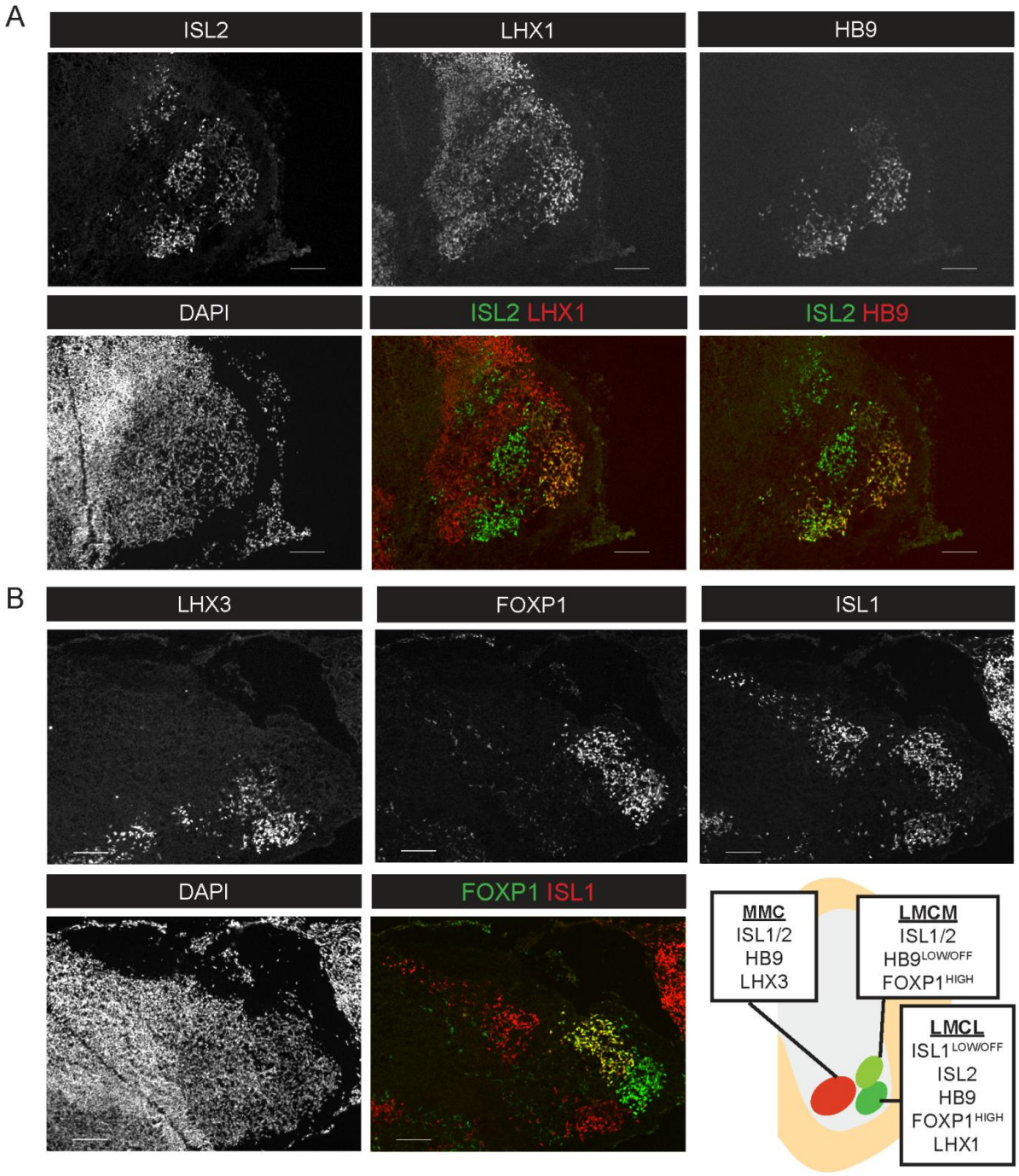
A
ISL2
LHX1
HB9
DAPI
ISL2 LHX1
ISL2 HB9
B
LHX3
FOXP1
ISL1
DAPI
FOXP1 ISL1
MMC
ISL1/2
HB9
LHX3
LMCM
ISL1/2
HB9LOW/OFF
FOXP1HIGH
LMCL
ISL1LOW/OFF
ISL2
HB9
FOXP1HIGH
LHX1

Figure 2.4. Human MNs express markers of LMC divisional identities

Human LMC_M was identified by FOXP1 and high ISL1 expression with low or no HB9, as previously shown, and also expressed ISL2 and was negative for LHX1. LMC_L as described expresses FOXP1, high HB9 and low or no ISL1, however it also marker by LHX1 and ISL2. LHX1 therefore serves as a marker that distinguishes lateral vs. medial LMC divisions. Serial sections from lumbar cord shown are representative of >4 limb level sections analyzed for n=3 embryos. Scale bars 100 um. Bottom right: summary of human LMC divisional gene expression profile.

Figure 2.5

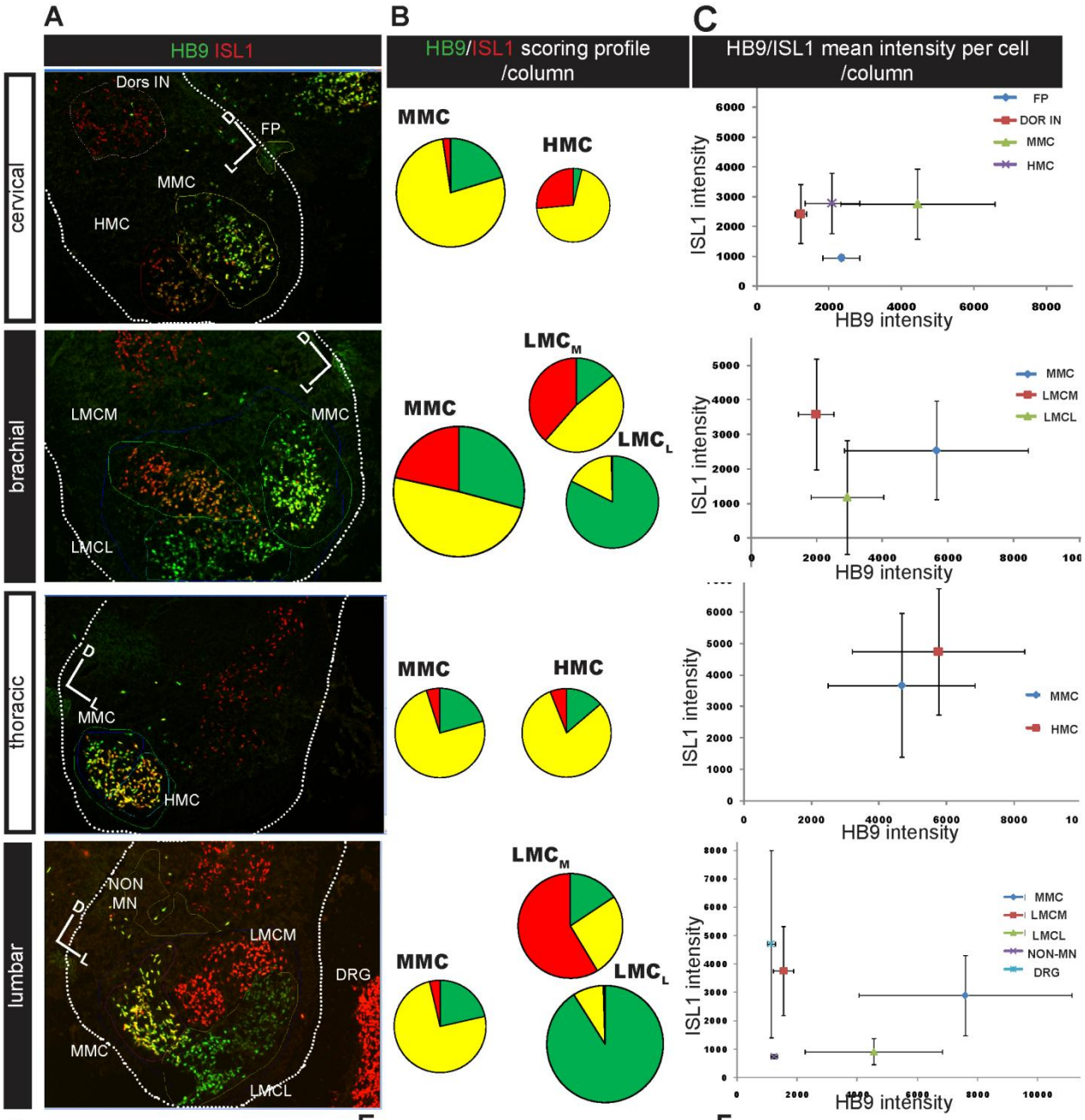

D

	Total MNs	% HB9	%HB9 ISL1	%ISL1
cervical MMC	128	20	77	2
cervical HMC	53	4	70	26
brachial MMC	202	29	49	22
brachial LMC_M	101	14	47	39
brachial LMC_L	93	83	17	0
thoracic MMC	75	21	74	5
thoracic HMC	94	14	80	6
lumbar MMC	96	21	75	4
lumbar LMC_M	115	16	26	59
lumbar LMC_L	144	91	9	0

Figure 2.5. HB9 and ISL1 expression levels in motor neuron columns, division, and control cells.

(A) motor neuron columns and divisions, as defined in serial sections by column and division markers described above, and control cell populations, were isolated as regions of interest (shown in dotted lines on sections: HMC, MMC, LMC_M, LMC_L, all motor columns at a given level considered together, $HB9^{low}$ sub floorplate cells (SUB FP), $ISL1^+$ dorsal interneurons (DOR IN), non-motor neurons (NON MN), and $ISL1^+$ dorsal root ganglia(DRG)) on representative sections from non-limb and limb levels and quantified for HB9 and ISL1 expression. (B) Cells in LMC, HMC, MMC anatomical regions were scored for high level of either HB9 or ISL1 were defined as motor neurons and pie charts show the percent of all motor neurons/column expressing either HB9 or ISL1: $HB9^+$ (green), $HB9^+ISL1^+$ (yellow), or $ISL1^+$ (red); n=1 cervical and mean of n=3 brachial or n=2 thoracic and n=2 lumbar sections, from one representative GW 7 embryo (#4). Individual motor neurons were not counted in more than one category. The area of the pie chart is proportional to the total number to motor neurons in the column, shown in (D). (C) Average intensity/cell in each motor column at each level and in control cell populations (mean+/-SD, n=1 section analyzed/level). For all regions with $HB9^+$ or $ISL1^+$ cells, intensity was analyzed among motor neurons only, except for the NON-MN region where intensity is for all cells in the region. (D-E) Total number of motor neurons per motor column (mean of n=2 sections/level except cervical n=1, and brachial n=3), and percentage of those cells in cell scoring categories as graphed in (B). (E) Total number of motor neurons in each cell scoring category, in all motor columns at each level (mean+/-SD, n=2 sections/level except cervical n=1, and brachial n=3). (F) Total number of motor neurons in each column and

for all motor neurons, mean+/-SD, All MMC n=8 sections, All HMC n=3 sections, All LMC_M n=5 sections, All LCM_L n=5 sections, and All MN section n=8 sections. 900 µm field width.

Figure 2.6

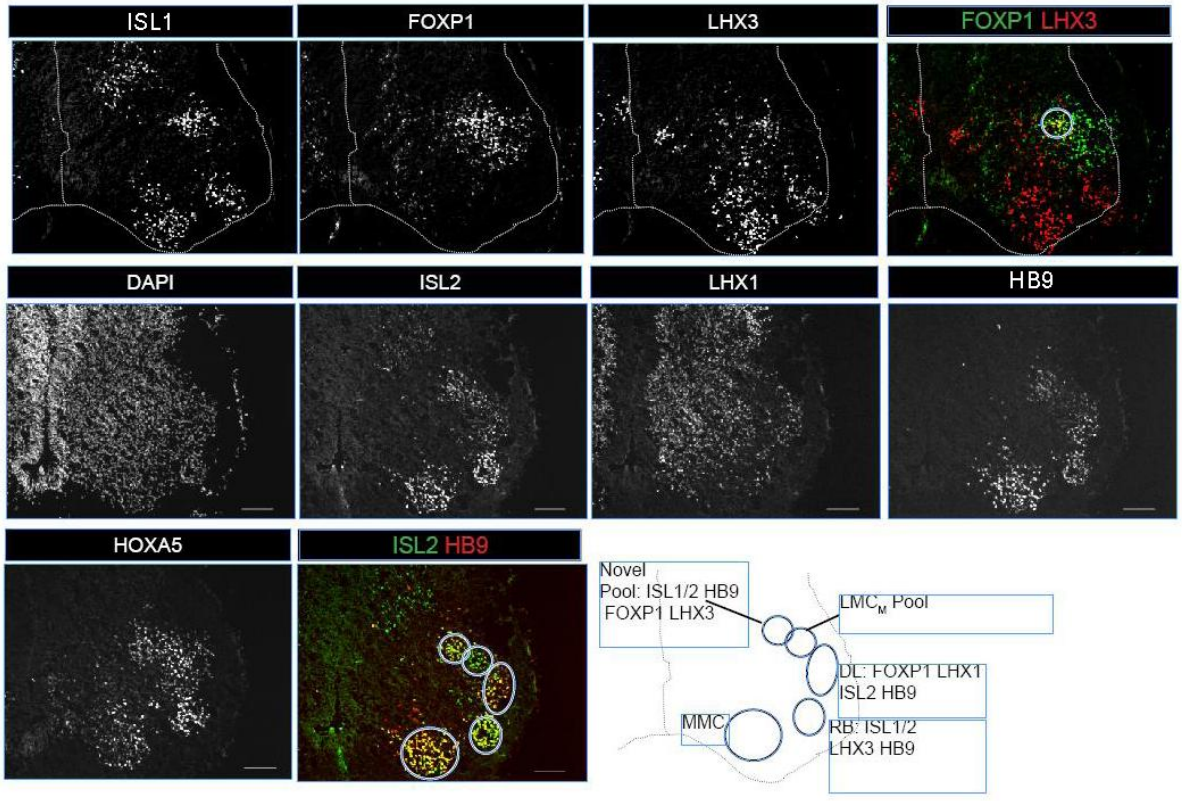

Figure 2.6. Some rostral brachial LMC pools identified by combinatorial expression of LIM-HD and column marker proteins. (A) Staining of serial sections of rostral ($HOXA5^+$) brachial spinal cord reveals LMC cells ($FOXP1^+$) can be subdivided into putative motor pools matching those in chick by expression profile of LHX1, LHX3, HB9, ISL1 and ISL2. Diagram at left indicates putative pool expression profiles matched for the MMC, rhomboideus (RB), deltoid (DL), and novel human specific putative motor pool which expresses LHX3 and FOXP1 (circled top right). Scale bar 100 um. Sections are representative of n=3 embryos examined.

Figure 2.7

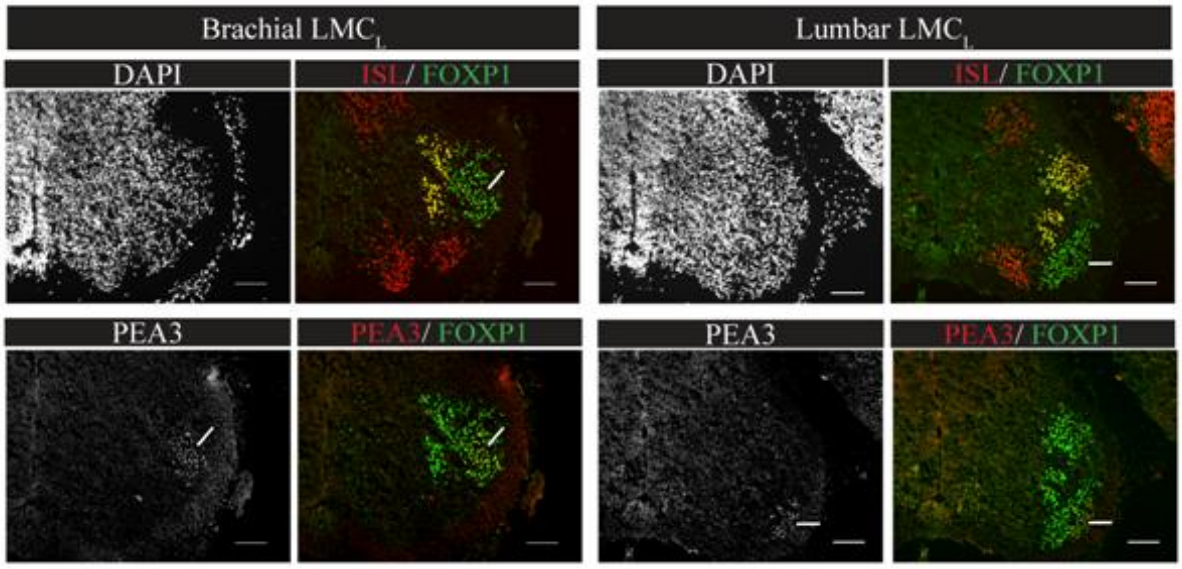

Figure 2.7. PEA3 marks brachial and lumbar LMC pools

At the HOXA5 level of the brachial spinal cord, and in the lumbar spinal cord, PEA3 selectively marks pool-size groups of LMC_L motor neurons. Representative sections of n=2 GW 7 and n=1 GW 8 embryos. Scale bar 100 um. Diagonal (left) and horizontal (right) bars indicate position of pools in each channel.

Figure 2.8

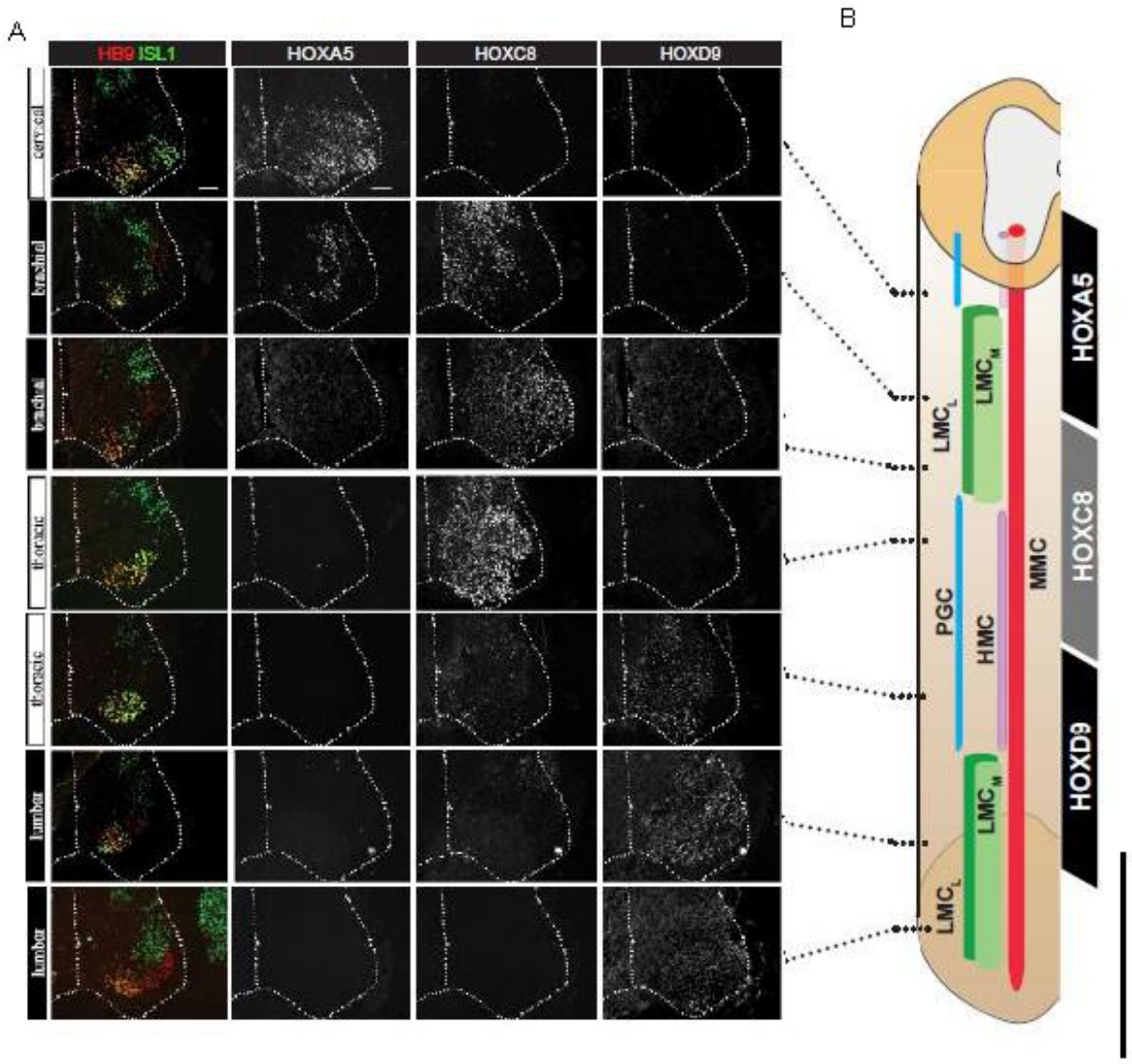
A
HB9 ISL1
HOXA5
HOXC8
HOXD9
cervical
brachial
brachial
thoracic
thoracic
lumbar
lumbar
B
LMC$_L$
LMC$_M$
PGC
HMC
MMC
LMC$_M$
LMC$_L$
HOXA5
HOXC8
HOXD9

Figure 2.8. Human motor neurons in vivo express HOX proteins in rostrocaudal collinear sequence

(A) HOXA5 was expression at cervical levels (rostral to the LMC) and persisted through the rostral half of the brachial LMC. The most rostral HOXC8 expression was detected in dorsal spinal cord cells rostral to the caudal limit of HOXA5 expression. Within 200 um HOXC8 displaced HOXA5 expression in motor neurons; in this intermediate brachial region some groups of motor neuron, likely LMC pools, expressed HOXA5 and some expressed HOXC8, but <20 individual cells, of thousands of motor neurons examined, expressed both HOX proteins. HOXC8 expression persisted caudally into thoracic levels until just short of halfway between brachial and lumbar LMC levels. HOXD9 expression was initiated in dorsal cells just after the caudal limit of HOXC8 expression and there was no overlap of expression at the same levels of the cord. HOXD9 expression in the cord and in motor neurons persisted caudally through the first half of the lumbar LMC. We did observe some low level HOXD9 staining at brachial levels, mostly in dorsal non-motor neurons. n=3 embryos showed the same expression pattern; representative sections from GW 7 embryo #4 shown. Length of spinal cord positive for: HOXA5= 3.7 +/-0.8 mm; HOXC8= 5.7 +/-0.7 mm; and HOXD9= 4.1 +/-0.3mm, (mean +/-SD of two GW 7 embryos). Scale bar 100 um. (B) Diagram summarizes HOX expression patterns with respect to motor neuron column marker staining pattern. Diagram drawn to scale along rostrocaudal axis (scale bar 5 mm) but mediolateral dimension is dilated for clarity of labeling; dotted lines indicate rostrocaudal level of representative sections.

Table 2.3

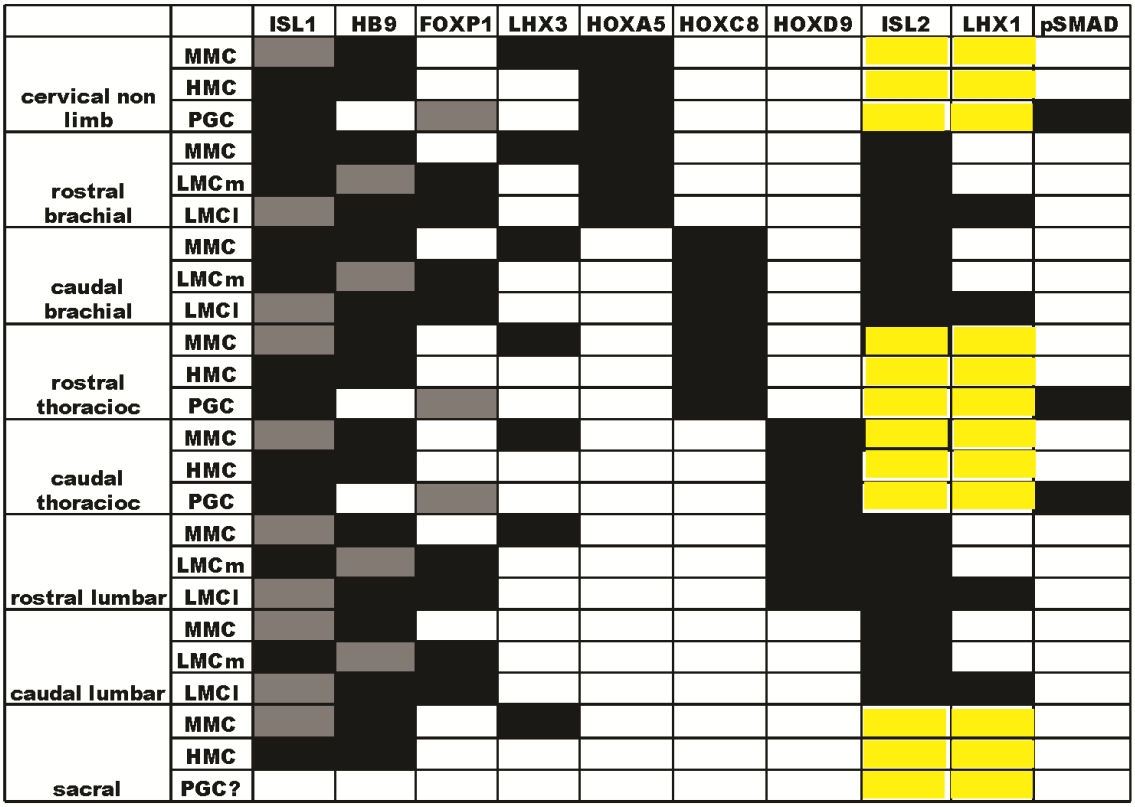

Table 2.3. Summary of motor neuron rostrocaudal, columnar and divisional subtype marker expression in human

The same expression profile was detected for HB9 and ISL1, and all column and divisional markers and HOX genes tested as found in mouse spinal cord, with the exception of the $LHX3^{+}FOXP1^{+}$ pool detected at $HOXA5^{+}$ levels of the brachial LMC. Black boxes, high level expression; grey boxes, low or low to no expression; white boxes, no expression; yellow boxes, not examined at indicated levels. Presence of sacral PGC not examined. n=3 embryos.

Chapter 3. Motor neuron differentiation from human embryonic stem cells: optimization, characterization of subtype diversity, and analysis of maturation

Introduction

The larger goal of these studies was to establish the conditions for modeling ALS using human ES cell-derived motor neuron subtypes. Our first goal in this chapter was therefore to systematically describe the subtypes of motor neurons differentiated from human stem cells. To do this we needed first to define a robust and reproducible method of differentiation which would be amenable to quantitative analysis. Next, in order to establish confidence in the relevance of ES-MN biology in vitro to motor neurons in vivo, we needed to demonstrate that key in vivo phenotypes would be manifested in vitro. Finally, since several hypotheses about the mechanisms of motor neuron degeneration in ALS hinge on mature characteristics of affected MNs, we needed to demonstrate maturation of ES-MNs in vitro and in vivo.

MNs have now been differentiated from human stem cells by many different groups. There is great variety among the protocols, methods of analysis, and efficiencies of differentiation in these reports. Our first goal was therefore to develop a reproducible and highly robust protocol for motor neuron differentiation which was compatible with quantitative analysis of the entire population of differentiated MNs. While some markers of motor neuron positional and columnar subtype identity have been tested in ES-MN cultures, in no case have these been systematically and representatively assessed in MNs as defined by HB9 and ISL1 expression. We therefore sought to determine the diversity of rostrocaudal and columnar motor neuron subtypes, using

markers and expression criteria defined in vivo in Chapter 2. This description would also provide a necessary starting point for designing strategies to control subtype identities in future studies (Chapter 5)

A general challenge for the utility of any stem cell-derived cell type is to demonstrate its in vivo bona fides. To address this we picked several characteristic features of motor neurons in vivo and asked if in vitro generated cells would meet these expectations. Expression of multiple subtype markers is in itself the first bar, but also allows us to ask if ES-MNs meet more subtle in vivo expression patterns, for example, mutual exclusion of specific HOX gene pairs and mutual exclusion of motor column markers. MN-selective electrophysiological features and the interpretation of in vivo axon guidance cues have also not been addressed in previous studies, but would support the functional equivalence of ES-MNs to their in vivo counterparts and thus argue for their utility in modeling motor neuron biology and disease.

Finally, several proposed mechanisms of MN-selective degeneration in ALS concern features typical of more mature motor neurons. The large total size of MNs, specifically axo-dendritic outgrowth, may place unusual demands on energy metabolism and mitochondrial function, and axonal transport, suggesting that ES-MNs should achieve significant total outgrowth in order to better study disease relevant pathologies. Finally, motor neuron degeneration may be linked to glutamate excitotoxicity. In order to adequately address this hypothesis it is necessary to demonstrate electrophysiological activity in vitro, which several groups have done. However an unmet need, with respect to designing in vitro assays of disease mechanisms is to systematically establish the timecourse and characteristics of ES-MN electrophysiological maturation in vitro.

Results

Defining a Standard Protocol for efficient and robust motor neuron differentiation

Our first goal was to define a simple and robust protocol for motor neuron differentiation from human ES cells, which was devoid of complicated manipulations and in which differentiated cells could be analyzed as a homogenized mixture. In order to support homogeneity, enhance neural induction, and reduce manual intervention we made several adaptations to a previously published embryoid body (EB)-based differentiation protocol from the Zhang lab (Li, Du et al. 2005). The Zhang protocol requires positive and negative manual selection to isolate rosette neuroepithelia and remove non-neural colonies during a period of transient attachment. We maintained EBs in suspension during the entire protocol to avoid potential bias of these manual interventions. In order to increase the efficiency of neural induction without manual intervention, we made two further modifications to the Zhang protocol. To both limit the size of EBs and ensure that their sizes were as regular and reproducible as possible we used a Rho kinase inhibitor (Y-27632) to maintain survival of individual ES cells at the pluripotent state (day 0 of differentiation) as they gradually nucleated EBs (Watanabe, Ueno et al. 2007). This produced an initial population of very small (5-20 cell) EBs which was extremely regular in its size distribution (Fig. 3.1B, day 4). Recombinant Noggin was also used during this time period to suppress induction of non-neural fates by BMP signaling (Munoz-Sanjuan and Brivanlou 2002; Watanabe, Ueno et al. 2007; Elkabetz, Panagiotakos et al. 2008). Beginning at day 10 RA and recombinant mouse SHH were used to impose the caudal (spinal) and ventral identity required for generation of motor neurons. EBs continued to expand and by day 24 almost all

EBs were composed of tightly packed neural rosettes (Fig. 3.1B) (Elkabetz, Panagiotakos et al. 2008). We also observed that nearly all cells in all EBs expressed the neuronal marker NCAM and/or the neuronal progenitor marker Nestin (Fig. 3.1C). We concluded that this protocol generated a highly regular population of EBs which was composed dominantly of neural derivates as judged by neural rosette morphology and neural lineage marker expression.

We next asked whether motor neuron progenitor (pMN) marker OLIG2 and the post-mitotic motor neuron marker genes ISL1 and HB9 were expressed by qPCR (Fig. 3.1D). As has been previously reported (Bock, Kiskinis et al. 2011) we detected low level expression of both ISL1 and HB9 in undifferentiated ES cells, but this was extinguished by day 6. HB9 expression increased at a relatively linear rate from day 6 to day 31, when it reached maximum measured levels. ISL1 expression increased at a lower linear rate from day 6-17 and then rapidly reached maximum levels between day 17 and day 31. OLIG2 expression, which we expected to precede the post-mitotic motor neuron markers, was only slightly increased at day 17 (<1%), but reached maximum expression by day 31. We then confirmed these gene expression data at the protein level by immunostaining cryosectioned EBs (Fig. 3.1F). These data showed that OLIG2 could be readily detected at day 17, but was considerably more prevalent at day 26 and 30. ISL1 protein was not detected until day 17, and then at low abundance, but was increased by 26 and at maximum by day 31. HB9 protein on the other hand was not detected until day 26, and increased substantially by day 31. To confirm the emergence of post-mitotic motor neurons we then tested this protocol on the motor neuron reported line HBG1, which expresses eGFP under control of the mouse HB9 promoter (Di Giorgio, Boulting et al. 2008). GFP was first expressed in scattered cells at day 24 (not shown) but was robustly expressed by day 31 (Fig. 3.1D). Interestingly day 25 in vitro precisely matches the estimated day 31 in vivo onset of motor

neurogenesis (Chapter 1, Part II) if 5 days are added to the developmental time of ES cell differentiation (since they are derived from day 5 blastocysts). We concluded from these data that under this protocol the motor neuron lineage was efficiently induced, that post-mitotic motor neurons were generated starting around day 25, and that they reached abundant levels by day 31.

We next sought to assess the efficiency of motor neuron generation by measuring the most selective motor neuron marker available, HB9 as well as the other selective marker, ISL1. We observed large differences within and between individual EBs in terms of the density of HB9 and ISL1 cells. In order to assess the entire population, EBs were therefore dissociated to single cells using trypsin and mechanical trituration, seeded on poly-amino acid and laminin coated substrate, and fixed two days later. Cells were then stained and scored for high level expression of HB9, ISL, and TuJ1 using the Multiwavelength Cell Scoring module in Metamorph (Fig. 3.2A). We observed a smooth continuum of expression levels for HB9 (and all other pan-MN and MN-subtype nuclear markers, not shown) (Fig. 3.2C). A threshold of staining intensity was set for each immunostain and then empirically optimized to score the maximum number of intensely stained HB9 cells as positive, and keep to an absolute minimum the number of cells with very low or no appreciable HB9 staining scored positive (Fig. 3.2D). The accuracy of utomated cell-scoring was therefore manually checked for each experiment and condition. The result of this conservative approach to automated cell scoring was that cells scored positive for HB9 were restricted to those with high intensity staining, although this population included a large range of staining intensity, as illustrated for individual scored cells (Fig. 3.2D) and by the standard deviation of the mean of HB9 or ISL1 cells (Fig. 3.2E). In addition some "HB9^{-}" cells showed some real level of HB9 staining (Fig. 3.2 D, #1). We therefore undercounted the total number of HB9 cells, however this approach maximized confidence that quantitated cells were

strongly positive. This same approach to cell scoring was also taken with ISL1 and all subsequently discussed subtype markers.

We then asked what fraction of cells co-expressed high levels of HB9 and ISL1. $HB9^{+}ISL1^{-}$ ($HB9^{high}$-only) cells constituted 6.1 ±1.0% of total cells, $HB9^{+}ISL1^{+}$ 6.5 ±1.0%, and $ISL1^{+}$ $HB9^{-}$ only 4.4 ±1.1% (mean ±SEM, n=5 independent experiments, Fig. 3.2B). The ratio of HB9 to ISL1 expression was continuous from 1:0 to 0:1 (Fig 3.2A) and included a broad range of values for both HB9 and ISL1 (Fig. 3.2E). This percentage breakdown, and deviation closely matched the profile to what we had observed for MNs in vivo (Chapter 2, Fig. 2.5). The percentage of in vitro cells expressing high level HB9, ISL1, or both was most similar to that produced when multiple in vivo columns were grouped together for analysis, and interestingly was closest of all to profile of the group of all MNs present at brachial levels (Fig. 2.5E). We concluded from these data that the distribution of pan-MN makers in ES-MNs reproduced the spectrum of values we defined for MNs in vivo.

Because HB9 and ISL1 are expressed in the pancreas and in other non-neural cells we co-stained cultures with HB9, ISL1, and the pan-neuronal marker βIII-Tubulin (TuJ1) to determine if all $HB9^{+}$ and $ISL1^{+}$ cells were indeed neurons (Fig. 3.2F). We found that 65 ±9% of all cells expressed TuJ1, and that 96 ±1% of $HB9^{+}$ cells were positive for TuJ1 (mean ±SEM, n=5 independent experiments). We concluded that this protocol efficiently generated a highly neuronal population, and when the large number of $Nestin^{+}$ presumable neural precursors (Fig. 3.1D) are included, a dominantly neural population. Importantly the TuJ1/HB9 stain demonstrated that $HB9^{+}$ cells were indeed neurons and not non-neural lineage $HB9^{+}$ cells. Importantly the dissociated-reseeded endpoint is almost unique among motor neuron protocols and allowed for a novel accurate quantitation of motor neuron efficiency in the entire

differentiation culture by unbiased sampling and cell scoring of thousands of cells in a homogenized population. This approach would also facilitate unbiased and representative analysis of motor neuron subtype frequencies (see below).

Testing optimizations for the Standard Protocol for motor neuron *differentiation*

In order to evaluate the effect of the optimizations we added to the Standard Protocol we tested them against the Zhang protocol. To determine whether Noggin played a strong role in preventing non-neural fates and supporting default (Munoz-Sanjuan and Brivanlou 2002) or spontaneous neural induction we performed Standard Protocol single cell start EB differentiations described above and in one pilot experiment omitted Noggin. We used %HB9 as the endpoint most relevant to our interest and also as a proxy for the efficiency of neural induction. We found that Noggin strongly increased the % HB9 (Fig. 3.2A). Since seeding density had been an important factor in optimizing mouse ES-MN differentiation protocols (Wichterle, Lieberam et al. 2002), we tested 3 different initial seeding densities, and found that without Noggin, only the highest was efficient for generating ES-MNs, and with Noggin all were efficient but the highest density was superior (Fig. 3.2A). When we compared our Standard Protocol with the EB protocol from which it was derived, and also tested the efficiency of positive and negative manual selection for neural rosettes we found only a slight increase in HB9 efficiency with manual selection, but both non-single cell EB protocols were less efficient than the Standard Protocol condition with Noggin. We concluded that Noggin supported more efficient ES-MN differentiation, likely by supporting more efficient neural induction, and we used Noggin and the higher EB-nucleation density for all subsequent experiments. We also

concluded that in our hands the protocol (referred to subsequently as Standard Protocol) was not only simpler but as or more efficient at ES-MN differentiation than published alternatives.

Since motor neuron differentiation requires a caudal spinal identity and Wnt signaling has been linked to the induction of caudal neural identity (Nordstrom, Jessell et al. 2002; Nordstrom, Maier et al. 2006) we decided to provide a Wnt signal on days 10-17 of differentiation (see Chapter 4 for logic and timing of this decision). To assess the impact of this decision we then asked if Wnt3a conditioned medium (Wnt3a-CM) (Willert, Brown et al. 2003) affected either the efficiency of neural induction, as measured by percent of cells staining for neuronal beta-III tubulin (TuJ1), or motor neuron induction efficiency, as measured by percent of cells positive for HB9 or ISL1. We found that there was no significant difference in the percent of differentiated neurons (62% vs. 63%, n=4 independent experiments, t-test, p= 0.66) with or without Wnt3a-CM. To exclude the possibility that Wnt-CM affected the $HB9^+$ cells differentially we measured the $\%TuJ1^+$ of HB9 cells and found no significant difference (92% vs. 94%, n=4 independent experiments, t-test, p= 0.79). We also found that the efficiency of motor neuron differentiation, as measured by %HB9- and %ISL1-expressing cells, was not affected by Wnt-CM (n=4 independent experiments, 11% vs. 12% HB9, t-test, p=0.93; 10% vs. 11%ISL1, t-test, p=0.37). We concluded from these data that exogenous Wnt-CM was not required for motor neuron generation, but also that it did not negatively affect differentiations. Furthermore, in anticipation that Wnt might work in cooperation with other caudal patterning cues (see Chapter 5) we elected to retain this signal in all subsequent experiments.

Accelerated Protocol

Subsequent to the completion of most studies in this report which used the Standard Protocol described above, new publications showed that pharmacological inhibition of TGF-β signaling increased the efficiency of neural induction to nearly 100%, and accelerated its timecourse by 7-10 days (Chambers, Fasano et al. 2009). We therefore asked if we could adapt our protocol with these inhibitors to increase the efficiency and speed of motor neuron differentiation (Fig. 3.4A). We substituted another inhibitor of TGF- β signal transduction for Noggin, which we report in a subsequent chapter and a previous publication (Boulting, Kiskinis et al. 2011). Because of the shorter overall timecourse of this protocol we reasoned that we could start with slightly larger EBs, and thus avoid the single-cell suspension process we used to initiate the Standard Protocol. We found that this protocol was indeed able to generate a uniform population of very small EBs which grew consistently throughout the differentiation (Fig. 3.4B, C). Initial experiments with the HBG1 MN-reporter line showed GFP expression at day 15 (data not shown): 10 days in advance of the Standard Protocol. EBs were therefore dissociated to single cells at day 21, seeded, and fixed at day 23 for analysis.

To ask if the Accelerated Protocol generated increased motor neuron percentages in this shorter timeframe we stained dissociated cultures with HB9 and ISL1, and NF (for wild type ES-MN) or GFP (for motor neuron reporter ES-MN) we observed a two-fold increase in the efficiency of motor neuron generation (22-31% HB9 depending on cell line, and 37% GFP) vs. Standard Protocol (Fig. 3.3D-G vs. Fig. 3.2). Accelerated Protocol ES-MNs expressed HB9 and ISL1 in the same partially overlapping pattern as described above for the Standard Protocol. When we analyzed the fidelity of the GFP reporter for ES-MNs we found that 70% of GFP cells expressed high levels of HB9 or ISL, and when considered together this figure was nearly 80% (Fig. 3.3H). We concluded that this protocol represented a faster and more efficient means to generate MNs

from ES cells. We could therefore use it to validate reagents and more rapidly test hypotheses about mechanisms of differentiation. For example, when a new lot of SHH protein was acquired, we titrated its activity using the accelerated protocol (Fig. 3.4F). Since the %HB9 was less than 1% in control or low SHH (200ng/ml) doses, this result also demonstrated the SHH dose-dependence of ES-MN differentiation. Accelerated protocol experiments were performed after the majority of work reported in these studies, therefore we used the Accelerated protocol for only a subset of studies and will indicate clearly where that is the case, while the Standard Protocol will be the default unless otherwise indicated.

In summary we developed two robust protocols that do not require manual intervention and that reproducibly generated motor neurons at consistent efficiencies. Both of these were established with dissociated re-seeded cells as the endpoint, and are therefore amenable to both bulk cryopreservation (see below) and homogenized phenotypic analysis. We next asked if and how the ES-MNs generated in our hands would be capable of maturation in vitro.

Maturational phenotypes of ES-MNs

Since many significant aspects of motor neuron biology—e.g., trophic factor dependent survival and axon pathfinding— require maturation beyond initial specification, and because modeling ALS in vitro may require the elaboration of specific mature characteristics, we next sought to characterize the state of maturation of ES-MNs over 2 weeks in vitro using electrophysiological, morphological and immunocytochemical approaches.

ES-MNs show progressive electrophysiological maturation during extended culture

In order to address the maturation of ES-MNs we turned first to the principal functional feature of all neurons: electrophysiological activity. Because of the prevalence of non-motor neurons in

our cultures, we used a motor neuron report line (HBG47) which expressed GFP under control of the mouse HB9 locus on transgenic bacterial artificial chromosome (Placantonakis, Tomishima et al. 2009) to prospectively identify ES-MNs for recordings.

Progressive changes in active membrane properties

To investigate the electrophysiological properties of ES-MNs over time we prepared low density cultures and our collaborator Tomonori Takazawa (Amy B. MacDermott's lab) tested passive and active membrane properties using patch clamp recordings between 2 and 13 days following seeding mat day 31 of dissociation. Recorded cells were backfilled with dye, fixed and then stained with motor neuron markers HB9 and ISL when cells were recoverable. We confirmed that all intact recorded cells (n=7) expressed both GFP and the motor neuron marker HB9 or ISL1 (Fig. 3.5A). When we asked if ES-MNs were competent to fire action potentials we found that 27 of 28 cells recorded were able to fire action potentials (APs) with depolarizing current injections, while the one AP-incompetent cell was at the youngest timepoint tested (day 2). Representative examples of voltage changes in response to depolarizing currents, and accompanying backfills are shown for 3 different cells at 3 different time-points (Fig. 3.5B-G). These data show an increase in repetitive firing accompanied by a decrease in input resistance over time in culture. We conclude from these experiments that ES-MNs showed rapid and progressive functional maturation over time in culture. We next sought to quantitatively describe these progressive changes in electrical properties.

Progressive changes in membrane properties

When input resistance was graphed as a function of time in culture, we found that it decreased significantly and progressively with time (Fig. 3.6A, n=28 cells, One-Way ANOVA, $p < 0.01$).

This decrease is consistent with an increase in the total number of ion channels contributing to leak conductance at resting potential. Resting potential did not change significantly over the timecourse studied, however the mean decreased from -50 mV to -60 mV by the latest timepoint (Fig. 3.6B). The rheobase—current step magnitude required to elicit AP—was also unchanged over this timecourse (Fig. 3.6C). We conclude from these data that ES-MNs show evidence of maturation, decreased input resistance, and may have been entering a phase of further maturation as indicated by the lowering of resting potential at the end of the timecourse. We next sought to examine more specific and quantitative changes in the APs generated by ES-MNS.

Progressive changes in AP characteristics

To understand in greater depth the maturational changes suggested by the increased frequency and number of APs fired by ES-MNs we next examined these spike trains quantitatively. The duration of APs (as measured by half-width) showed a significant decrease from the earliest timepoint to all older time-points ((Fig. 3.6D) n=25 cells, One Way ANOVA, $p < 0.01$). This result suggested a more mature profile of acute AP discharge which implied a more mature constellation of voltage gated Na^+ and K^+ channels. Because both AP-half-width measures and rheobase showed a range of values even at the oldest time-points, we plotted rheobase vs. half-width for individual cells at day 43 (Fig. 3.6E). This analysis suggested that two distinct populations were present in older cultures: one with low rheobase and broad action potentials, and another with tight action potentials and higher rheobase. This result could be interpreted as evidence of two different ES-MN subtypes, or as evidence for a less and a more mature population of ES-MNs.

To distinguish between the two possibilities we examined maturation state of ES-MNs more directly. As motor neurons mature they develop the ability to fire repetitive trains of action potentials (Gao and Ziskind-Conhaim 1998). We next investigated whether a similar change had occurred with time in vitro. At the earliest timepoint studied, no ES-MN recorded was able to fire more than one action potential even during extended (1s) current injections. Many ES-MNs however showed repeated AP-trains on subsequent days in vitro (Fig. 3.5B-G). Indeed the maximum frequency of AP firing showed a progressive and significant increase over time ((Fig. 3.6F) n=28 cells, One-Way ANOVA, $p<0.05$,). Interestingly, even at the latest age measure, some ES-MNs were capable of firing only a single action potential, even during injections of large depolarizing current (>140 pA), showing that even after 13 days of maturation, ES-MNs are a mixture of cells with less and more mature properties. We concluded from these experiments that in aggregate ES-MNs underwent progressive functional maturation, as shown by their membrane properties and increasing ability to fire repeated high frequency AP-trains and that late time point cultures consist of a mixture of more and less mature ES-MNs.

Progressive development of motor neuron selective electrophysiological signatures

We next asked if we could detect more subtle aspects of maturation consistent with motor neuron firing properties in vivo. First, we noticed that the timing of APs within repeated spike trains gradually increase, a phenomenon identified in vertebrate motor neurons in vivo and termed spike frequency adaptation (SFA) (Fig. 3.7A). When we graphed the ratio of last to first spike interval over time, we found a progressive increase with time in culture (Fig. 3.7B, n=8 cells, $R=0.73$, $p= 0.05$, Pearson's linear regression). We concluded from this analysis that ES-MNs progressively acquired more mature physiological profile with time, and that this profile was consistent with the in vivo motor neuron firing properties.

We also noted that some ES-MNs showed depolarizations in response to hyperpolarizing current injections. In some cases these post-inhibitory rebound depolarizations triggered APs, a phenomenon described in vertebrate MNs and termed rebound action potentials (RAPs) (Fig. 3.7C). No ES-MNs displayed RAPs at day 33; however at this timepoint one neuron did exhibit post-inhibitory rebound depolarization. At every other subsequent time however nearly half of ES-MNs displayed RAPs (Fig. 3.7D). We concluded from this analysis that many ES-MNs exhibit mature firing properties characteristic of MNs in vivo.

ES-MNs show progressive morphological maturation with time in culture

We have seen that ES-MNs showed a maturation of electrophysiological properties over time in culture. But we also observed a second population of cells with immature characteristics at later time-points in culture. The less mature cells might either correspond to a subset of ES-MNs refractory to maturation or to a population of newly born MNs generated during the maturation period. We favor the latter, as parallel studies in the lab following HB9:GFP expression have seen dramatic increases in GFP^+ cells after a week in culture (Nuno Lamas, Bethany Kerner, unpublished data). Furthermore BrdU labeling of mitotic cells demonstrated ongoing birth of new motor neurons during this time period (Nuno Lamas, Bethany Kerner, unpublished data). This interpretation also fits both with the high level of OLIG2 expression we observed at day 31, and with the evidence for an extended timecourse of human motor neurogenesis in vivo: day 25-56 (Hagan, Ross et al. 2000; Altman and Bayer 2001; Bayer and Altman 2002). To address the extent of motor neurogenesis in our cultures we next used alkyne conjugated EdU, a nucleotide

analog used to label dividing cells which is more compatible with immunostaining. When we stained cultures with or without EdU we first observed that the number of total cells in EdU treated cultures was greatly decreased (not shown). This suggested that EdU was acting as a mitotic poison at the dose used (0.5 μM). When GFP cells were co-stained with EdU we found that at each timepoint fewer than 10% of cells were labeled with Edu and we observed a gradual decrease in GFP cell numbers rather than the dramatic increase reported by colleagues above (Fig. 3.8). We concluded from these experiments that maturation with EdU treatment was able to almost completely eliminate newborn ES-MNs from our cultures. We could therefore examine the non-mitotic ES-MN population for progressive features of maturation in EdU treated cultures.

Morphological maturation of ES-MNs

In order to determine if surviving ES-MNs showed progressive maturation at the morphological level, we quantitated neurite outgrowth of all GFP^+ cells during a 14 day timecourse subsequent to plating on day 31 of differentiation. We optimized analysis parameters for each timepoint and condition separately to ensure the most accurate tracing possible, and then applied these to all cells for each of two coverslips per condition per timepoint. First we noticed a clear increase in the extent of neurite projections with time (Fig. 3.9A), and determined that automated tracing could accurately quantify this morphological phenotype. This outgrowth phenotype is represented at the qualitative level by camera lucida overlays of an unbiased sample (the first ten fields imaged) (Fig. 3.9B). This analysis indicated that at a qualitative level cell outgrowth was progressive and substantial. Quantitative analysis of morphometric parameters showed progressive increases in all measures of neurite outgrowth, complexity, and cell body size (Fig. 3.9 C). Day 33 vs day 45 values for both cell soma area and total outgrowth were distributed

non-normally (Shapiro-Wilk tests failed, P <0.050) therefore a Mann-Whitney Rank Sum Test was performed which showed a significant difference between the population of day 33 and day 45 cells in both cell soma area (median 88 vs. 158 μm^2, U=9723.000, T=29757.000 n(small)=105 n(big)=323 P= <0.001) and total outgrowth (median 110 vs. 406 µm, U=5535.000, T=34374.000 n(small)=106 n(big)=323 P= <0.001) (Fig 3.9D, E). Population histograms showed the contribution of increasing numbers of very large and complex cells to the mean outgrowth and cell body size (Fig. 3.9F, G). Finally, in order to estimate the morphological characteristics of cells which were recorded in the previous experiment, all recorded, backfilled cells which were recoverable for staining were imaged and their morphometry was quantified as for the morphological time series and plotted on histograms (Fig. 3.9F, G).

We conclude from this series of morphometry experiments that while ES-MNs are undergoing electrophysiological maturation they are also undertaking morphological elaboration. This maturation consisted of progressive somatic growth and elaboration of neurites which were increasingly long and complex. By eliminating proliferative cells that disrupt the growth of more differentiated cells and are capable of giving rise to new, smaller, ES-MNs, this morphological maturation could be quantified directly. We next asked if there were any molecular changes which paralleled this morphological and functional maturation.

ES-MN maturation marked by a switch to NF-H expression

We next asked if we could detect any changes in the molecular profile of surviving matured ES-MN under the anti-mitotic conditions defined above. We have previously shown that short term (2 days after dissociation at Standard (day 31) or Accelerated (day 21)) cultures were composed of ES-MNs which were uniformly positive for TuJ1 and only some of which were positive for

NF-H. We therefore seeded differentiated cells from two different ESC lines (RUES1 and HB9:GFP) in parallel: a replicate well was fixed at day 2, and another allowed to mature with mitotic inhibition for 8 days and then fixed. Both sets were then stained for motor neuron markers HB9:GFP or HB9/ISL1(for RUES1 cells) and NF-H. First, we noted a dramatic increase in the percent of MNs expressing NF-H and the intensity of expression: at day 2 only some ES-MN (HB9/ISL$^+$ or GFP$^+$) expressed NF-H, however by day 8 every single HB9/ISL1 or GFP cell (n >50 cells per cell line in one experiment each) expressed high level NF-H (Fig. 3.10). We also observed a strong qualitative increase in the intensity of NF-H staining in each cell suggesting a maturational switch to a higher expression level of NF-H. Qualitatively, ES-MNs showed long primary axons and dendrites in the older cultures compared to the bipolar or spindle shaped ES-MNs at day 2. Surprisingly, EdU-mediated suppression of motor neurogenesis in culture was accompanied by a dramatic increase in the percent purity of motor neurons. We observed at a qualitative level nearly every cell (n>50 cells for each cell line in one experiment each) positive for NF-H was also positive for HB9 or ISL1 or for HB9:GFP. These striking differences are representative of 3 additional independent experiments, but should be more precisely quantified in future studies. In combination with the previous data on functional and morphological maturation, we concluded that mitotic inhibition allowed us to observe a maturational switch from TuJ1 expressing MNs with immature morphology, to morphologically elaborate NF-H$^+$ phenotypes. And surprisingly, simply by eliminating dividing cells the fraction of motor neurons in culture rose nearly to purity.

In conclusion our morphological, electrophysiological and molecular data demonstrate that ES-derived motor neurons mature but that there is ongoing neurogenesis resulting in a mixed

population of mature and immature cells in aged cultures. Interestingly this can be suppressed by EdU treatment and the maturational fraction can be observed independently.

Characterization of ES-MN diversity in vitro

ES-MNs express all motor column markers found in vivo

We next asked if ES-MNs co-expressed the markers of motor column identity we had validated in vivo by staining cultures for the MMC marker LHX3 and the LMC/PGC marker FOXP1. We found that most $HB9^+$ or $ISL1^+$ cells expressed neither columnar marker, 57% and 54% respectively; 27% and 25 % expressed only LHX3 respectively; 9% and 10% respectively expressed only FOXP1; and 7% and 8% respectively expressed both LHX3 and FOXP1 (Fig. 3.11A-C, n=4 independent experiments). Cells expressing HB9 or ISL1 and neither columnar marker match the expression profile for the human HMC in vivo and those expressing LHX3-only match the expression profile of the MMC. Cells expressing FOXP1-only could match the profile of the LMC or PGC, however, since high level FOXP1 expression was required to score a cell as positive for FOXP1, these cells are a better match for the LMC. Cells with lower level FOXP1 (not included in the scored total fro FOXP1+) would then match the PGC (and would come out of the current putative HMC subset). Cells expressing both LHX3 and FOXP1 do not match any defined motor columns, however they did match a group of MNs that we identified in the dorsal $HOXA5^+$ brachial LMC_M observed in vivo (Fig. 3.11D and Chapter 2). Alternatively these cells may have confused or transitional identity. We concluded from these analyses that ES-MNs expressed marker combinations consistent with all in vivo motor column identities:

HMC, MMC, LMC, and PGC, and also with the novel $LHX3^+/FOXP1^+$ population. We next turned to the issue of rostrocaudal identity.

HOX protein expression in ES-MN

To determine the rostrocaudal identity of ES-MNs we next tested the HOX protein antibodies which had shown specific rostrocaudal domains of expression in vivo (Chapter 2). We found that many cells expressed HOXA5 whereas a much smaller number of cells expressed HOXC8 or HOXD9 (Fig. 3.12A, B). This suggested that most cells with a positively identifiable rostrocaudal identity were cervical. When HOX gene expression gated on MNs (cells with high HB9 or ISL1) we found that about half of ES-MNs expressed HOXA5 (45% of $HB9^+$ and 50% of $ISL1^+$ cells, n=4 independent experiments) with significantly smaller percentages which were $HOXC8^+$ (3% of $HB9^+$ and 13% of $ISL1^+$ respectively, n= 4 independent experiments, unequal variance rank sum test p=0.029 and t-test p=.008 respectively) or $HOXD9^+$ (3% of $HB9^+$ cells n= 3 independent experiments and 3% of $ISL1^+$ cells n=4 independent experiments, unequal variance rank sum test p=0.029 each) (Fig. 3.12C, D). Interestingly the percent of MNs positive for each HOX gene was much higher than the percent of all cells, suggesting that HOX gene expression was somewhat selective to MNs as in vivo. We also noted that $ISL1^+$ cells had a larger fraction of $HOXC8^+$ cells. We concluded that under RA based differentiation conditions, ES-MNs adopted a predominantly $HOXA5^+$ HOX phenotype, and based on our in vivo data this suggests a cervical or rostral brachial positional identity. Interestingly, the group of motor neurons co-expressing FOXP1 and LHX3 was detected in cervical spinal cord expressing HOXA5 in vivo, suggesting that the minority of $LHX3^+/FOXP1^+$ ES-MNs might correspond to this newly identified motor neuron subtype. A small percentage of ES-MNs did exhibit HOXC8

or HOXD9 expression, suggesting that small number of ES-MNs adopted caudal brachial or thoracic identity.

Because MNs in vivo expressed only one of these three HOX genes depending on their rostrocaudal location, and mutually exclusive expression is a key outcome of repressive inter-HOX interactions in mouse and chick, we asked if ES-MNs would conform to in vivo standards and express HOX proteins in a mutually exclusive manner. When we triple stained cultures for a motor neuron marker (HB9 or ISL) and HOXA5 and HOXC8, or HOXA5 and HOXD9 we found that the majority (>96%) of ES-MNs expressing either HOX gene did so exclusively (Fig. 3.12E, F). We concluded from these results that ES-MNs adopt a range of coherent rostrocaudal phenotypes, strongly centered on the cervical spinal region.

Cryopreserved ES-MN can be thawed for subsequent analyses

Finally, because of the length of differentiation protocols, and the anticipated needs to revisit experiments, use differentiated motor neurons for either bulk screening purposes or transplantation experiments—either of which would be difficult to precisely time with respect to the end of differentiations—we next asked if it would be possible to cryopreserve motor neurons for subsequent live culture and analysis. At the day of dissociation MNs were seeded as described and analyzed, while some were cryopreserved. When these were later thawed, seeded as described for fresh MNs, and stained for motor neuron markers, we found that the matched cultures still contained robust populations of neurons and motor neurons (Fig. 3.13A). The percentage of neurons was not significantly affected (n=3 independent experiments, t-test p=0.292) but the % $HB9^+$ or %$ISL1^+$ MNs of all cells were still robust but were significantly lower (n=5 independent experiments, t-tests, p=0.028 and p=0.020 respectively) than the same

freshly dissociated cultures (Fig. 3.13B, C). When we examined the expression of HOX proteins we also found a reduction in percentage, though this was not significant (HOXA5 fresh n=5 and frozen n=3 experiments, t-test p=0.131; HOXC8 fresh/frozen n=4 experiments, t-test p=0.846; and HOXD9 fresh n=3, frozen n=4, t-test p=0.296), and the same relative HOX distribution was preserved (Fig. 3.13D). When we analyzed the motor column marker expression we found no change in %LHX3 of all cells (fresh n=2 and frozen n=3 experiments, t-test p=0.544) and a small but significant increase in %FOXP1 of all cells (n=5 experiments, t-test p=0.022) (Fig. 3.13E). We concluded from these experiments that while ES-MNs were sensitive to cryopreservation compared to all cells, they could in general be cryopreserved with limited reduction in survival or purity and limited effect on the distribution of rostrocaudal or columnar subtypes.

Matured cells increase LMC marker FOXP1 expression in percent and quantity

Having established the columnar identities among freshly dissociated ES-MNs we next asked if these identities changed during the maturation period described above using EdU treatment. Surprisingly, when EdU-treated matured cells were stained with FOXP1 and LHX3, we found that the vast majority (85%) of cells at 8 days after dissociation expressed extremely high levels of FOPX1 protein (Fig. 3.14). This is in striking contrast to the 12% of ES-MNs which expressed FOXP1 at 2 days after dissociation. Additionally the staining intensity for FOXP1 was much brighter by eye at this later timepoint suggesting a large increase in expression level. One interpretation of this result is that only $FOXP1^{+}$, putative LMC cells were able to survive under these conditions. This interpretation does not explain the dramatic up-regulation in FOXP1 expression level for individual cells however. These data therefore better support the idea of maturational conversion to a nearly uniform $FOXP1^{+}$ LMC phenotype, but they also do not contradict the idea that FOXP1/LMC cells have preferential survival under these conditions

compared to any other columnar subtype. To determine if this column phenotype conversion or survival was a direct effect of anti-mitotic treatment, or the result of selective survival under these conditions, we next asked if we could devise non-EdU conditions under which to observe exclusively post-mitotic cells.

FOXP1 cells show a distinctive morphological phenotype

To ask if non-mitotically poisoned cells would show an increased percent and expression level of FOXP1, we used FACS to purify cells which expressed high levels of GFP immediately after dissociation. These were then seeded at very low density on monolayers of commercially available human fetal spinal cord astrocytes and allowed to mature for 12 days. When these cultures were fixed and stained 12 days later we again observed a percent of FOXP1 cells (72%), far higher than at day 31 and a complete lack of LHX3 staining (Fig. 3.15A, B). These cells again displayed extremely high intensity FOXP1 staining typical of matured ES-MN. We concluded from these results that the increase in FOXP1 percentage and intensity was not a byproduct of selective resistance to mitotic poison. Because of the generally low survival following FACS these experiments did not however address whether the resulting increase in percentage of surviving $FOXP1^{+}$/LMC ES-MNs was a result of selective survival or a conversion of columnar phenotype.

We next wanted to ask if FOXP1 cells would show a functional phenotype correlated with their expression profile. Since these cultures were seeded at very low density we were able to perform automated neurite outgrowth morphometry analysis of individual cells. In the few (n=10) fields

where cells were in direct contact, the field was excluded from quantitation. We found that FOXP1^{+} (n=39) cells had trend increases in most aspects of neurite length and complexity, and the mean and median process length compared to FOXP1^{-} (n=20) cells were significantly larger (t-test, $p<0.05$, Fig. 3.15C). This morphological phenotype was specific to neurite outgrowth since while both FOXP1^{+} and FOXP1^{-} cells showed large increases in cell soma area; there was no significant difference between the two populations. Since the total outgrowth of cells is traditionally a robust metric reflecting their morphological maturation, and FOXP1^{+} cells trended higher but not significantly so, we next examined the population distribution by cumulative percentage (Fig. 3.15D). This analysis revealed both populations contained the same percent of smaller cells: 50% of cells had total outgrowth <0.91mm). However The FOXP1^{+} cells contained many more cells with much larger total outgrowth. This analysis shows that the divergence between FOXP1^{+} and FOXP1^{-} cells was mostly accounted for by a larger number of large (>0.1 mm: 43% vs. 20%) and very large (>1.8 mm: 20% vs. 5%) cells. First we concluded that FOXP1^{+} putative LMC cells may exhibit a motor column-specific functional morphological phenotype in vitro consisting of more extensive neurite outgrowth in vitro. Second we concluded from these pilot data that low density non-mitotic culture conditions are another promising assay in which to search for motor neuron subtype-specific phenotypes.

ES-MNs show behavior on transplant consistent with functional subtype identities

Finally we asked if human ES-MN would be competent to interpret in vivo cues directing motor axons projection patterns. To do this we conducted a series of pilot experiments in which GFP^{+} ES-MNs were transplanted to the chick neural tube at HH stage 15-16 and allowed to develop for 2-3 days (Wichterle, Peljto et al. 2009; Peljto, Dasen et al. 2010). We found that many ES-MNs were able to survive during this time period, some settled into ventral positions appropriate for

MNs and maintained expression of motor column markers FOXP1 or LHX3, and extended projections towards ventral roots (Fig. 3.16A, B). We also found that transplanted ES-MNs were able to project axons very long distances (> 1.8 linear mm) out of the spinal cord, towards epaxial, hypaxial and limb muscles (Fig. 3.16C, D). We also noted that the proportion of $FOXP1^{+}$ ES-MNs in this context was again disproportionately high compared to pre-transplant cultures. We conclude from these preliminary results that hES-MNs were able to respond to chick axon guidance cues in vivo and projected axons along in vivo paths muscle targets which were consistent with the columnar diversity of transplanted cells. However, without backfilling projections and labeling for motor column markers, we have no evidence that individual ES-MNs exhibited column-specific axonal pathfinding.

Discussion

Summary of findings

We have defined 2 robust protocols for differentiating MNs from human ES-cells. Both protocols are simple, robust, do not require manual intervention and utilize a homogenized dissociated cell endpoint. This allowed us to perform the first systematic description of the diversity of ES-MNs. ES-MNs are defined, like their in vivo counterparts, by expression of the motor neuron markers HB9 and or ISL and we found that the spectrum of expression matched that observed in vivo: a continuous range from 1:0 to 0:1. We then showed that ES-MNs expressed motor column marker combinations consistent with all motor columns (MMC, HMC, LMC, and PGC) and describe their relative abundance. The rostrocaudal diversity of ES-MNs on the other hand was restricted mostly to cervical and rostral brachial cells ($HOXA5^{+}$) although

smaller populations of caudal brachial to rostral lumbar ($HOXC8^+$ and $HOXD9^+$) cells were generated as well. We also show that ES-MNs displayed several phenotypes characteristic for motor neurons in vivo. HOX genes were expressed in a mutually exclusive fashion, and column markers were expressed in a mostly exclusive fashion. ES-MNs displayed electrophysiological features (spike frequency adaptation and rebound depolarizations) consistent with in vivo physiology and they could pursue a variety of axonal trajectories in the periphery consistent with their transcriptional diversity. Finally, we show that ES-MNs undergo progressive and rapid maturation in vitro characterized by a conversion to mature neurofilament expression, extensive neurite outgrowth, and maturation of passive and active electrophysiological properties culminating in action potential spike trains. Unexpectedly, during maturation in three different paradigms—EdU mitotic inhibition, low density culture of FACS purified cells on astrocyte monolayer, and in chick transplant—the percentage of $FOXP1^+$ (LMC) MNs was increased dramatically and LHX3 expression was lost.

Simple, robust and quantitative protocols for ES-MN differentiation and phenotypic analysis

Optimized protocols for ES-MN differentiation

The Standard Protocol we describe relied upon facilitated spontaneous neural induction and proceeded at an in vivo-like developmental timecourse. This direct comparison with in vivo timing should facilitate modeling developmental events with aim of controlling ES-MN subtype identities (Chapter 5). The second, Accelerated Protocol increased the efficiency of neural induction using TGF-β signaling inhibitors and attained ~2 fold higher ES-MN differentiation efficiency in 10 fewer days than the Standard Protocol.

Efficiency of motor neuron induction

In comparison to previously published results the pan-MN efficiency of our protocols (12% HB9 for the Standard Protocol, and 25% HB9 for the Accelerated Protocol) are lower than most reports. However, reported ES-MN differentiation efficiency is determined by different approaches. The group of Su Chun Zhang was among the first three papers to describe human ES-MN differentiation, and this group consistently reports higher HB9% than our data, and generate what appear to be very high quality and bona fide motor neurons. However their analysis of pan-MN differentiation efficiency (%HB9) is conducted when EBs are attached whole to substrate and some cells migrate out from clusters. They report that HB9 rarely occurs outside of these clusters and HB9 was quantified by taking several fields surrounding, or perhaps within, several 3-dimensional masses of cells. When we dissociated cells we are therefore killing some $HB9^{+}$ motor neurons, and we are certainly looking at substantially different endpoint. Based on their own statements, we can only assume that if their differentiations were quantified from dissociated re-seeded cell suspensions, their HB9 efficiency would be much lower.

Additionally, as we have shown, HB9 is detected in a nearly smooth continuum from extremely bright, >10,000 grey levels above background, to 1 grey level above background. When we assessed methods for quantifying HB9 we decided to restrict ourselves to scoring only the brightest and most unambiguously positive HB9-expressing cells in order to be certain that co-expression analyses were restricted exclusively to MNs. In the zero sum game of cell scoring, this decision minimized false positives, and as we have shown, necessarily increased the rate of false negatives, thereby depressing our %HB9 relative to less conservative approaches to cell scoring. Most published reports are not explicit about cell scoring methods, but close

examination of published immunocytochemical results suggests that we have placed ourselves, as intended, at the most conservative end of the most conservative group. Under our Accelerated Protocol however, our conservative estimate of motor neuron efficiency (25%) compares favorably with top echelon of reliable reports in the literature. Most importantly we achieved our goal to develop robust differentiation protocol with high efficiency of motor neuron differentiation which would be amenable to rigorous quantitative analyses.

Homogenized cultures

Our decision to treat differentiations as a homogenous whole had direct implications for both the differentiation protocol we chose to develop and the endpoint, and was motivated by several factors. First we elected not to perform any manual selection during the differentiation. This undoubtedly retained some non-neural derivatives in Standard Protocol cultures. Although in agreement with previous reports (Chambers, Fasano et al. 2009), these were minimized to apparently zero under the Accelerated Protocol. The "hands-off" design of both of our protocols simplifies them and minimizes variability between experiments and operators. Most importantly this decision was taken so that different populations of motor neurons were not inadvertently selected for or against at any stage. This decision will become especially important when we turn to the topic of manipulating subtype identity by changing differentiation conditions in Chapter 5.

Since few robust methods have been reported for purification of motor neurons, or efficiency of differentiation approaching 100%, all current ES-MN cultures are a mixed population of ES-MNs and other cells. The second implication of our commitment to homogeneity was therefore that our endpoint for analysis must assay the population as a homogenized whole. We reasoned

that dissociating all EBs and re-seeding cells in a homogeneous mixture would provide the most rigorous approach to unbiased sampling of the population to quantitatively assess its constitution. One drawback of this approach is that we could not directly measure heterogeneity between EBs. Second this method engendered a non-zero level of cell death, of MNs and non-MN alike, due to trypsinization and physical trituration, which likely lowered our total efficiency of motor neuron induction. An alternative approach such as acute fixation and intracellular staining of dissociated cells could provide an interesting window into the changes introduced by EB dissociation and reseeding in the future. The motivation for this decision was four-fold. First, when we later attempt to manipulate rostrocaudal identity by adding posterior patterning factors (Chapter 5) we did not want to bias results by excluding any EBs or cell types affected by these treatments. Second, we anticipated that defining and studying more mature phenotypes of motor neurons and motor neuron subtypes, especially disease related or survival phenotypes, would be greatly simplified by assaying a homogenous population which started from the same state of individual single cells, rather than cells emerging from distinct and variable 3-dimensional EB matrices. Third, in order to study motor neuron subtype phenotypes, we sought render any intercellular effects homogenously distributed throughout the culture. Fourth, we wanted to be able to cryopreserve motor neurons for future phenotypic or screening studies. Our short term and mature cultures were completely homogeneous across culture surfaces and the variability between fields in a sample was therefore extremely low. We conclude that our protocols meet the above requirements and using very strict and conservative quantification show respectable and highly reproducible motor neuron yields.

ES-MN subtype diversity

Precise characterization of pan-MN markers

We have provided here the first detailed and quantitative treatment of co-expression of the pan-MN transcription factor markers HB9 and ISL, which ranged continuously from an expression ration of 1:0 to 0:1. Our data confirms the widespread co-expression of these markers in many cells, which has been reported previously (Li, Du et al. 2005; Di Giorgio, Carrasco et al. 2007; Li, Hu et al. 2008). We substantiate these reports as well as contribute previously undocumented detail of the wide spectrum of expression levels which constitute this overlap. The extent of apparent co-expression varies inversely with the strictness of thresholding used to score cells as positive for either marker. Therefore our reported % of co-expressing cells does not include many cells which express low levels of the other marker. However our analysis points to the real existence of many ES-MNs which are completely devoid of one or the other pan-MN marker. This finding matches the in vivo staining we show for human ES-MN in vivo in Chapter 2. The in vivo suggested interpretations for the identity of HB9 and ISL1 expressed cells as well. The in vivo cognate of any cell expressing appreciable levels both HB9 and ISL1 cannot be other than a spinal motor neuron. Cells which express HB9 predominantly could match a minority of MNs in the MMC or many MNs in the LMC_L, especially at lumbar levels. While we observed few $HB9^+$ interneurons in vivo, these are known to exist in other species at other timepoints, so it is formally possible that some in vitro generated $HB9^+$ $ISL1^-$ cells correspond to these. Given the approximate stage of these cultures this interpretation is unlikely. The $ISL1^+HB9^-$ cells could match a small subset of low/no-HB9 MMC, a slightly larger subset of HMC, many LMC_M, especially at lumbar levels, or any PGC motor neuron. However we identified three other in vivo $ISL1^+HB9^-$ cellular identities in human samples in vivo, which are also found in rodent: scattered ventral $ISL1^+HB9^-$ cells, a population of $ISL1^+HB9^-$ dorsal (presumably interneurons)

at all levels of the spinal cord, as well as dorsal root ganglion cells. Given the high level of SHH signaling used in our protocols we predict that $ISL1^{+}HB9^{-}$ cells are unlikely to be dorsal interneurons and less likely to be neural crest-derived DRG neurons, and therefore that most of the $ISL1^{+}HB9^{-}$ cells are ventral motor neurons, however additional markers would be needed to address this proposition. Choline Acetyltransferase (ChAT) would be a good marker to support motor neuron identity for HB9- or ISL1-only cells, however congruent with previous reports that ChAT is not expressed by ES-MNs until 6-8 weeks in vitro (Li, Du et al. 2005) , we observed no robust staining for this enzyme, although qPCR did indicate transcript was expressed (data not shown).

When we examined the expression of GFP driven by the HB9 promoter in transgenic ES-MNs we found that most GFP^{+} cells expressed either HB9 or ISL1 (70%) and the vast majority (80%) expressed high levels of one or the other. We also observed that many of the remaining 20% of cells expressed low levels of one or both motor neuron markers, but due to our conservative approach to thresholding were not included in this figure. Our data supports previous publications using this reporter line, showing that its GFP expression is MN-specific, but shows that some cells express very little of one or both pan-MN markers. Given the distribution of HB9 and ISL1 both in vivo and in wild type cells, the expression pattern of this reporter appears more faithful to pan-MN identity, than it is to strictly HB9 protein expression per se. Furthermore the high level of LHX3 expression in our cultures supports the likelihood of this idea since LHX3 and ISL1 are known to act directly on the HB9 promoter (in concert with NGN2, which we did not measure).

In summary we have provided the most specific and systematic description, informed by in vivo expression patterns, of what ES-derived neurons may be safely or speculatively called “MNs”.

HB9 is the much more selective marker in vivo therefore the most conservative approach would denominate almost any $HB9^+$ neuron as a motor neuron with high confidence. Of these most should express high or intermediate levels of ISL1, while some should have low or no ISL1 expression, especially if LMC cell types have been induced. $ISL1^+$ cells are also likely MNs under strong ventralizing protocols; again most but not all of these should co-express some level of HB9. Finally, especially if LMC subtypes have been induced, some ES-MNs should express high ISL1 and low or no HB9. Therefore from our data we suggest that some or all of these ISL1-only cells should be considered "MNs" but without additional markers it is not possible to positively determine what percent.

Quantitation of motor neuron column markers

We also provide a quantitative description of the motor column diversity present in hES-MNs using the LMC/PGC and MMC specific markers FOXP1 and LHX3. This is the first quantitative description which is strictly gated by validated markers of pan-MN identity, HB9 or ISL1. Most ES-MNs expressed neither marker suggesting an HMC phenotype, while many expressed LHX3 suggesting an MMC phenotype, and fewer still expressed FOXP1 at the high level required for scoring, suggesting an LMC phenotype. The prevalence of LHX3 expressing cells matches with other anecdotal reports showing LHX3 expression in ES-MN cultures as well as with the evidence of overwhelming LHX3 expression in mouse RA-based ES-MN differentiation (Wichterle, Lieberam et al. 2002; Soundararajan, Miles et al. 2006; Peljto, Dasen et al. 2010). Only one previous reports has shown FOXP1 expression in human neurons (putative LMC), and also shown FOXP1-LHX3- neurons (putative HMC) (Patani, Hollins et al.

2011), however neither of these markers were gated by either motor neuron transcription factor marker, but rather by non-phosphorylated neurofilament (SMI-32). Furthermore these authors do not undertake to demonstrate the MN-specificity of SMI-32 in vitro. On the other hand we have observed (data not shown and corroborated by Bethany Kerner, unpublished observations) has found that SMI-32 reactivity in ES-MN containing cultures is not selective for cells expressing HB9 or ISL1.

Since we stained for LHX3 and FOXP1 in separate channels, as opposed to same species same fluorescent channel (Patani, Hollins et al. 2011), we could document 2 additional features not previously appreciated in any report on human cells. First, these markers were expressed in most cells exclusively. This suggests that the columnar phenotypes within individual cells are molecularly coherent. Second we identified a subset of cells expressing both column markers in vitro. This molecular phenotype has no cognate in mouse in vivo. We considered two possibilities which could account for this hybrid identity. First we did identify a hybrid population expressing this combination of markers in human in vivo. This population was located in the $HOXA5^{+}$ rostral brachial spinal cord, which is also the identity of most hES-MNs in our cultures. Therefore these $LHX3^{+}FOXP1^{+}$ are a likely match the molecular profile of this newly identified population in terms of both HOX protein and column marker expression. However we did not directly co-stain LHX3, FOXP1, HB9 or ISL, and HOXA5 simultaneously, which could directly test the idea of an equivalence between our LHX3/FOXP1 coexpressing cells and those found in vivo. Another possible interpretation of this molecular profile is that these hybrid cells have a confused or transient molecular identity. Since LHX3 is a known determinant of pan-MN identity, it is possible that in vitro its down-regulation in non-MMC cells is delayed. Delayed down-regulation of LHX3 has indeed been observed for mouse ES-MNs

(personal communication Hynek Wichterle). And when more caudal conditions generated FOXP1^{+} cells from mouse ES-MN, most FOXP1^{+} cells were LHX3^{-}, however a subset of cells was positive for both markers ((Peljto, Dasen et al. 2010) and M.W. Amoroso personal communication of unpublished observations).

The broad diversity of MN-subtypes we describe has important implications for future studies on hES-MNs. Because ES-MNs are a mixed population studies directed at defining motor neuron phenotypes, normal or diseased, will need to carefully address the possibility that different motor neuron subtypes may show different responses based on columnar and or rostrocaudal identity. Because of the consistencies between our results and protocols and other reports, the map of potential identities we provide is likely to be relevant for most hES-MN differentiations using RA for caudalization. Whether or not the precise percentages are similar in our study or others, the markers we describe can be used to identify many subpopulations, and will therefore enable investigation of their specific properties. Indeed when we began to look for such behaviors we found that LMC-phenotype MNs showed enhanced outgrowth characteristics. Future studies directed at defining disease related phenotypes may benefit from this approach as well. For example, will LMC subtype ES-MNs show enhanced or accelerated sensitivity to ALS genotypes or pathogenic triggers? The ability to define LMC vs. non-LMC ES-MNs in vitro using molecular markers lays the technical foundation for asking this question.

Precise characterization of rostrocaudal HOX profile

Finally we have provided the first quantitative description of the rostrocaudal identity of hES-MNs which is gated directly by motor neuron markers. Previous work has not quantified the percent of hES-MNs expressing one or multiple HOX markers, and usually not reported HOX

expression in the context of an independent marker of pan-MN identity. Our data show a strong cervical bias (~50%HOXA5^{+}) but also trace populations of HOXC8 and HOXD9 expressing ES-MNs. The predominance of HOXA5 expression squares with evidence from developmental models systems showing direct action of RA on anterior HOX gene promoters. Other reports have documented some HOXA5 expressing hES-MNs (Elkabetz, Panagiotakos et al. 2008).

The presence of small but identifiable populations of HOXC8 and HOXD9 positive hES-MNs is at odds with the largely cervical nature of mouse ES-MN expressing HOXC4 and HOXA5 but lacking HOXC8 or HOXD9 positive MNs (Wichterle, Lieberam et al. 2002; Soundararajan, Miles et al. 2006; Peljto, Dasen et al. 2010). This suggests that human ES-MN differentiations may develop some endogenous caudalizing activities during differentiation, or that human mechanisms of development are more open to caudal identity. Our data fits with reports of more caudal HOX gene expression, HOXC6, HOXC8, HOXC9, HOXC10 in hES-MN containing cultures (Li, Du et al. 2005; Lee, Shamy et al. 2007; Patani, Hollins et al. 2011). Although HOXC8 expression was not gated by a pan-MN marker in any report, the impressively high and believable % of HB9 expression in at least one publication (Li, Du et al. 2005) suggests that this HOXC8 expression may indeed have been in motor neurons. Another report indicated even more caudal HOX genes HOXC9 and HOXC10, but this was without RA and in the presence of FGF and will be discussed in Chapter 5 (Patani, Hollins et al. 2011). Gene expression studies on hES-MN-enriched vs. control cultures have also show induction of preferentially rostral HOX genes HOX1-6, which fits very well with the rostrally biased profile we show here (Lee, Shamy et al. 2007).

While we have presented the first systematic account of rostrocaudal identity in ES-MNs, over 40% of ES-MNs failed to stain for one of three confirmed markers available. We speculate that

based on the rostral HOX activity of RA that many of these cells express HOX genes found in the vertebrate hindbrain, HOX1-4. Our studies of gene expression also indicated the presence of HOXC6 (see Chapter 5) which fits with the identification of FOXP1 cells since evidence from chick and mouse shows HOXC6 is required for brachial LMC identity. A more comprehensive description of the rostrocaudal profile at the level of individual motor neurons will require the generation of new reagents to specifically detect human HOX proteins and mRNA by in situ in vivo and in hES-MNs in vitro.

Maturational phenotypes

Timecourse of physiological maturation and emergence of motor neuron selective characteristics

We described for the first time the rapid timecourse under which ES-MNs acquire electrophysiological activity. The characteristic of repeated action potential firing matches many previous studies done on ES-MNs but most of these were performed several weeks or months later than in this report. Therefore our findings show that physiological maturity is attained by ES-MN earlier than has been previously appreciated and show the rapid and progressive nature of this maturation. We also demonstrate two features which are characteristic for motor neuron firing properties in vivo. Rebound action potentials are associated with rhythmic locomotor activity and spike frequency adaptation in AP trains is an optimal electrical strategy for inducing muscle contraction. This report is therefore the first description of physiological properties beyond pan-neuronal characteristics, and therefore provides strong evidence of functional maturation of ES-MNs into cells indistinguishable from in vivo MNs.

The identification of MN-selective electrophysiological phenotypes and the description of mature physiological characteristics have important implications for studying ALS pathology in vitro. First, since glutamate excitotoxicity has been identified as a potential mechanism of degeneration, it is important to rapidly achieve physiologically active motor neurons in vitro. Second, circuit and firing properties—loss of inhibition and relative vulnerability of fast vs. slow twitch motor neurons—selective to motor neurons have been implicated in ALS as well. ES-MNs have now been shown to adopt several in vivo motor neuron functional firing properties which increase the likelihood of modeling disease which is associated with connectivity and electrical activity.

Molecular changes in matured ES-MNs

Coincident with electrophysiological maturation we report progressive maturation in morphology and expression of the NF-H subunits. These characteristics have not been investigated in previous studies, and add to our electrophysiological results in suggesting that ES-MNs rapidly acquire more mature features. Surprisingly in both FACS and mitotic inhibition experiments we saw a dramatic increase in the relative proportion of $FOXP1^{+}$ ES-MNs at later timepoints. This observation could be explained by either a selective survival advantage of $FOXP1^{+}$ vs. $FOXP1^{-}$ cells or a conversion of columnar identity in favor of LMC in older cells. Our data does not strongly support either possibility preferentially. It is also possible that at later timepoints FOXP1 becomes a less specific marker for LMC identity, although there is no evidence for this in mouse or human to date. The only other report showing FOXP1 staining in hES-MN containing cultures examined cells after 9 weeks of differentiation (Patani, Hollins et al. 2011). Again, the expression was not gated for a validated motor neuron marker, but the

overall percent of FOXP1 expression, especially in the context of low HB9 efficiency, was extremely low. Future studies are needed to address this point in detail.

We also observed that LHX3 expression was extinguished in mature cultures. Whether this is explained by late down-regulation of pan-MN-progenitor LHX3 expression, the loss of $LHX3^{+}$/MMC cells, or both is not addressed by the scope of our studies. HB9 and HB9-driven GFP expression were also down-regulated in our hands at this timepoint. The down-regulation of HB9 supports a previous report in older ES-MN cultures (Lee, Shamy et al. 2007), however, the timecourse of HB9 and ISL1 down-regulation has not been carefully defined in vivo in mouse and not addressed in human. These findings suggest that early pan-MN markers may not retain their relevance as motor neurons mature and this in turn has implications for studying ES-MNs for extended periods in vitro

One important unresolved question which follows from these studies is what underpins the dramatic increase in the number of $FOXP1^{+}$ cells? As discussed we do not have experimental grounds to speculate on the relative contributions of $FOXP1^{+}$/LMC-specific survival vs. a developmental conversion from $FOXP1^{-}$ to $FOXP1^{+}$ phenotypes. Future studies should directly address this issue since it has important implications for the utility of this system and may in itself constitute an interesting LMC vs. MMC/HMC phenotype.

Morphological maturation of ES-MNs

The progressive elaboration of large and complex neurites we describe for ES-MNs has implications for modeling ALS in vitro. The extraordinary size of MNs, specifically their extremely long axons has been suggested as one characteristic leading to their selective vulnerability in ALS. Axonal dieback is one of the first clinical features of disease and suggests

a pathology which may also begin in the axon or neuromuscular junction. Deficiencies in axonal transport and accumulations of proteins and varicosities are also hallmarks of disease and were speculated to trigger the degeneration. Finally the energy demands of large cells and mitochondrial dysfunction have been identified as potentially relevant players (Boillee, Vande Velde et al. 2006). We present methods to culture ES-MNs for extended time period, to very large sizes with increasingly complex and mature morphologies, which provides a novel and appropriate cellular substrate for testing these hypotheses.

Future Directions

Searching for functional and subtype specific phenotypes

Data from mouse ES-MN studies argues that molecular motor column phenotypes are strong predictors of functional motor column phenotypes. When mouse ES-MNs were xenotransplanted to the chick neural tube they showed significant preference for column-appropriate settling position dependent on whether they had a MMC ($LHX3^+$) or LMC ($FOXP1^+$) transcriptional identity (Peljto, Dasen et al. 2010). MMC or LMC transcriptional identities also resulted in column-appropriate axial vs. limb muscle axonal trajectories (Soundararajan, Miles et al. 2006; Peljto, Dasen et al. 2010).

Will human ES-MN's with LMC vs. MMC molecular marker expression shown functional motor column-specific phenotypes? To begin to answer this question we conducted several pilot experiments to look for functional motor column-specific phenotypes. First, in a preliminary study we found that $FOXP1^+$ cells showed a larger total outgrowth than non-$FOXP1^+$ cells after FACS sorting and low density culture. While preliminary this the first in vitro evidence to date

of a human motor neuron phenotype which is potentially specific to motor neuron subtype. Second, we observed a dramatic increase in the relative abundance of FOXP1 cells in this assay, as well as when mitotic cells were killed by EdU. Third, when ES-MNs were transplanted to the chick, the incidence of $FOXP1^+$ cells was again higher than in the starting population. The relative abundance of FOXP1 vs. non-FOXP1 cells which we observed in these three different paradigms may constitute a column-specific phenotype. However we cannot say if this was the result of selective survival of $FOXP1^+$ cells, or initially-$FOXP1^-$ cells turning on FOXP1 expression. It will be of great interest to determine the mechanism underlying these results.

Our transplantation also showed many limb-projecting ES-MN axons. In the future it will be crucial to use backfills to establish whether $FOXP1^+$ putative LMC ES-MNs preferentially interpret chick axon guidance cues to seek limb muscle targets.

Motor pools

Many interesting aspect of motor neuron biology emerge at the level of the motor pool: the group of motor neurons dedicated to synapse on a particular muscle. These include later stage axon pathfinding and arborization, gene expression changes in MNs, competence to selectively engage circuit afferents (Dalla Torre di Sanguinetto, Dasen et al. 2008), as well as disease associated survival differences. For any study directed at motor pool identity or phenotype one must ask first if motor pool identities will emerge in human ES-MNs in vitro. This final level of motor neuron specificity was not addressed in these studies. However experience from mouse ES-MN differentiation predicts by analogy that they will. When mouse ES-MNs were specified to express HOXC8 and the LMC marker FOXP1, and provided with GDNF, it appeared that a *cutaneous maximus* motor pool identity emerged: $PEA3^+$ $HOXC8^+$ cells expressed ISL1 (LMC_M

marker) and not LHX1 (LMC_L marker) (Peljto, Dasen et al. 2010). Moreover, this transcriptional profile appear to be functional since PEA3 expression was dependent on exogenously added GDNF as it is in vivo. Motor pool identity emerges within the context of established columnar identity, which in turn depends upon rostrocaudal identity. Therefore our efforts to precisely identify the rostrocaudal profile of ES-MNs were a necessary prerequisite to an informed search for motor pool identities and phenotypes in vitro. For example, phrenic motor neurons which innervate the diaphragm are generated in the $HOXA5^+$ region of mouse the spinal cord. This population does not show a differential response to ALS; however its function is crucial to patient survival. Since we have established that the rostrocaudal identity of hES-MNs is dominantly focused on this HOX region, it is therefore reasonable to begin looking for phrenic motor pool motor neurons in these cultures, or in matured cultures derived from them. If phrenic motor neurons could be defined from these cultures in vitro, their specific survival requirements, naïve or in the context of ALS genotypes, could be tested in vitro. In turn this could lead to the development of new cell replacement strategies for reinnervation of diaphragm in ALS patients or for discovery of new drug candidates.

Two motor pools show a unique resilience to ALS degeneration: the oculomotor neurons of cranial motor nucleus III, and the MNs of Onuf's nucleus in the sacral spinal cord which innervate sphincters subserving urinary continence and male sexual functions. Because of the rostral bias to defined rostrocaudal subtypes in our system it is unlikely that progenitors of Onuf's nucleus MNs are present in our cultures. However since our cultures are rostrally biased, and 50% HOX-, it is not impossible that oculomotor motor neurons were generated, but we find it unlikely since different patterning cues are active in midbrain where they reside. However it

would be of great interest to pursue strategies designed to generate these disease refractory motor neurons.

Because of the scalability and reproducibility of the ES-MN differentiation protocols we have described, and the precisely defined mixture of subtypes generated, these populations may be a propitious substrate for drug screens to identify ALS pathologic pathways and drug targets within them.

Figure 3.1

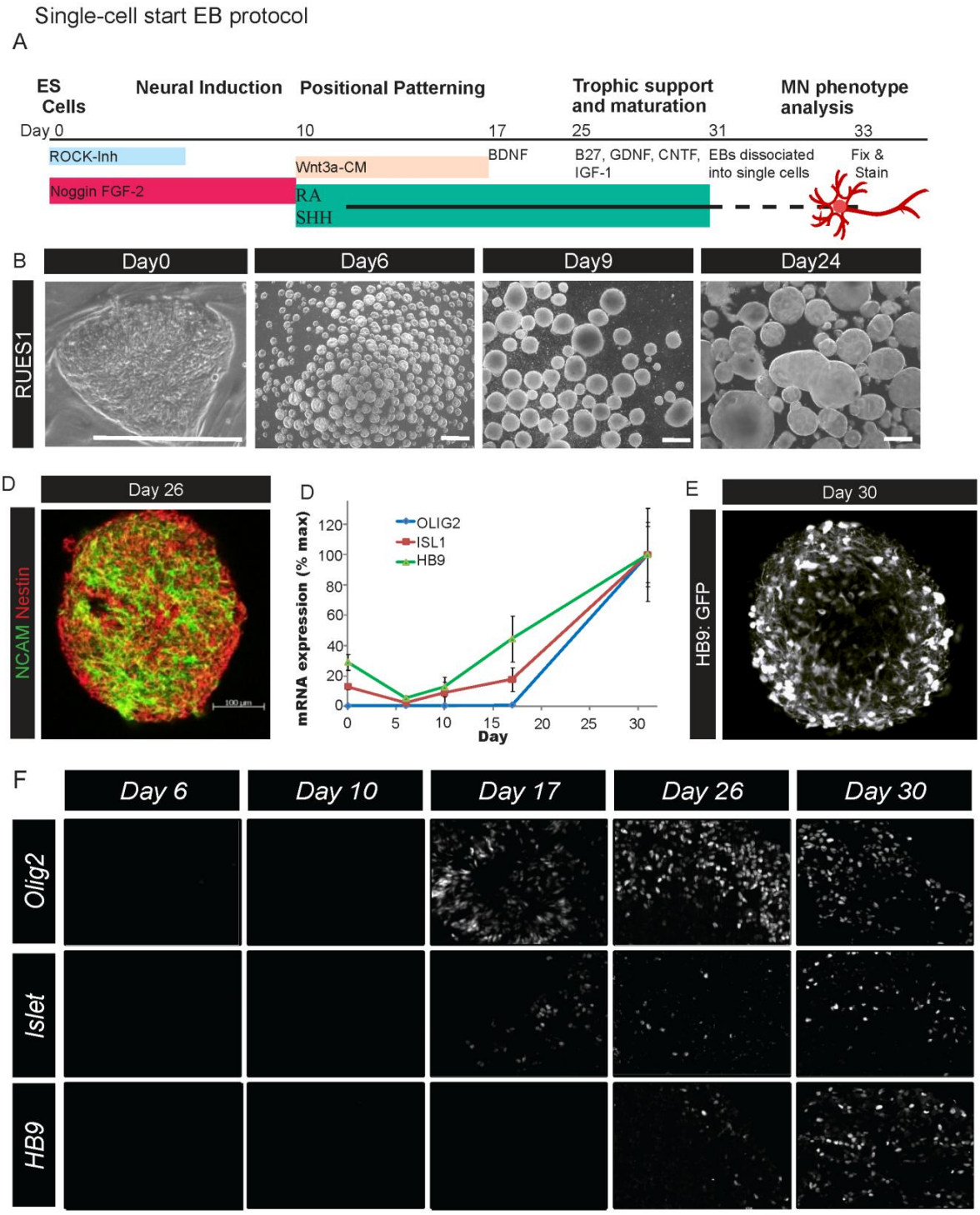
Single-cell start EB protocol
A
ES Cells
Neural Induction
Positional Patterning
Trophic support and maturation
MN phenotype analysis
Day 0
10
17
25
31
33
ROCK-Inh
Noggin FGF-2
Wnt3a-CM
RA
SHH
BDNF
B27, GDNF, CNTF, IGF-1
EBs dissociated into single cells
Fix & Stain
B
Day0
Day6
Day9
Day24
RUES1
D
Day 26
NCAM Nestin
D
mRNA expression (% max)
OLIG2
ISL1
HB9
Day
E
Day 30
HB9: GFP
F
Day 6
Day 10
Day 17
Day 26
Day 30
Olig2
Islet
HB9

Figure 3.1. Establishing a Standard Protocol for ES-MN differentiation

(A) Schematic of motor neuron differentiation protocol showing drugs, morphogens, and growth factor treatments. (B) Phase timecourse of ESC and EB morphology: day 0 typical ES colony morphology; day 6 EBs are small, uniform spheres; day 9 smoothness typical of neural spheres; day 24 large EBs showing high purity closely packed neural rosettes, scale bars 436 µm. (C) Day 26 fixed, whole-mount stained EB, 10x Apotome optical section shows some differentiated neurons (NCAM) and abundant neural precursors (Nestin), scale bar 100 µm. (D) qPCR for motor neuron lineage genes OLIG2, ISL1, and HB9, % of maximum value/gene normalized to GAPDH (mean ±SEM), n=4 independent experiments. (E) Day 30 fixed , whole-mount EB, with abundant HB9:GFP^+ ES-MNs 10x Apotome optical section, scale same as (D). (F) Representative staining of fixed EB cryosections shows ordered progression of MN-lineage protein expression.

Figure 3.2

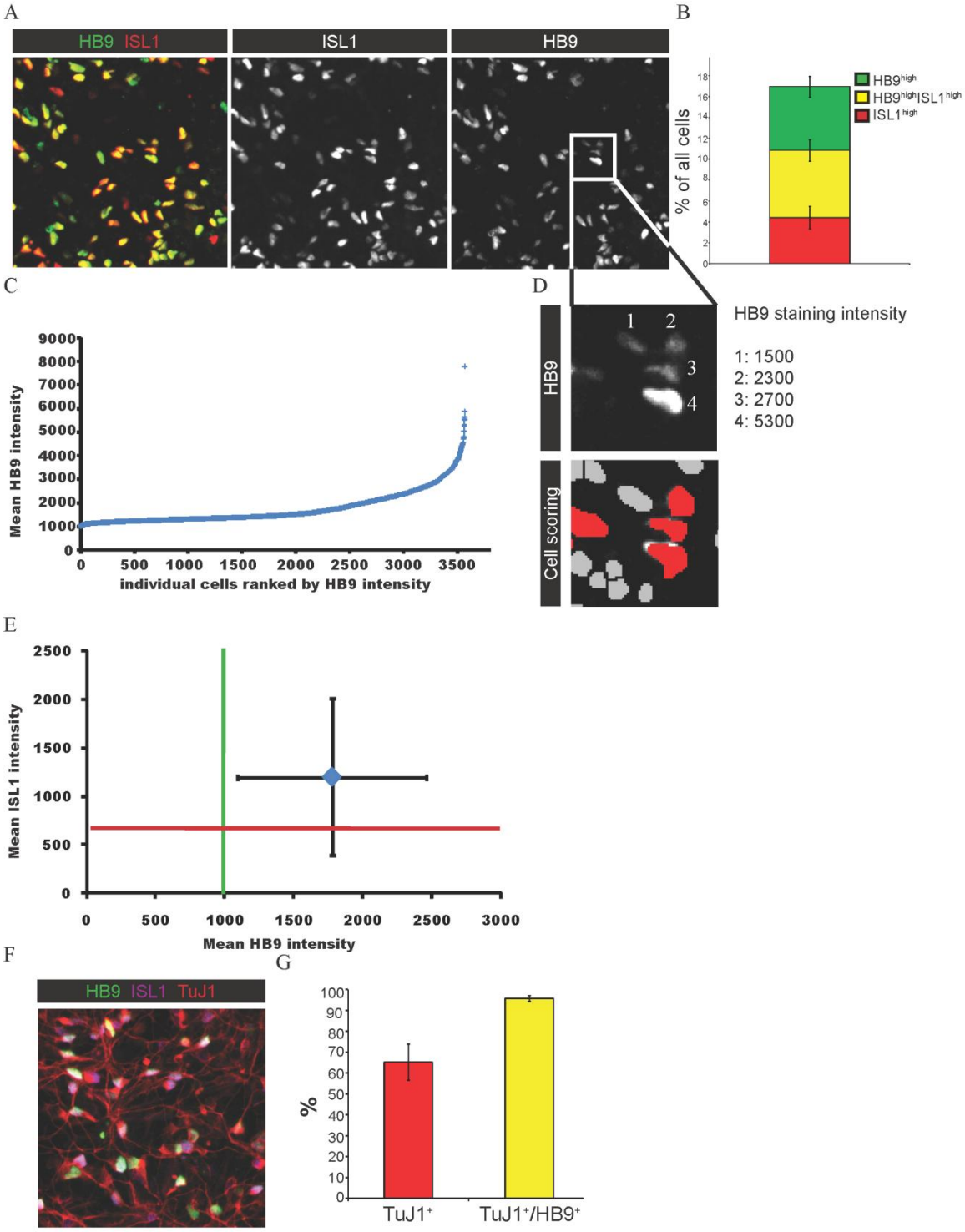
A
HB9 ISL1
ISL1
HB9
B
% of all cells
HB9high
HB9highISL1high
ISL1high
C
Mean HB9 intensity
individual cells ranked by HB9 intensity
D
HB9
Cell scoring
1
2
3
4
HB9 staining intensity
1: 1500
2: 2300
3: 2700
4: 5300
E
Mean ISL1 intensity
Mean HB9 intensity
F
HB9 ISL1 TuJ1
G
%
TuJ1+
TuJ1+/HB9+

Figure 3.2. ES-MNs are defined by expression of HB9 and/or ISL1 at varying ratios

(A) Day 33 cultures stained for HB9, ISL1 (B) % of all DAPI nuclei with high intensity staining for HB9, HB9 and ISL1, or ISL1 (mean ±SEM, n=5 independent experiments), ES-MNs exhibit a balanced, partially overlapping profile. (C-D) The wide range of mean HB9 fluorescence intensity grey levels (gl) per nucleus generates a smooth curve when (C) ranked and (D) includes high and low expressing cells (top, grey levels at left); typical Metamorph scoring result in subfield from (A) using a typical conservative 1600 gl above background threshold shows some cells scored $HB9^+$ have high intensity, some less so, and some low expressers are scored DAPI-only (grey), though most DAPI-only have no obvious HB9 signal. (E) Mean HB9 and ISL1 intensity (±SD) for the ~950 of 3500 cells ranked in (C) which were $HB9^+$ and/or $ISL1^+$ shows an equally broad range of intensities for both markers within "ES-MN" population which is similar to the profile for MNs in vivo (Fig. 2.5). Colored lines indicate background intensity ISL1 (red) and HB9 (green). (F) $HB9^+$ and $ISL1^+$ cells are neurons by morphology and TuJ1 staining. (G) 65% of all cells in culture were neurons and 95% of $HB9^+$ cells were neurons, (mean ±SEM, n=5 independent experiments).

Figure 3.3

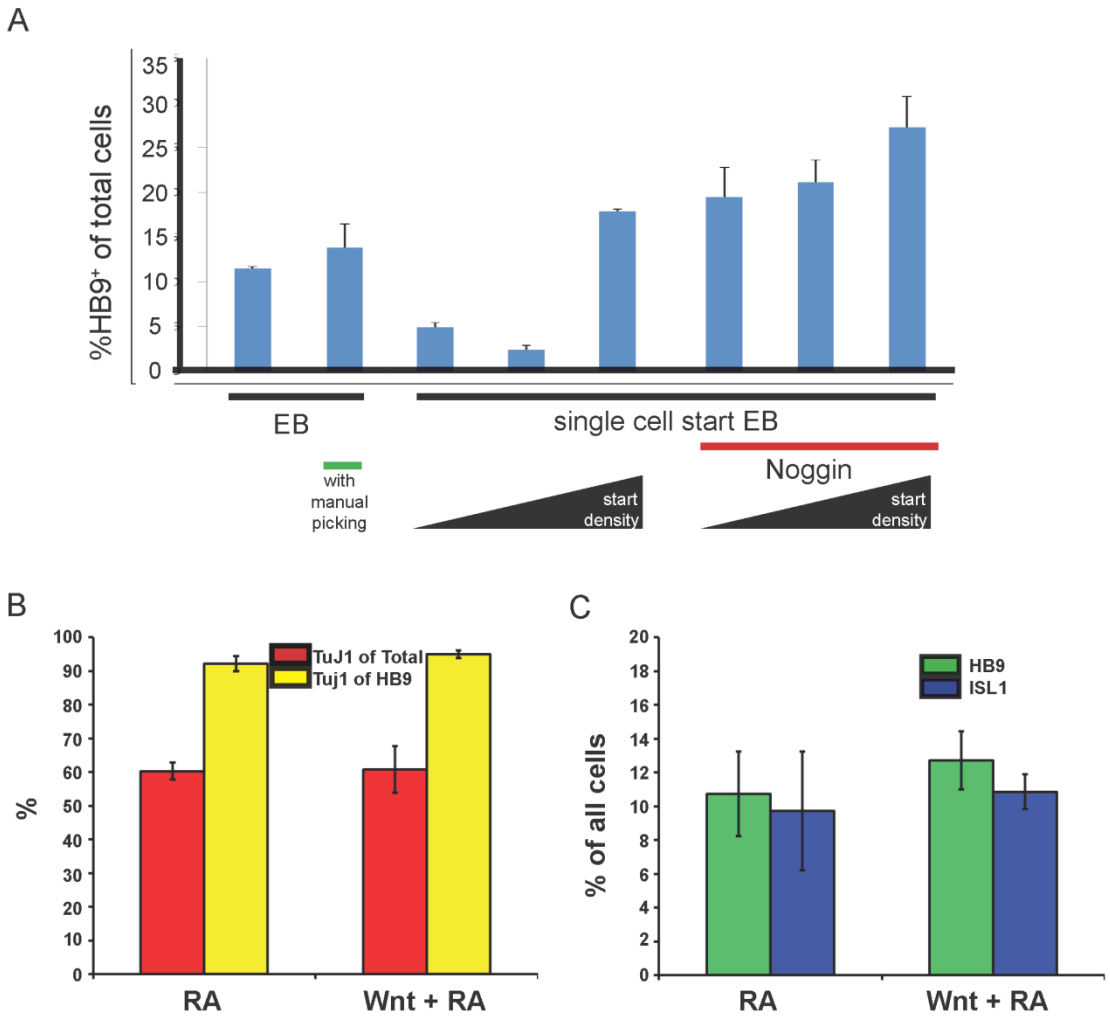
A
%HB9+ of total cells
35
30
25
20
15
10
5
0
EB
single cell start EB
with manual picking
start density
Noggin
start density
B
%
100
90
80
70
60
50
40
30
20
10
0
TuJ1 of Total
Tuj1 of HB9
RA
Wnt + RA
C
% of all cells
20
18
16
14
12
10
8
6
4
2
0
HB9
ISL1
RA
Wnt + RA

Figure 3.3. Optimization of a Standard Protocol for ES-MN differentiation

(A) Single cell seeding and Noggin enhance motor neuron differentiation efficiency. % $HB9^+$ of total cells, (mean of 8 fields/condition ±SEM, n=1 experiment) shows Standard Protocol (single cell start) protocol is the most efficient tested when supported by Noggin. Higher density is more efficient and much more efficient than traditional EB protocol even with manual selection (day 17-28) for rosettes; single-cell start densities tested: 0.1, 0.2, 0.4M cells/ml. (B) Wnt3a-conditioned medium(CM) had no significant effect on neuronal differentiation, % TuJ1 of total cells (red), or the neuronal identity of $HB9^+$ cells, %TuJ1 of $HB9^+$ cells (yellow) (mean ±SEM n=4 independent experiments, t-tests, p=0.66 and 0.79 respectively. (C) Wnt3a-CM also had no effect of on the efficiency of motor neuron differentiation % HB9 (green) or %ISL1 (blue) of total cells, (mean ±SEM, n=4 independent experiments), t-tests p=0.93 and 0.37 respectively.

Figure 3.4

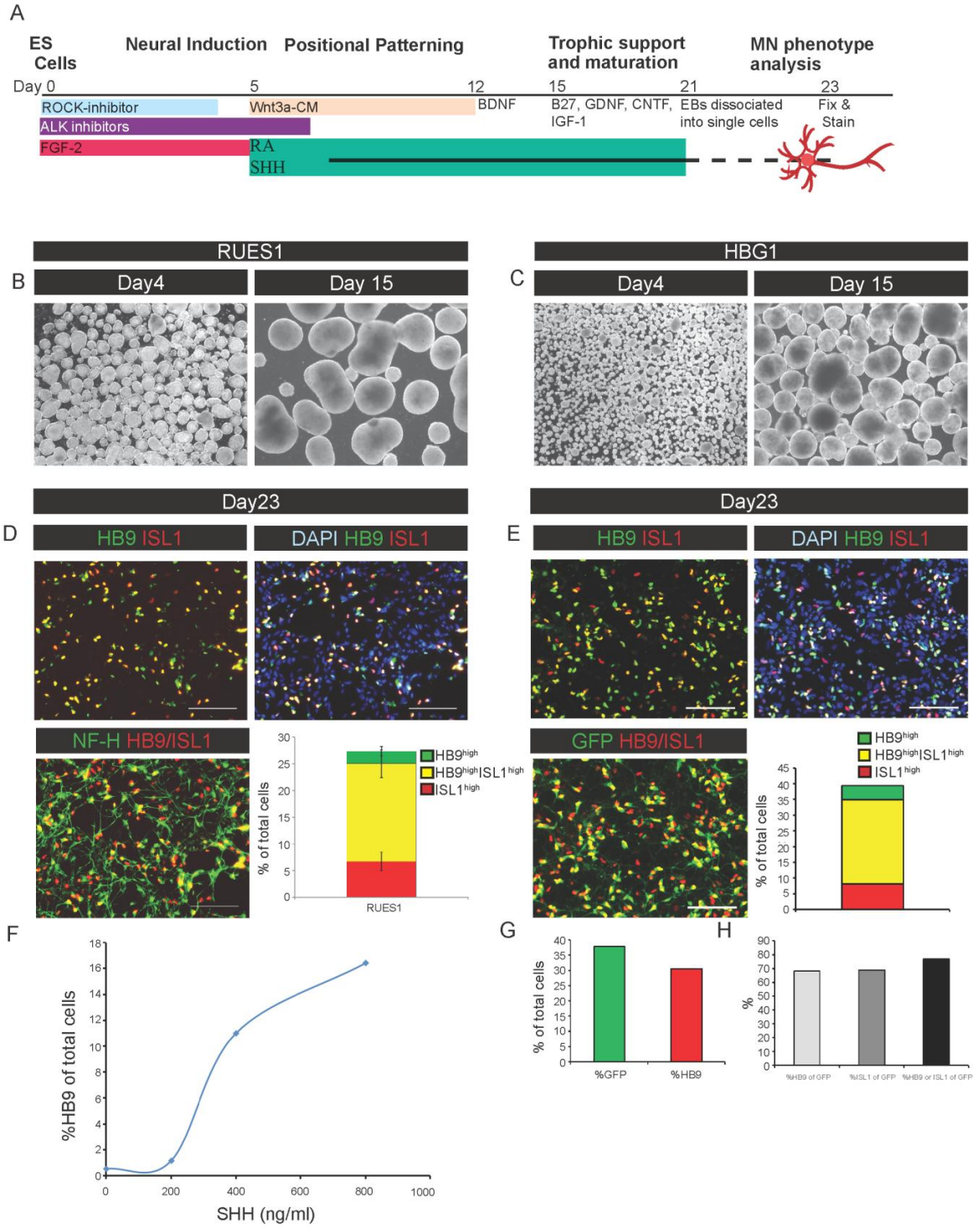
A
ES Cells
Neural Induction
Positional Patterning
Trophic support and maturation
MN phenotype analysis
Day 0
5
12
15
21
23
ROCK-inhibitor
ALK inhibitors
FGF-2
Wnt3a-CM
BDNF
B27, GDNF, CNTF, IGF-1
EBs dissociated into single cells
Fix & Stain
RA
SHH
RUES1
HBG1
B
C
Day4
Day 15
D
E
Day23
HB9 ISL1
DAPI HB9 ISL1
NF-H HB9/ISL1
GFP HB9/ISL1
% of total cells
HB9high
HB9high ISL1high
ISL1high
RUES1
F
G
H
%HB9 of total cells
SHH (ng/ml)
%GFP
%HB9
%

Figure 3.4. Defining an Accelerated Protocol for high efficiency ES-MN differentiation

(A) Schematic of Accelerated protocol for the differentiation of ES-MNs showing drugs, morphogens, growth factors, and time. (B-C) EBs were homogeneous and smooth when small (day 4) and after expansion (day15) for both (B) RUES1 and (C) HBG1 (HB9:GFP) ES lines, 4x phase-2 (D-E) Accelerated protocol generates ES-MNs at high purity by day 23 from both RUES1, 27% $HB9^+$ or $ISL1^+$ of total cells (mean ±SEM, n=3 independent experiments), and HBG1, 40% (n=1 experiment), with normal partial overlap of these markers. (F) Accelerated Protocol can be used to optimize reagents and test differentiation conditions: dose response curve for recombinant SHH protein shows activity plateau at 800ng/ml, no MNs with negative control or 200ng/ml, n= 1 experiment, mean of 8 fields/condition. (G-H) HBG1 HB9:GFP reporter retains high fidelity to endogenous HB9 expression under this protocol (70% of GFP^+ cells express HB9 or express ISL1, while 80% express one or the other motor neuron marker, n=1 experiment).

Figure 3.5

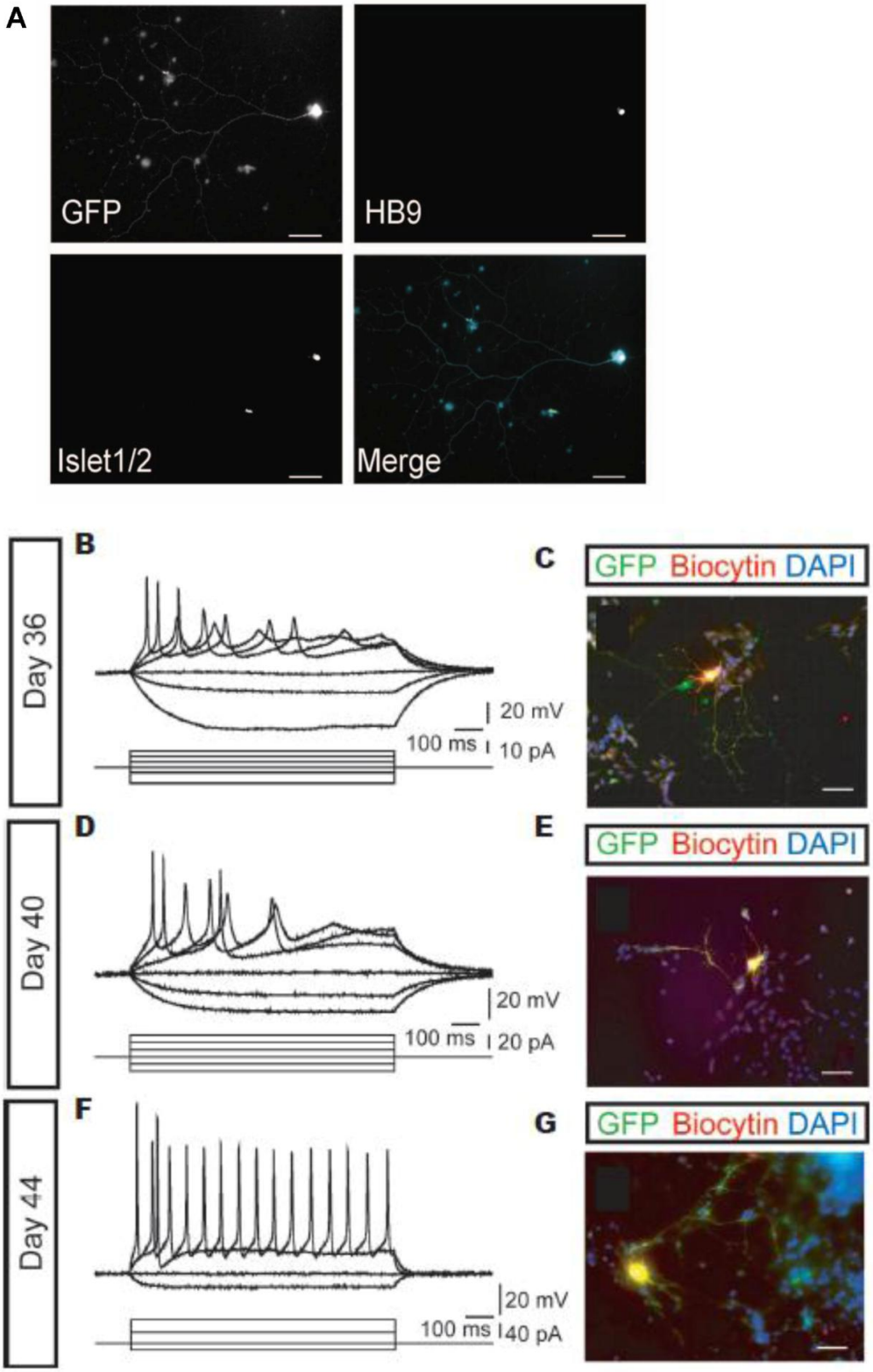
A
GFP
HB9
Islet1/2
Merge
Day 36
B
C
GFP Biocytin DAPI
20 mV
100 ms
10 pA
Day 40
D
E
GFP Biocytin DAPI
20 mV
100 ms
20 pA
Day 44
F
G
GFP Biocytin DAPI
20 mV
100 ms
40 pA

Figure 3.5. ES-MNs progressively acquire action potential firing capacity

(A) Representative image of day 36 HBG47 BAC-HB9:GFP human ESMNs showing mature neuronal morphology and coexpression of GFP with motor neuron marker HB9 and ISL1, scale bar 50 μm (B,D,F) Current-clamp voltage recordings of representative cells show GFP^+ ES-MN action potential spiking increases consistently over 13 days, bottom traces show injected currents. (C,E,G) all recorded cells were injected with biocytin and example cells and GFP^+ status was confirmed by post-staining. Scale bars 50 μm.

Figure 3.6

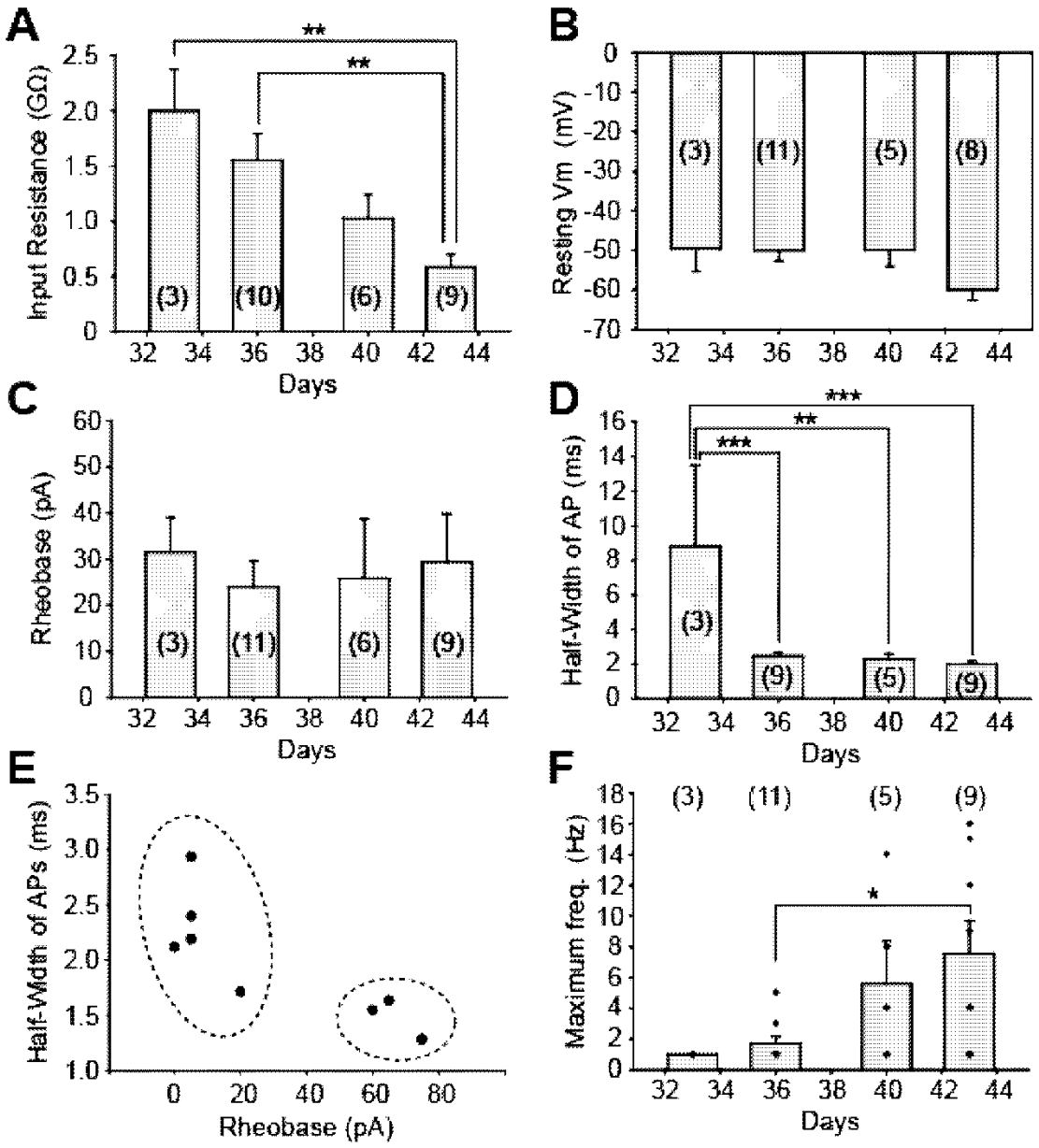
A
Input Resistance (GΩ)
Days
(3)
(10)
(6)
(9)
B
Resting Vm (mV)
(3)
(11)
(5)
(8)
C
Rheobase (pA)
(3)
(11)
(6)
(9)
D
Half-Width of AP (ms)
(3)
(9)
(5)
(9)
E
Half-Width of APs (ms)
Rheobase (pA)
F
Maximum freq. (Hz)
(3)
(11)
(5)
(9)

Figure 3.6. Progressive maturation in passive and active ES-MN membrane properties

(A) Input resistance decreased over time in vitro (n = 28, $P < 0.01$, one-way ANOVA). ** $P < 0.01$, Tukey's *post hoc* test. (B) Resting membrane potential and (C) rheobase did not change (n = 27 and 29, respectively). Rheobase was defined as the current step magnitude required to activate the minimum number of action potentials. Positive current steps were in 5 pA increments to distinguish small difference in rheobase among individual neurons. (D) Half-width of action potentials (APs), measured at 50% of peak amplitude at rheobase, changed over time in vitro (n = 26, $P < 0.001$, one-way ANOVA). ** $P < 0.01$, *** $P < 0.001$, Tukey's *post hoc* test. (E) hESMNs at 43 days (n= 8) appeared to be divided into two distinct populations: neurons having small rheobase with narrow APs, and neurons having large rheobase with wide APs. (F) Maximum frequency of APs after current injection increased over time *in vitro* (n = 28, $P < 0.05$, one-way ANOVA). * $P < 0.05$, Tukey's *post hoc* test. Dots shows frequency values for individual neurons. The numbers in parenthesis indicate the number of neurons used for analysis taken from 22 dishes in total.

Figure 3.7

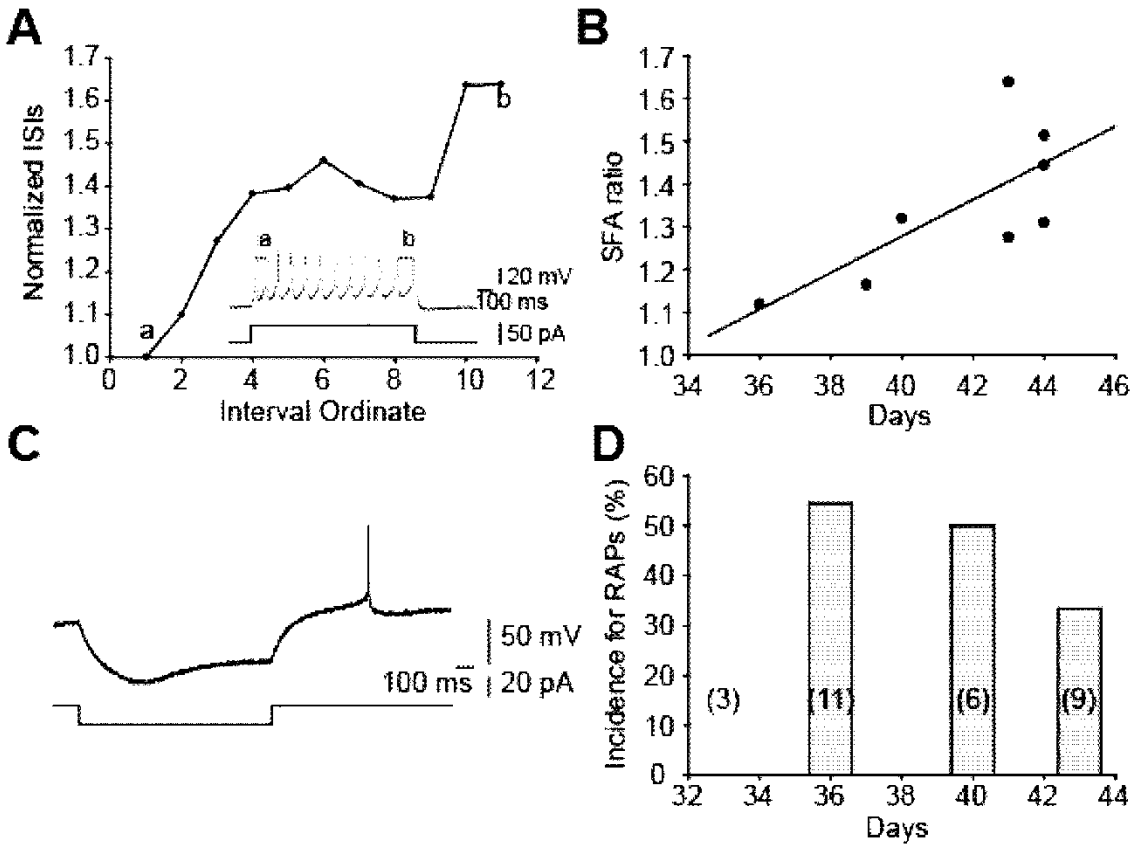
A
Normalized ISIs
Interval Ordinate
a
b
120 mV
100 ms
50 pA
B
SFA ratio
Days
C
50 mV
100 ms
20 pA
D
Incidence for RAPs (%)
(3)
(11)
(6)
(9)
Days

Figure 3.7. ES-MNs display two characteristic features of in vivo motor neuron firing

ES-MNs displayed spike frequency adaptation (SFA), and rebound action potentials (RAPs). (A) Inter spike intervals (ISIs) after positive current injection increased gradually during 1 sec steps. ISIs were normalized to the first ISI. Inset shows APs (upper) and injected currents (bottom). APs between which 'a' and 'b' ISI values were measure are indicated in the inset as a and b, respectively. (B) SFA ratio, calculated as the maximum value of normalized ISIs after any amplitude of positive current injection, increased developmentally ($n = 8$, $R = 0.73$, $P < 0.05$, Pearson's linear regression). (C) RAPs were observed in a subset of hESMNs . Upper trace shows voltage change after negative current injection. Bottom trace shows injected negative current steps. RAP follows the return of current to baseline after the hyperpolarizing step. (D) Incidence of RAPs in hESMNs at 4 different ages ($n = 29$). Negative current steps with 5 pA increments (to at least 20 pA) were injected while checking for RAPs.

Figure 3.8

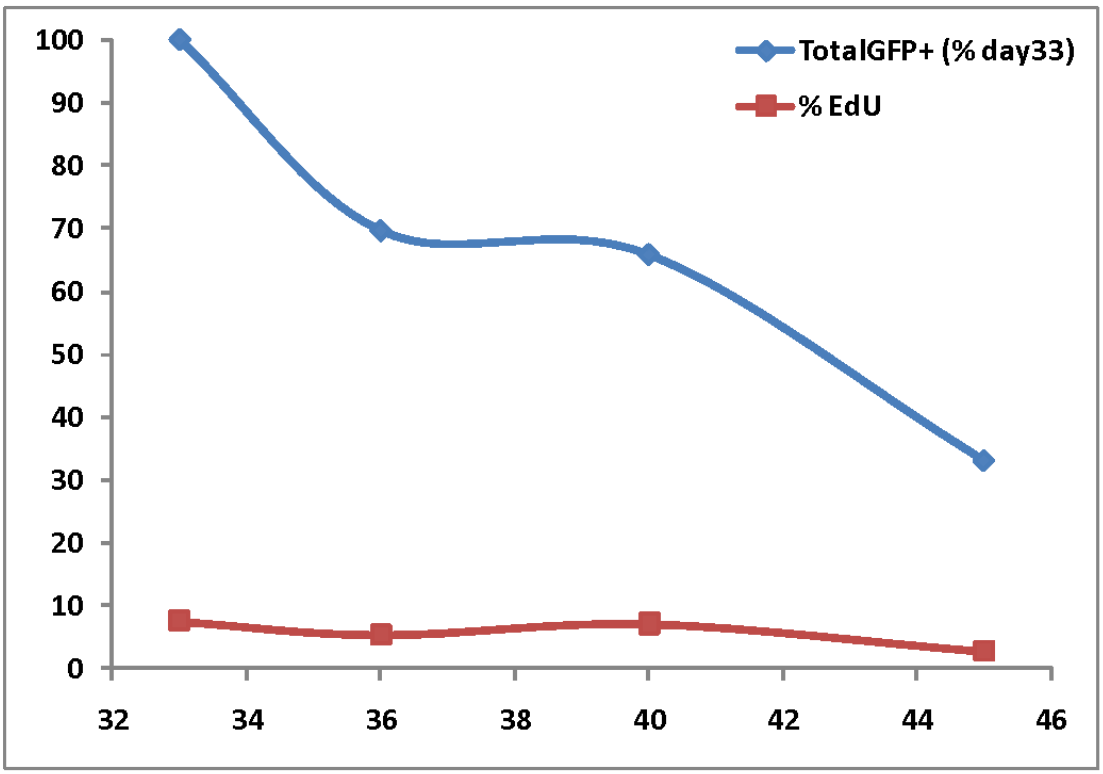

Figure 3.8. EdU inhibits motor neurogenesis

Fewer than 10% of ES-MNs (%Edu of GFP, red) costained for EdU; scattered flat non-neuronal cells with very large (>60 µm diameter) nuclei were internal positive control for EdU labeling. Total GFP^+ ES-MN numbers declined steadily (323, 312, 135, and 105 cells at day 33, 36, 40, and 45 respectively), % of day 33 (blue), in stark contrast to the much high numbers in parallel cultures without EdU (362, 405, 300, 265 cells at days 33, 36, 40, and 45 respectively). This accords with unpublished data Nuno Lamas and Bethany Kerner, Project ALS lab, however they report larger increases in cell numbers rather than the relatively steady state that we observed.

Figure 3.9

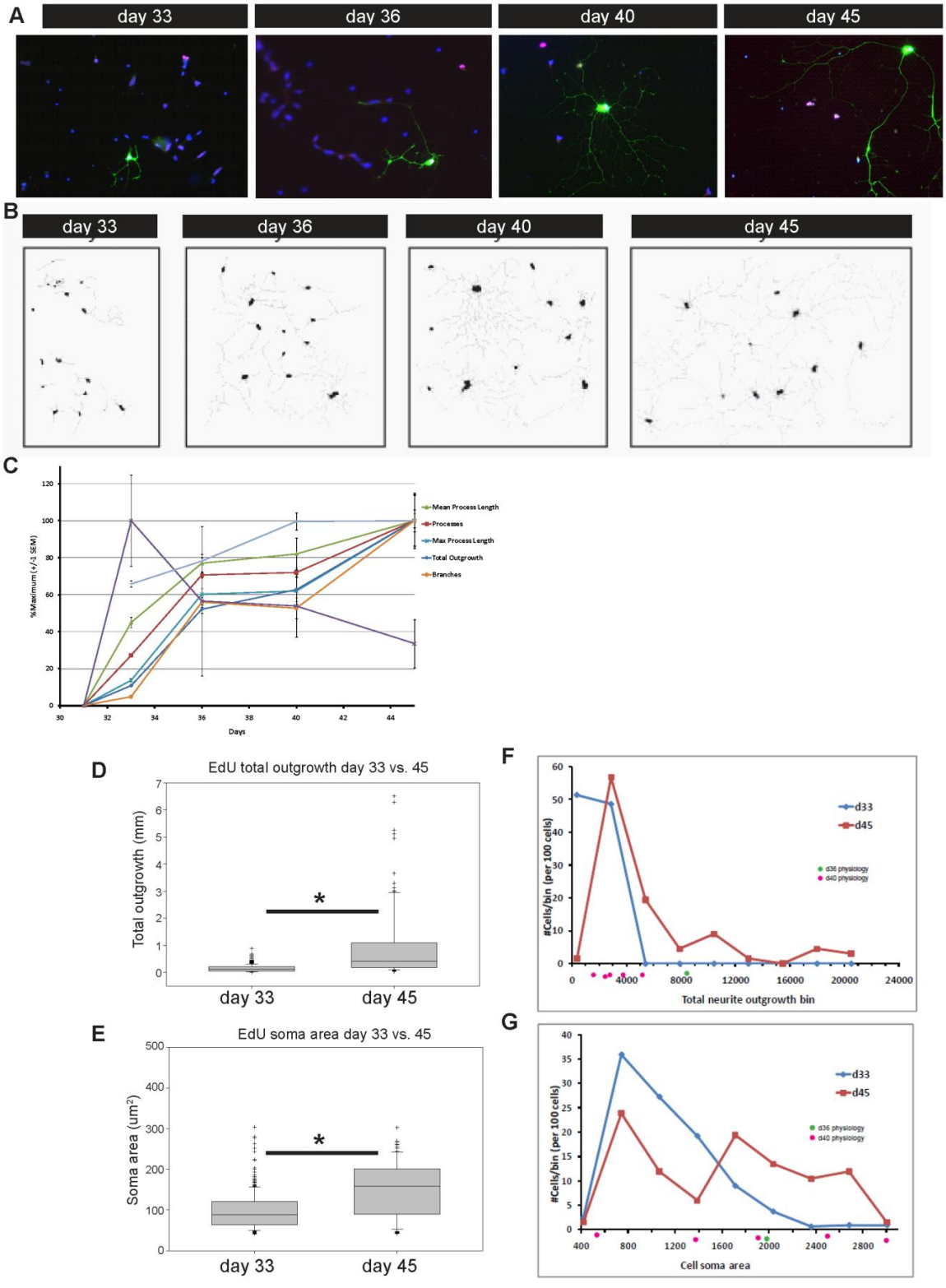
A
day 33
day 36
day 40
day 45
B
day 33
day 36
day 40
day 45
C
%Maximum (+/-1 SEM)
Days
Mean Process Length
Processes
Max Process Length
Total Outgrowth
Branches
D
EdU total outgrowth day 33 vs. 45
Total outgrowth (mm)
day 33
day 45
E
EdU soma area day 33 vs. 45
Soma area (um²)
day 33
day 45
F
#Cells/bin (per 100 cells)
Total neurite outgrowth bin
d33
d45
d36 physiology
d40 physiology
G
#Cells/bin (per 100 cells)
Cell soma area
d33
d45
d36 physiology
d40 physiology

Figure 3.9. Progressive morphological maturation of ES-MNs

(A) Representative images of HBG47 BAC-HB9: GFP^+ ES-MNs cultured with EdU and stained for GFP (green) and HB9 (red) show progressive elaboration of increasingly complex projections between day 33 and 45. (B) Metamorph automated neurite tracing was performed on all GFP^+ neurons on two coverslips (n=323-105 cells/timepoint, n=1 experiment). Camera lucida traces from the first 10 fields encountered show qualitative increases in outgrowth and complexity. (C) Mean cell body size, neurite outgrowth length and complexity increased over the timecourse (mean % of maximum value/metric +/-SEM, n=323, 312, 135, and 105 cells at days 33, 36, 40, and 45, respectively, in one experiment). We confirmed zero values for the >100 cells counted by hemacytometer after dissociation at day 31 for number of neurites, branches, and total outgrowth, therefore these metrics include a day31 nominal 0 value (D-E) Total mm of neurite outgrowth (D) and um^2 soma area (E) increased significantly between day 33 and 45 (mean/cell) Mann-Whitney Rank Sum Test $P < 0.001$, black line is median, grey boxes 25th-75th percentiles, whisker bars 10^{th}-90th percentiles, and outliers individual hashes. (F-G) Total neurite outgrowth per cell (F) and cell soma area (G) Population histograms, normalized to 100 cells, for day 33 and day 45, revealed many cells with only modest increases, but a population of cells with much larger outgrowth and soma area. Backfilled cells from physiology experiments (Fig. 3.5) which were successfully recovered for staining (n=6), were subjected to morphometry and plotted on population histogram in the appropriate bins showing that physiology studies were performed on cells with broad range of soma areas but not in the larger component for outgrowth (day 33, blue; day 45, red).

Figure 3.10

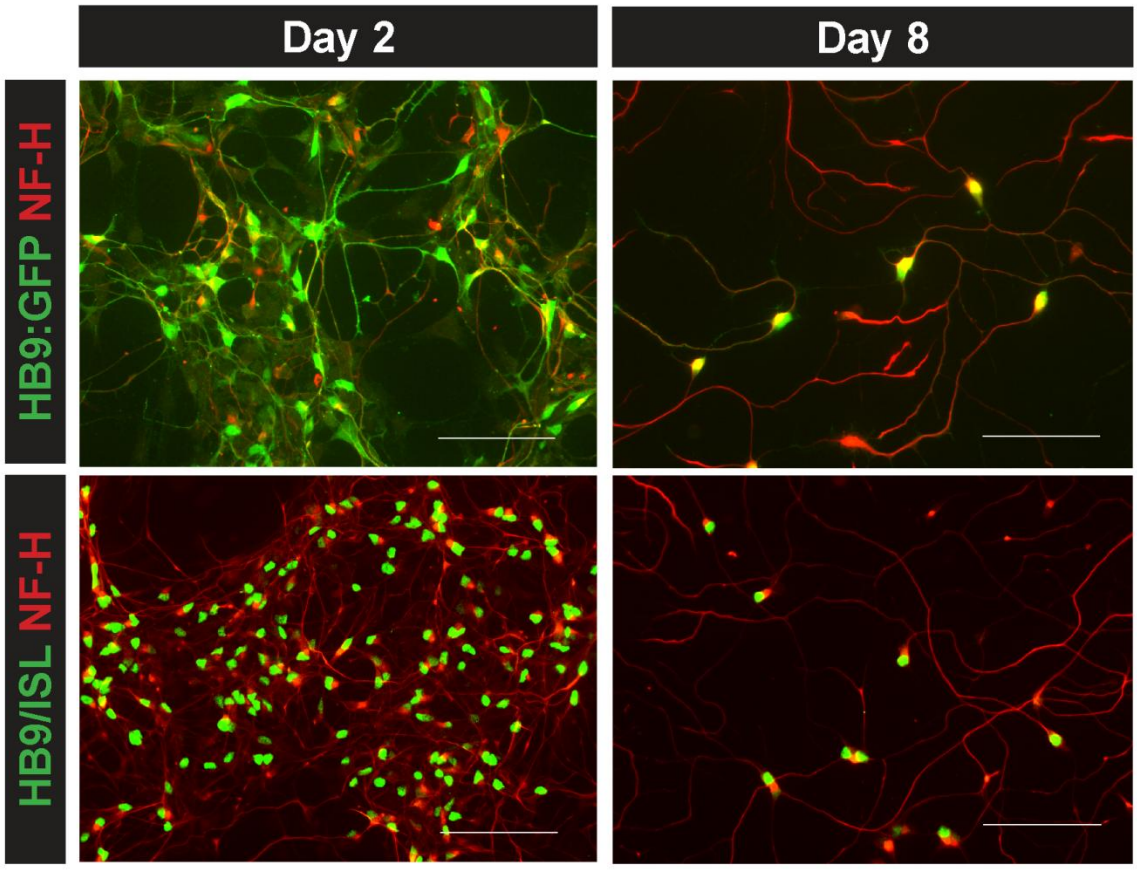

Figure 3.10. ES-MNs rapidly acquire mature NF-H expression profile

Accelerated Protocol ES-MNs HBG1(HB9:GFP) (top) or RUES1 (bottom, HB9/ISL) seeded at day 21 at high density (0.5M/12mm coverslip) and fixed two days later (day 2) showed moderate intensity NF-H staining in only a little over half of cells, however ES-MNs seeded at low density (0.05M/12mm coverslip) , incubated with EdU for 8 days with a 2/3 media change at day 4 and then fixed, all showed high intensity NF-H staining in all observed cells. With mitotic inhibition ES-MN purity was greatly increased: almost all (>80%) of NF-H$^+$ cells were GFP$^+$ or HB9$^+$/ISL1$^+$. This clear qualitative result was consistent across 3 independent experiments, n>100 cells examined/ experiment at day8. Scale bar 100 µm.

Figure 3.11

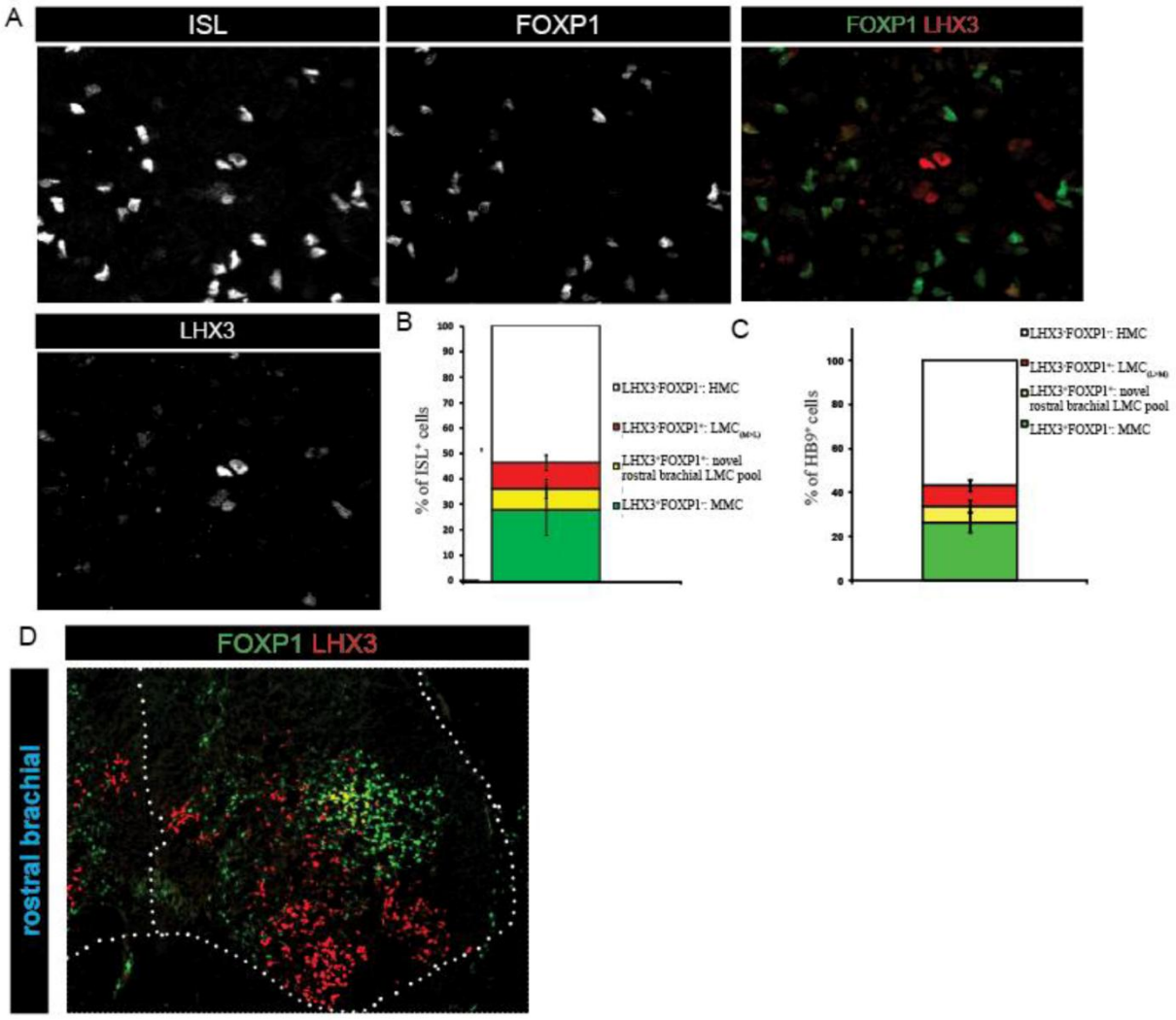

Figure 3.11. ES-MNs express marker combinations matching all in vivo motor columns

(A) Standard Protocol RUES1 ES-MN differentiations were stained for ISL1 (or HB9, not shown), FOXP1, and LHX3 to determine the presence and frequency of putative motor column subtypes. (B-C) $ISL1^{+}$ (B) or $HB9^{+}$ (C) cells which showed quantitatively high intensity staining for FOXP1 only, LHX3 only, neither, or both, correspond to the expression profiles of human LMC, MMC, HMC, and the novel $HOXA5^{+}$ brachial pool shown in Fig. 2.6 and again here. (mean ±SEM, n=4 independent experiments).

Figure 3.12

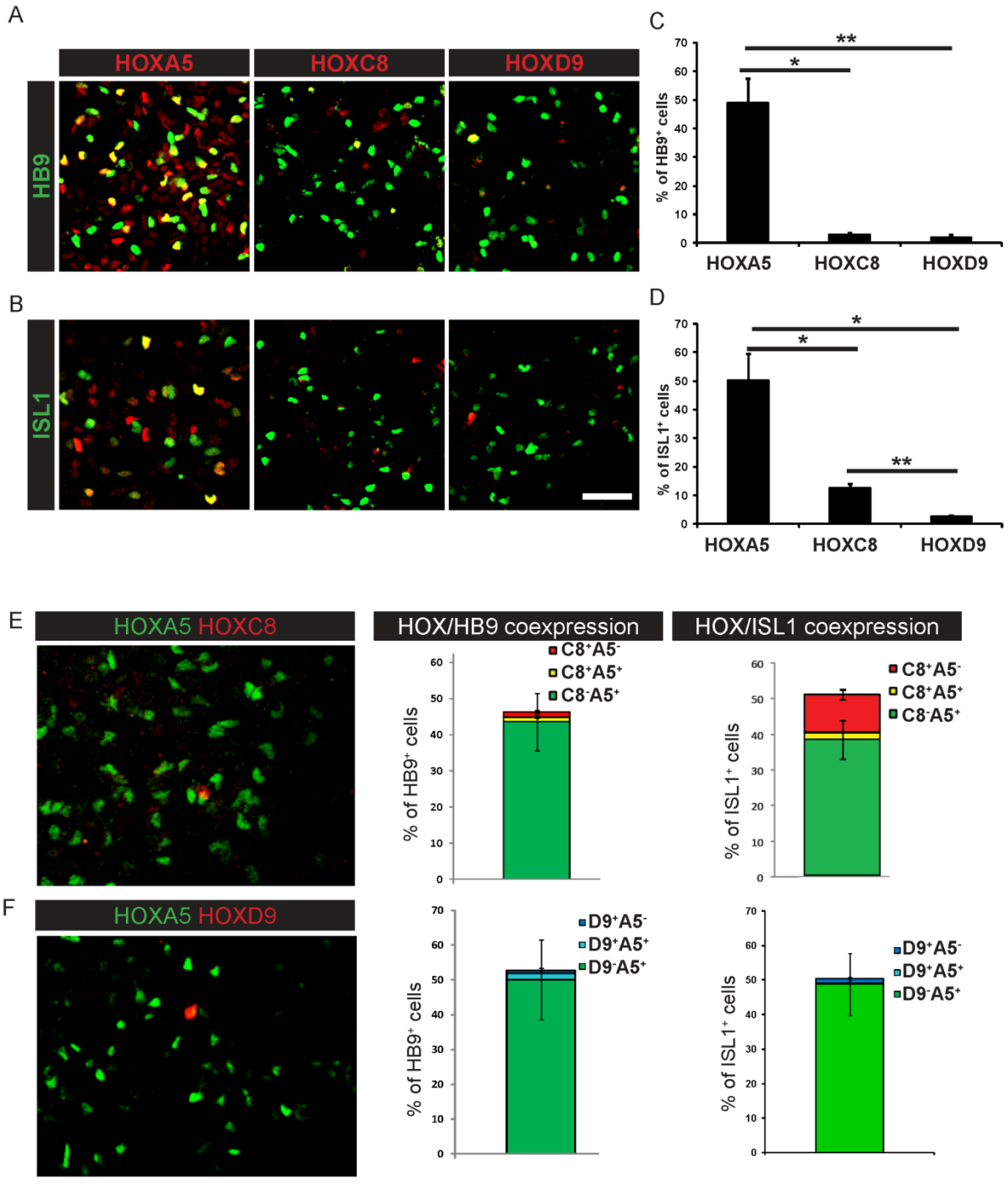
A
HOXA5
HOXC8
HOXD9
HB9
B
ISL1
C
% of HB9⁺ cells
HOXA5
HOXC8
HOXD9
D
% of ISL1⁺ cells
HOXA5
HOXC8
HOXD9
E
HOXA5 HOXC8
HOX/HB9 coexpression
HOX/ISL1 coexpression
C8⁺A5⁻
C8⁺A5⁺
C8⁻A5⁺
% of HB9⁺ cells
% of ISL1⁺ cells
F
HOXA5 HOXD9
D9⁺A5⁻
D9⁺A5⁺
D9⁻A5⁺
% of HB9⁺ cells
% of ISL1⁺ cells

Figure 3.12. ES-MNS express predominantly HOXA5 and exclude HOX-protein coexpression

(A) Day 32 Standard Protocol RUES1 ES-MNs were stained for HB9 (A, red) or ISL1 (B, red) and HOXA5 (green), HOXC8 (green), or HOXD9 (green) to profile their rostrocaudal identities, scale bar 50 μm. Both HB9 (C) and ISL1 (D) MNs were predominantly $HOXA5^+$ (45% and 50% respectively), and only small percentages coexpressed HOXC8 (3% and 13% respectively) or HOXD9 (3% and 3% respectively), indicating a dominantly cervical identity. (mean ±SEM, n=4 except n=3 for HB9 HOXA5 HOXD9 stain. Significant differences were found between the % of $HB9^+$ or ISL^+ cells stained for HOXA5 vs. either HOXC8 or HOXD9; and also the % of ISL^+ cells which stained for HOXC8 vs. HOXD9. (E-F) When cultures were costained for HB9 or ISL1(not shown) and both HOXA5(green) and HOXC8 (red) or HOXA5 and HOXD9 (red) we observed that fewer than 5% of $HB9^+$ or $ISL1^+$ cells positive for either HOX gene coexpressed the other (yellow bar for $HOXA5^+HOXC8^+$, aqua bar for $HOXA5^+HOXD9^+$). (mean ±SEM, n=4 independent experiments). Statistical Analyses: *$p<0.05$ for unequal variance Rank Sum test for all comparisons except $HB9^+HOXA5^+$ vs. $HB9^+HOXD9^+$, and $ISL1^+HOXC8^+$ vs. $ISL1^+HOXD9^+$, where equal variance test passed $p<0.05$ and t-test was used, * $p<0.05$.

Figure 3.13

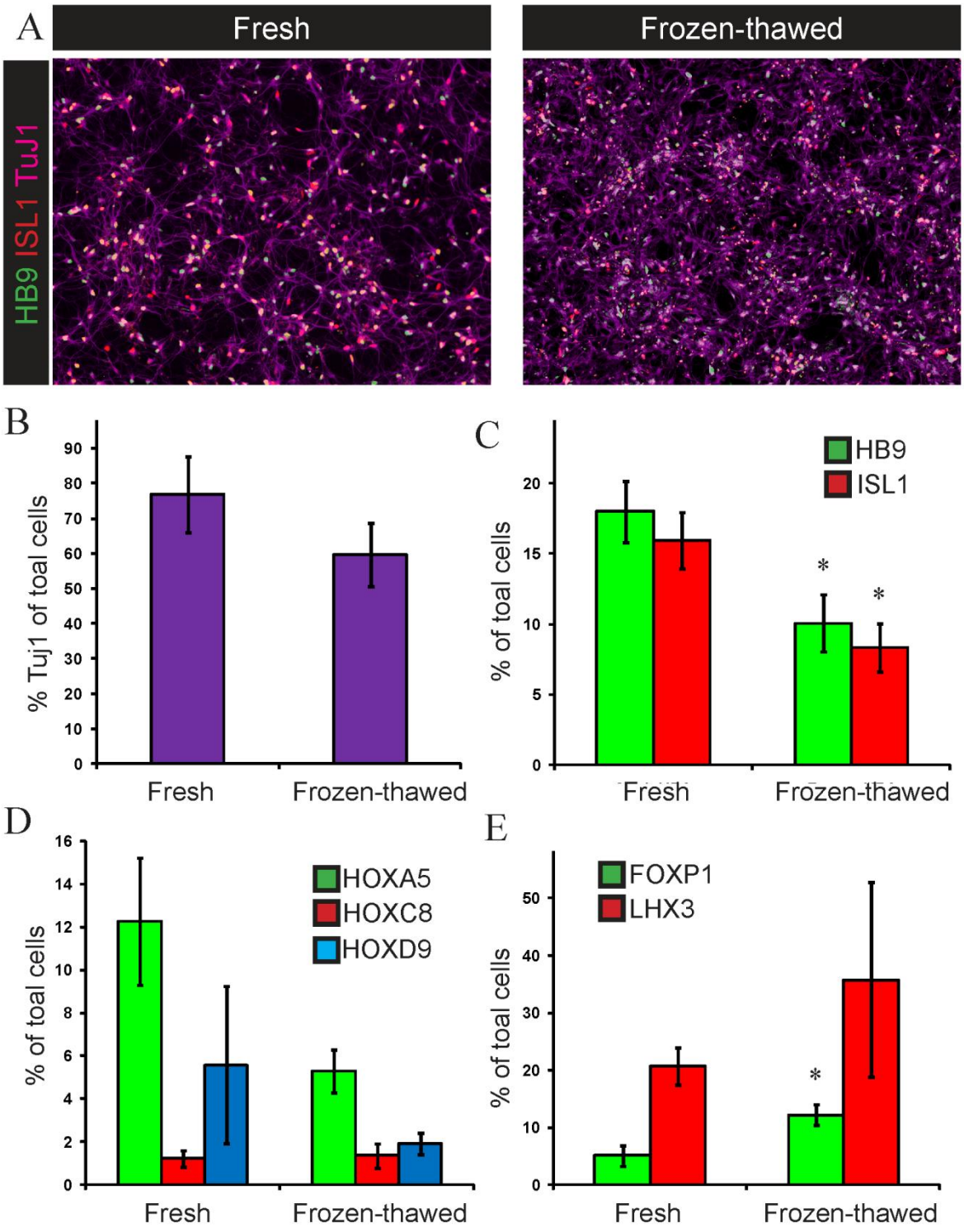
A
Fresh
Frozen-thawed
HB9 ISL1 TuJ1
B
% Tuj1 of toal cells
0
10
20
30
40
50
60
70
80
90
Fresh
Frozen-thawed
C
% of toal cells
0
5
10
15
20
HB9
ISL1
*
*
Fresh
Frozen-thawed
D
% of toal cells
0
2
4
6
8
10
12
14
16
HOXA5
HOXC8
HOXD9
Fresh
Frozen-thawed
E
% of toal cells
0
10
20
30
40
50
FOXP1
LHX3
*
Fresh
Frozen-thawed

Figure 3.13. ES-MNs can be cryopreserved with limited effects on subtype identity

(A) Day 31 RUES1 Standard Protocol ES-MNs from the same experiment were either seeded for fixation and analysis at day33, or cryopreserved, thawed and seed for analysis at +2 days; both cultures showed abundant live ES-MNs neurons by $Tuj1^+$ morphology and HB9, ISL1 staining. (B) The mean $\%Tuj1^+$ of total cells was decreased but not significantly t-test $p>0.05$, (mean ±SEM , n=3 experiments). (C) The percentage of $HB9^+$ or $ISL1^+$ of total cells were significantly reduced (t-tests, $p<0.05$), but many ES-MNs survived (mean ±SEM, n=5 experiments). (D) surviving cells showed reduced percentage of HOXA5 and HOXD9 cells, but no changes were significant (mean ±SEM; HOXA5, n=5 fresh, n=3 frozen; HOXC8, n=4; and HOXD9, n=3 fresh, n=4 frozen, t-tests, $p>0.05$). (E) Surviving cells showed an increased %FOXP1 and LHX3 of total cells (mean ±SEM ; FOXP1, n=5; LHX3, n=2 fresh, n=3 frozen) which was significant in the case of FOXP1 (t-test, $p<0.05$).

Figure 3.14

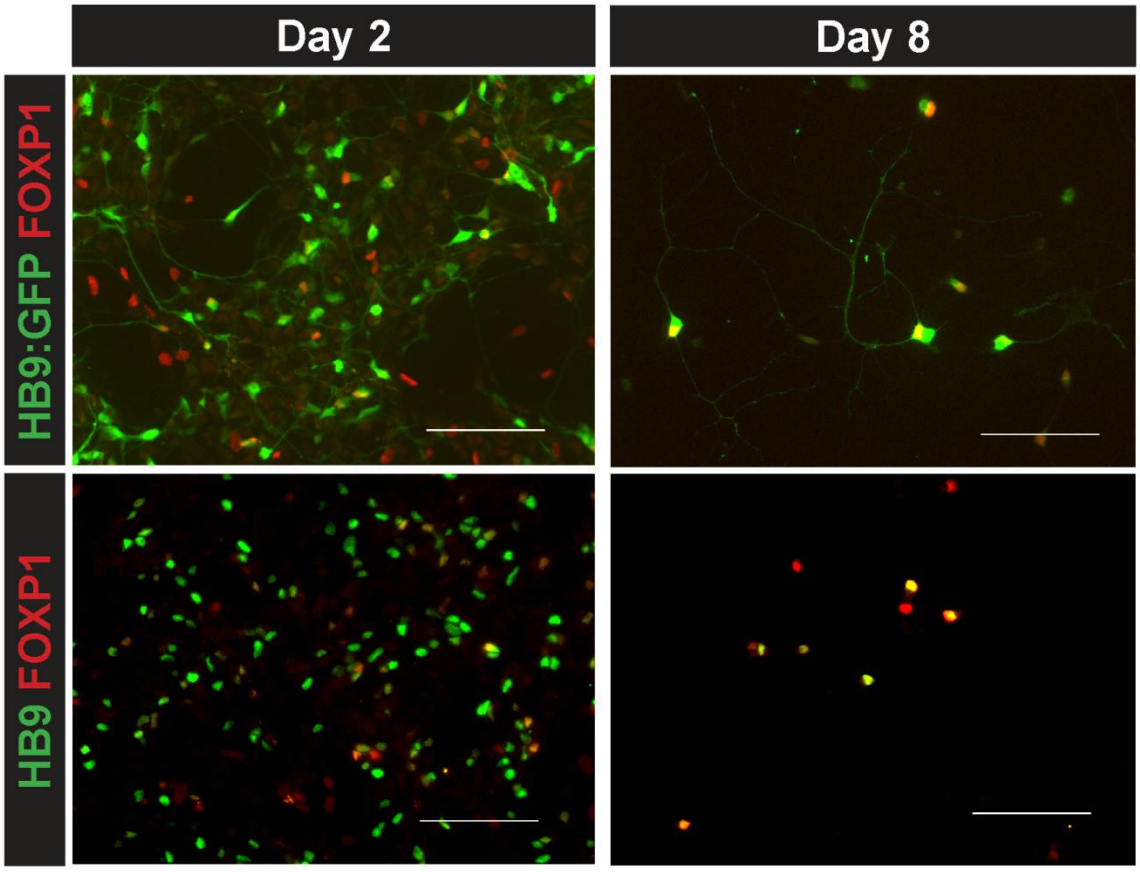

Figure 3.14. ES-MN in matured cultures are predominantly FOXP1^{+}

Accelerated Protocol HBG1(HB9:GFP) (top) or RUES1 (bottom) ES-MNs seeded at high density (0.5M/12mm coverslip) and fixed at day 2 show the normal 5-10% range of %FOXP1 of ES-MNs we have described above. However when seeded at low density and matured for 8 days in the presence of EdU, almost every ES-MN examined (n>100 cells for each of 2 ESC lines in 1 experiment/line) stained intensely for FOXP1. In addition these cultures were stained for LHX3 (not shown) which identified abundant ES-MNs at day 2, but almost no MNs at day 8. This clear qualitative result was consistent with 3 other independent experiments. Scale bar 100 µm.

Figure 3.15

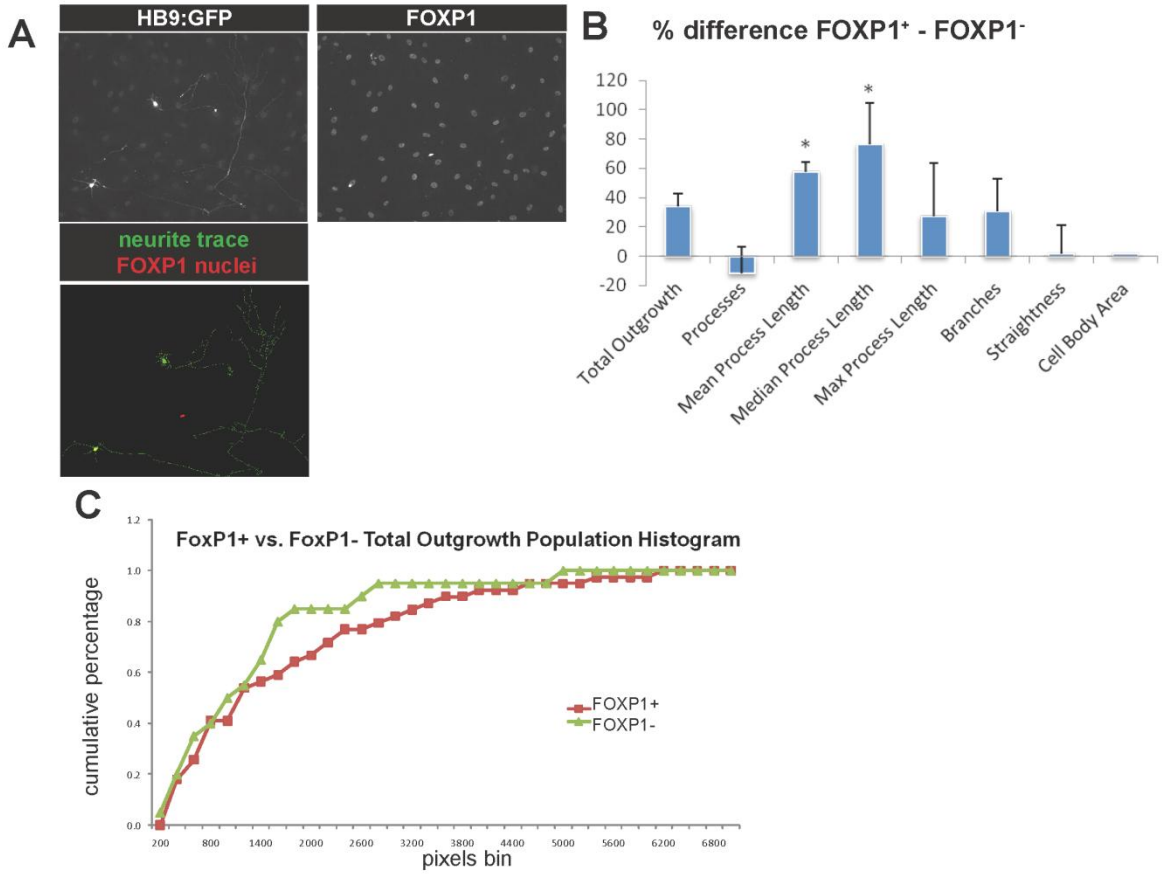
A
HB9:GFP
FOXP1
neurite trace
FOXP1 nuclei
B
% difference FOXP1+ - FOXP1-
120
100
80
60
40
20
0
-20
Total Outgrowth
Processes
Mean Process Length
Median Process Length
Max Process Length
Branches
Straightness
Cell Body Area
C
FoxP1+ vs. FoxP1- Total Outgrowth Population Histogram
cumulative percentage
pixels bin
FOXP1+
FOXP1-

Figure 3.15. FOXP1^{+} ES-MNs show a subtype-specific morphological phenotype

(A) HBG1 (HB9:GFP) Standard Protocol ES-MNs were FACS sorted for GFP and seeded at ultra low density (0.01 M/12 mm coverslip) onto confluent layers of commercially available human fetal spinal cord astrocytes in one pilot experiment. After 12 days 72% of surviving ES-MNs showed intense FOXP1 staining, while LHX3 could not be detected (not shown), field width 900 µm. We also observed that astrocyte nuclei showed very weak but above background FOXP1 staining. (B) FOXP1^{+} cells (n=39) showed significantly (t-tests $p<0.05$) longer mean and median process lengths and trend increases in all other aspects of neurite outgrowth, but no change in cell soma area compared to FOXP1^{-} cells (n=20); Metamorph neurite outgrowth morphometry was paired with a custom interactive journal to score celsl for FOXP1 and analyze neurite outgrowth. Any GFP cells in direct contact with other GFP cells were manually excluded from analysis (C) Cumulative percentage population histogram showed that FOXP1^{+} cells had the same proportion of smaller cells, but more cells with much longer outgrowth (0.66 µm/pixel).

Figure 3.16

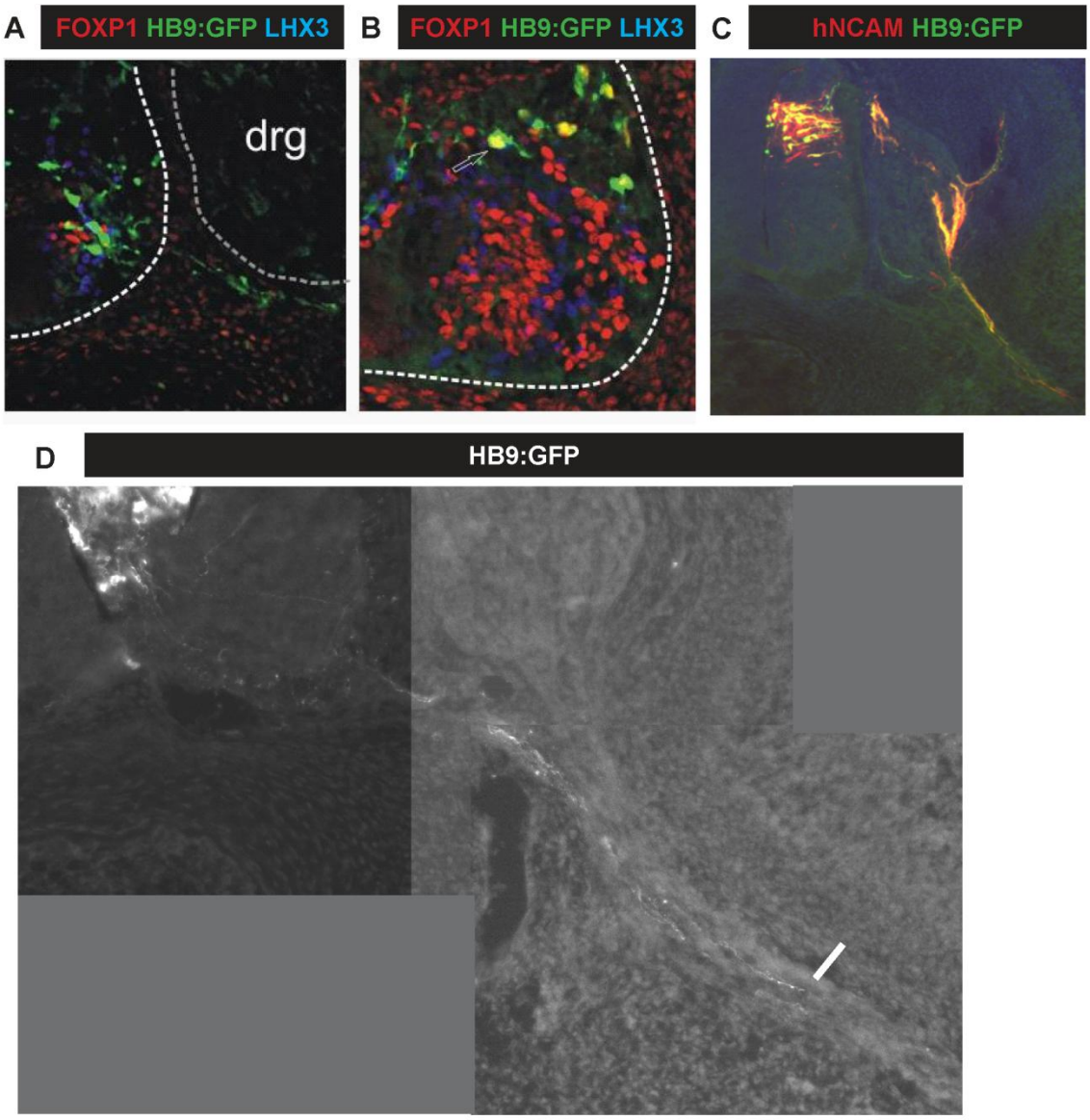
A
FOXP1 HB9:GFP LHX3
drg
B
FOXP1 HB9:GFP LHX3
C
hNCAM HB9:GFP
D
HB9:GFP

Figure 3.16. Human ES-MNs respond to in vivo cues in xenotransplant to chick spinal cord.

(A-D) Standard Protocol HBG1 (HB9:GFP) ES-MNs were transplanted to the prospective brachial level of HH stage 15-16 embryos and allowed to develop for 2-3 days. When chicks were sacrificed and cryosectioned we observed GFP^+ human cells in many embryos (n=8 of 16 surviving embryos). Many GFP^+ also expresssed FOXP1, and some but fewer which expressed LHX3. Human ES-MNs extended projections (>1.8 linear mm in C and D) through ventral roots (A, C, D) or ectopic dorsal exit point in the case of one dorsal transplant (C) and in most cases along motor nerve paths and often into the limb (C, D).

Chapter 4. Motor neuron differentiation from human induced pluripotent stem cells: comparison to embryonic stem cells, sources of variability and motor neuron subtype diversity

Introduction

The discovery that somatic cells could be reprogrammed to a pluripotent state opened the door to the study of previously unavailable cell types with relevance to human disease (Takahashi and Yamanaka 2006). The precise genotype of patients with disease could now be captured in a pluripotent cell with the potential to generate unlimited quantities of affected cell types in vitro (Park, Arora et al. 2008; Lee, Papapetrou et al. 2009; Soldner, Hockemeyer et al. 2009). ALS-iPSC lines were among the first human lines generated from patients because the human motor neurons affected in ALS were not otherwise available and their differentiation from human ES cells had been established. Subsequent studies, however, have reported differences between iPSC and ESC lines. In order for ALS-iPS-MNs to become a productive tool to model ALS it will be necessary to determine the reproducibility with which they can generate motor neurons. In addition it will be necessary to show that motor neurons derived from iPSC are bona fide motor neurons and capable of functional maturation. Our first goal was therefore to generate a large test set of iPSC lines and compare these to ESC lines for their ability to generate motor neurons. Second, we wanted to establish that motor neurons generated from iPSCs were functional and met specific criteria established by in vivo studies and for ESC-derived motor neurons. Third, we designed this test set so that we could ask if several key variables, which

would routinely be encountered when building disease models, affect the performance of iPSC lines.

Are iPSC lines comparable to ESC lines in making motor neurons?

Several concerns have been raised about the general comparability of iPS to ES cells. Some groups have reported epigenetic and gene expression differences between iPS and ES cells, potentially the result of incomplete reprogramming or epigenetic memory of their somatic cells of origin (Chin, Mason et al. 2009; Doi, Park et al. 2009; Taura, Noguchi et al. 2009; Armstrong, Tilgner et al. 2010; Ghosh, Wilson et al. 2010; Grigoriadis, Kennedy et al. 2010; Stadtfeld, Apostolou et al. 2010; Tokumoto, Ogawa et al. 2010; Xi, Khalil et al. 2010). From the perspective of modeling ALS in vitro, the most relevant and troubling report concluded that iPSC lines have categorically and substantially lower rates of neural induction and more variable differentiation to motor neurons compared to ESC lines (Hu, Weick et al. 2010). This study, however, used a relatively small number of iPSC lines, which limits the strength of conclusions about the general and motor neuron-specific comparability of iPS to ES cells. Therefore a larger study which methodically addressed these issues was required.

Does individual genetic background influence iPSC performance?

The small sample sizes of previous comparative studies have also limited the investigation of potential sources of variability between iPSC lines. This issue is no less acute in the case of ESC lines, where many studies have described large variability between lines. The sources of this variability are poorly understood. Methods of derivation, culture, and differentiation vary widely. However because of the extremely limited availability of fertilized embryos from which ESC lines have been derived, and the lack of control over or publication of demographic

variables, it has not been feasible to study the contributions of these variables to ESC performance. iPSC lines on the other hand are easily derived from any individual and it is therefore now possible to begin to ask what impact demographic factors and individual genetic background have on stem cell properties. Understanding these effects will have major implications for the use of iPS-derived cell types to study cellular physiology and disease models. Studies of a large number of iPS lines distributed across several demographic variables which will be commonly encountered as researchers undertake disease modeling are required.

We have seen that some variability among ES lines may be related to the method of derivation. However a direct test of this idea is not possible since it is possible to derive a line only once from a unique embryo. Multiple iPSC lines however can be derived from the same donor. Studying multiple lines from the same donor in comparative studies should contribute two related insights. First, this could help define the extent of variability associated with the one-time event of reprogramming since all lines will start from the same individual genotype. At the same time, if conserved properties are found between lines from the same donor vs. other donors, this would provide the first demonstration of the effect of human genetic background on pluripotent cell properties and differentiation potential. Studies aimed at assessing sources of variability should therefore also include multiple iPSC lines derived from the same donor.

Are iPS-MNs functionally comparable to ES-MNs?

The last question raised by studies of gene expression and epigenetic differences between iPSC and ESCs is whether terminally differentiated cells will be functionally compromised in important ways. For example we have seen that ES-MNs acquire a specific set of dominantly cervical HOX-protein identities, and that HOX-proteins are mutually excluded from individual

ES-MNs as they are by motor neurons in vitro. Since HOX-protein mutual exclusion is a principal mechanism by which limb-innervating motor pool identity is acquired, it is important that iPS-MNs not only respond similarly at the first level to patterning cues (by expressing HOXA5 in response to RA for example) but that the subtleties of gene expression are also preserved (mutual HOX-exclusion). We have also defined the short timecourse during which ES-MNs acquire electrophysiological activity in vitro, which mirrors important aspects of motor neuron physiology in vivo. If iPS-MNs are to be used to model disease in which electrophysiological activity may play a role, it is important that iPS-MNs are able to attain functional electrical properties matching or relevant to motor neurons in vivo as well. While many groups have now reported the expression of pan-motor neuron transcription factors in iPS-MNs, the rostrocaudal HOX subtype and HOX exclusion have not been tested. And while others (Hu and Zhang 2009; Karumbayaram, Novitch et al. 2009; Hu, Weick et al. 2010) have shown that iPS-MNs can acquire functional physiological properties, this has not been done systematically on a large set of iPS lines. It was therefore important to ascertain if iPS-MNs would display in vivo-like transcriptional identities, and to test their functional maturation.

Statement of Contributions

This chapter contains work which was highly collaborative; performed exclusively by collaborators; or led and performed almost entirely by myself at the experimental level, in that order. Figures 4.1, 4.2, 4.3 (with the exception of Figure 4.3D which was performed by myself contemporaneously), and 4.4A were adapted from a publication by the Eggan Laboratory, and the experiments described therein were performed entirely by members of the Eggan Laboratory

as described in the published manuscript (Dimos, Rodolfa et al. 2008) with the following exceptions: for this publication I optimized skin biopsy and fibroblast culture methods and initiated and maintained cultures with technical help from Mary Lee; I also adapted and optimized motor neuron differentiation and staining protocols which did not appear in, but contributed to the technical basis for this publication. The remaining figures are adapted from (Boulting, Kiskinis et al. 2011) and Figure 4.18 from (Bock, Kiskinis et al. 2011) with the exception of my unpublished data (Fig. 4.4B-D, and Fig. 4.8). GFC performed biopsies and fibroblast cultures with technical help from Mary Lee, and some help from Annie Hon, MWA, and DHO. CTR and JTD reprogrammed all iPS lines. GLB and EK initially expanded all iPS lines and GFC, Annie Hon, MWA, and DHO expanded early passage lines at the PALS lab. FACS experiments of day 0 and day 29 cells were optimized and overseen by GFC with technical advice from KTR and some technical help from MWA, and analyses were performed by DJK with help from GFC, MWA, and DHO. Standard motor neuron differentiations in the PALS lab were performed by MWA and GFC with some help from DHO. Optimal motor neuron differentiations were performed by MWA and GFC. HOX analyses were performed by GFC and MWA. ABM, DJW, and DHO designed and carried out $Ca2^{+}$ imaging experiments. BJW, GLB, and CJW performed physiological recordings. MY assisted with teratomas. LD assisted with quantitative cell scoring of imaging data in the Eggan Lab. MWA and GFC performed quantitative cell scoring of imaging data in the PALS lab. Southern Blots were performed by GFC and MWA with technical advice from Andrew Sproul (NYSCF) and the Eggan lab. Statistical analysis was performed by GFC, with the following exceptions: FACS statistics performed by DHO, and sex difference ANOVA by MWA, 2 correlations performed by EK. GLB and EK led and contributed equally to all other experiments in the Eggan Laboratory.

Scorecard analyses of iPS lines was conducted entirely in the Meissner/Eggan laboratories as described in their publication (Bock, Kiskinis et al. 2011).

Results

iPS-MNs and iPS-astrocytes: proof of principle experiments

iPS cells from older ALS patient donors are pluripotent

Since ALS is an adult-onset disease it was important to determine whether iPSC lines could be derived from ALS patients of advanced age, and to show that these lines could generate cell types of disease relevance. We therefore obtained informed consent and cultured ALS patient skin biopsies to derive primary fibroblast cultures (Fig. 4.1A) (Dimos, Rodolfa et al. 2008). Cultures were transduced with 4 reprogramming factors and after several weeks colonies with ES-like morphology were observed (Fig. 4.1B). These colonies stained with conventional markers of human ES and iPS cells (Fig. 4.11C, and (Dimos, Rodolfa et al. 2008)) These lines showed the same genetic mutation in the SOD1 gene (L144F) as the patient donor (data not shown, (Dimos, Rodolfa et al. 2008)) confirming that they were generated from patient fibroblasts. Under a non-directed spontaneous differentiation protocol (Fig. 4.2A) these iPSC lines demonstrated pluripotency by generating cells expressing proteins indicative of differentiation to all three primary germ layers (Fig. 4.2B). We concluded from these data that age and disease status were not obstacles to generating iPSC lines from ALS patients. We next asked if these lines could generate the cell types of primary interest for modeling ALS in vitro, motor neurons and astrocytes.

ALS patient-derived iPS cells are competent to generate motor neurons

To test the ability of patient-derived iPS cells to generate spinal motor neurons we applied a standard protocol from the Zhang lab used to induce motor neurons from human ES cells (Li, Du et al. 2005) described in Chapter 3, with minor modifications. Retinoic acid was used to induce caudal, and SHH to induce ventral positional identity, and we maintained EBs in suspension until dissociation or seeding, rather than manually select rosettes (Fig. 4.3A). When these cultures were stained for the markers of pan-MN identity, HB9 and ISL1, we observed that 20% of cells expressed HB9, and 90% of these co-expressed ISL1 (Fig. 4.3B). The neuronal identity of these cells was confirmed by strong reactivity for the neuronal marker βIII-tubulin (TuJ1) and neuronal morphology (Fig. 4.3C, D) and over half of $HB9^{+}$ cells stained for the MN-neurotransmitter synthetic enzyme ChAT (not shown). We concluded from these data that patient-derived iPS cells were capable of generating motor neurons. We next asked if astrocytes, which manifest a strong toxicity for motor neurons in mouse models of ALS in vivo (Boillee, Vande Velde et al. 2006) and mouse and human in vitro models of ALS (Di Giorgio, Carrasco et al. 2007; Nagai, Re et al. 2007; Di Giorgio, Boulting et al. 2008), could also be generated from ALS-iPS cells.

iPS cells are competent to generate astrocyte-like cells

To determine the ability of patient-derived iPS cells to generate astrocytes we assessed the expression of the astrocytic marker glial fibrillary acidic protein (GFAP). At the same timepoint that the above iPS-MN phenotype was observed (~40days of differentiation) many cells that stained strongly for GFAP had small somata and few and very long processes suggestive of a radial glial rather than astrocytic identity (Fig. 4.4A). Cells with similar morphology also stained

for the radial glia antigen RC-2 (not shown) at this timepoint, supporting this idea. Since gliogenesis begins around 3-4 months in human in vivo (Bayer and Altman 2002), we maintained cultures for this time in vitro with infrequent passaging. After 120 days we observed that nearly all cells in the culture displayed flattened multipolar astrocytic morphology, most expressed GFAP in all possible permutations with the early astrocyte marker CD44 and the glial progenitor marker Vimentin (Fig. 4.4B-D). While astrocyte generation was not the focus of our studies, and this novel qualitative result was not quantified, and further gene expression and functional analysis would be required to substantiate an astrocytic identity, we concluded from these experiments that ALS-iPS cells were capable of giving rise not only to motor neurons, but to cells with key molecular and morphological features of astrocytes as well.

Establishing a test set of iPSC lines

In order to address general concerns about the comparability of iPS and ES cells, specific concerns about reduced motor neuron differentiation efficiency, and test potential sources of variability, we set out to construct a large "test set" of iPSC lines. We generated 14 new iPSC lines, which, combined with the 2 lines reported above were derived from seven different donors, healthy or diagnosed with ALS, male and female, and whose ages ranged from 29 to 82 years (Table 4.1). All 14 new lines were generated by 3-factor reprogramming, i.e., without c-MYC, to allow us to test for the impact of this oncogene by comparison to the two previously described iPSC lines. To determine if individual genetic background had a strong impact on phenotype we included several independent lines derived from the several individual donors. To compare iPSC lines as a group to ESC lines we included 6 well-characterized ESC lines.

All test set iPSC lines are pluripotent

To determine whether these iPS cell lines met the established criterion for human ES cells we first assayed them using standard assays for marker expression and functional pluripotency. All iPSC colonies showed classical ESC-like cellular and colony morphology, stained for cell-surface, cytoplasmic, and nuclear markers of pluripotency, and showed active cell-cycle parameters similar to ESC controls (Fig. 4.5A, B, C). All iPSC lines generated cells from all 3 embryonic germ layers in undirected differentiation (Fig. 4.5D) and all tested lines formed typical teratomas including tissues from all 3 germ layers when injected into immune-compromised mice (Fig. 4.5E). These data demonstrated that all iPSC lines in our test set passed all conventional assays of pluripotency for human ES cells. We then asked how these lines would perform in motor neuron directed differentiation.

Most iPS cell lines generate functional motor neurons with in vivo-like molecular identities

To compare the ability of iPSC and ESC lines to properly specify motor neurons, all lines were differentiated under standard protocols previously shown to generate motor neurons from ES cells (Fig. 4.6A). To determine the robustness of these lines, differentiations were conducted in parallel in the Eggan laboratory and in the Project ALS laboratory. We found that 81% (13/16) of iPSC lines, and all ESC lines generated robust populations of $ISL1^{+}$ cells which also stained for TuJ1 and showed typical neuronal morphologies (Fig. 4.6B). Of the lines tested in parallel in both labs there was a striking consistency in the quantitative %ISL1 for individual lines (Fig 4.6C). A Pearson correlation, however, did not show a strong correlation between lines tested in both labs however (n=10 lines, r=0.5038). However, in both labs the same 3 of 16 iPSC lines failed to generate almost any ISL^{+} neurons (27e, 29e, and 11b, see below Sources of variability).

The striking consistency of line malperformance between labs could not be included in the Pearson correlation because these are non-numerical values (Fig. 4.6C). If lab was considered as an independent variable, on the other hand, then there was no significant difference between the aggregate efficiency observed between labs (ANOVA, $p>0.05$, Table 4.2). We therefore pooled the data between labs for subsequent analyses of all 13 lines which had generated $ISL1^+$ neurons. Importantly, as a group, the 13 iPSC lines that generated $ISL1^+$ cells did not show a significantly different efficiency compared to ESC lines (Table 4.2). There were, however, significant differences in %ISL1 efficiency between lines, and post-hoc tests showed that lines 11a and 11c in particular were significantly different from 18c (Fig. 4.6D, Table 4.3). We concluded from these data that iPSC lines show robust and characteristic behavior in multiple settings, suggesting that motor neuron differentiation efficiency was a stable and intrinsic property of individual iPSC lines. These data also showed that iPSC lines did not have more variable or lower efficiency motor neuron differentiation than ESC lines.

To further validate the motor neuron phenotype defined by ISL1 expression, we tested several other endpoints required for more definitive assignment of motor neuron identity. First, we found that all 13 lines tested generated $HB9^+$ cells which stained for TuJ1 and showed neuronal morphologies (Fig. 4.7A). We again observed characteristic differences between lines which paralleled the differences observed for %ISL1 (Fig. 4.7B). Many $ISL1^+$ cells from iPS and ES lines alike expressed the characteristic motor neuron neurotransmitter synthetic enzyme ChAT (Fig. 4.7C). To ask if stem cell derived motor neurons were post-mitotic we stained cultures for the cycling cell marker Ki67, and found that $ISL1^+$ cells were not positive, while $PAX6^+$ progenitor cells served as an internal positive control (Fig. 4.7D). Finally we used qPCR to show that motor neuron lineage and marker genes (OLIG2, HB9, ISL1, ChAT, CHT1) and the

neuronal marker TuJ1 were strongly upregulated in these cultures compared to undifferentiated ESC or IPSC, or fibroblasts (Fig 4.7E). We concluded from these data that iPSC-derived neurons met all established in vitro criteria to be considered bona fide motor neurons. We next wanted to ask if these iPS-MNs met the criteria of coherent positional identity as defined by patterns of HOX protein expression as we have shown that ES-MNs did in Chapter 3.

To determine if iPSC lines would respond to the patterning cue RA in a similar fashion to ESC we tested the expression of HOXA5 and HOXC8 (Fig. 4.8A). iPS-MNs adopted a strikingly similar positional profile to that of ES-MNs (Fig 4.8B). The largest fraction of iPS- and ES-MNs expressed HOXA5 (42% vs. 41% respectively), indicative of a cervical positional identity, whereas about ~4 fold fewer motor neurons from both cell types expressed HOXC8 (14% vs. 12% respectively), indicative of a brachial to thoracic identity. Impressively, the fraction of motor neurons abnormally expressing both HOXA5 and HOXC8 was extremely small and was consistent between iPS- and ES-MNs (4% and 2% respectively). We concluded from these data, that iPSCs appear to interpret the positional cue RA with the same results as ESCs. Furthermore, iPS-MNs are no less faithful to the in vivo phenomenon of HOXA5-HOXC8 mutual exclusion than are ES-MNs. This phenomenon is particularly important since it controls the diversification of several brachial motor pools from generic LMC precursors.

To test whether iPS-MNs were functional we compared the electrophysiological activity of neurons from four iPSC and two ESC lines using the Ca^{2+} sensitive dyes Fura Red AM (Fig. 4.9A, B) and Fluo-4 AM (Fig. 4.9C). Spontaneous Ca^{2+} transients were observed in many cells from all iPSC and ESC lines tested (Fig. 4.9C, H, J). When cells were exposed to the ionotropic glutamate receptor agonist kainate (KA) 78% of cells with neuronal morphology (n=132 cells) responded with rapid increases in intracellular Ca^{2+} (Fig. 4.9E, I, K). When KCl was then used

to depolarize cells by shifting the electrochemical equilibrium of the perfusion medium, many KA responsive cells again showed Ca^{2+} fluxes (Fig. 4.9G, I, K). Post-imaging stains of these cultures confirmed that many active cells were $ISL1^{+}$ motor neurons. These data showed that iPS-MNs, like ES-MNs, had spontaneous and evocable electrical activity consistent with functional neuronal identity. To further examine the basis for this activity and to ascertain if iPS-MNs could fire action potentials, we performed whole cell patch clamp recordings on cells with neuronal morphology from an ESC control (HuES3 HB9:GFP, n=9) and iPSC lines (18a, n=10; 27b, n=10). All cells showed fast voltage-activated inward currents followed by slow outward currents, consistent with voltage-activated sodium and potassium channels (Fig. 4.10A, B). Inward currents were blocked by TTX, a specific inhibitor of voltage-gated sodium channels (Fig. 4.10C). Finally, current clamp recordings revealed that action potentials could be elicited by current injection in both ESC- (n=2) and iPSC-derived neurons (n=2), as well as repetitive firing from one neuron derived from iPS line 18a (Fig. 4.10 D). We concluded from these studies that iPSC lines generated electrically active functional neurons similar to ESC lines.

Potential sources of iPSC variability and rescue of atypical lines

Our data demonstrated that iPSC lines were able to generate functional motor neurons with coherent (HOX-mutually exclusive) positional identities with equivalent efficiency to ESC lines. The variability between iPSC lines was no greater than between ESC lines however our data did show significant line-dependent differences in motor neuron differentiation efficiency. We also noted that 3 lines showed a defective phenotype of near complete failure to generate $ISL1^{+}$ motor neurons. We therefore investigated several potential sources of inter-line variability and for this defective phenotype: persistent transgene expression, karyotypic instability, the effect of any of the demographic or technical variables in our test set, and neural lineage failure.

Persistent transgene expression

We and others have reported some persistent or reactivated expression of viral reprogramming transgenes in iPSC lines. To gauge the extent of this phenomenon in our test set and to see if this correlated with variable motor neuron differentiation efficiency we monitored expression of endogenous and viral reprogramming genes in undifferentiated and differentiated iPSC cultures (Fig. 4.11). For most cell lines viral transcription was very low, and for SOX2 it was undetectable (Fig. 4.11A-C). Many iPSC lines however expressed varying levels of KLF4 (11b, 11c, 15b, 18b, 18c, 27b, 27e, and 29e) in both undifferentiated and differentiated cultures (Fig. 4.11B). Several lines also expressed viral OCT4 (15b, 18c, and 27b) in both undifferentiated and differentiated cultures (Fig. 4.11C). Notably, transgene expression was stable: present in undifferentiated and differentiated cultures from that line, not reactivated on differentiation. To determine if OCT4 protein was expressed in differentiated neurons we double-stained cultures for ISL1 and OCT4 and found, surprisingly, that many individual $ISL1^+$ neurons in viral OCT4-expressing lines co-expressed nuclear OCT4. Despite this inappropriate gene expression, there was no correlation between total transgene expression and motor neuron differentiation efficiency as measured by $\%ISL1^+$ cells (R^2=0.1687). Furthermore many of the lines showing transgene expression were those that had previously been shown to generate electrically active motor neurons with normal HOX profiles. We concluded from these data that although some iPS lines maintained transgene expression, it had no detectable effect on the differentiation efficiency or quality of motor neurons.

Karyotypic instability

Karyotypic instability is a well described phenomenon in both mouse and human stem cell cultures. We therefore asked if irregular karyotypes might have affected iPSC performance. The majority of iPSC lines tested (9/15) retained normal karyotype at both early and late passage whereas 6 lines (29d, 27b, 29e, 11a, 11b, and 15b) showed abnormal karyotypes of varying severity (Table 4.4). Only two (29e, 11b) of the three defective lines showed abnormal karyotypes therefore this alone could not explain the defects. Furthermore line 27e had a normal karyotype and showed the same specific defective phenotype as 29e (see below). Finally, excluding defective lines (11b, 27e, 29e) there was no significant difference in $ISL1^{+}$ motor neuron differentiation efficiency between lines with normal vs. abnormal karyotype (Table 4.2). We concluded that abnormal karyotype could not explain variability or defective lines. We next sought to establish quantitative phenotypes for the 3 failed lines and to investigate the nature of their defects.

Identification and rescue of defective iPSC lines

Two of three defective lines (27e and 29e) showed a dramatic cystic disaggregated EB phenotype at day just after day 10, which first distinguished them from all other stem cell lines studied (Fig. 4.12A). When EBs were dissociated and seeded at the same density we found a significant difference in the total number of attached cells at day 32 for both of these lines (Fig. 4.12B, Table 4.5). Since these lines were easily identifiable by the qualitative EB and quantitative dissociated-cell phenotypes, and since the remaining cells were not positive for TuJ1 or ISL1, we excluded these lines as outliers from subsequent analyses. The third defective iPS line, 11b, showed a normal EB phenotype throughout differentiation and a normal number of

total cells at day 32. However, when cultures were stained for the neuronal marker TuJ1 we observed a significant decrease in the percent of neurons (Fig. 4.13A, B and Table 4.6). Because the first defective phenotype (for 27e and 29e) occurred during the period of consolidation of neural identity and the second phenotype (11b) was a reduced percent of neurons, we hypothesized that both phenotypes might be underpinned by a defect in neural induction.

To test whether these abnormal phenotypes were related to failed or low efficiency neural induction, we attempted to rescue them using essentially the Accelerated Protocol (described in Chapter 3, Fig. 3.3) which forces rapid neural induction using two ALK inhibitors. We found that both defective lines and two ES control lines displayed normal, smooth and round EB morphology throughout differentiation and generated robust populations of $ISL1^+$ $TuJ1^+$ neurons (Fig. 4.14A). All iPSC and ESC lines showed very high neuronal differentiation efficiency (70-90% $TuJ1^+$) (Fig. 4.14B) and comparable percentages of both $ISL1^+$ (10-20%) and $HB9^+$ (3-6%) (Fig. 4.14C, D). Since strong inducers of neural identity were able to completely rescue both defective phenotypes, we concluded that the defects were somewhere in the pathway of neural induction.

Sources of variation

To understand the line-specific variability observed for %ISL1 efficiency in the 13 of 16 normal iPSC lines, we next investigated whether any of the demographic or technical variables which we built into the test set had an effect on the outcome. There was no difference between ALS and control or between 3- and 4-factor lines (Fig. 4.15 A, B; Table 4.2). Similarly there was no correlation between donor age and %ISL1 (R^2=0.0084). However iPSC lines derived from female donors did show a significantly higher percentage of $ISL1^+$ cells (Fig. 4.15C, Table 4.7).

When ESC lines were included in this comparison the mean difference between male and female lines was smaller but still significant (Fig. 4.15D, Table 4.7). Since our test set was included multiple lines from 3 donors, we could assess whether individual genetic background affected differentiation efficiency. Indeed we observed very low variability between lines from the same donor and large variability between the means of all lines from one donor compared to another. ANOVA revealed that donor genetic background significantly affected differentiation efficiency (Fig 4.15E, Table 4.7). Post hoc pairwise comparisons comparing all individual donors did not however identify significant differences between any individual donors. However, the n for lines from the same donor (1-3; Table 4.7) was too low to reasonably expect any pairwise comparisons to be statistically significant, and the lack of significant pairwise comparisons should not detract from the significant finding in the more powerful ANOVA. Finally, because donor sex is part of donor genetic background we cannot be certain that the sex-specific difference does not alone account for the difference between donor genetic backgrounds. We concluded from these data that donor genetic background, including or in addition to sex had significant effects on the motor neuron differentiation efficiency of individual lines.

We next considered an alternative explanation for the low variability in $ISL1^{+}$ performance for lines from the same donor. Since most lines from individual donors were derived from the same reprogramming cultures, it was formally possible that cells from an initial clonal transduction event had physically moved in culture and were subsequently isolated and mistakenly considered to be independent lines. To directly address this possibility we conducted Southern blots using probes for 2 different viral transgenes, SOX2 and OCT4 (Fig. 4.16). The SOX2 probe showed a differential pattern of molecular weight species for all of the lines from donor 29, 18, and 11. These data demonstrated that these lines are the result of independent viral insertion events and

are not the same line. We concluded from these data that the low intra-donor variability was not the result of the same line being erroneously considered as multiple lines, and therefore that these effects on performance were likely the result of donor genetic background and or sex.

Scorecard predictions match line-specific empirical behaviors

During the course of our experiments, which showed significant differences between individual lines in motor neuron differentiation efficiency, another group was using a subset of this test set of iPSC lines to develop comprehensive reference maps of variation among ES and iPS lines (Bock, Kiskinis et al. 2011). Additionally these authors developed a targeted microarray approach to predict the differentiation propensities of individual lines based on short-term spontaneous EB differentiation: a "scorecard" for pluripotent cell differentiation potential. For each cell line we plotted the neural and ectodermal lineage indices generated by this scorecard analysis against the percentage of $ISL1^+$ neurons we had measured empirically for that line, and we found a strong correlation for both lineages (Fig. 4.17A, B). As a control for specificity we showed that there was not a strong correlation between endoderm and mesoderm lineages and $ISL1^+$ efficiency (Fig. 4.17C,D). We concluded that the same result was obtained by both methods, thereby cross validating both our empirical and their scorecard approach to estimating the intrinsic lineage competence and proclivity for individual lines.

Discussion

Summary of Findings

We have shown that patient derived iPSC lines can generate motor neurons and astrocytes: two key cell types affected in ALS. Next we constructed a large set of iPS lines encompassing several demographic variables likely to be encountered when attempting to model disease using iPS-derived cells. We demonstrated that 1 in 5 iPSC lines had a serious defect in neural differentiation, but these were easily detectable. The remaining iPSC lines generated motor neurons with positional identities and functional electrophysiological behavior equivalent to ESC-derived motor neurons. Finally, we excluded several of the demographic variables—age, disease status, number of reprogramming genes—as sources of variation among iPS-MNs, but identified donor genetic background (including and potentially limited to sex) as a significant factor. These studies provide a resource of disease and control cell lines for studying ALS and also provide practical guidelines for the derivation and analysis of iPSC lines. Most importantly they provide confidence that iPSC lines can generate differentiated motor neurons with comparable functional characteristics to those derived from ESC lines, and set the stage for making models of genetic disease.

iPS-MNs are functional and show in vivo like transcriptional phenotypes comparable to ES-MNs

iPS-MNs showed spontaneous and evoked electrophysiological activity no different than ES-MNs. Since adult-onset diseases like ALS affect cells that are developmentally mature in vivo, studying more mature motor neurons in vitro may increase the chances of defining disease relevant phenotypes. Indeed, several hypotheses about the mechanisms of motor neuron degeneration in ALS hinge on characteristics that appear only with maturity. For example glutamate excitoxicity has been implicated in ALS, and to adequately address this hypothesis it would be useful to test ALS-MNs which have functional glutamate receptors and maturing firing properties in response to depolarization. Our results show both the presence of functional

glutamate receptors—in Ca^{2+} imaging experiments—as well as electrophysiological maturity capable of sustaining repeated action potential spike trains. These functional electrophysiological characteristics suggest that iPS-MNs may be able to model activity-dependent aspects of ALS. In the future it will be important to demonstrate that iPS-MNs can achieve the type of mature and motor neuron-typical physiological activity which we have described for ES-MNs in Chapter 3. Other hypothetical ALS mechanisms have pointed to relatively unique morphological features of motor neurons to explain their selective vulnerability: the giant cell size (mostly axonal) may be linked to the pathology observed in axonal dieback and varicosities, ubiquisome overload, protein folding dysfunction and aggregation, axonal dieback, axonal transport defects, and energy metabolism and mitochondrial dysfunction. In order to adequately address these hypotheses it will be important to demonstrate that iPS-MNs can undergo morphological maturation as we described for ES-MNs in Chapter 3.

Another aspect of in vivo motor neuron biology that may be leveraged to study ALS in vitro is the differential susceptibility shown by specific motor column and motor pool subtypes. We know from studies in mouse and chick that these subtype identities emerge downstream of rostrocaudal patterning as articulated by HOX genes. Because iPS cells can differentiate to motor neurons, in our hands and in others', shows that they can respond to developmental cues (RA and SHH) and assume differentiated identities. In order to generate specific motor column or motor pool subtypes the fidelity of this developmental response must be high enough to generate the coherent HOX identities that drive those subtypes. We show that all iPS lines tested, just like ES lines, generated motor neurons with HOX profiles congruent with natural in vivo cervical positional identities (Chapter 2 and 3): they expressed mostly HOXA5 (cervical) and some HOXC8 in mutual exclusion. This is important since HOX cross-repression underpins

the diversification of motor pool (HOXA5-C8 and others) and column (HOXC-6, -9, -10) subtype identities. Since our data suggest the functional activity of these HOX mechanisms, it predicts that they may be used to generate specific motor neuron subtypes with enhanced utility for modeling ALS. The equivalent ability of iPSC and ESC to follow developmental cues and mechanisms in order to make highly-specific neuronal subtype cell-fate choices supports the idea that iPSC will be able to follow developmental trajectories to specific cell types relevant to other diseases.

Reproducibility and net equivalence with ES

By using a large set of iPSC lines and ES lines and a standardized differentiation protocol we showed that iPSC lines are no worse and no more variable than ESC lines in generating motor neurons. This result is at odds with the most in-depth previous study of this question (Hu, Weick et al. 2010). One explanation for this discrepancy is that the manual selection protocol used previously for motor neuron differentiation (see Chapter 3 for discussion) unintentionally biased the results against iPSC lines. Another explanation might be that the cell bank fibroblasts used to make those iPS lines had accumulated cytogenetic problems or mutations during indeterminate periods of culture, passage, or cryostorage. Additionally, the number and variety of iPSC and ESC lines which we used was much larger than in the previous study (16 iPSC and 5 ESC vs. 4 iPSC and 1 ESC), allowing us to test variability within iPSC and ESC categories independently and also compare the two statistically. Additionally, the ESC lines used for motor neuron comparison in the previous report (H9) is well known to show better than average efficiency for basal neural conversion. On the other hand the authors show a very clear difference in early neural induction between a large set of both iPSC (12) and ESC (4) lines, for

which none the above explanations can fully account, except cell bank degradation. More studies will be needed to resolve these issues in the future.

The performance of individual iPSC lines was remarkably similar between the two different labs involved in our study. This shows that lines retain intrinsic properties across passages, and their performance in well defined differentiation protocols (with at least 4 different operators) was highly robust. This finding gives confidence that iPSC are reproducible tools: an important criterion required for cellular substrates of disease modeling and drug screening.

While the majority of iPSC lines (81%) were equivalent to ESC lines, we did identify 3 defective lines. These defective lines were easily detectable and at a rate of just under 1 in 5 lines, we conclude that this error rate is an acceptable cost of making iPSC lines. Although motor neuron differentiation in these lines could be rescued with a forced neuralization protocol, for all practical purposes we recommend that simple steps be taken to remove lines like these from experimental sets. Since we excluded transgene expression and karyotypic instability as sufficient causes for these defects, we hypothesize that random viral integration events are responsible for these defects, and therefore newer reprogramming techniques such as synthetic RNA, non integrating vectors, or chemicals should avoid this complication altogether. Indeed, whether viral genomic lesions are responsible for causing these particular defects, non-integrating approaches are clearly a more conservative approach to generating iPSC lines.

Sources of variation

Our results showed that donor sex/genetic background significantly affected motor neuron differentiation efficiency. This result could explain some of the variation which others have reported among iPSC lines (Hu, Weick et al. 2010). Other studies have found that ES cells as

well show marked differences in differentiation efficiencies for the motor neuron (Di Giorgio, Boulting et al. 2008) and other lineages (Osafune, Caron et al. 2008). This finding was made possible by the categorically greater capacity of iPS vs. ES cells to sample and study individual genetic variation. This capacity is a double edged sword however: because of the tremendously greater natural variation in human populations than in any model system for genetics we predict the issue of unexpected variation in differentiation phenotypes will arise repeatedly in years to come as more terminal cell types become the subject of directed differentiation studies using iPS cells. This will need to be carefully controlled for in future studies as it could complicate or confound disease phenotypes. On the other hand the abundance of human genetic variant alleles may provide a unique opportunity to study gene function in the mechanisms of differentiation in vitro (see Chapter 6).

Because donor sex is part of donor genetic background it is possible that the sex-specific difference alone accounts for the difference between donor genetic backgrounds. Because we did not have a balanced number of lines from each donor and across sexes, we could not perform a 2-factor ANOVA to directly test this possibility. However, consistent with this possibility the lowest performing lines, from donor 11, were male, while the highest performing lines, from donors 18 and 29, were both female. Based on the large variability between lines from different donors, and very small variability between lines from the same donor in our study, a new study with 3-4 lines/donor from a 5 male and female donors each could address this question.

The variable phenotype (%ISL1^{+}) which we describe was unlikely to be related to ALS. However, ALS is less common in females, therefore it is tempting to speculate that some sex-linked genetic determinant may link depressed basal rate of in vitro motor neuron differentiation to ALS susceptibility. More intriguingly our measurement of %ISL1^{+} cells could equally well

represent a motor neuron survival difference in response to some in vitro stressor (EB dissociation for example). On the other hand the %ISL1^{+} phenotype may be completely unrelated to ALS, and the mechanisms and potential linkage of these phenomena were not within the scope of our study.

There is also one technical caveat for the donor-genetic background result, which applies less strongly to the sex-difference result. Because independent lines from the same donor were derived from the same specific culture well which subjected to repeated retroviral transductions, it is possible that these lines are derivatives of single transduction event. In this case, the n for each donor would be reduced to 1, reducing the power of our statistical inference. Although we could prove by Southern blot that lines were independent, we cannot experimentally prove or falsify a lineal relationship between these lines. However future studies could eliminate this possibility simply picking independent clones from the same donor from physically or temporally separate reprogramming cultures.

We chose an unbiased and functional—ability to make a defined cell type—approach to characterizing the utility of pluripotent cell lines. Our collaborators used this same test set and a larger set of ES lines to generate an unbiased predictive scorecard, based on several short-term experimental differentiations, to evaluate pluripotent cell lines (Bock, Kiskinis et al. 2011). Our empirical results correlated very well with the predictions of this scorecard for the lineage represented by our terminal phenotype (ectoderm/neuroectoderm) and were not correlated with other lineages tested. This result confirms the accuracy and utility of their expression profiling approach. Conversely, it validates our empirical approach as well, and suggests that for disease models where only one particular cell type is of primary interest immediate differentiation of candidate iPSC lines to that terminal cell type of interest will provide as accurate and arguably

more directly relevant index of the behavior individual lines which is faster, cheaper, and accessible to any lab.

Conclusion and Perspectives

In summary, our data provide new confidence in the ability of iPSCs to give rise to functional differentiated cell types of disease interest with the same efficiency and fidelity as ESCs. Our study provides the first analysis of the rate and nature of the potential pitfalls of defective lines and practical recommendations for how to handle them. We also demonstrate that human genetic variation may be an important and previously underappreciated factor to consider when constructing iPSC line sets, for interpreting iPSC or ESC phenotypes, and for studying gene function. Together this work establishes a strong empirical foundation and guidelines for launching disease-phenotype directed studies of ALS and other genetic diseases using iPSCs.

The outstanding question for the field is whether iPSC motor neurons will show ALS disease phenotypes in vitro. This was not addressed by our studies and will not be addressed within the scope of this thesis. However, in addition to looking for pan-motor neuron ALS phenotypes, a complementary approach is to use the differential response of specific motor column and motor pool subtypes to search for disease phenotypes or disease modifying mechanisms. We showed that iPS-MNs, like ES-MNs have dominantly cervical to brachial rostrocaudal identities. This regional identity includes brachial LMC motor neurons which are typically affected first in disease. Studying LMC motor neurons derived from ALS-iPS cells may reveal distinct or accelerated disease phenotypes in vitro. However, two of the most disease resistant motor neuron subtypes are caudal to the HOXA5 domain—$HOXC9^{+}$ thoracic PGC motor neurons and

HOX10/11^{+} sacral Onuf's nucleus motor neurons—and these are unlikely to have been generated in significant numbers in our population. It will thus be critical to ask if more caudal motor neuron subtypes can be generated from human ESCs and iPSCs. The question of caudal patterning of human stem-cell derived motor neurons will be the subject of Chapter 5.

Figure 4.1

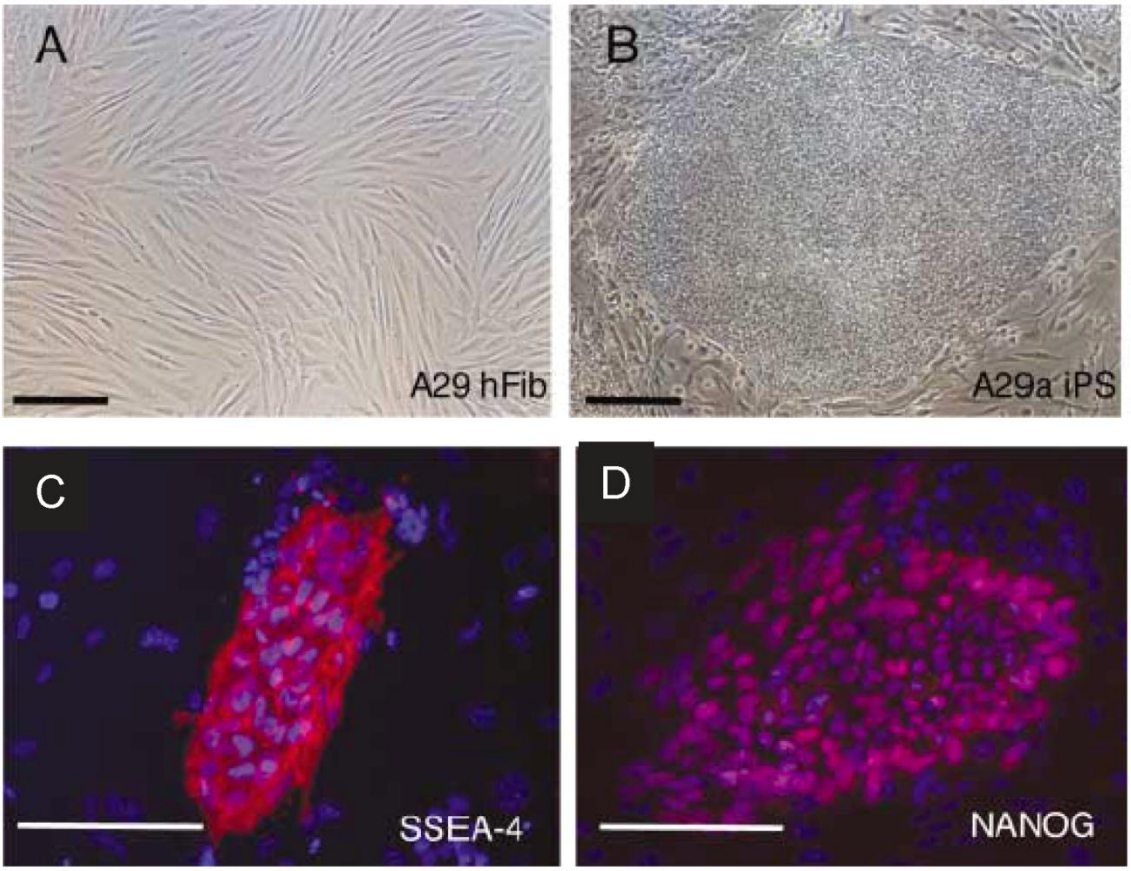

Figure 4.1. iPS cells can be established from patient fibroblasts after biopsy

(A) Primary dermal fibroblasts (hFib, human fibroblasts) derived from an 82-year old female ALS patient, A29. (B) iPS cells produced from patient A29. (C and D) SSEA-4 and NANOG protein expression in A29 iPS cells. Scale bars 200 µm.

Figure 4.2

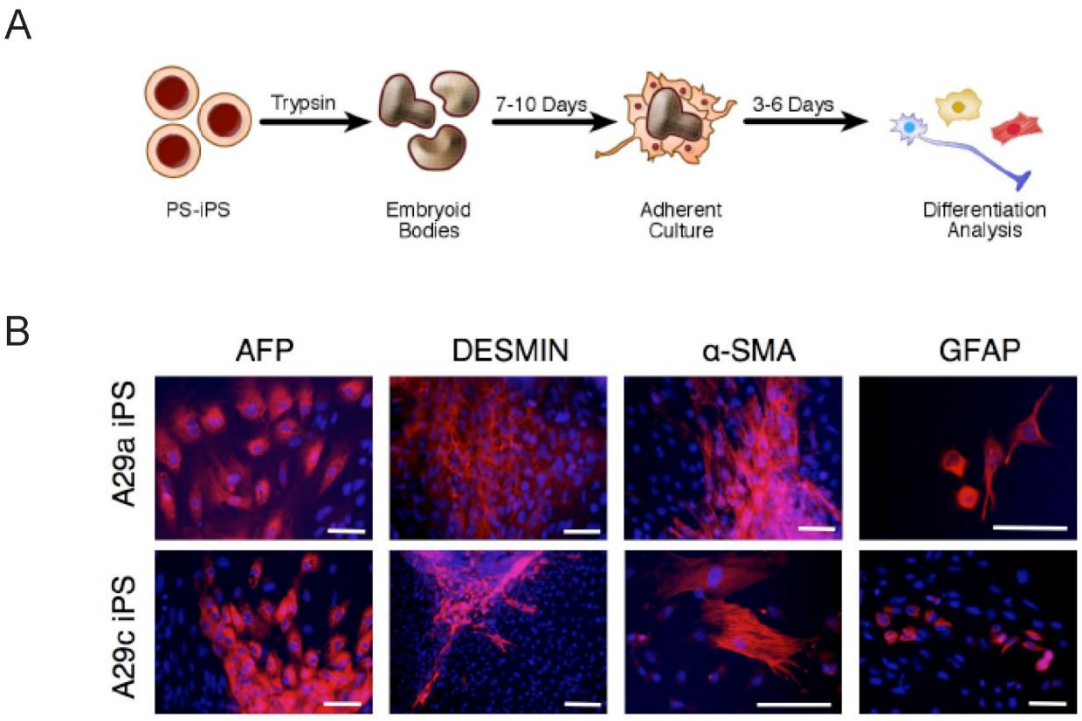

Figure 4.2. Patient-specific iPS cells are pluripotent

(A) Schematic illustrating the spontaneous differentiation of iPSC in embryoid bodies (EBs) and subsequent adherent culture. iPSCs were used to seed EBs and grown in suspension for 7-10 days before attachment to tissue culture plastic and analysis for the production of cell types representative of the three embryonic germ layers. (B) Attached EBs contained cells characteristic of each of the three germ layers: endoderm (AFP), mesoderm (Desmin, alpha-SMA), and ectoderm (GFAP). Scale bars 100 µm.

Figure 4.3

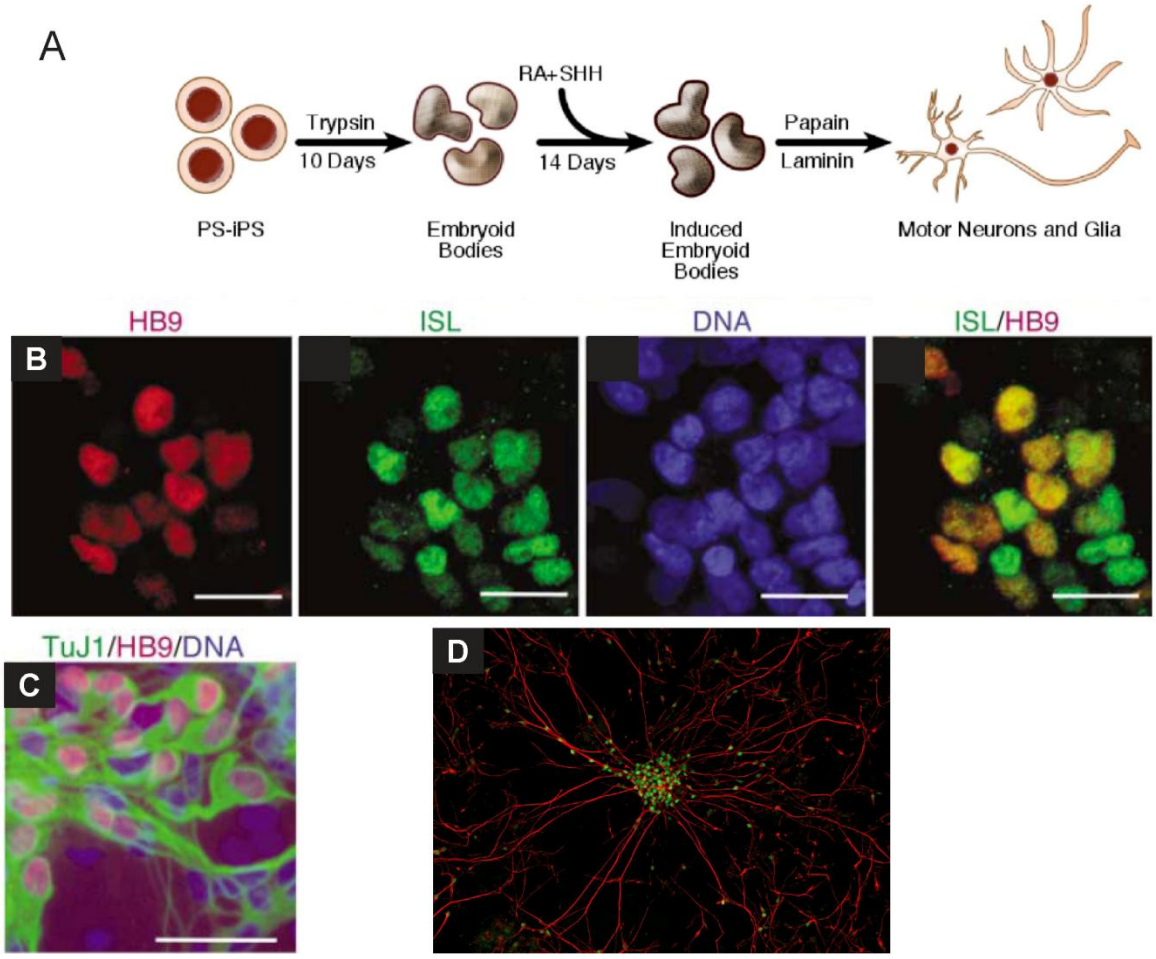
A
Trypsin
10 Days
RA+SHH
14 Days
Papain
Laminin
PS-iPS
Embryoid Bodies
Induced Embryoid Bodies
Motor Neurons and Glia
HB9
ISL
DNA
ISL/HB9
B
TuJ1/HB9/DNA
C
D

Figure 4.3. ALS iPSC lines can be differentiated to motor neurons

(A) Schematic of protocol used to direct the differentiation of patient-specific iPSC to motor neurons. EBs derived from iPS cell line A29a were grown for 10 days before treatment with retinoic acid (RA) and a small molecule sonic hedgehog (SHH) signaling agonist. After two weeks of continued suspension culture in the presence of these inductive molecules, EBs were dissociated and cells plated on laminin. (B) The motor neuron identity of $HB9^{+}$ and $TuJ1^{+}$ cells is confirmed by the coexpression of HB9 and ISL1 (ISL), scale bar 75 μm (C and D) Neuronal identity of $HB9^{+}$ cells is confirmed by (C) high-magnification image of HB9 and TuJ1 coexpression in dissociated patient-specific motor neuron cultures, Scale bar 100 μm, and (D) abundant $HB9^{+}$ cells (green) with extensive neurite outgrowth (TuJ1, red) field width 900 μm.

Figure 4.4

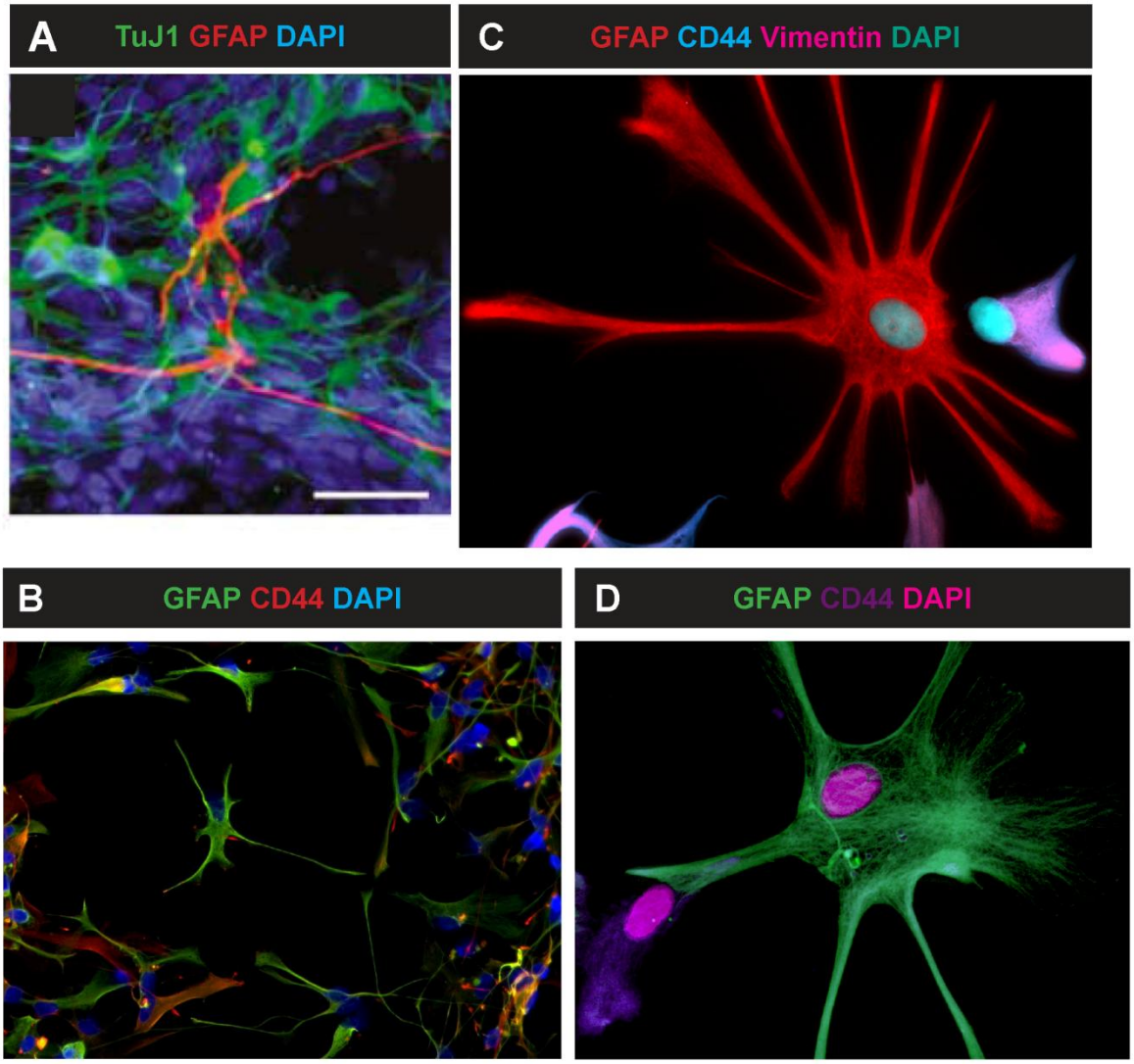

Figure 4.4. ALS iPSC lines generate cells with astrocyte-like phenotypes

(A) Cells expressing the astrocyte marker GFAP show radial glial morphology after 3 weeks of culture, scale bar 100 µm (B-D) after 120 days of continuous culture most cells show astrocytic morphology and express combinations of GFAP, the immature astrocyte marker CD44, and the glial progenitor marker Vimentin, and are costained for DAPI. (B) 450 µm field width (C and D) 225 µm field width.

Table 4.1

Cell type	Donor fibroblast	Cell line	ALS diagnosis	Reprogramming factors	Sex	Donor age	Reference
iPS	11	11a	Healthy control	OCT4/SOX2/KLF4	M	36	This report
iPS	11	11b	Healthy control	OCT4/SOX2/KLF4	M	36	This report
iPS	11	11c	Healthy control	OCT4/SOX2/KLF4	M	36	This report
iPS	15	15b	Healthy control	OCT4/SOX2/KLF4	F	48	This report
iPS	17	17a	Healthy control	OCT4/SOX2/KLF4	F	71	This report
iPS	17	17b	Healthy control	OCT4/SOX2/KLF4	F	71	This report
iPS	18	18a	Healthy control	OCT4/SOX2/KLF4	F	48	This report
iPS	18	18b	Healthy control	OCT4/SOX2/KLF4	F	48	This report
iPS	18	18c	Healthy control	OCT4/SOX2/KLF4	F	48	This report
iPS	20	20b	Healthy control	OCT4/SOX2/KLF4	M	55	This report
iPS	27	27b	*SOD1*G85S	OCT4/SOX2/KLF4	F	29	This report
iPS	27	27e	*SOD1*G85S	OCT4/SOX2/KLF4	F	29	This report
iPS	29	29A	*SOD1*L144F	OCT4/SOX2/KLF4/c-MYC	F	82	2
iPS	29	29B	*SOD1*L144F	OCT4/SOX2/KLF4/c-MYC	F	82	2
iPS	29	29d	*SOD1*L144F	OCT4/SOX2/KLF4	F	82	This report
iPS	29	29e	*SOD1*L144F	OCT4/SOX2/KLF4	F	82	This report
ES	–	HuES-3	–	–	M	–	23
ES	–	HuES-6	–	–	F	–	23
ES	–	HuES-9	–	–	F	–	23
ES	–	HuES-13	–	–	M	–	23
ES	–	HuES-3 hb9:GFP	–	–	M	–	12
ES	–	RUES1	–	–	M	–	24

Table 4.1. iPSC and ESC lines used for comparative studies

Sixteen human iPSC lines were used for comparison with each other and with six ESC lines. iPSC lines include 14 newly generated three-factor lines from two ALS patients and five controls, and two previous four-factor lines from one ALS patient. This cohort of human stem cell lines allows comparisons to be made between ESCs and iPSCs, between three-factor and four-factor iPSC lines, between male and female lines, between lines derived from the same donor and those derived from another donor, and between cells derived from ALS patients and control donors.

Figure 4.5

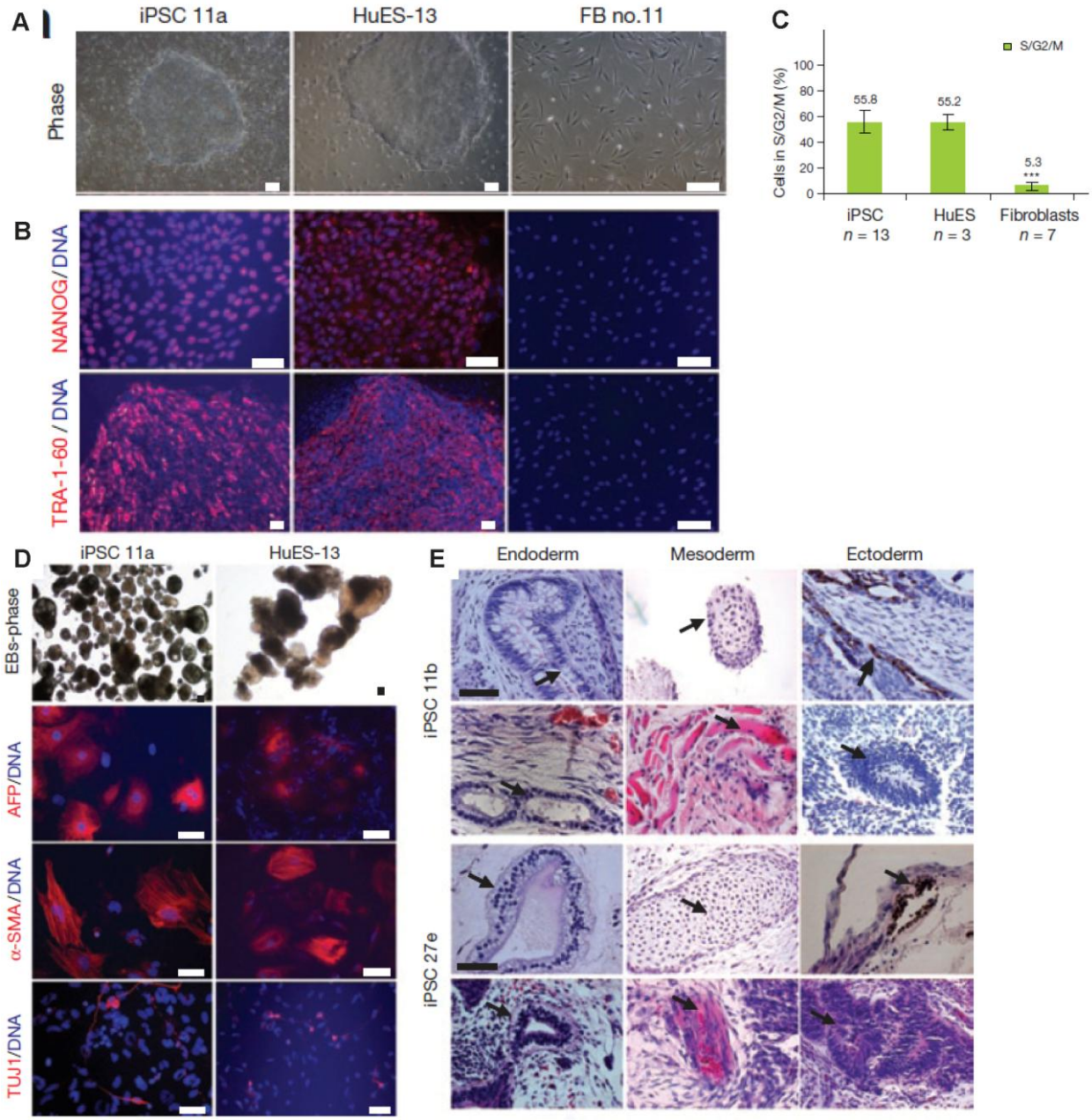
A
iPSC 11a
HuES-13
FB no.11
Phase
B
NANOG/DNA
TRA-1-60 / DNA
C
S/G2/M
Cells in S/G2/M (%)
100
80
60
40
20
0
55.8
55.2
5.3
***
iPSC
n = 13
HuES
n = 3
Fibroblasts
n = 7
D
iPSC 11a
HuES-13
EBs-phase
AFP/DNA
α-SMA/DNA
TUJ1/DNA
E
Endoderm
Mesoderm
Ectoderm
iPSC 11b
iPSC 27e

Figure 4.5. All test set iPSC lines pass standard assays of pluripotency

(A) iPSC colonies were morphologically identical to ESC colonies and (B) expressed the pluripotency markers NANOG and TRA-1-60, unlike the patient fibroblasts (FB). Scale bars, 200 μm. (C) iPSC lines' cell cycle profiles are similar to those of ESCs and different from parental fibroblasts. T-test, ***P < 0.001, mean ±SD. (D and E) ESCs and iPSC lines generated cell types of all 3 embryonic germ layers (endoderm, AFP; mesoderm, α-SMA; ectoderm, TUJ1) in vitro from EBs, scale bars 100 μm, and when injected into mouse kidney capsules and allowed to form teratomas in vivo (E; scale bars 50 μm). Representative images of H&E-stained sections are shown for lines 11b and 27e. Glands and goblet cells (endoderm), cartilage and muscle (mesoderm), pigmented neural epithelium and neural rosettes (ectoderm) are shown in the top and bottom panels, respectively, for both lines.

Figure 4.6

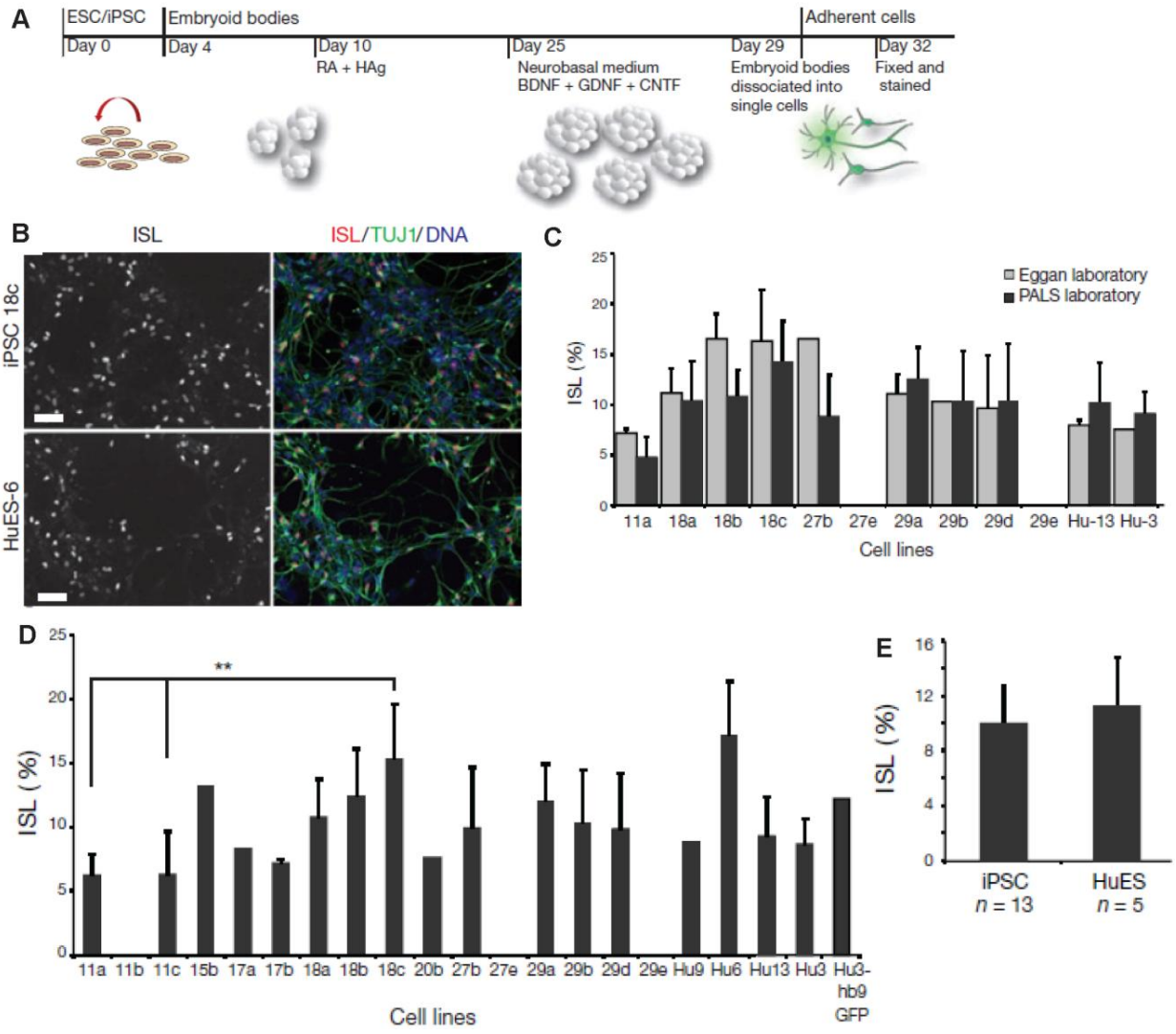
A
ESC/iPSC
Day 0
Embryoid bodies
Day 4
Day 10
RA + HAg
Day 25
Neurobasal medium
BDNF + GDNF + CNTF
Day 29
Embryoid bodies
dissociated into
single cells
Adherent cells
Day 32
Fixed and
stained
B
ISL
ISL/TUJ1/DNA
iPSC 18c
HuES-6
C
Eggan laboratory
PALS laboratory
ISL (%)
11a 18a 18b 18c 27b 27e 29a 29b 29d 29e Hu-13 Hu-3
Cell lines
D
**
ISL (%)
11a 11b 11c 15b 17a 17b 18a 18b 18c 20b 27b 27e 29a 29b 29d 29e Hu9 Hu6 Hu13 Hu3 Hu3-hb9 GFP
Cell lines
E
ISL (%)
iPSC
n = 13
HuES
n = 5

Figure 4.6. iPSC lines show characteristic motor neuron differentiation efficiencies, but no global difference from ESC lines

(A) Protocol for directed differentiation of human stem cell lines into motor neurons. Cells were differentiated to motor neurons as described previously. EBs were dissociated and single cells plated for adherent culture on day 29. On day 32 cultures were analyzed. (B) Representative immunostaining results for iPSC (18c) and ESC (HuES-6) cultures show many $ISL1^+$ $TUJ1^+$ motor neurons (scale bars 50 μm). (C) The percentage of all nuclei that were $ISL1^+$ was quantified from differentiations performed independently in the Eggan and PALS laboratories. Data sets from lines differentiated in both laboratories are highly similar and lines have reproducible, characteristic % $ISL1^+$ efficiencies. 29e and 27e did not differentiate efficiently in either laboratory. Hu-13, HuES-13, Hu-3, HuES-3. (D) Percent $ISL1^+$ data from both laboratories were pooled for each iPSC and ESC line, and comparisons between lines showed that individual lines had different efficiencies and iPSC lines 11a and 11c were significantly different than 18c ($p < 0.05$). (E) The efficiency of IPSC lines as a group was not significantly different than for ESC lines. See Tables 4.2 and 4.3 for statistical analyses.

Table 4.2

% ISL+ cells (One Way ANOVA)					
Eggan v PALS	n= # of lines	experiments	mean +/- SEM	F-value	p-value
Eggan	10	30	11.6 +/-1.1		
PALS	10	42	10.1 +/-0.8	1.132	0.301
ES v. iPS	n= # of lines	experiments	mean +/-SEM		
ES	5	13	11.2 +/-1.6		
iPS	13	59	10.0 +/-0.8	0.629	0.439
3 v. 4 factor	n= # of lines	experiments	mean +/-SEM	F-value	p-value
3 factor	11	45	9.7 +/-0.9		
4 factor	2	14	11.2 +/-0.9		
0 - hES	5	13	11.2 +/-1.6	0.49	0.622
ALS v. control	n= # of lines	experiments	mean +/-SEM	F-value	p-value
ALS	4	26	10.6 +/-0.5		
control	9	33	9.7 +/-1.1		
0 - hES	5	13	11.2 +/-1.6	0.413	0.669
Norm v Abnormal Karyotype	n= # of lines	experiments	mean +/-SEM	F-value	p-value
normal	9	41	10.0 +/-1.0	0.007	0.932
abnormal	4	18	9.9 +/-1.4		

Table 4.2. Statistical analysis of categorical variables on %ISL1 differentiation efficiency

ANOVAs on %ISL1$^+$ values show no difference between performance in Eggan vs. PALS Laboratories, iPSC vs. ESC lines, 3-factor vs. 4-factor vs. 0-factor (ESC) reprogramming, ALS vs. control vs. ESC, or normal vs. abnormal karyotype. Day 32 differentiations were stained, imaged, and quantitated for mean % ISL1$^+$ cells (of all DAPI$^+$ cells) per image field per line, and then mean %ISL1$^+$ was compared for n different lines per grouping variable. Mean ±SEM is shown for each variable setting. All comparisons showed no significant difference between groups.

Table 4.3

% ISL+ cells (One Way ANOVA)				
line	**N**	**mean +/- SEM**	**F-value**	**p-value**
11a *	5	6.2 +/-0.7		
11c +	4	6.3 +/-1.7		
15b	1	13.3 +/-na		
17a	1	8.3 +/-na		
17b	2	7.2 +/-0.2		
18a	6	10.7 +/-1.2		
18b	7	12.4 +/-1.4		
18c * ÷	6	15.3 +/-1.8		
20b	1	7.6 +/-na		
27b	7	9.9 +/-1.8		
29A	10	12.1 +/-0.9		
29B	4	10.3 +/-2.1		
29d	5	10.0 +/-2.2		
HUES13	5	9.3 +/-1.4		
HUES3	4	8.7 +/-1.0		
HUES3-GFP	1	12.2 +/-na		
HUES6	2	17.2 +/-2.9		
HUES9	1	8.8 +/-na	3.355	0.001
Holm Sidak pairwise	**Difference of means**		**t value**	**p-value**
* 11a vs. 18c	9.03		4.176	0.017
÷ 11c vs. 18c	9.008		3.908	0.039

Table 4.3. %ISL1$^+$ cells varies by cell line

Day 32 differentiations were stained, imaged, and quantitated for mean % ISL1$^+$ cells (of total DAPI$^+$ cells) per image field per experiment, and then mean % ISL1$^+$ was compared for n different experiments per line. Mean +/-SEM is shown for each line. ANOVA revealed that there were significant differences based on line, and post hoc pairwise comparisons showed that lines 11a and 11c were each significantly different than line 18c.

Figure 4.7

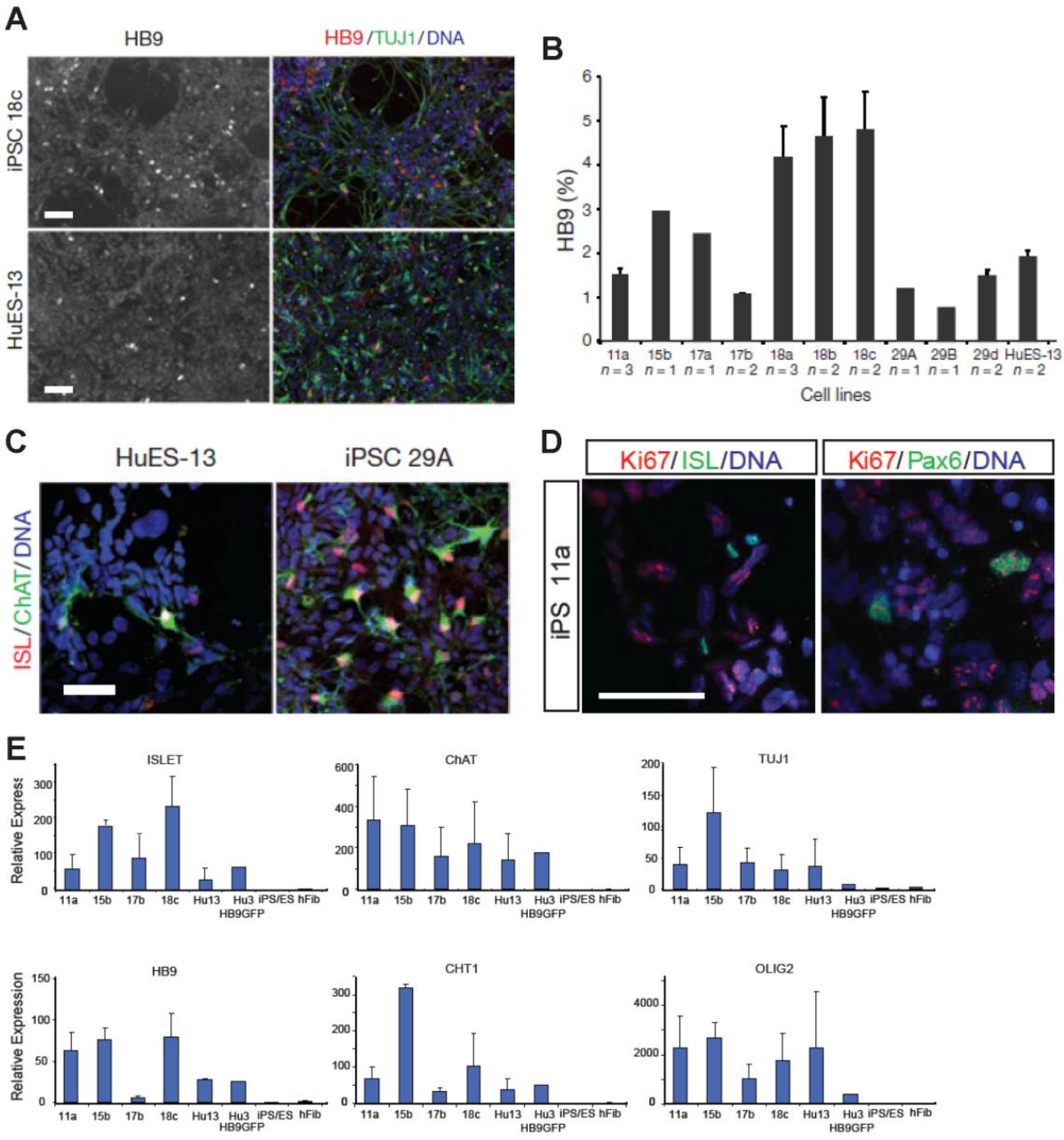
A
HB9
HB9/TUJ1/DNA
iPSC 18c
HuES-13
B
HB9 (%)
11a n=3
15b n=1
17a n=1
17b n=2
18a n=3
18b n=2
18c n=2
29A n=1
29B n=1
29d n=2
HuES-13 n=2
Cell lines
C
HuES-13
iPSC 29A
ISL/ChAT/DNA
D
Ki67/ISL/DNA
Ki67/Pax6/DNA
iPS 11a
E
ISLET
ChAT
TUJ1
HB9
CHT1
OLIG2
Relative Expression
11a 15b 17b 18c Hu13 Hu3 iPS/ES hFib
HB9GFP

Figure 4.7. iPSC motor neuron cultures show phenotypes consistent with motor neuron identity

(A) Efficiency of motor neuron differentiation was also measured by the motor neuron marker HB9. (B) The percent of $HB9^+$ nuclei were compared for a subset of iPSC lines and HuES-13. Although comparisons again suggest donor- and line-specific differences, iPSC lines were overall equally capable of generating $HB9^+$ motor neurons as HuES-13 (n experiments shown under bars for mean ±SD). (C) Many ISL^+ motor neurons were also $ChAT^+$, indicating proper maturation toward a cholinergic transmitter phenotype. (D) $ISL1^+$ motor neurons are not dividing since they did not stain for Ki67, as expected of post-mitotic cells, while $PAX6^+$ neural progenitor cells were $Ki67^+$. (E) The expression of motor neuron markers ISL1, ChAT, TUJ1, HB9, CHT1, and the motor neuron progenitor gene OLIG2 were assessed by qPCR. iPS/ES represents the average expression level in undifferentiated HuES-3 Hb9:GFP and iPSC line 18c. The relative expression of these genes in undifferentiated HuES-3 Hb9:GFP is set as 1. (mean ±SD). All scale bars 50μm.

Figure 4.8

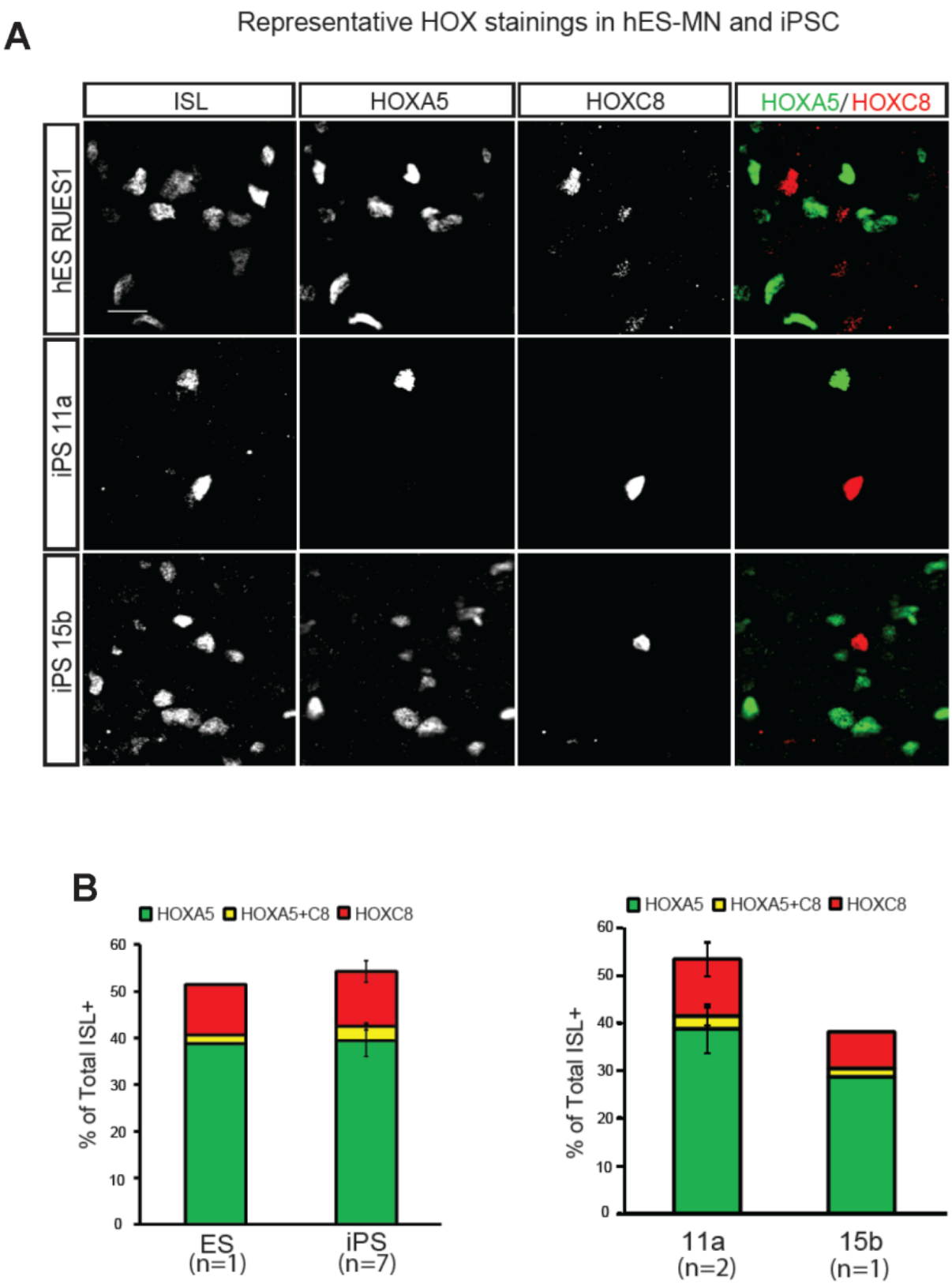
A
Representative HOX stainings in hES-MN and iPSC
ISL
HOXA5
HOXC8
HOXA5/HOXC8
hES RUES1
iPS 11a
iPS 15b
B
HOXA5
HOXA5+C8
HOXC8
% of Total ISL+
60
50
40
30
20
10
0
ES
(n=1)
iPS
(n=7)
11a
(n=2)
15b
(n=1)

Figure 4.8. iPS- and ES-MNs exhibit the same coherent cervical HOX phenotypes

(A) Day 32 cultures were triple stained for ISL1, HOXA5, and HOXC8. (B) 41% of IPS- and 42% of ES- $ISL1^{+}$ cells expressed HOXA5 (green) and 12% and 13% expressed HOXC8 (red) respectively. The number of HOXA5 HOXC8 coexpressing cells (yellow) was extremely low (<5% of all HOXA5 or HOXC8 expressing cells) for iPS- as well as ES-MN. Left panel, mean of 4 experiments on n=1 (RUES1) ESC line, and mean ±SEM of n=7 individual iPS lines tested (18a, 18c, 11a, 11b, 11c, 15b, 29A). Right panel, individual percentages for representative lines shown in (A).

Figure 4.9

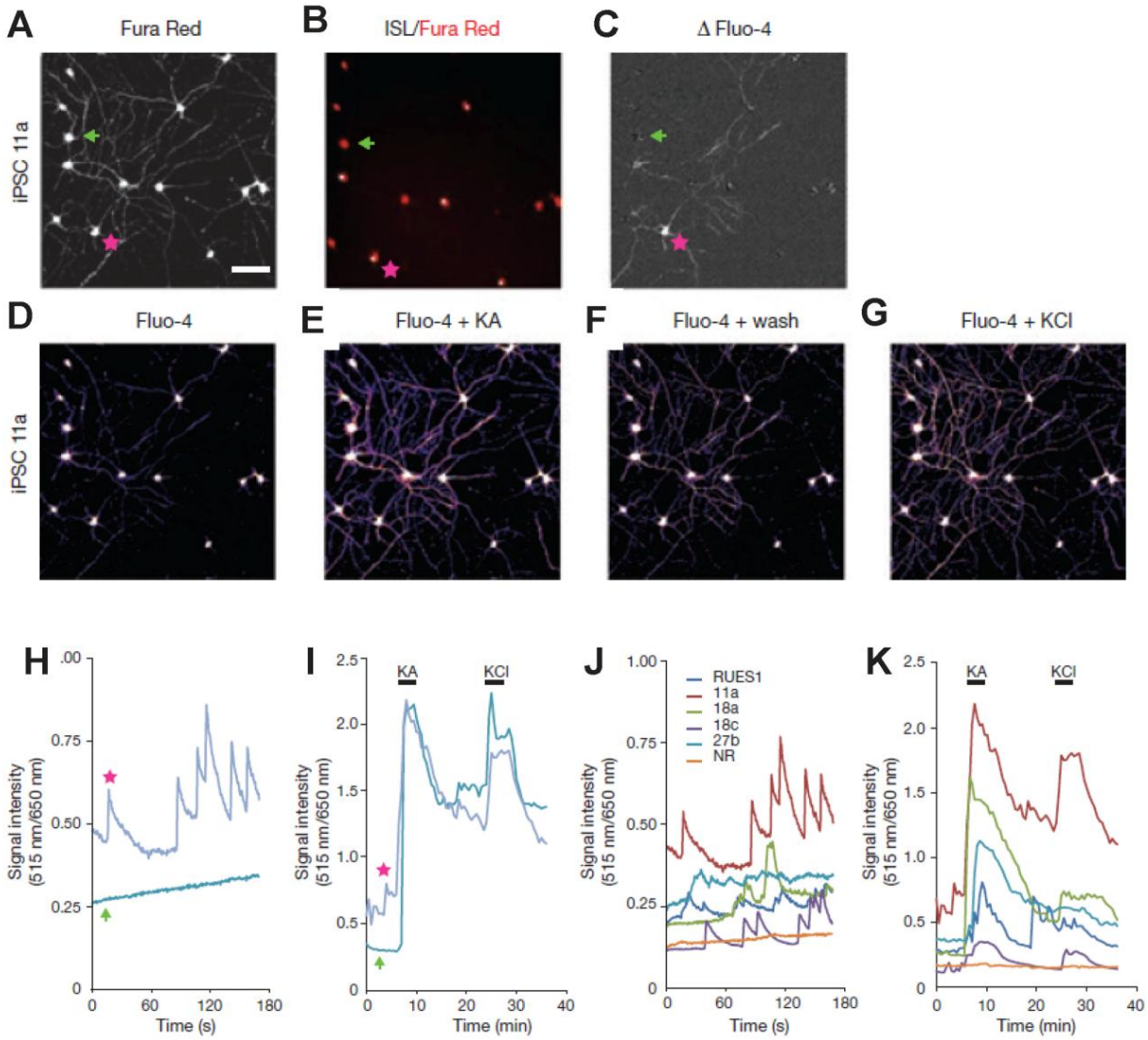
A
Fura Red
B
ISL/Fura Red
C
Δ Fluo-4
iPSC 11a
D
Fluo-4
E
Fluo-4 + KA
F
Fluo-4 + wash
G
Fluo-4 + KCl
iPSC 11a
H
Signal intensity (515 nm/650 nm)
Time (s)
I
KA
KCl
Signal intensity (515 nm/650 nm)
Time (min)
J
RUES1
11a
18a
18c
27b
NR
Signal intensity (515 nm/650 nm)
Time (s)
K
KA
KCl
Signal intensity (515 nm/650 nm)
Time (min)

Figure 4.9. iPSC- and ESC-derived neurons are physiologically active

(A) Fura Red channel image of iPSC 11a–derived neurons filled with Fura Red AM and Fluo-4 AM dyes, same field as in (B-G). Activity of labeled cells is represented in (H) and (I). Scale bar, 100 μm. (B) immunostaining shows $ISL1^+$ (star) and ISL^- neurons (arrow). (C) Spontaneous electrical activity in cultured iPSC-derived neurons visualized by a 'subtracted image' that shows the difference in pixel intensities between two images acquired 1.7 s apart in the Fluo-4 channel. Higher gray values represent increased pixel intensity. (D–G) Identically exposed pseudocolored averages of ten Fluo-4 AM images taken during the control period (D), after treatment with 100 μM KA (E), after KA washout (F) and after treatment with 50 μM KCl (G). Warmer colors represent increased fluorescence intensity. (H-K) Plots of Fluo-4/Fura Red intensity ratios in the somata of (H) example $ISL1^+$ (*) and $ISL1^-$(arrow) cells show spontaneous activity in the $ISL1^+$ cell, (I) both cells are activated by KA and KCl, (J) examples of spontaneous activity in cultures of ESC RUES1–, and iPSC 11a–, 18a–, 18c– and 27b–derived neurons as well as one example of a nonresponsive (NR), non-active cell for RUES1, and (K) KA and KCl response of cells from (J).

Figure 4.10

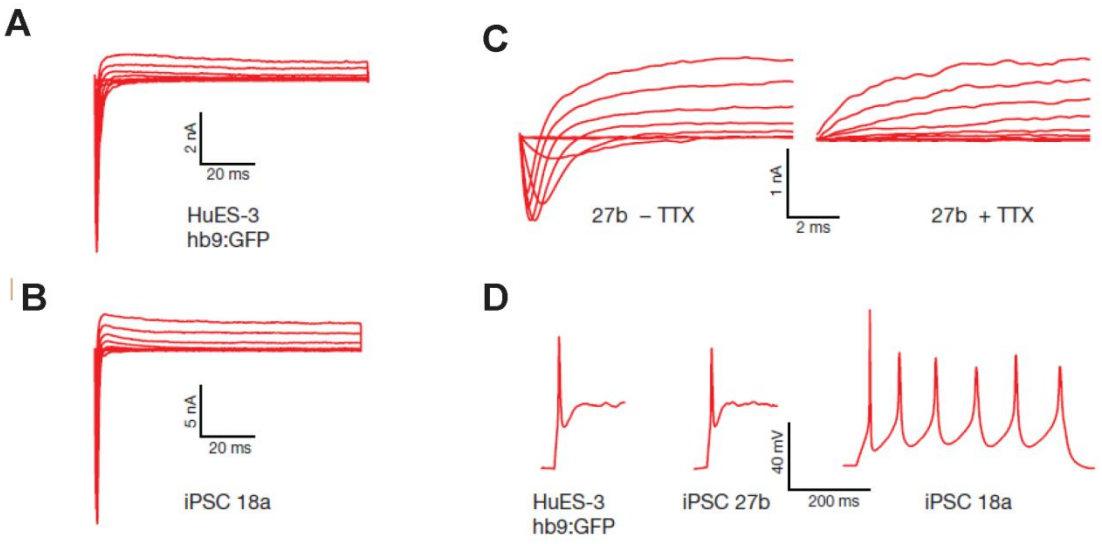

Figure 4.10. iPSC- and ESC-derived neurons show voltage gated sodium channels and fire action potentials

(A–D) Sample voltage-clamp traces from ESC (A) and iPSC 18a–derived (B) neurons. (C) Blowup of an iPSC 27b–derived neuron recording reveals typical sodium currents (left), which are blocked by TTX (right). (D) Current-clamp recordings of single action potentials in ESC and iPSC 27b–derived neurons as well as multiple action potentials in an iPSC 18a–derived neuron.

Figure 4.11

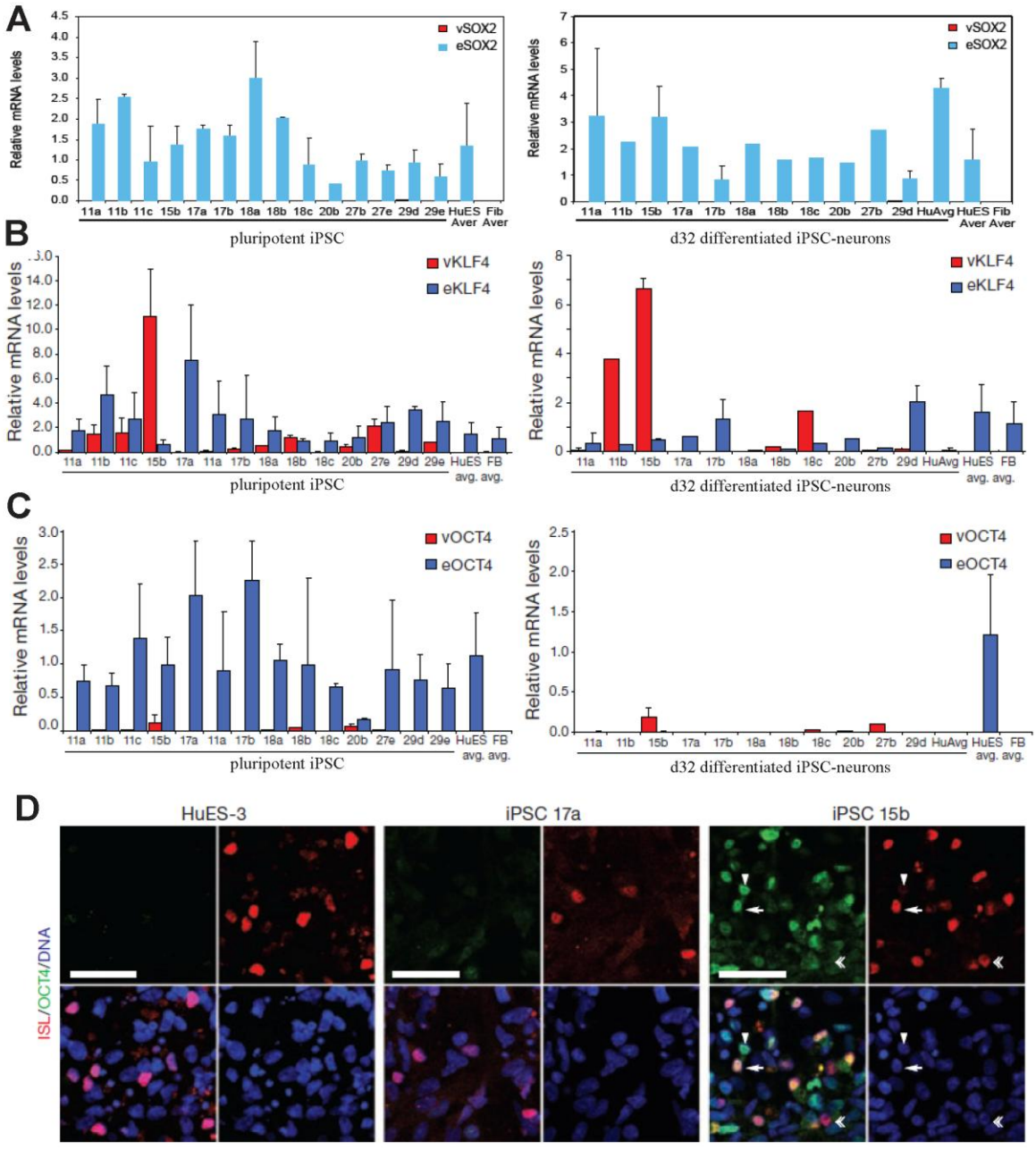
A
Relative mRNA levels
vSOX2
eSOX2
11a 11b 11c 15b 17a 17b 18a 18b 18c 20b 27b 27e 29d 29e HuES Aver Fib Aver
pluripotent iPSC
11a 11b 15b 17a 17b 18a 18b 18c 20b 27b 29d HuAvg HuES Aver Fib Aver
d32 differentiated iPSC-neurons
B
vKLF4
eKLF4
11a 11b 11c 15b 17a 11a 17b 18a 18b 18c 20b 27e 29d 29e HuES avg. FB avg.
pluripotent iPSC
11a 11b 15b 17a 17b 18a 18b 18c 20b 27b 29d HuAvg HuES avg. FB avg.
d32 differentiated iPSC-neurons
C
vOCT4
eOCT4
11a 11b 11c 15b 17a 11a 17b 18a 18b 18c 20b 27e 29d 29e HuES avg. FB avg.
pluripotent iPSC
11a 11b 15b 17a 17b 18a 18b 18c 20b 27b 29d HuAvg HuES avg. FB avg.
d32 differentiated iPSC-neurons
D
HuES-3
iPSC 17a
iPSC 15b
ISL/OCT4/DNA

Figure 4.11. Persistent transgene expression in some iPSC lines does not inhibit MN differentiation

(A-C) qPCR measurement of relative levels of transcript from endogenous ‘e’ (blue) and viral “v” (red) reprogramming factors (A) SOX2, (B) KLF4, and (C) OCT4 in undifferentiated iPSCs (left) and ESCs, and in day 32 neuron cultures (right). The expressed/silenced status of transgene is constant before or after differentiation. Relative levels in undifferentiated HuES-3 were set as 1. FB, fibroblasts. (D) Day 32 motor neuron cultures were co-stained for ISL1 and OCT4. HuES-3– and iPSC 17a–derived cultures, which do not express viral OCT4, did not stain for OCT4. However, iPSC 15b–derived cultures, which do express viral OCT4, contained many $OCT4^+$ $ISL1^+$ motor neurons (arrow) and $OCT4^+$ ISL^- cells (arrowhead), scale bars 50 μm.

Table 4.4

Cell Line and passage (p)	# of cells normal	Abnormalities Detected
11a p19 Eggan	**18/20**	**10% additional marker chromosome unidentified**
11a p27 Eggan	1/21	95% extra Y chromosome
11b p13 Eggan	**19/20**	**5% Tri-1**
11b p39 PALS	1/20	95% Tri-Y
11c p42 PALS	**15/20**	**25% small deletion in Ch2**
15b p27 Eggan	11/20	40% +(1)(q25.3), 5% Tri-X, +(1)(q25.3)
15b p34 Eggan	10/20	45% +(1)(q25.3), 5% Tri-X, +(1)(q25.3)
17a p17 Eggan	**21/21**	**none**
17b p13 Eggan	**20/20**	**none**
18a p30 Eggan	**18/20**	**10% -X**
18b p29 Eggan	**20/20**	**none**
18c p27 Eggan	**20/20**	**none**
20b p18 Eggan	**18/20**	**10% non-clonal tetraploid with loss**
27b p40 Eggan	2/20	80% Tri-17, addition to Ch9
27b p42 PALS	1/20	85% Tri-17, 10% Tri-17, Tri-12
27e p32 Eggan	**19/20**	**5% Tri-17**
29B p21 PALS	**19/20**	**5% -X, Tri-17, Tri-15**
29d p24 PALS	1/20	95% Tri-15
29e p29 PALS	0/20	100% Tri-20

Table 4.4. Some iPSC lines show abnormal karyotypes

A number of iPSC lines are summarized including the percentage of normal cells as well as abnormalities detected. Passage number (p) and lab that cells were grown is indicated for each report. Bold fonts indicate normal lines. We have previously reported iPS cell line 29A as having a normal karyotype (Dimos, Rodolpha et al. 2008). Abnormalities found in only one of twenty metaphase spreads (5% of cells) are considered "non-clonal" variants and were assumed to be technical artifacts. Lines with >75% normal karyotype were considered normal. Of lines able to generate $ISL1^{+}$ neurons under standard differentiation protocol 69% (9/13) had normal karyotypes; of ISL1-incompetent lines 33% (1/3) had continuous normal karyotypes: 27e was normal, 11b was normal at early and abnormal at later passage, and 29e was abnormal.

Figure 4.12

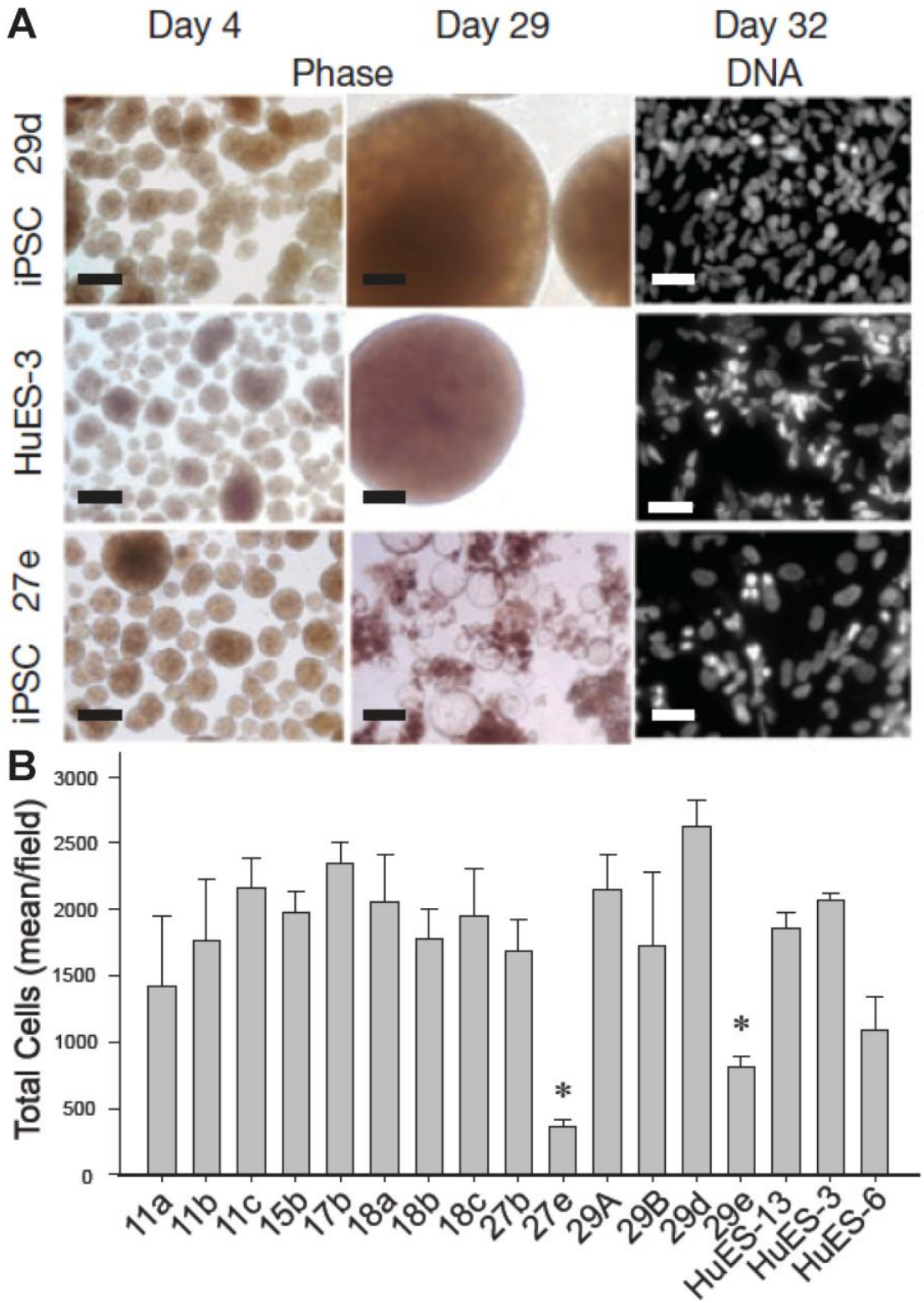
A
Day 4
Day 29
Day 32
Phase
DNA
iPSC 29d
HuES-3
iPSC 27e
B
Total Cells (mean/field)
3000
2500
2000
1500
1000
500
0
*
*
11a
11b
11c
15b
17b
18a
18b
18c
27b
27e
29A
29B
29d
29e
HuES-13
HuES-3
HuES-6

Figure 4.12. 2 of 16 iPSC lines display a defective EB and total cell number phenotype during motor neuron differentiation

(A) During standard motor neuron differentiation, iPSC lines 27e and 29e showed abnormal embryoid body morphology and dissociated cell survival phenotype compared to all other iPSC and ESC lines (HuES-3, 29d, 27e shown), phase scale bar 500 μm; DNA scale bar 129 μm. (B) Total cell output was quantified for each line at day 32 of differentiation by averaging the total number of $DAPI^+$ nuclei per image field and taking the mean of n experiments for each line (see Table 4.5) ±SEM. Kruskal-Wallis One Way ANOVA on Ranks showed a significant difference between lines ($p=0.027$) and Dunn's post-hoc tests showed that both 27e and 29e were significantly different than line 29d (* $p<0.05$), see Table 4.5

Table 4.5

Total cells per image field (Kruskal-Wallis One Way ANOVA on Ranks)				
line	n	mean +/- SEM	H(°s freedom)=	p-value
11a	3	1395 +/-532	H(19)=32.585	0.027
11b	3	1762 +/-463		
11c	4	2162 +/-220		
15b	2	1894 +/-151		
17a	1	1501 +/- na		
17b	2	2240 +/-155		
18a	5	2012 +/-336		
18b	7	1751 +/-227		
18c	6	1906 +/-347		
27b	7	1678 +/-241		
27e *+	3	360 +/-58		
29A	10	2135 +/-264		
29B	4	1693 +/-529		
29d *	5	2578 +/-200		
29e +	6	816 +/-77		
HUES13	5	1817 +/-120		
HUES3	4	2043 +/-53		
HUES3-GFP	1	2007 +/- na		
HUES6	2	1036 +/-72		
HUES9	1	1425 +/- na		
Dunn's pairwise	Diff of Ranks	Q	p-value	Dunn's pairwise
* 27e vs. 29d	65.267	3.799	<0.05	27e vs. 29d
+ 29e vs. 29d	55.767	3.915	<0.05	29e vs. 29d

Table 4.5. Statistical analysis of mean total cells numbers per line after dissociated cell seeding identifies 2 defective iPS lines

Kruskal-Wallis One Way ANOVA on Ranks for total cell number shows that the 2 of 16 iPSC lines with abnormal EB phenotype have significantly different total cell numbers. Day 32 differentiations were stained, imaged, and quantitated for mean cells ($DAPI^+$) per image field, and then compared for n different experiments per line. Mean ±SEM is shown for each line. The ANOVA showed a significant effect of line identity. All significant post hoc pairwise comparisons are shown.

Figure 4.13

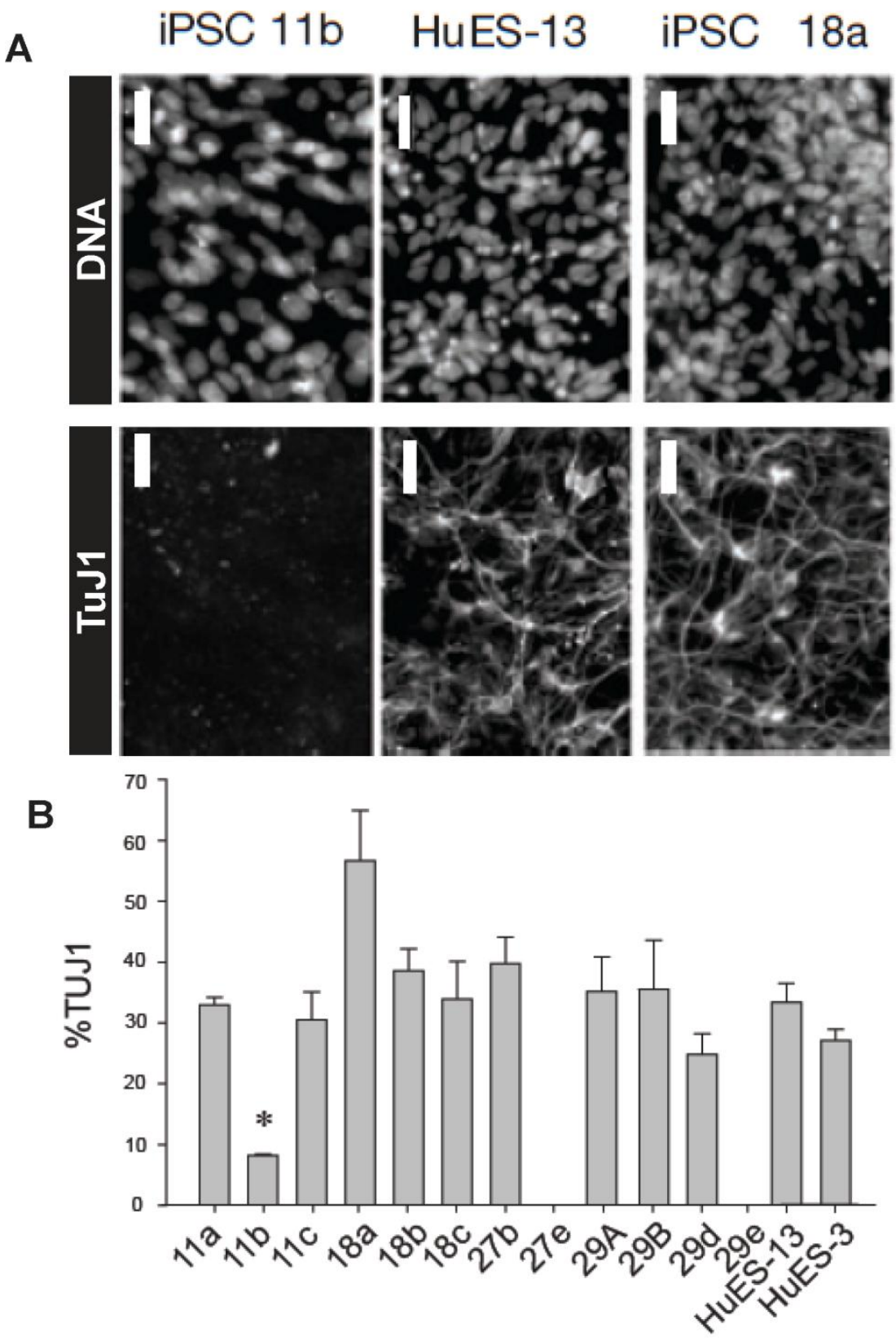
A
iPSC 11b
HuES-13
iPSC 18a
DNA
TuJ1
B
%TUJ1
70
60
50
40
30
20
10
0
*
11a
11b
11c
18a
18b
18c
27b
27e
29A
29B
29d
29e
HuES-13
HuES-3

Figure 4.13. 1 of 14 iPSC lines shows a neuronal defect after standard motor neuron differentiation

(A) During standard motor neuron differentiation, iPSC line 11b had typical EB morphology and normal total cell numbers, but showed drastically reduced neuronal TuJ1 staining compared to all other lines (iPSC 11b, HuES-13, and iPSC 18a shown), scale bar 129 μm. (B) The percentage of $TuJ1^{+}$ cells was quantified for n experiments (see Table 4.6) and the mean %TuJ1 of all cells ±SEM is shown. One Way ANOVA showed line identity significantly affected %TuJ1 ($p=0.012$) and Holm Sidak post-hoc pairwise comparisons showed 11b was significantly different than 18a, see Table 4.6.

Table 4.6

% TUJ1+ cells (One Way ANOVA)				
line	N	mean +/- SEM	F-value	p-value
11a	3	32.9 +/-1.2		
11b *	3	8.1 +/-0.2		
11c	4	30.4 +/-4.6		
18a *	5	56.6 +/-8.3		
18b	7	38.5 +/-3.6		
18c	6	33.9 +/-6.2		
27b	7	39.7 +/-4.3		
29A	10	35.1 +/-5.7		
29B	4	35.5 +/-8.0		
29d	5	24.8 +/-3.4		
HUES13	5	33.3 +/-3.1		
HUES3	4	27.0 +/-1.8	2.934	0.012
Holm Sidak pairwise	Difference of means		t value	p-value
* 18a vs. 11b	48.495		5.037	0.002

Table 4.6. ANOVA for %TuJ1 showed line 11b had a significantly different phenotype.

Day 32 differentiations were stained, imaged, and quantitated for mean %TUJ1$^+$ cells (of DAPI$^+$ cells) per image field. The mean of n different experiments per line ±SEM is shown. All significant post hoc pairwise comparisons are shown.

Figure 4.14

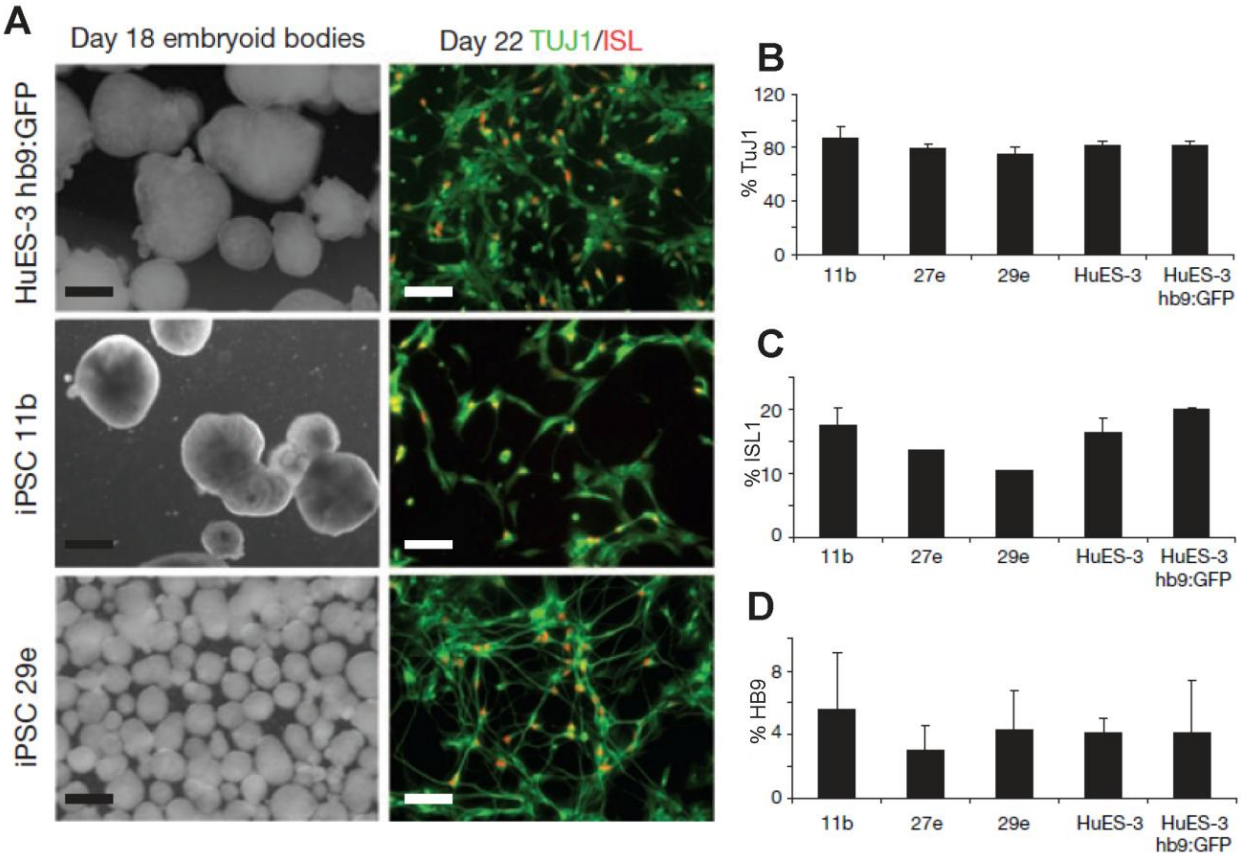

Figure 4.14. Pharmacological neuralization completely rescues all three defective-phenotype iPSC lines

(A) Dual inhibition of TGF-beta type I signaling rescues the defective EB and total cell number phenotype of both affected iPSC lines (27e not shown and 29e shown) and also rescues the Tuj1 phenotype for line 11b, HUES-3 HB9:GFP shown as ES control. Phase scale bars 500 μm, immunostaining scale bars 100 μm. (B-D) Quantification of immunostaining for defective lines (11b, 27e, 29e) and ESC controls shows complete rescue for: (B) %TUJ1^{+} of all cells; (C); %ISL1^{+} of all cells; and (D) %HB9^{+} of all cells, n=3 independent experiments, Mean ±SEM shown.

Figure 4.15

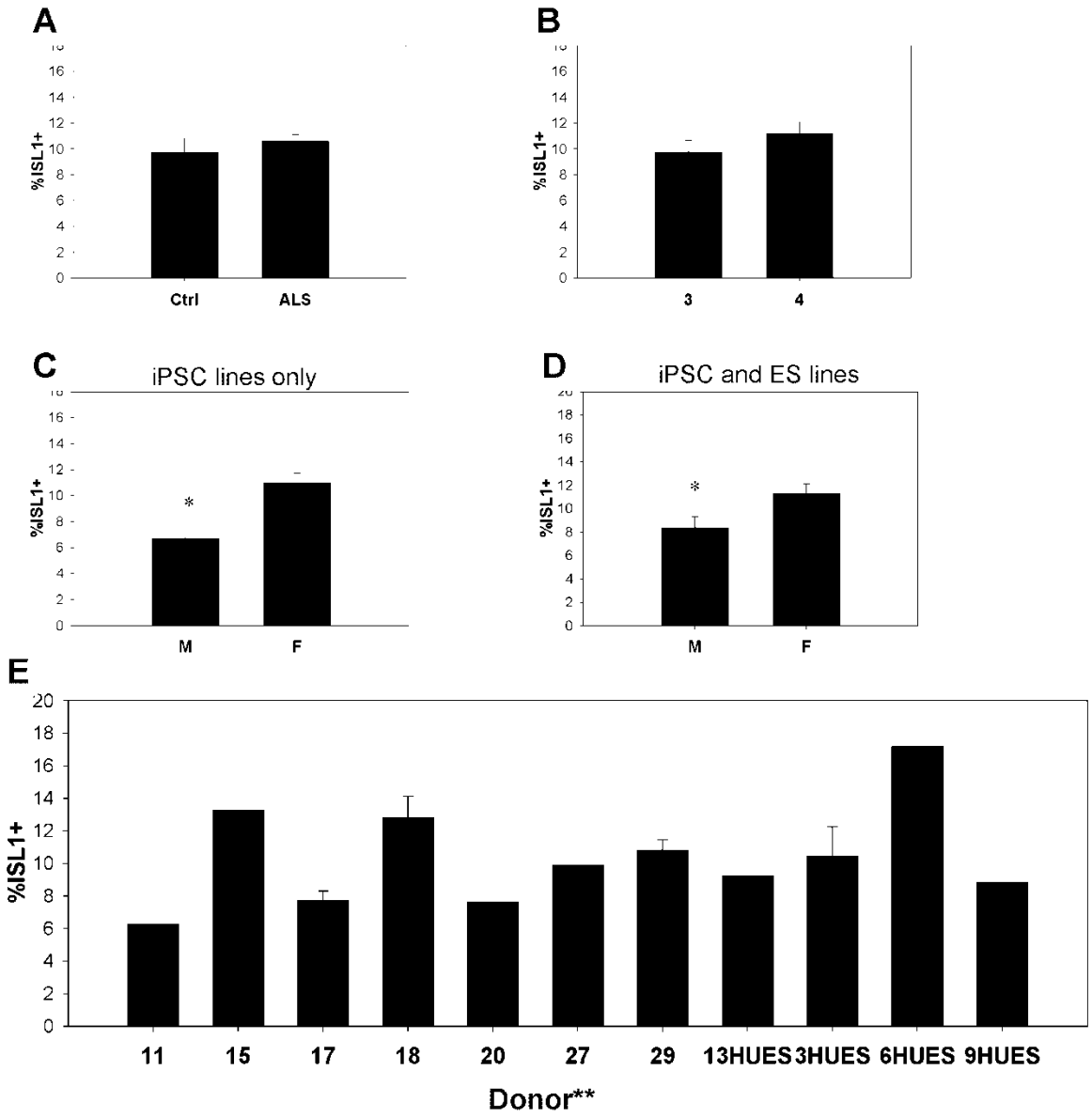
A
%ISL1+
Ctrl
ALS
B
%ISL1+
3
4
C
iPSC lines only
%ISL1+
*
M
F
D
iPSC and ES lines
%ISL1+
*
M
F
E
%ISL1+
11
15
17
18
20
27
29
13HUES
3HUES
6HUES
9HUES
Donor**

Figure 4.15. Sources of variability in motor neuron differentiation between iPSC lines

(A-E) The mean of all experiments per line were averaged and the mean of n lines per category ±SEM is shown. There was no significant difference (A) between control (Ctrl) and ALS lines or (B) between 3- and 4-factor reprogrammed lines. (C) iPSC lines and (D) all stem cell lines from male donors showed a significantly different %ISL1 efficiency from female, (*$p<0.05$). (E) lines from individual donors showed characteristic efficiencies and ANOVA showed that donor identity had a significant effect on %ISL1 (**, $p=0.003$), however no pairwise post-hoc tests reached significance. See Table 4.2 and 4.7.

Table 4.7

% ISL+ cells (One Way ANOVA)					
Male v. Female	n= # of lines	experiments	mean +/- SEM	F-value	p-value
Male	6	13	8.4 +/- 0.9	4.595	0.048
Female	12	57	11.3 +/-0.8		
Holm Sidak pairwise	Difference of means		t value		p-value
M vs. F	2.92		2.144		0.048

% ISL+ cells (One Way ANOVA)						
donor	iPS/ES	n= # of lines	experiments	mean +/- SEM	F-value	p-value
11	iPS	2	9	6.2 +/-0.01		
15	iPS	1	1	13.3 +/- na		
17	iPS	2	3	7.7 +/-0.6		
18	iPS	3	19	12.8 +/-1.3		
20	iPS	1	1	7.6 +/- na		
27	iPS	1	7	9.9 +/- na		
29	iPS	3	19	10.8 +/-0.6	11.816	0.006
HUES13	ES	1	5	9.3 +/- na		
HUES3	ES	2	5	10.5 +/-1.8	Including ESC	Including ESC
HUES6	ES	1	2	17.2 +/- na	lines:	lines:
HUES9	ES	1	1	8.8 +/- na	11.655	0.003
Holm Sidak pairwise						
none significant						

Table 4.7. ANOVAs on %ISL1 show significant effects of donor identity and sex

Mean %ISL$^+$ of all cells (DAPI$^+$ nuclei) per image field were averaged for all experiments per line and then the mean ±SEM of n different lines per sex, and n different lines for each donor were compared. ANOVA indicated a significant effect of donor sex and donor identity, but no post-hoc pairwise comparisons for donor identity were significant.

Figure 4.16

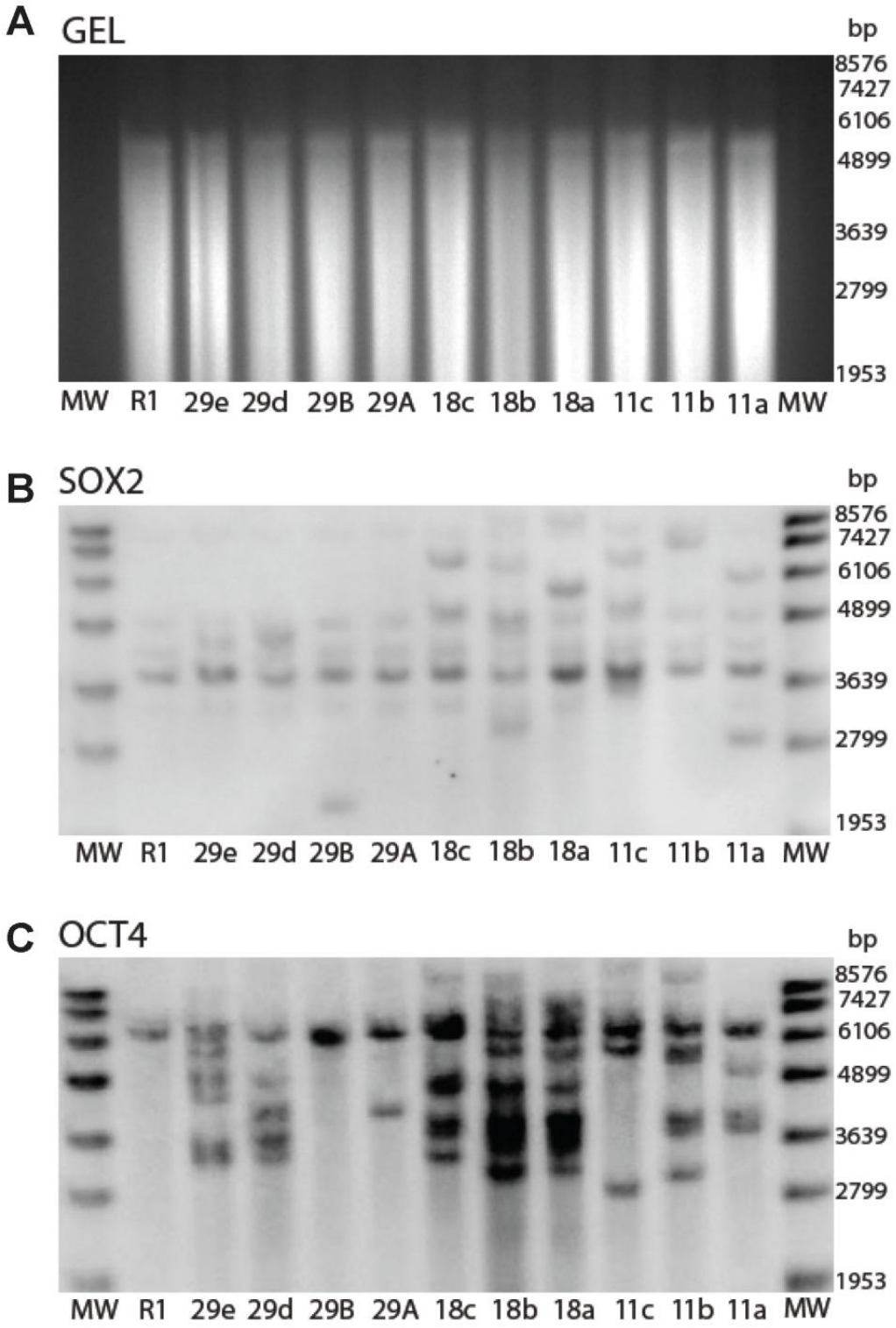
A
GEL
bp
8576
7427
6106
4899
3639
2799
1953
MW R1 29e 29d 29B 29A 18c 18b 18a 11c 11b 11a MW
B
SOX2
bp
8576
7427
6106
4899
3639
2799
1953
MW R1 29e 29d 29B 29A 18c 18b 18a 11c 11b 11a MW
C
OCT4
bp
8576
7427
6106
4899
3639
2799
1953
MW R1 29e 29d 29B 29A 18c 18b 18a 11c 11b 11a MW

Figure 4.16. Southern blots show multiple lines from the same donor are independent lines (A) 6.5 μg BglII digested genomic DNA was separated by electrophoresis on an agarose gel, (B) Southern Blot and hybridization with DIG-labeled probe for SOX2 cDNA transcript showed a conserved $SOX2^{+}$ restriction fragment at ~3800bp in the control ESC line and all iPSC lines, as well as a unique pattern of bands for each iPSC line demonstrating unique transgene insertion sites and therefore unique line identities. (C) Hybridization with OCT4 cDNA probe showed endogenous bands at ~6000bp in ESC control and iPSC lines, as well as unique MW species indicative of unique transgene integration sites, confirming unique line identities.

Figure 4.17

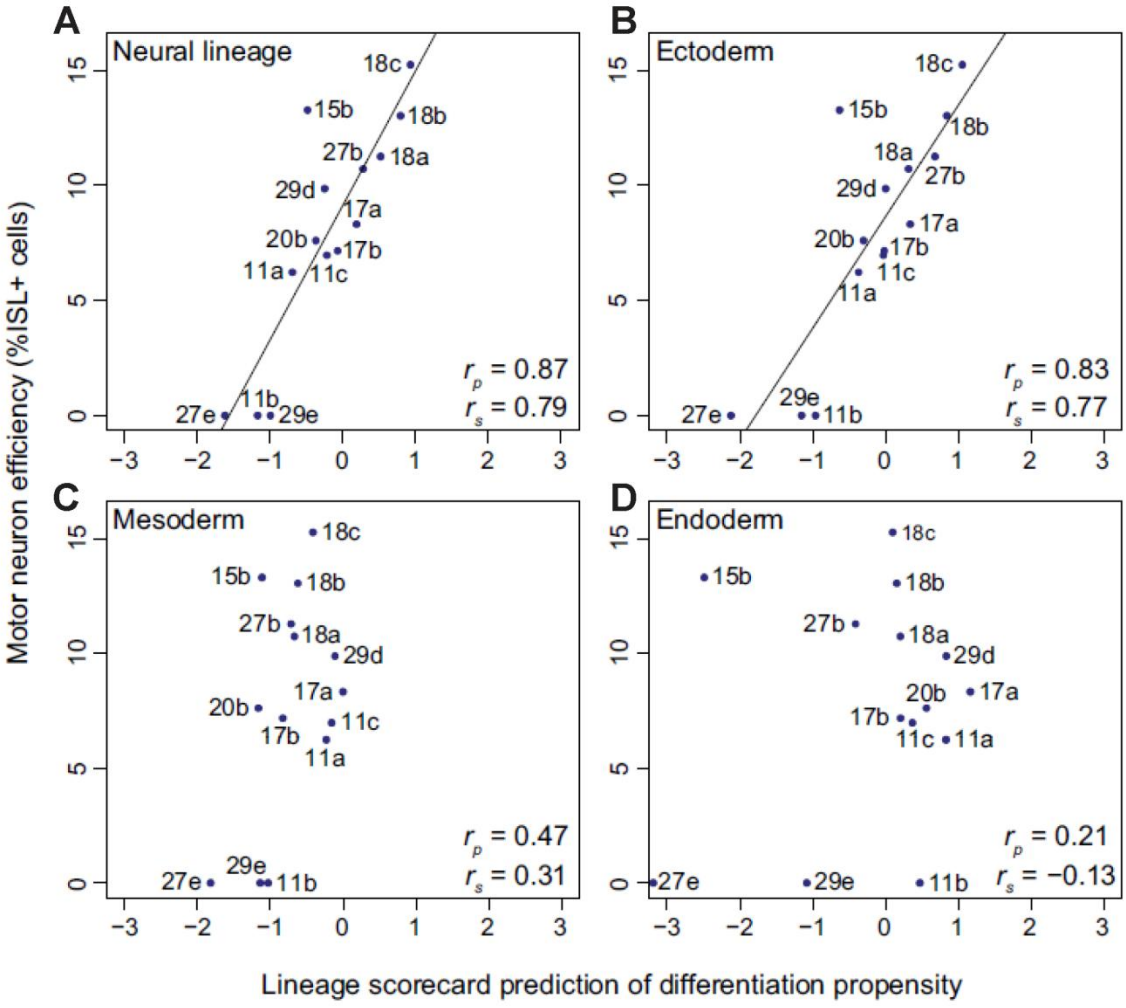
A
Neural lineage
r_p = 0.87
r_s = 0.79
B
Ectoderm
r_p = 0.83
r_s = 0.77
C
Mesoderm
r_p = 0.47
r_s = 0.31
D
Endoderm
r_p = 0.21
r_s = −0.13
Motor neuron efficiency (%ISL+ cells)
Lineage scorecard prediction of differentiation propensity

Figure 4.17. Empirical measures of cell-line-specific motor neuron efficiency correlate with lineage scorecard predictions for germ layer and neuronal differentiation proclivity. Correlation between the lineage scorecard estimates for the neural lineage and three germ layers versus the cell-line-specific efficiency of directed differentiation into motor neurons (rp, Pearson's correlation coefficient; rs, Spearman's correlation coefficient). Motor neuron efficiencies were measured by the percentage of $ISL1^{+}$ cells at the end point of a 32 day neural differentiation protocol. Further details including biological replicates and standard errors are available from Table S7 (Bock, Kiskinis et al. 2011)

Chapter 5. Controlling the rostrocaudal subtype diversity of human stem cell-derived motor neurons.

Introduction

While spinal motor neurons selectively degenerate and die in ALS, their susceptibility is not uniform. Distal muscle-innervating motor neurons of LMC subtype for example are more typically the site of onset than proximal thoracic muscle innervating HMC/MMC motor neurons (Ravits, Paul et al. 2007). On the other hand sympathetic chain innervating PGC motor neurons may be relatively preserved, and eye and pelvic sphincter innervating motor neurons are almost completely spared—oculomotor and Onuf's nuclei motor pools (Kanning, Kaplan et al. 2010). If motor neuron subtypes with strong differential responses to ALS could be generated in vitro, their comparison could sharpen the resolution of in vitro disease phenotypes or molecular changes and allow direct investigation of the mechanisms underlying those differences. However as we have shown in Chapters 3 and 4, ES- and iPS-MNs are predominantly cervical, and therefore are unlikely to contain a robust cohort of either thoracic PGC or lumbar Onuf's nuclei motor neurons. As we have discussed (Chapter 1 Part I) early rostrocaudal patterning events control the diversification of motor neurons into these and other subtypes. In order to contemplate generating these more caudal motor neuron subtypes we would have to generate motor neurons with more caudal identities. We therefore asked how more caudal motor neurons are generated during development of vertebrate model organisms—chick and mouse—and then sought to recapitulate these events in vitro at a timecourse appropriate to human development.

During early spinal cord development the morphogens Wnt and FGF and later FGF and RA are produced from specific anatomic sources and act over two specific embryonic phases. In the

first phase—from the mid-primitive streak stage to the 4-somite stage—Wnt from the paraxial mesoderm and FGFs from the primitive streak activate *CDX* gene expression which encodes caudal neural character in prospective hindbrain and spinal cord progenitor cells (Fig. 5.1A) (Nordstrom, Maier et al. 2006).

In the second phase—from the 4-somite to the 16-somite stage—FGFs secreted from the regressing node expose progressively more caudal prospective spinal cord progenitors to higher concentrations of FGF for longer durations while RA synthesized by the somites formed lateral to the neural tube in the rostral wake of the node exposes more rostral spinal progenitors to higher levels of RA (Fig. 5.1C) (Liu, Laufer et al. 2001; Nordstrom, Maier et al. 2006). Spinal progenitor cells exposed to RA, RA and FGF, or FGF alone assume positional identities from caudal hindbrain to lumbar spinal cord as marked by the combinatorial expression of *HOXB* and *HOXC* cluster genes (Bel-Vialar, Itasaki et al. 2002; Nordstrom, Maier et al. 2006). These rostrocaudal domains, with the additional influence of node derived GDFs on the prospective lumbar region, give rise to the code of HOXC protein expression which determines motor column identities (Liu, Laufer et al. 2001).

While these patterning morphogens and *CDX* and *HOX* caudal identity genes are not described in human, a recent study has identified neural marker genes whose temporal expression profiles bracket the cognate phases of human embryonic development: late primitive streak to 16 somite stage. PAX6 shows a novel expression pattern in early primate and human embryos, compared to mouse and chick, appearing as a selective marker of early neuroectoderm by the neural plate stage, day 18 (Zhang, Huang et al. 2010) (Fig. 5.2). By day 26—the 19 somite stage—PAX6 no longer serves as a pan-neural marker, but is restricted to its role as an effector of dorsoventral positional identity as it is in mouse and chick. By this stage SOX1 is expressed in all neural cells

in human embryos. The molecular profile of human spinal neuroectodermal cells in vivo during the patterning period we inferred is therefore bracketed at the onset by the initiation of PAX6 expression and at the end by the pan neural expression of SOX1. These markers might therefore be used to correlate the developmental status of in vitro cultures with in vivo development during the time period of caudal patterning.

If an appropriate time window for inducing more caudal neural pattern can be defined in vitro, we could then test the combinations of Wnt, FGF and RA which the vertebrate model predicts should determine rostrocaudal identity. We would use the RA-only condition, which we previously described in Chapter 3, as a rostral spinal control and starting point. The predicted outcomes of more caudalizing FGF-containing conditions are motor neuron populations with reduced cervical HOXA5^{+}-, increased caudal brachial and thoracic HOXC8^{+}-, and increased thoracic and lumbar HOXD9^{+}-motor neuron subtypes.

Results

Inferring a time window for caudal neural patterning in human

The events leading to caudal neural patterning and the graded expression of HOX genes in post-mitotic motor neurons occur in two embryonic phases in chick. In the first phase (primitive streak to 4 -somites) Wnt and FGF demarcate the caudal neural plate (prospective hindbrain and spinal cord) from more rostral neural tissues. While the expression and activity of Wnt and FGF are not described in the human system, the human embryo passes through nearly identical stages of early embryonic development as the chick. The human embryo is at mid primitive streak at

day 15, and 4 somite stage at day 18; we therefore inferred that Wnt and FGF may be acting in the human embryo during this time (Fig. 5.1B).

In the second phase (4 to 16 somites) RA and FGF gradients lead to the differentiation of caudal neural tissues into caudal hindbrain, rostral and caudal spinal cord**.** Again, these morphogens are not described in the human embryo, but the human embryo reaches 17 somites by day 22 (Fig. 5.1D). These comparisons predict that Wnt and FGF act from day 15-18 and that FGF and RA act from day 18 -21 of human development to generate spinal positional identities (Fig. 5.1D). In order to translate this inferred patterning period to our in vitro system we made two final assumptions. First, we assumed that in vitro development would proceed at an in vivo rate. Second, since human ES cells are derived from day 5 blastocysts, we subtracted 5 days of development from the inferred period of human in vivo caudal neural patterning to project an in vitro timing window of day 10-17.

Molecular markers of neural lineage induction correlate in vitro timing with in vivo

To monitor the transition away from pluripotency we quantified expression of the core pluripotency gene *OCT4 (*Nichols, Zevnik et al. 1998). *OCT4* mRNA levels were 95% of day 0 (maximum) at day 6, but reduced to 10% of maximal expression at day 10 and completely extinguished by day 17; this was confirmed at the protein level by immunostaining (Fig. 5.3A, B). In order to confirm our assumption that the time course of neural differentiation in vitro would parallel that observed in vivo, and thereby validate the choice of days 10-17 for caudal patterning, we tested the expression of two key markers of neural identity, *PAX6* and *SOX1*, whose expression profile in vivo (Zhang, Huang et al. 2010) (Fig 5.2) marks the same period we inferred above. The first neural lineage marker, *PAX6,* was upregulated at day 10 (18% of

maximum) whereas *SOX1* expression at the same stage was only 4% above baseline. Both proteins however could be detected at low frequency in some EBs (Fig. 5.3B). By day 17 however, both *PAX6* and *SOX1* had reached peak expression levels. Subsequently *SOX1* expression decreased slightly (to 80% of maximum), while *PAX6* decreased substantially (to 22% of maximum). The decline of *PAX6* after day 17 fits with its later in vivo function in dorsoventral patterning in vertebrates, since the increased concentration of SHH protein at day 17 should ventralize cultures and inhibit *PAX6* expression. We concluded from these data that in vitro differentiation matched the time course of in vivo development since days 10-17 in vitro showed a similar molecular profile to that observed over the corresponding period (day 15-26) in vivo. Having inferred a patterning window in vivo, and then correlated in vitro marker expression with in vivo markers, we designed an experiment to test the effect of the relevant in vivo morphogens during this in vitro time window.

Rostrocaudal patterning with Wnt, FGF, and RA

The model of vertebrate rostrocaudal positional patterning reviewed above suggests that Wnt and FGF first define caudal neural identity, and then combinations of FGF and RA subdivide the hindbrain and spinal cord into hindbrain, rostral spinal cord, and caudal spinal cord. Although node-derived GDFs are required for lumbosacral HOXC10 expression in chick (Liu, Laufer et al. 2001), for simplicity we chose to focus on the initial two periods when caudal identities are determined and refined by Wnt, FGF and RA (Nordstrom, Maier et al. 2006) and to collapse these two patterning periods together. We predicted that Wnt+RA, Wnt+RA+FGF, or Wnt+FGF if applied during the appropriate time window, would generate progressively more caudal sets of spinal motor neurons, as they had been shown to do in chick explants (Nordstrom, Maier et al. 2006). To test this hypothesis we treated EBs with these combinations during the in vitro time

window we identified (Fig 5.4). The endpoint of this analysis was the HOX profile of post-mitotic motor neurons.

FGF treatment induces a caudal shift in HOX gene expression

We first asked if FGF treatment induced a caudal shift in the expression of *HOX* genes in the whole culture (Fig. 5.5). qPCR analysis of *HOX* gene mRNA expression showed that when FGF was added to RA there was a small decrease in *HOXA5* (0.8 fold RA) and an increase in all caudal *HOX* genes tested (*HOXC6*, 4 fold; *HOXC8*, 17 fold; *HOXD9*, 4 fold; and *HOXC10*, 2 fold), although this difference only reached significance for *HOXC6* (t-test p=0.02) (Fig. 5.5A). When FGF was used in the absence of RA we observed a significant decrease in *HOXA5* levels as compared to RA alone (0.2 fold), a significant decrease in *HOXC6* and a large decrease in *HOXC8*, when compared to RA+FGF , suggesting a shift away from cervical through rostral thoracic spinal identities. FGF alone compared to RA+FGF also showed unchanged *HOXD9* and increased *HOXC10* suggesting stable caudal thoracic and increased lumbar gene expression. We concluded from these data that FGF, when added to RA, generated a more caudal positional profile of *HOX* gene expression, as shown by decreased *HOXA5*, and increases in all caudal *HOX* genes. Notably the largest increases were in *HOXC6* and *HOXC8* which suggested brachial to mid-thoracic positional identities, although the increase in *HOXD9* and *HOXC10* was consistent with some mid-thoracic to lumbar gene expression as well. We also concluded that FGF alone induced an even more caudal profile of *HOX* gene expression, based on the significant decrease in *HOXA5* from RA and the trend decrease compared RA+FGF, the decreases in *HOXC6* and *HOXC8* compared to RA+FGF, the increase in *HOXD9* compared to RA, and importantly the increased *HOXC10* compared to RA+FGF.

We then asked whether HOX proteins were affected by FGF treatment by staining cells for HOXA5, HOXC8, and HOXD9 (Fig. 5.5B, C). We observed a trend decrease in the percent of total cells staining for HOXA5 when RA was compared to RA+FGF (11% vs. 5% respectively), a trend increase in HOXC8 (1% vs. 7% respectively), and a significant increase in HOXD9 (2% vs. 8% respectively, $p<0.05$). FGF alone induced significantly fewer $HOXA5^+$ cells compared to RA (2% vs. 11% respectively, $p<0.05$), and fewer than RA+FGF. FGF alone also induced more $HOXC8^+$ (3%) and $HOXD9^+$ (3%) cells. This was elevated as compared to RA alone but less than with the combination of RA+FGF, significantly so in the case of HOXD9 ($p<0.05$). We concluded from these data that HOX protein expression showed a clear caudal shift in positional identity when FGF was added to RA. When FGF was used alone we saw a stronger and significant decrease in $HOXA5^+$ cells suggesting a less rostral identity. The decrease in $HOXC8^+$ and $HOXD9^+$ cells could supports the idea that FGF alone generated even more caudal positional identities than RA+FGF, but could also mean that cultures were less spinal in identity.

FGF leads to a reduction in the number of neurons and motor neurons

To determine whether FGF treatment affected the efficiency of neuronal or motor neuronal differentiation we stained cultures for the neuronal marker TuJ1, and the motor neuron markers HB9 and ISL1 (Fig. 5.6A,B,C). The percent of total cells positive for TuJ1 was slightly but significantly decreased when RA was compared to RA+FGF (65% vs. 56%, $p<0.05$), and was further decreased when FGF was used without RA (53%, $p<0.05$ vs. RA). We concluded from these data that FGF significantly decreased the percentage of differentiated neurons present in culture, although the magnitude of this change was relatively small (-9% for RA FGF vs. RA and -3% for FGF vs. RA+FGF). From these data we could not discriminate whether this effect was

the result of increases in the numbers of undifferentiated neural progenitor cells or the preferential specification of non-neuronal cell types.

Because FGF reduced the percentage of differentiated neurons, we next wanted to determine whether the efficiency of motor neuron induction was decreased and if the pattern of motor neuron marker expression was changed. It was also important to establish that the motor neuron markers HB9 and ISL1 were still expressed exclusively by neurons and not by non-neural cells which also express these markers in vivo. We therefore stained cultures for HB9, ISL1, and TuJ1 and found that >90% of $HB9^+$ or $ISL1^+$ cells co-expressed TuJ1, and there was no significant difference between conditions (Fig. 5.6A, B). These data demonstrated that virtually all $HB9^+$ or $ISL1^+$ cells were neurons under all conditions tested. The percent of cells expressing HB9 however was significantly decreased under RA+FGF conditions vs. RA (8% vs. 13% respectively, $p<0.05$), and was significantly decreased with FGF-only compared to RA+FGF or RA (4%, $p<0.05$) (Fig. 5.7C). The percent of $ISL1^+$ cells was also significantly decreased with FGF-only (5%, $p<0.05$) compared to either RA (11%) or RA+FGF (9%) (Fig 5.6C). The degree of HB9 and ISL1 coexpression however, was not significantly changed by either treatment (Fig. 5.6C). We concluded from these data that FGF treatment reduced the efficiency of neuronal differentiation and of motor neuron differentiation. However $HB9^+$ and $ISL1^+$ cells generated in these conditions remained predominantly neuronal and their pattern of ISL1/HB9 co-expression continued to match that described in vivo. We could therefore use these motor neuron markers with confidence in all conditions tested.

FGF induced caudal motor neuron subtypes at the expense of rostral

To determine whether FGF affected the positional identity of motor neurons specifically we costained cultures for HB9 or ISL1, and HOXA5, HOXC8, or HOXD9 (Fig. 5.7A). The percent of $HB9^+$ cells expressing HOXA5 was significantly decreased from RA (34%) under both RA+FGF (18%, $p<0.05$) and FGF-only (9%, $p<0.05$) conditions. The percent of $HB9^+$ cells expressing HOXC8 or HOXD9 was also increased from RA (13% HOXC8, 7% HOXD9) under RA+FGF treatment (34% HOXC8, 24% HOXD9) but this difference was only significant for HOXD9 ($p<0.05$). When FGF alone was used, the fraction of HOXC8 (37%) and HOXD9 (29%) of $HB9^+$ cells was further increased and significantly different from RA alone ($p<0.05$) (Fig. 5.7B). When the shift in HOX expression was gated for $ISL1^+$ cells, the results were virtually identical (not shown). We concluded from these data that FGF induced a caudal shift in ES-MN positional identity. When FGF was used in the absence of RA, the trend toward even lower HOXA5, and higher HOXC8 and HOXD9, compared to RA+FGF suggested an even more caudal positional identity.

ES-MN HOX protein expression is mutually exclusive even in more caudal populations

Because we now observed substantial numbers of motor neurons expressing more caudal HOX proteins we asked whether caudalized ES-MNs would adopt coherent positional identities characterized by mutually exclusive HOX protein expression as reported in vivo (Chapter 1) and for predominantly rostral ES- and iPS-MNs (Chapter 2 and Chapter 3). Because of the strongly reduced total motor neuron numbers in the FGF-only condition, and the clearly caudalized identities observed in the RA+FGF condition, we restricted these analyses to the RA and RA+FGF conditions. When cultures were triple stained for HB9 or ISL1 and either HOXA5 and

HOXC8 or HOXA5 and HOXD9 (Fig. 5.8A, B) we found that under rostral or caudal conditions fewer than 5% of $HB9^+$ cells expressing either HOX protein coexpressed the other (Fig. 5.8C, D). We concluded from these data that ES-MNs were successfully able to interpret competing patterning cues, RA and FGF, and resolve coherent, mutually-exclusive HOX identities. We next wanted to ask if the caudal shift in rostrocaudal identity coincided with any change in the distribution of columnar subtypes.

Caudalization does not change motor column subtype distribution

In order to determine whether the caudal shift in HOX expression would lead to a shift in motor column identity, we stained caudalized and control (RA) cultures for markers of LMC (FOXP1) and MMC (LHX3) identities (Fig. 5.9A). We found that the percentage expression profile of LHX3 and FOXP1 for $HB9^+$ motor neurons was not significantly different in caudal cultures (Fig. 5.9A, B, $p>0.05$). This result is consistent with the in vivo expression profile for $HOXA5^+$, $HOXC8^+$, and $HOXD9^+$ motor column subtypes, because each of these HOX genes is expressed by motor neurons in nearly equal proportions of limb and non-limb innervating spinal regions in vivo and therefore includes, MMC, HMC, PGC, and LMC columnar subtypes in relatively equal proportions. Therefore taking away motor neurons positive for any one of these HOX genes, and adding any another would not be predicted to substantially change the motor column profile.

HOX and column marker staining more precisely classifies potential subtype identities

To more precisely classify in vitro-generated ES-MNs using in vivo expression patterns, we stained control and caudalized cultures for HB9 or ISL1, a positional marker (HOXA5, HOXC8, or HOXD9), and the LMC column marker FOXP1, the marker for LMC/PGC motor column identity and quantitated expression profiles for all $HB9^+$ and $ISL1^+$ cells (Fig. 5.10A). When

these in vitro combinatorial expression patterns were matched to in vivo correlates (Fig. 5.10B) the range matched all motor neuron staining profiles found in the spinal cord between cervical and mid lumbar levels in vivo (Fig. 5.10C). Because each marker combination we measured was consistent with more than one in vivo motor neuron subtype, in vitro staining combinations yielded several potential identities. We therefore list the possible in vivo identities based on our evidence. We concluded however that the rostrocaudal and columnar range of potential subtypes included several with differential responses to ALS in vivo: LMC vs. thoracic HMC/MMC, and thoracic PGC.

Testing caudal patterning on accelerated protocol differentiations and iPS cells

In order to search for motor neuron-intrinsic subtype-selective ALS phenotypes, these specific subtypes must be differentiated from stem cells with ALS genotypes. We showed in Chapter 3 that iPS cells generate the same range of predominantly cervical motor neuron subtypes in vitro. In order to study ALS-refractory thoracic or lumbar subtypes, iPS cells must be competent to generate these more caudal subtypes as well. We therefore next tested whether iPS cells would respond similarly to the rational approach for generating caudal motor neurons we developed using ES cells.

As discussed in Chapter 2, recent developments in pharmacological control of neural induction led us to establish an Accelerated Protocol (Fig. 3.4A) which more than doubled motor neuron differentiation efficiency. This technical development may prove to be a superior strategy for generating motor neurons for disease studies and may be useful for studies of development as well. However since by intention it deviates from some aspects of in vivo neural development,

especially temporal, we wanted to ask how amenable it would be to our developmentally based patterning approach.

Accelerated cultures show early expression of neuroectodermal markers

To target a developmental time window in accelerated cultures that was similar to that used for Standard Protocol patterning experiments above, we reasoned that the same early neural lineage markers, PAX6 and SOX1 could again be used to define an appropriate patterning window. Colleagues in the lab (Mackenzie Amoroso, Andrew Brunswick, Laurent Roybon, unpublished) found that by day 10 accelerated cultures showed the same widespread expression of PAX6 and SOX1 observed at day 17 under Standard Protocol conditions (not shown) indicating an acceleration of at least 7 days. These result corroborated previously published findings showing that neural induction may be largely complete by day 5 under similar conditions (Chambers, Fasano et al. 2009), which suggested an acceleration of at least 5 days. Finally we had observed that the onset of HB9-driven GFP expression was accelerated by 10 days (Chapter 2). This suggested that the only acceleration was in the early phase of neural induction and that subsequent development proceeded in parallel with Standard Protocol differentiations. We therefore shifted the patterning window for Wnt3a and FGF exposure backwards to day 5-12.

Accelerated Protocol cultures generate comparable motor neuron populations

We first wanted to test whether FGF-treated accelerated differentiations would generate a comparable spectrum of motor neurons. Both iPSC lines and ESC control generated abundant $HB9^+$ and or $ISL1^+$ neurons with RA, and slightly fewer motor neurons with FGF treatment (28%, 18%, and 17% under RA and 17%, 13%, and 15% $HB9^+$or $ISL1^+$ of total cells under RA+FGF treatment for RUES1-ES, iPS-29A, and iPS-18c respectively) (Fig. 5.11A, B). The

pattern of HB9 and ISL1 overlap was very similar between iPS lines and RUES1 control, although it appeared there was more overlap and fewer $HB9^{HIGH}$-only cells compared to Standard Protocol conditions (Fig. 5.11B). We concluded that using the Accelerated Protocol with iPS and ES cells generated motor neurons with similar profiles of pan-motor neuron marker expression and at similar efficiencies.

iPS-MNs respond to caudal patterning similarly to ES-MNs

We next asked if iPS cells would be competent to respond to FGF and generate caudal motor neurons. When we stained iPS- and ES-MNs for HOXA5 and HOXC8, we observed that for iPSC as well as ESC lines, only under caudalizing conditions were many $HB9^{+}$ cells stained with HOXC8 (Fig. 5.11C). Both iPS lines showed a decrease in the percent of $HOXA5^{+}$ motor neurons, and an increase in the percent of $HOXC8^{+}$ motor neurons, similar to the RUES1 control (Fig. 5.11D). We concluded from these data that differentiating iPS cells responded to developmental mechanisms to generate more caudal motor neuron subtypes in a fashion comparable to ES cells. We also concluded that the Accelerated Protocol, and accelerated differentiation approaches more broadly, may be compatible with developmentally based patterning approaches.

Discussion

FGF induces more caudal motor neuron subtypes

Vertebrate embryos use rostrocaudal patterning as a means to specify a diversity of motor neurons which are genetically, functionally and somatotopically matched to their muscle targets.

This model of development predicts that controlling rostrocaudal identity is necessary and sufficient to generate specific functional motor neuron subtypes at the level of both motor column and pool. In accord with the predictions of this model, we found that FGF, when added to RA, or used alone, generated a group of motor neurons with significantly more caudal positional identities. This shows that human spinal neuroepithelial cells can operate by the developmental rules defined in model systems. This finding also supports, though cannot not directly test, the idea that human motor neuron diversification in vivo is enacted by the same mechanisms as model vertebrates. Importantly these findings act as a proof of principle that complex developmental events defined in model systems can be translated to rational approaches for engineering the differentiation of highly specific cellular subtype of intellectual and disease relevance from human ES and iPS cells.

The profile of motor neurons was most rostral with RA alone, was caudalized by FGF addition in the presence of RA, and was the most caudal with FGF in the absence of RA. Generating specific cell types from stem cells is crucial to their use for studies of development and cellular function in health and disease. Therefore our results have broad implications for developmentally-based approaches to generating specific and hitherto unavailable cell types from human stem cells. Most specifically our findings render rostral and caudal motor neuron subtypes available for functional and disease-related studies.

A broad diversity of coherent subtypes generated across conditions

When we used the three HOX genes and two positive markers of motor column identity for which we had previously defined in vivo expression patterns we could assign a set of potential rostrocaudal and columnar identities to motor neurons generated in vitro. In aggregate these

potential identities spanned each motor column residing in spinal regions from cervical to mid-lumbar human spinal cord. However, because the HOX proteins we tested each span limb and non-limb-innervating territories, because FOXP1 is expressed by both LMC and PGC cells, and because we could not identify a human-reactive antibody for the HMC marker ER81, most of the transcription factor expression combinations we identified could potentially be assigned to several potential identities. Resolving these ambiguities is a major unsolved task looking forward since motor column-specific disease phenotypes can only be studied if motor column identities can be definitively monitored.

In cases where it was possible to test, we found a striking coherence of cellular identities at the level of transcription factor expression. For example, the mutual exclusion of HOXA5 and HOXC8 or HOXD9 matches the pattern found in vivo. Importantly under caudalizing conditions when a large percent of motor neurons expressed HOXC8 or HOXD9, these proteins were still expressed exclusively. This result shows that even in the context of competing positional information, differentiating ES cells are able to interpret these cues to resolve coherent identities. Furthermore, since the elaboration of motor pool subtype identity at the forelimb level depends on cross repressive interactions between many *HOX* genes, including *HOXA5-HOXC8* pair, our results suggest that ES- and iPS-derived motor neurons manifest an intact network of functional *HOX* responses which is required for coherent motor pool identities.

The interpretation of ES-MN identity based on column marker expression was less clear cut. The majority of motor neurons in vivo expressed the motor column markers LHX3 (MMC) and FOXP1 (LMC/PGC) mutually exclusively (Chapter 2). This was the case for most in vitro ES-MNs as well (Chapter 3). However a subset of cells inappropriately coexpressed these markers. As discussed in Chapter 3, one potential interpretation of this expression pattern is that these

cells match the novel brachial LMC putative motor pool identified in human fetuses in vivo. Alternatively, as seen in mouse ES-MN differentiation LHX3 expressed inappropriately according to mouse in vivo expectations, i.e., appears it is coexpressed by some $FOXP1^{+}$ motor neurons ((Peljto, Dasen et al. 2010) and Mackenzie Amoroso unpublished observations). This expression pattern may therefore be an in vitro artifact which could be interpreted as cells with confused molecular identities. The shift to dominant FOXP1 expression in matured cultures and loss of LHX3 expression, which we describe in Chapter 3, supports the interpretation that this cellular confusion is transient, and resolves in favor of clean LMC identities however. In either case this is small subset of cells, but future studies are needed to address its significance.

iPS cells are similarly responsive to caudal patterning

Finally we found that iPS cells showed the same response to caudal patterning as ES cells. Importantly, this result shows that human iPS cells regain the ability to execute specific developmental pathways when they are reprogrammed. This result is also critical for the larger goal of these studies: to generate ALS motor neuron subtypes in vitro which show differential disease responses in vivo. Identifying motor neurons which show unambiguous expression of thoracic and rostral lumbar HOX markers puts several of these subtypes in reach. The full rostrocaudal diversity of brachial LMC subtypes is likely represented by these cultures which will allow investigation of the mechanisms of heightened sensitivity of distal, limb projecting motor neurons to degeneration in comparison with proximal projecting motor neurons. Thoracic motor neurons (HOXC8 or HOXD9) that express no or low-level FOXP1 are consistent with either HMC/MMC or PGC identities respectively, and represent disease-delayed and disease-resistant populations. It will therefore be of great interest to determine if these motor neuron subtypes show differential disease responses in vitro.

Conclusions and Perspectives

Motor neuron functional and subtype-specific ALS phenotypes

As discussed above, the assignment of subtype identity based on combinatorial expression of the markers we validated in vivo lead to a set of several possible in vivo cognate identities for each combination. Disambiguation could be achieved in the future by several means. First, reagents to monitor expression of purely thoracic (HOXC9) or purely limb-level (HOXC6: brachial and HOXC10: lumbar) motor neurons would help to eliminate or support specific identities for in vitro cells. Since these genes also play functional roles in limiting and enabling position-specific columnar identities it is critical that their expression patterns be defined in human in vivo and in vitro. Their functional roles in determining motor column identity also make them crucial candidates to test using gain and loss of function strategies in vitro with motor column identity as the endpoint. Additional markers of subtype identity like RALDH2 (LMC), ER81 (HMC), and nNOS and pSMAD (PGC) would greatly add to the certainty of specific assignments. Furthermore, markers for individual motor pools are needed to investigate the biology of these specific subtypes.

The ultimate proof of identity however, no matter how precise the assemblage of correctly overlapping markers, will be to define functional phenotypes which are specific to motor columns and pools. These phenotypes could consist of column or pool-specific behavior in xenotransplantation assays (motor column settling position and axonal pathfinding) or in vitro assays which mimic aspects of these or other phenotypes defined in vivo. In addition, motor pools which show defined gene expression and functional responses to exogenous target derived factors (pSMAD expression via BMP signaling in PGC motor neurons, and PEA3 expression via

GDNF in CM/LD and followed by cell body settling position and endplate arborization for CM/LD motor neurons) will be attractive targets to test the functionality of human stem cell-derived motor neurons.

Establishing bona fide functional motor column and motor pool identities, and reliable markers and functional assays for ES-derived motor neurons are important goals to study the specific biology of these cell types in human development. However these are equally important from a translational perspective. ES- or iPS-MN subtypes must be identifiable and should reproduce functional phenotypes in order to increase their relevance to in vivo subtypes and therefore increase the chances of success in searching for differential disease phenotypes. This imperative is relevant at the level of both motor column and motor pool. LMC neurons are typically affected first in clinical presentation, whereas thoracic columns are less quickly affected and PGC motor neurons may show some resistance. Oculomotor and Onuf's nucleus motor neurons show strong resilience even at end stages of disease both clinically and in animal models. Future work to establish unambiguous and functional columnar identities, as well as to generate specific affected and resistant motor pools would allow direct investigation of the pathways contributing to this selective susceptibility and resistance.

Figure 5.1

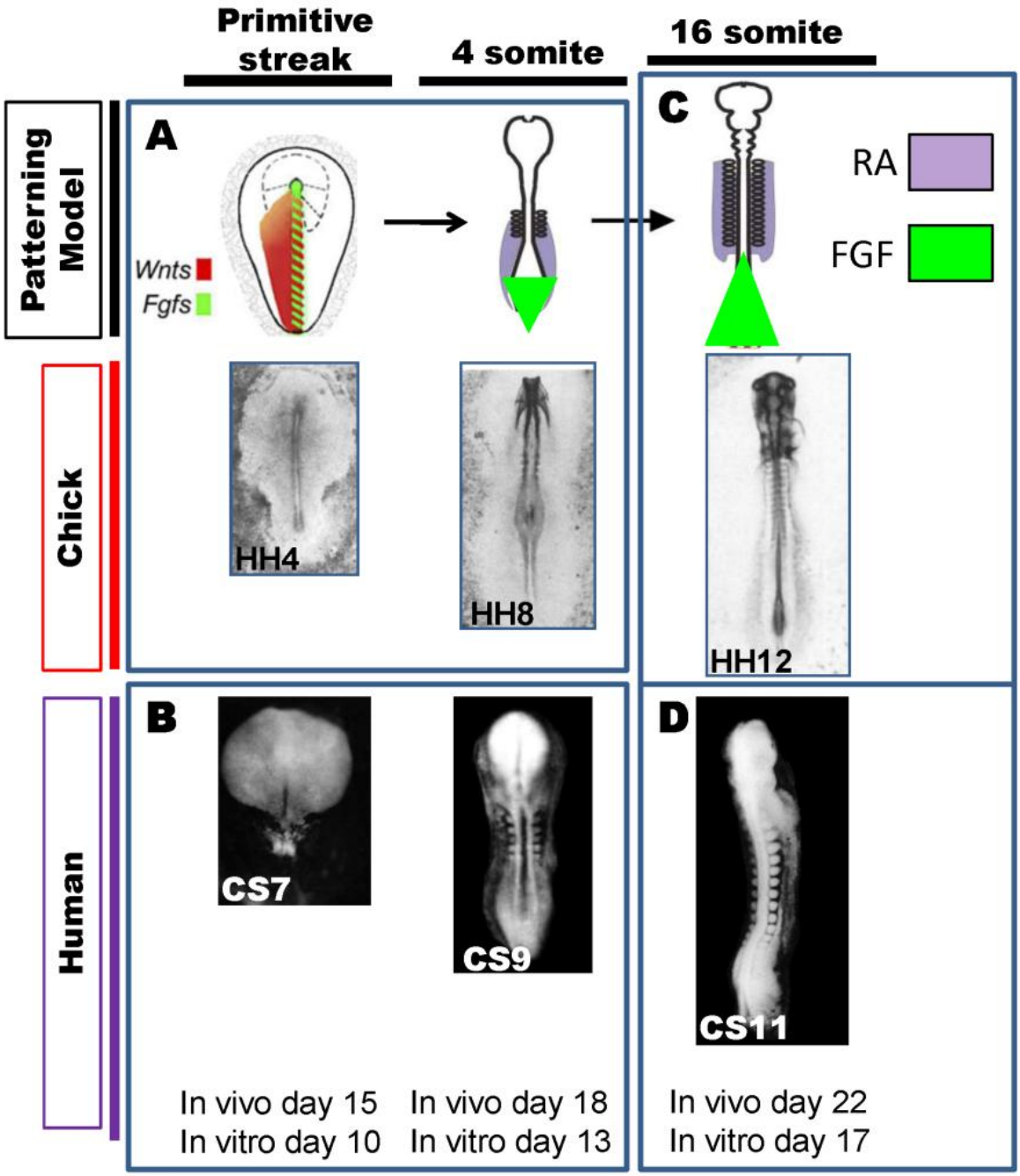
Primitive streak
4 somite
16 somite
Patterning Model
Chick
Human
A
Wnts
Fgfs
HH4
HH8
C
RA
FGF
HH12
B
CS7
CS9
D
CS11
In vivo day 15
In vitro day 10
In vivo day 18
In vitro day 13
In vivo day 22
In vitro day 17

Figure 5.1. Comparison of chick and human embryos during the period of caudal neural patterning

(A) In the model of caudal neural patterning defined in chick Wnt and FGF activity from the paraxial mesoderm and primitive streak are required from primitive streak to the 4 somite stage, HH stages shown. (B) Human embryos at matched developmental stages, Carnegie stages shown, in vivo developmental day, and assumed in vitro cognate (in vivo -5 days) shown. (C) RA and FGF secreted from somites and the node between 4 somite and 16 somite stages refine and subdivide caudal neural identity, chick HH stage 12 shown. (D) Human matched equivalent is ~CS 10.5 (CS 11 shown) and in vivo and in vitro days of human development. Model and cartoon adapted from Nordstrom, Maier et al. 2006; and Liu, Laufer et al. 2001; chick embryo pictures from Hamburger and Hamilton 1956; human embryo pictures from UNSW embryology website.

Figure 5.2

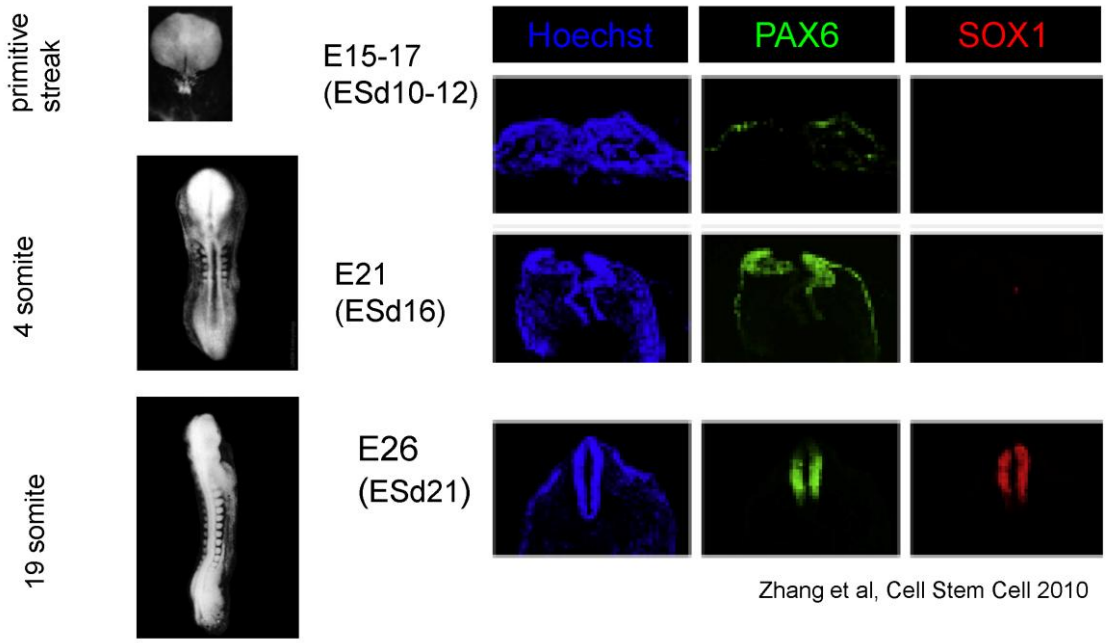

Figure 5.2. Transition to PAX6 marks the beginning and SOX1 the end of inferred patterning window

PAX6 expression is initiated at low levels in human embryos in the neuroectoderm during late primitive streak stage (embryonic day 15), is upregulated as the first selective marker of neural plate by day 21, and subsequently serves as a restricted marker of dorsoventral positional identity as it does in mouse and chick. SOX1 is expressed in all neuroectodermal cells of the neural tube by embryonic day 26. Embryonic day -5 = assumed in vitro ES cell day of development are shown. Human protein expression data from Zhang, Huang et al. 2010; human embryo pictures are from UNSW embryology website.

Figure 5.3

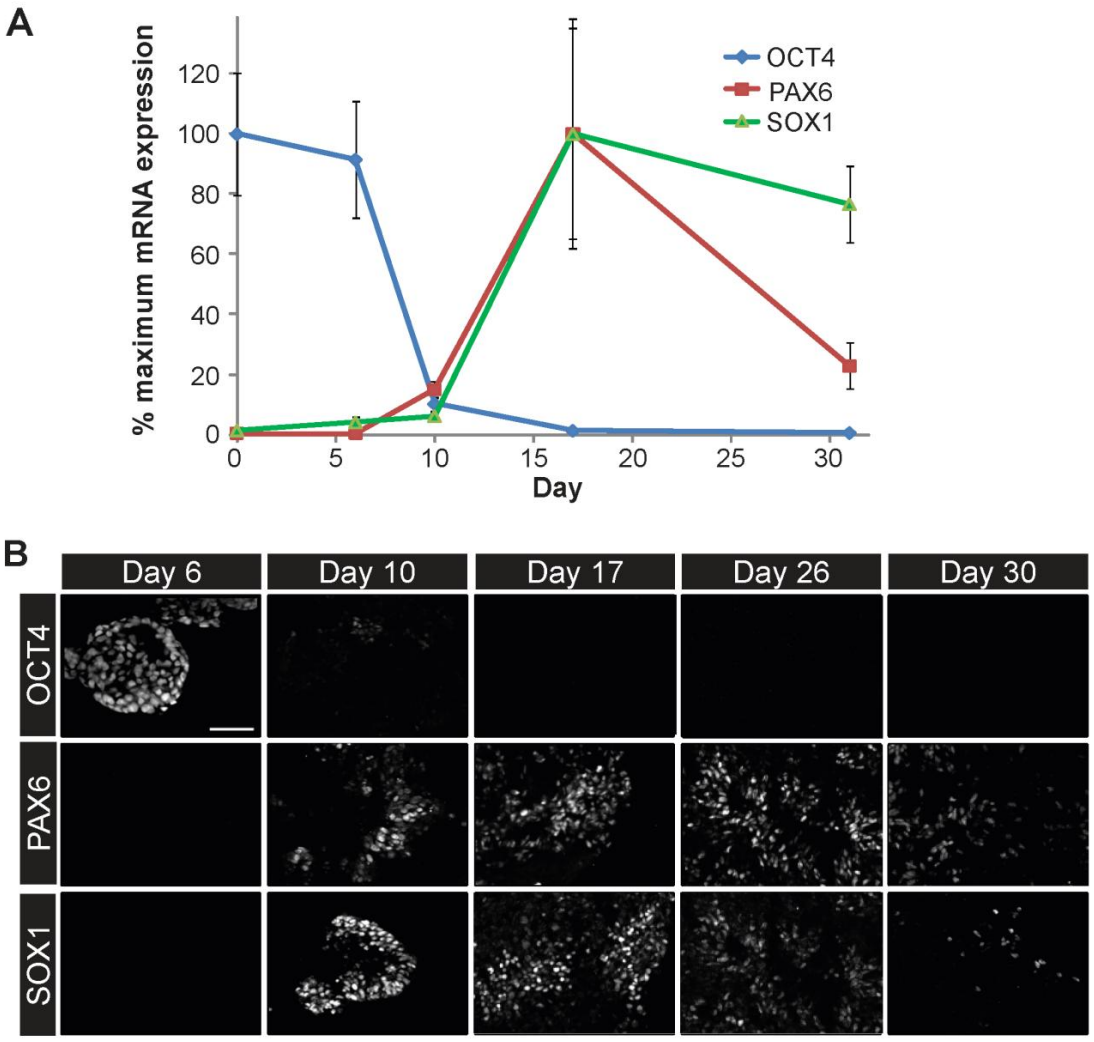
A
% maximum mRNA expression
120
100
80
60
40
20
0
0
5
10
15
20
25
30
Day
OCT4
PAX6
SOX1
B
Day 6
Day 10
Day 17
Day 26
Day 30
OCT4
PAX6
SOX1

Figure 5.3. In vivo markers of human neural plate to neural tube stages define cognate developmental stages in vitro

(A) qPCR for pluripotency gene OCT4 and neuroectodermal markers PAX6 and SOX1 shows neural induction initiated around by day 10, and consolidated by day 17. Mean ±SEM of n=4 experiments. (B) Immunostaining of representative cryosections of EBs for OCT4, PAX6, and SOX1 confirms qPCR data showing transition to definitive neuroectoderm by day 17 in vitro, scale bar 50 μm.

Figure 5.4

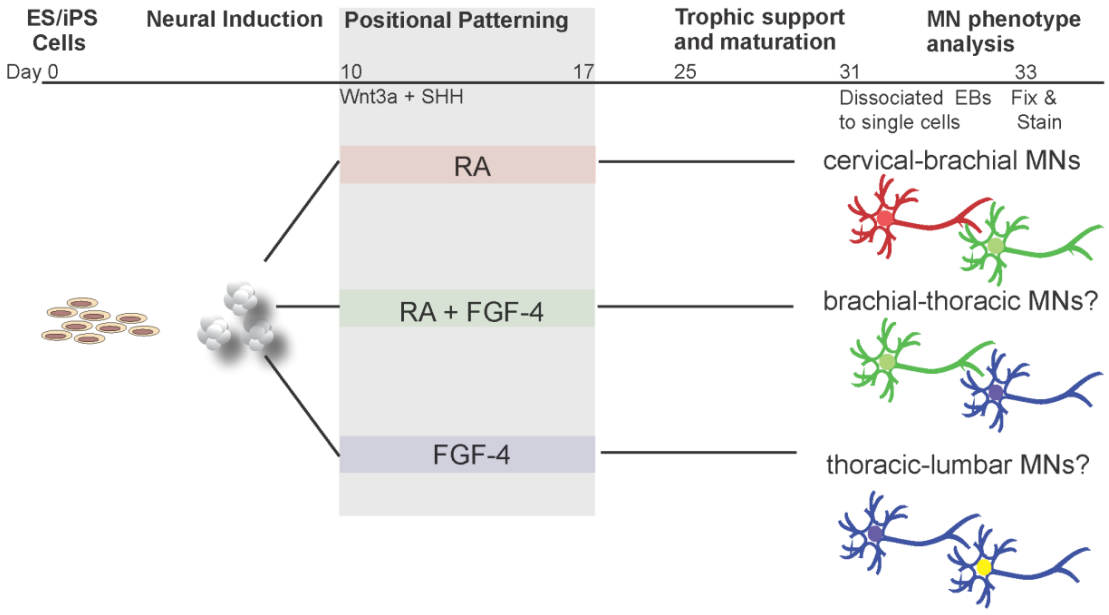

Figure 5.4. Design of caudal patterning ES-MN differentiation experiment

Motor neuron differentiations were conducted as described previously (Chapter 3 Fig3.1). The in vivo caudal morphogen FGF-4 (100ng/ml) was used alone or in combination with RA during the putative patterning window, in vitro day 10-17. As described previously, all EBs were dissociated to single cells at day 31, analyzed for HOX gene mRNA expression, and seeded at a fixed density for fixation and immunostaining for HOX markers of positional identity. Our hypothesis was that combinations of RA and FGF-4 would generate progressively more caudal motor neuron subtypes as they do in chick in vivo.

Figure 5.5

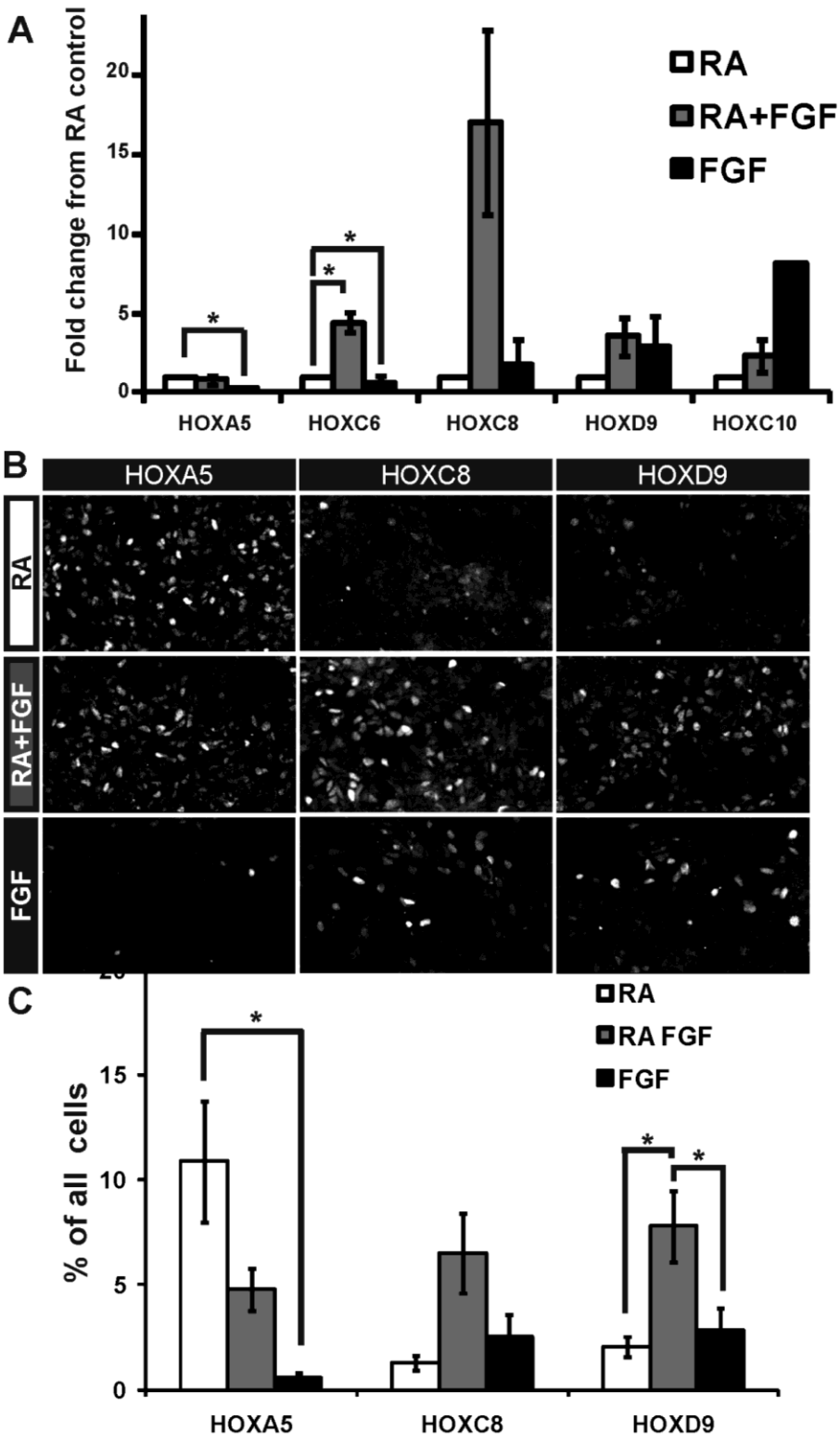
A
Fold change from RA control
20
15
10
5
0
RA
RA+FGF
FGF
*
*
*
HOXA5
HOXC6
HOXC8
HOXD9
HOXC10
B
HOXA5
HOXC8
HOXD9
RA
RA+FGF
FGF
C
% of all cells
15
10
5
0
RA
RA FGF
FGF
*
*
*
HOXA5
HOXC8
HOXD9

Figure 5.5. FGF induces a caudal shift in HOX expression

(A) qPCR for HOXA5, HOXC6, HOXC8, HOXD9, and HOXC10 shows a caudal shift in HOX gene expression when FGF-4 is added to RA. Mean ±SEM from n experiments (HOXA5, HOXC6, and HOXD9: RA n=5; RA+FGF and FGF n=4; HOXC8: n=3; HOXC10: RA n=5; RA+FGF n=4; FGF n=1. HOX gene expression was normalized to GAPDH and expressed as fold change from RA control. All significant comparisons from paired 2-tailed t-tests are indicated, * $p<0.05$. (B) Immunostaining for HOXA5, HOXC8, and HOXD9 proteins confirmed a caudal shift in HOX protein expression with FGF. (C) % of total cells expressing HOX proteins, mean ±SEM, n=4 experiments. One Way Repeated Measures ANOVA indicated that treatments affected HOXA5, HOXC8, and HOXD9 ($p= 0.010, 0.042, 0.021$ respectively). * significant ($p<0.05$) post-hoc pairwise comparisons are shown.

Figure 5.6

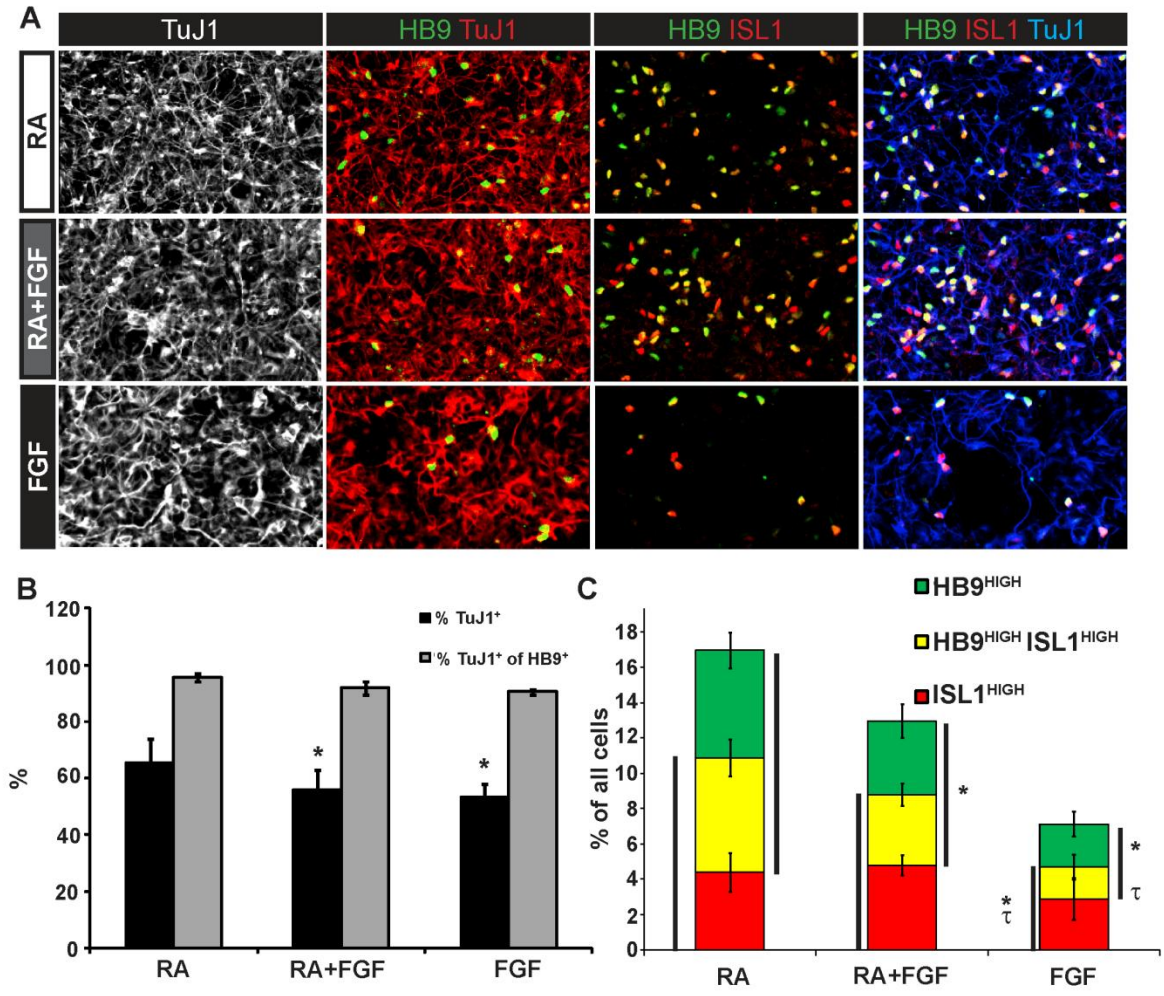
A
TuJ1
HB9 TuJ1
HB9 ISL1
HB9 ISL1 TuJ1
RA
RA+FGF
FGF
B
% TuJ1+
% TuJ1+ of HB9+
%
120
100
80
60
40
20
0
RA
RA+FGF
FGF
C
HB9HIGH
HB9HIGH ISL1HIGH
ISL1HIGH
% of all cells
18
16
14
12
10
8
6
4
2
0
RA
RA+FGF
FGF

Figure 5.6. FGF treatment reduces the percent of neurons and motor neurons, without affecting their phenotype and MN-marker profile

(A) Immunostaining of representative fields for TuJ1 and HB9 (left columns), or HB9, ISL1, and TuJ1 (right columns). (B) % $Tuj1^+$ of total cells (black bars) and % of $HB9^+$ cells expressing TuJ1 (grey bars), mean ±SEM of n=4 experiments. Significant differences ($p<0.05$) in paired two-tailed t-test, * = RA vs. RA+FGF, and RA vs. FGF. There were no significant differences between %Tuj1 of HB9. (C) % of total cells expressing only high level HB9 (green), only high level ISL1 (red), or both (yellow), mean ±SEM, n=5 experiments. Significant differences ($p<0.05$) in paired two-tailed t-test for ISL1 (black bars at left) or HB9 (black bars at right), * = RA vs. RA+FGF or vs. FGF, and τ = RA+FGF vs. FGF.

Figure 5.7

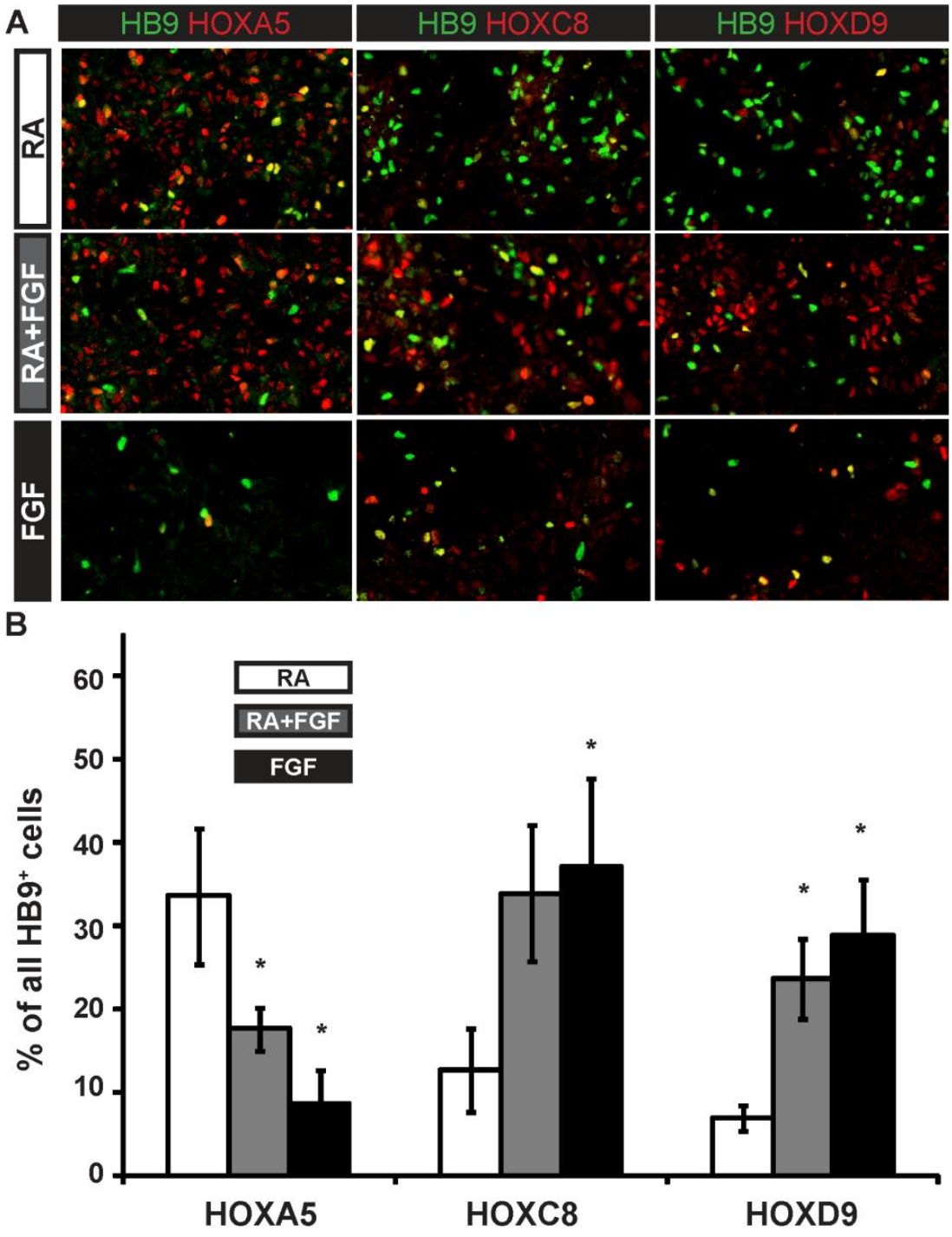
A
HB9 HOXA5
HB9 HOXC8
HB9 HOXD9
RA
RA+FGF
FGF
B
RA
RA+FGF
FGF
% of all HB9+ cells
0
10
20
30
40
50
60
HOXA5
HOXC8
HOXD9
*

Figure 5.7. FGF induces caudal motor neuron subtypes at the expense of rostral

(A) Immunostaining for HB9 and HOXA5, HOXC8, or HOXD9 proteins shows a caudal shift in motor neuron HOX-subtype with FGF treatments. (B) % of all $HB9^{+}$ cells coexpressing HOXA5, HOXC8, or HOXD9, mean ±SEM, n=5 experiments. Repeated Measures ANOVA showed significant differences between treatments for HOXA5 ($p= 0.008$), HOXC8 ($p= 0.026$), HOXD9 ($p= 0.012$). All pairwise Holm-Sidak post-hoc tests showing significant ($p< 0.05$) differences are shown, *= RA vs. RA+FGF or RA vs. FGF.

Figure 5.8

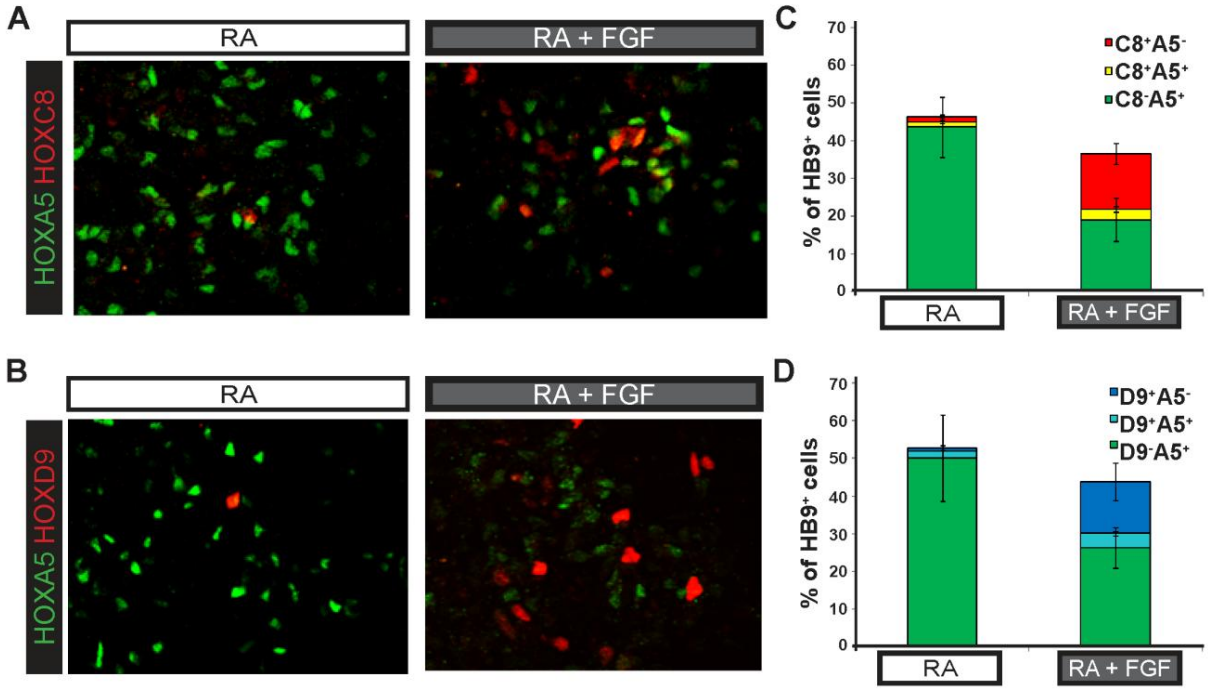

Figure 5.8. HOX protein expression is mutually exclusive in caudalized ES-MNs.

(A, C) Triple immunocytochemistry for HOXA5 (green) and HOXC8 (red, A) or HOXD9 (red, C) and HB9 (not shown) shows these HOX pairs are mutually exclusive. (B, D) Quantitation of HOX expression by $HB9^{+}$ MNs shows most ES-MNs expressed HOXA5 (green) and HOXC8 (red) or HOXD (blue) mutually exclusively, with less than 5 % of all MNs (yellow (B) or aqua (D)) coexpress HOX genes, n=4 experiments, mean ±SEM.

Figure 5.9

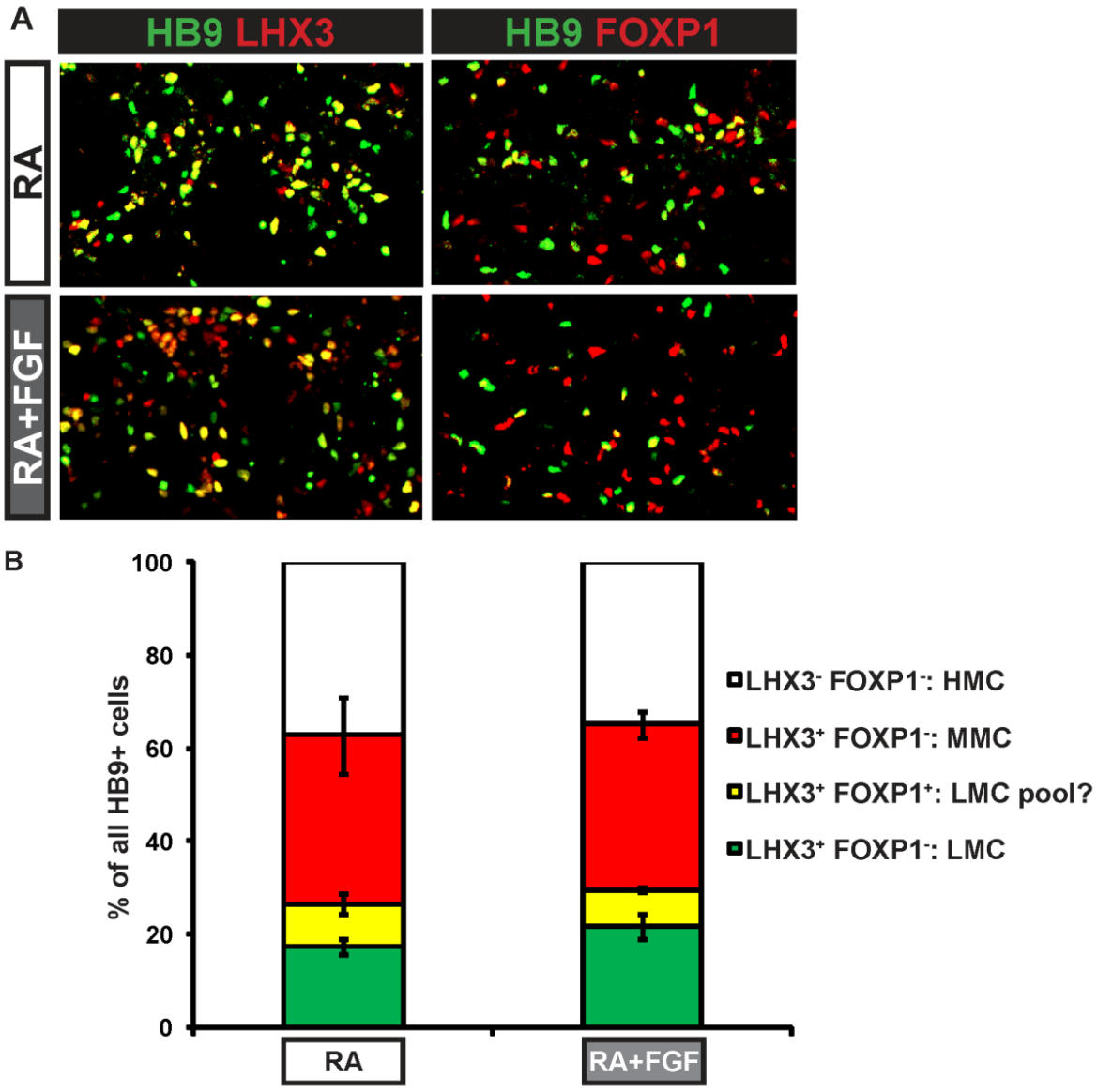
A
HB9 LHX3
HB9 FOXP1
RA
RA+FGF
B
100
80
60
40
20
0
% of all HB9+ cells
RA
RA+FGF
LHX3- FOXP1-: HMC
LHX3+ FOXP1-: MMC
LHX3+ FOXP1+: LMC pool?
LHX3+ FOXP1-: LMC

Figure 5.9. Motor column diversity preserved in caudal ES-MNs

(A) immunostaining for HB9 (green) and LHX3 (left, red) or FOXP1(right, red) (B) When HB9 LHX3 and FOXP1 were stained simultaneously, the %of all $HB9^{+}$ cells expressing all combinations of markers and their putative columnar identities could be assessed: LHX3 alone(red: MMC), FOXP1 alone (green: LMC), both LHX3 and FOXP1 (yellow: novel brachial LMC pool?) or neither (white: HMC). There was no significant difference between control (RA) and caudalizing (RA+FGF) conditions for any scoring category (paired 2-tailed t-tests $p>0.05$) mean ±SEM for n=3 independent experiments.

Figure 5.10

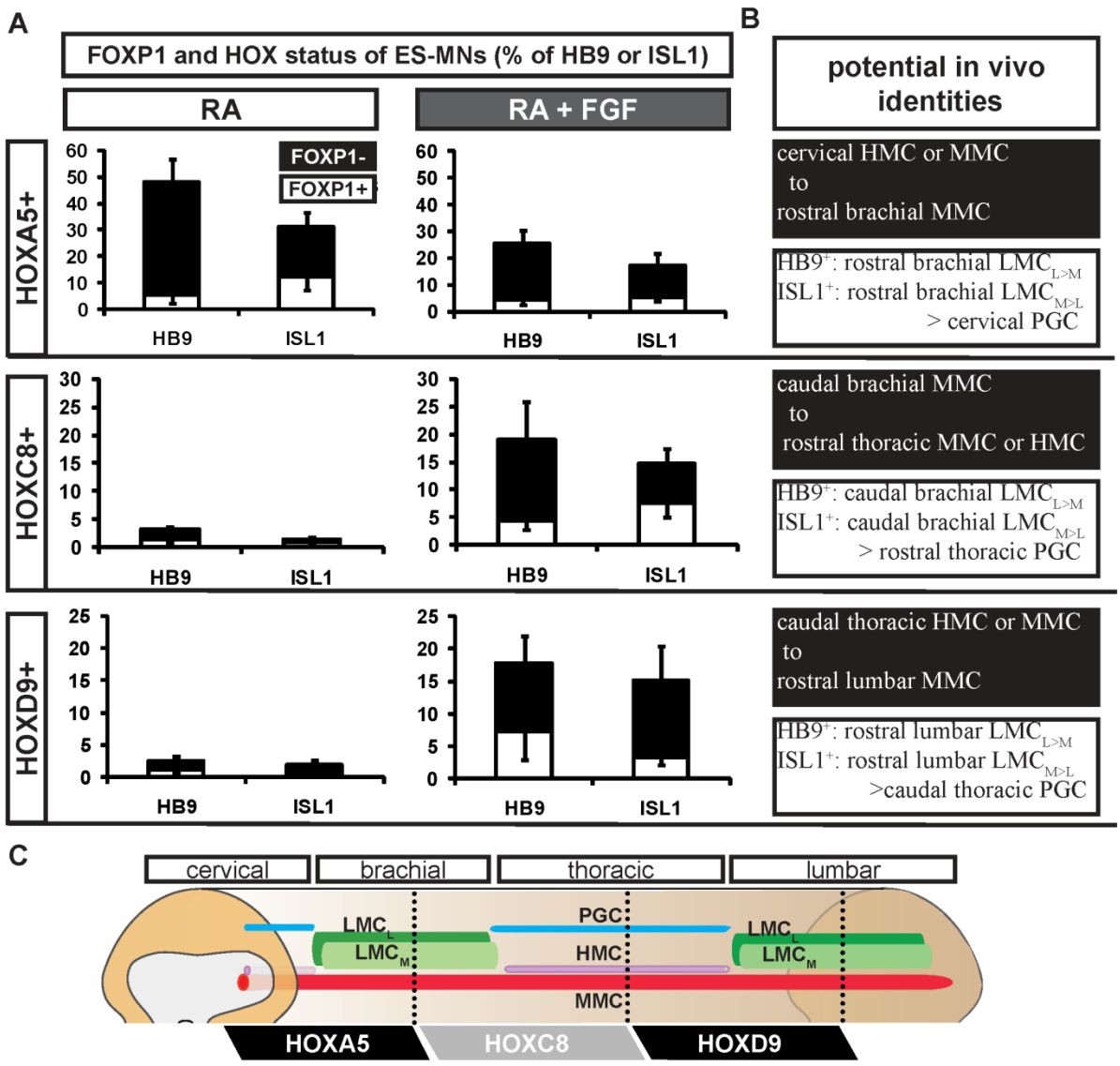
A
FOXP1 and HOX status of ES-MNs (% of HB9 or ISL1)
RA
RA + FGF
HOXA5+
HOXC8+
HOXD9+
FOXP1-
FOXP1+
HB9
ISL1
B
potential in vivo identities
cervical HMC or MMC to rostral brachial MMC
HB9+: rostral brachial LMCL>M
ISL1+: rostral brachial LMCM>L > cervical PGC
caudal brachial MMC to rostral thoracic MMC or HMC
HB9+: caudal brachial LMCL>M
ISL1+: caudal brachial LMCM>L > rostral thoracic PGC
caudal thoracic HMC or MMC to rostral lumbar MMC
HB9+: rostral lumbar LMCL>M
ISL1+: rostral lumbar LMCM>L >caudal thoracic PGC
C
cervical
brachial
thoracic
lumbar
LMCL
LMCM
PGC
HMC
MMC
HOXA5
HOXC8
HOXD9

Figure 5.10. HOX proteins and column markers jointly classify more precise ES-MN subtypes

(A) RA and RA+FGF treated differentiations were stained with FOXP1 and either HB9 or ISL and either HOXA5, HOXC8, or HOXD9. Mean of n=4 experiments ±SEM are shown for cells expressing marker combinations. Black bars show FOXP1- staining combinations, white bars show FOXP1 positive expression profiles (B) The set of in vivo human MNs (Chapter 2) which matches each of the expression profiles graphed at left. (C) Summary diagram of potential human motor neuron subtypes differentiated across control (RA, rostral) and caudalizing (RA+FGF) conditions.

Figure 5.11

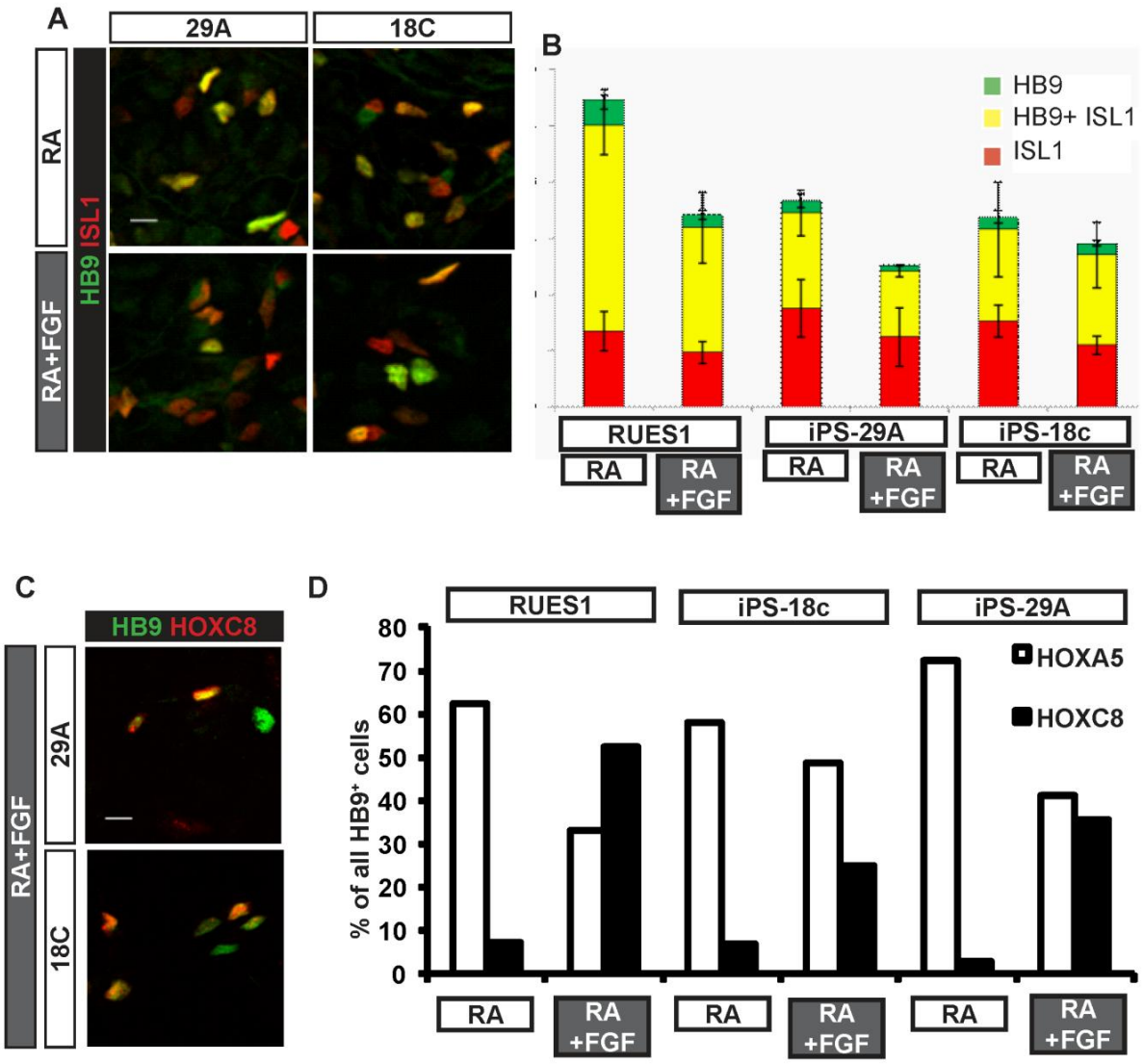
A
29A
18C
RA
RA+FGF
HB9 ISL1
B
HB9
HB9+ ISL1
ISL1
RUES1
iPS-29A
iPS-18c
RA
RA +FGF
C
HB9 HOXC8
RA+FGF
29A
18C
D
RUES1
iPS-18c
iPS-29A
HOXA5
HOXC8
% of all HB9+ cells
80
70
60
50
40
30
20
10
0
RA
RA +FGF

Figure 5.11. FGF induces more caudal motor neuron subtypes from iPS and ES cells

(A) iPS cells stain for motor neuron markers HB9 and ISL1 after Accelerated differentiation with rostral or caudal patterning treatment. Scale bar 10 um (B) iPS and ES cells generate similar distribution of HB9 and ISL1-expressing MNs under Ra or RA+FGF conditions, mean +/-SEM, n=3 experiments (C) FGF treatment induces $HOXC8^+$ MNs ($HB9^+$ neurons) from iPS lines, scale bar 10 um. (D) FGF treatment (grey box label below) decreased rostral ($\%HOXA5^+$ (white bars)) and increased caudal ($\%HOXC8^+$ (black bars)) MNs derived from both ES (RUES1) and iPS (18c and 29A) cells , mean % HOX^+ of $HB9^+$ cells / field, n=1 experiment / line.

Chapter 6. General Discussion: Conclusion and Perspectives

ALS is an intractable and fatal neurodegenerative disease with poorly understood causes and mechanisms resulting in cell loss. Principal and most obvious among the human cell types lost are the spinal motor neurons which directly innervate muscles, however this human cell type has been historically unavailable for direct study. This has changed since human ES and iPS cells have been differentiated to motor neurons. Recently, attention has become more focused on the diversity of responses to ALS among motor neuron subtypes. Motor neuron subtypes innervating specific categories of muscles (motor columns), muscle fiber-types (fast vs. slow), and specific individual muscles (eye and pelvic sphincters) show differential vulnerability or resistance to degeneration in ALS (Kanning, Kaplan et al. 2010). It was the aim of this thesis to set the stage for modeling ALS in vitro using specific motor neuron subtypes differentiated from ALS-patient iPS cells.

To study human motor neuron subtypes we first needed to translate the rich understanding of chick and mouse motor neuron diversity into the human system. To this end we characterized the subtype diversity of human embryonic motor neurons in vivo at the molecular level. These studies defined a set of antibodies that label human spinal motor neurons and their subtypes, and established that human motor neuron subtype diversity and organization are overwhelmingly similar to vertebrate models. Practically, they also provide validated tools to identify human motor neuron subtypes in vitro. The similarity of human motor neuron diversity to chick and mouse at the molecular level also provides confidence that in vitro directed differentiation strategies based on developmental mechanisms in chick and mouse may be highly applicable to human stem cells.

In order to quantitatively characterize motor neuron subtypes and generate cell preparations compatible with high throughput studies of ALS in vitro, we developed robust protocols for the differentiation of motor neurons from human ES and iPS cells. We then used the in vivo categories we defined to systematically categorize the diversity of motor neuron subtypes generated in vitro from human stem cells for the first time. First, we showed that the traditional in vitro perspective that motor neurons are defined by coexpression of HB9 and ISL1 is inadequate to describe the diversity of motor neurons present in vivo or in vitro, and provided a detailed profile of their combinatorial expression. Then we showed that ES and iPS derived motor neurons are predominantly cervical and brachial but contain cells matching all motor column subtypes. Because of the broad diversity of motor neuron subtypes in vivo, and their differential responses to ALS, it is critical to be able to account for the diversity of stem cell derived motor neuron subtypes that would potentially be used for disease modeling and drug screening.

In order to make more relevant models of ALS in vitro we anticipated the need to generate mature motor neurons which better match the cells affected in vivo. We therefore developed assays to characterize the rapid morphological and electrophysiological maturation of ES-MNs. We showed that ES-MNs rapidly acquired large size and mature morphologies, and that this was accompanied by a functional maturation of electrophysiological activity. Since both cellular size and electrical activity are implicated in ALS pathology, defining them in vitro should improve the prospects for disease modeling. The electrical activity we defined also mimicked key features of in vivo motor neuron physiology thought to underpin their circuit properties. These findings provide added confidence that ES derived neurons can reach states of maturity and in

vivo similarity which makes ES-MNs a favorable tool to model the disease affecting their in vivo correlates.

One of the most promising new approaches to modeling human disease is to derive iPS cells from patients with defined familial forms of disease, generate the relevant cell types, and identify disease relevant defects and phenotypes that manifest in vitro. In order to access motor neuron subtypes with ALS genotypes we participated in a collaboration to generate a large collection iPS cells from ALS patients and unaffected controls. We then used these cells to demonstrate the equivalence of iPS and ES cells for making functional motor neurons, classify their subtypes, and establish that they assumed coherent in vivo-like identities. Since maturation and activity may be important for modeling ALS, we also demonstrated that ALS-iPS motor neurons achieved functional electrical activity comparable to ES-derived motor neurons.

Finally, in order to generate thoracic and lumbar motor neuron subtypes that show differential susceptibility or resistance to ALS we needed to first control the rostrocaudal identity of differentiating ES and iPS cells to generate more caudal motor neurons. We developed a rational approach, based on developmental patterning mechanisms, to recapitulate the rostrocaudal patterning which orchestrates motor neuron diversification in vivo. We then used this approach to generate motor neuron populations with more caudal subtype identities in vitro. The rostral and caudal populations we describe collectively span the length of the spinal cord from cervical to mid-lumbar (Fig. 5.10). We generated cells that match the profile of several motor columns with potential differential responses to disease (LMC vs. MMC vs. PGC), and defined caudalizing conditions that might lead to specification of a key ALS-resistant motor pool (Onuf's nucleus). These findings theoretically put several motor neuron subtypes with differential ALS responses within experimental reach. Additionally we demonstrated that ES- and iPS-MNs were

able to resolve competing patterning signals (RA and FGF) into coherent positional identities characterized by mutually exclusive HOX protein expression as do motor neurons in vivo. Since HOX cross-repression is a fundamental mechanism for resolving motor column and motor pool identity this finding suggests that stem cell derived motor neurons are following the in vivo developmental path leading to defined columnar and motor pool identities.

As intended this work moves the field closer to making novel and highly specific models of ALS using motor neuron subtypes. However in the light of what we now know several major questions remain to be resolved. First, how can we more definitively identify specific motor neuron subtypes? Second, can we develop rational means to more precisely control the subtypes of motor neurons? Third, how might these subtypes actually be used to model disease?

Definitive identification of specific motor neuron subtypes

While we have generated motor neurons with individual expression profiles matching those in vivo from cervical to mid-lumbar spinal cord and including all motor columns, each of these in vitro motor neurons could match several in vivo subtypes. For example, because HOXC8 expression in vivo straddles brachial LMC and thoracic regions, and because FOXP1 is expressed by both PGC and LMC motor neurons, $HOXC8^{+}$ $FOXP1^{+}$ ES-MNs are a transcriptional match for both caudal brachial LMC and thoracic PGC motor neurons (Fig. 5.10). Although FOXP1 expression levels, especially if coupled with anatomic position, can easily distinguish between these identities in vivo, expression level does not translate well as a marker of identity in the in vitro setting. Indeed, like other markers tested in vitro there is a smooth continuum of staining intensity and no objective, unambiguous, or most importantly, verifiable means to set a threshold intensity to discriminate low from high expression and thus PGC vs.

LMC identity. And while the high level expression of FOXP1 in all ES-MNs we scored as positive strongly suggests they are LMC rather than PGC, and while we can easily identify lower level FOXP1 expression in $HOXC8^{+}$ or $HOXD9^{+}$ $ISL1^{+}$ cells consistent with PGC identity, we have no reliable way to positively identify disease-refractory PGC motor neurons. In order to study the behavior of specific motor column or motor pool subtypes for basic or disease modeling purposes it will therefore be crucial to push the resolution and certainty with which we can identify these cells at least one step further.

One approach to resolving this ambiguity would be to generate human reactive antibodies for more definitive markers. HOXC6 vs. HOXC9, if these prove in human spinal cords to match chick and mouse expression patterns, would cleanly discriminate between LMC and PGC identities. HOXC10 vs. HOXC9 would resolve the same current ambiguity for $HOXD9^{+}$ $FOXP1^{+}$ expressing cells in favor of lumbar LMC or thoracic PGC. These reagents would also be extremely useful for determining if the system of HOXC6, C9, and C10 cross repression controls limb vs. non limb motor column identities in human as it does in chick and mouse (see below). In addition to resolving ambiguous identities, we noted that almost 40% of ES-MNs did not stain for either of the HOX markers we profiled. It is therefore important that in addition to HOXC9 and HOXC10, which should account for some of these unlabeled cells, that antibodies be developed and validated for hindbrain and cervical motor neurons HOX1-4, and for HOX negative midbrain motor neurons like the disease relevant oculomotor motor neurons. While HOX markers will be crucial for assigning identities to ambiguous or unlabeled cells, there will be no substitute for generating more direct markers of motor column identity. Reagents to detect the known markers of LMC (RALDH2), HMC (ER81), and PGC (nNOS) need to be developed and validated on human spinal cords and tested in vitro.

Another approach would be to identify new markers for these columnar identities. Laser capture microdissection (LCM) on motor columns from new fresh-frozen human spinal cords, or even from the current tissue resource described above (Table 2.1) followed by microarray expression profiling or deep sequencing, could identify differentially expressed genes, which could then be validated on human samples and serve as new specific markers. Validated markers could be used for immunostaining and potentially for MACS or FACS sorting on endogenous surface epitopes. Indeed the LCM-microarray approach has already been used to great effect to isolate gene expression profiles for oculomotor and Onuf's nucleus motor neurons (Artem Kaplan, unpublished findings) which have shed light on novel mechanisms of disease resistance and susceptibility, and additionally provided gene expression profiles including candidate marker genes which could be screened against human samples in vivo and in vitro.

If more specific columnar identities can be definitively established in vitro for ES/iPS-MNs, will these show functional phenotypes? The pilot studies we performed suggesting a FOXP1 specific outgrowth phenotype are suggestive of an LMC-specific functional phenotype, which can be rationalized since LMC cells must extend longer axons to reach peripheral targets. While this study was far from conclusive it is a proof of principle for searching for biologically interesting phenotypes for human motor neuron subtypes in our preparations in vitro. Furthermore, the evidence from chick in vivo experiments (Dasen, Liu et al. 2003; Dasen, Tice et al. 2005; Jung, Lacombe et al. 2010) and mouse ES-MN studies suggests that if cells express a coherent profile of HOX genes and column markers then functional phenotypes will follow. When mouse ES-MNs were specified with LMC ($HOXC6^{+}$ $FOXP1^{+}$) (Peljto, Dasen et al. 2010) or MMC ($LHX3^{+}$ $HOXA5^{+}$) (Soundararajan, Miles et al. 2006) identities and xenotransplanted to chick embryos, they demonstrated motor column specific settling position and axonal pathfinding phenotypes.

We have shown that xenotransplantation of hES-MNs to chick is feasible and that axons extended millimeters into the periphery along endogenous spinal motor nerve paths. These early pilot studies were complicated by the presence of very large quantities of cycling human neural progenitors, low motor neuron yields, limited trials, and a transplant technique which was a work in progress. Since we can now generate robust populations of high purity $FOXP1^{+}$ GFP labeled human ES-derived motor neurons, in the absence of mitotic progenitors, the question of whether these human motor neurons can interpret cell body settling position and axon guidance cues in the chick xenotransplantation assay, according to their column identity, is begging to be asked. In addition, we predict that the mitotically-inhibited preparation of nearly pure GFP^{+} $FOXP1^{+}$ human motor neurons that we describe, which contains a balanced mix of HOXA5 and HOXC8 expressing subtypes, might be able rescue the functional phenotype of the FOXP1 knockout mouse (Dasen, De Camilli et al. 2008), at least in the forelimb, if transplanted *in utero* to the spinal cord of these animals.

Other functional phenotypes can be examined for specific motor columns and motor pools. For example pSMAD marks the PGC motor column and PEA3 marks the CM/LD motor pool. Since these subtype markers depend on peripheral cues (BMP5, Ed Laufer, personal communication, and GDNF (Haase, Dessaud et al. 2002; Livet, Sigrist et al. 2002) respectively) their expression in hES-MNs in response to these ligands would itself constitute functional column- or pool-specific phenotypes respectively. Pilot experiments using BMP5 and GDNF in attempt to elicit pSMAD expression in $HOXC8^{+}$ or $HOXD9^{+}FOXP1^{LOW}$ putative PGC motor neurons or PEA3 expression in $HOXC8^{+}FOXP1^{HIGH}$ putative brachial LMC motor neurons, either in dissociated cultures or in EBs, failed to show any specific staining for either pSMAD or PEA3. It remains to be seen whether the failure is due to inadequate reagents, low abundance of MNs that acquired

specific pool or columnar identities, or functional divergence between human and non-human spinal motor neurons.

More precise control of motor neuron subtype identity and purity

We have shown that we can inflect the distribution of motor neuron rostrocaudal identity from largely rostral to largely caudal, however these populations are still each composed of a very broad rostrocaudal range of identities. Furthermore, while we detected lumbar (HOXC10) gene expression we did not have reagents to show that ES-MNs expressed this marker. Because Onuf's nucleus motor neurons are lumbosacral HOXC10-expressing cells, we need to be able to generate higher purity lumbar cultures in an effort to isolate this disease refractory population.

In order to exert more precise control over rostrocaudal identity and thereby generate more focused lumbar MN populations, we suggest a return to the *in vivo veritas* approach, the success of which we report in Chapter 5. In this case, the aim would be to one, better understand the mechanisms of human development in vitro, and two, better mimic in vivo mechanisms in vitro. The first approach would be to use genetic gain and loss of function strategies to test the sufficiency and requirement of *HOXC* genes in controlling motor column subtypes as has been done so fruitfully in the chick. Overexpression studies and dominant negative constructs or RNAi for *HOXC6*, *HOXC9*, and *HOXC10* could be transiently transfected into differentiating human EBs and motor column identity would serve as the readout. Understanding whether human motor column diversity is controlled by the interaction of these genes will be of basic interest but also critical to designing strategies to differentiate, for example, high purity cultures of limb level or thoracic motor neurons. Additionally, recent success in transcription factor reprogramming of fibroblasts to nerve cells (Vierbuchen, Ostermeier et al. 2010) suggests that

this type of gain of function expression approach could serve as an alternate means to program motor neuron columnar or other subtype identities in order to isolate and study those columnar subtypes for disease or basic purposes. Applying this strategy to ES-derived cell types which already possess correct lineage, region, and generic cell type identity could only increase the chances of success and the potential relevance and in vivo similitude of resulting cells.

The second approach would be to return again to what is known about embryonic development. Our approach in Chapter 5 was to crudely approximate the timing of 3 overlapping positional cues. However for simplicity we made several sacrifices of fidelity to in vivo events. First, we collapsed the earlier developmental phase of Wnt/FGF pan-spinal caudal patterning with the subsequent FGF/RA phase which subdivides spinal identity. Second, we did not account for the importance of concentrations of patterning factors. And third, we could not, in the scope of these studies, account for the spatio-temporally dynamic nature of rostrocaudal patterning and motor neurogenesis. The pursuit of more fine grained approximations of developmental events should therefore include separating the early period of Wnt/FGF patterning from the subsequent RA/FGF patterning period. Additionally, since FGF is thought to act in a concentration dependent manner, the effect of different doses of this and other morphogens should be tested with HOX protein expression as endpoints. In addition, the spinal cord is patterned by FGF and RA over a long time period acting on different rostrocaudal regions at different times from initial somite stages until 16-17 somite stages when FGFs and GDFs act on the prospective lumbar spinal cord. A series of experiments should therefore be done to present cues in a temporally dynamic and combinatorial fashion to better approximate the embryonic events leading to motor neuron diversification in vivo. Finally, node-derived GDFs are necessary for the proper elaboration of $HOXC10^{+}$ lumbar motor neurons (Liu, Laufer et al. 2001). Indeed, one pilot

experiment showed that GDF11, when added to FGF treatment, substantially increased *HOXC10* transcription (data not shown). Therefore future studies should incorporate this cue at a developmentally relevant timepoint: that is, towards the end of the patterning period we defined here.

Refining the rostro-caudal patterning of ES-MNs should provide better access to defined clinically relevant motor neuron subtypes. The pools of greatest interest in the context of disease resistance, oculomotor and Onuf's, are midbrain HOX^- and sacral $HOX10^+$, respectively. The oculomotor motor neurons are rostral to the region on which we have focused. Alternative differentiation strategies, based on rhombomeric segmentation mechanisms in vivo should therefore be designed for this target population. The targeted strategies we suggest above should help to refine differentiation conditions to increase the abundance of these lumbar and midbrain regional subtypes. Pool specific markers can then be validated in vivo and screened in vitro so differentiation conditions can be optimized to support their differentiation and survival.

Differentiation strategies alone however are unlikely to produce target cell types of interest at high purity. It is more likely that the cells will acquire a positionally appropriate range of motor neuron subtypes as seen in our experiments and in mouse ES-MNs (Peljto, Dasen et al. 2010). Therefore, means to purify cells are clearly needed for subtype-specific disease modeling studies. One approach is the identification of endogenous surface markers that could be used for FACS or MACS sorting. Alternatively appropriate marker genes and their regulatory sequences could be harnessed to generate transgenic fluorescent and/or surface marker reporter cell lines, which would allow sorting of relevant MN populations to purity. FOXP1, LHX3, or ER81 and nNOS genetic elements, if validated in human, could potentially be used to purify LMC, MMC, HMC or PGC columnar subtypes for example.

Towards disease phenotype assays

How can the populations we have described, or those achieved by the approaches discussed above, be used to model ALS? While in vitro disease phenotypes do not necessarily have to mimic the disease pathology in vivo in order to generate useful insights, the most parsimonious approach is to first attempt to recapitulate in vivo pathology in vitro. *Prima facie,* the survival of motor neurons would then be the most relevant assay. Since we have generated and cultured a population of almost pure $FOXP1^{+}$ presumably limb innervating motor neurons which show high sensitivity to ALS in vivo, simply following the survival of ALS and control $FOXP1^{+}$ motor neurons might be a useful strategy. If these could be compared to more resistant non limb innervating motor neurons at the level of survival, gene expression changes, morphology, or biochemical endpoints this would significantly increase the power, sensitivity and relevance of the assays. Hopefully, more disease refractory populations of human MNs can be generated using the approaches discussed above.

The only clear in vitro phenotype identified in ALS is the motor neuron selective toxicity of ALS astrocytes (Di Giorgio, Carrasco et al. 2007; Nagai, Re et al. 2007; Di Giorgio, Boulting et al. 2008), or organophosphate treated astrocytes (Marine Prisette and Derek Oakley, unpublished). Whether control or ALS motor neurons respond differentially to this challenge remains a matter of controversy (Di Giorgio, Carrasco et al. 2007; Nagai, Re et al. 2007), raising the possibility that the degree of motor neuron degeneration might depend on MN subtype identity. It is therefore our high priority to test human ALS-motor neurons in these assays and to determine whether the presence of predominantly $FOXP1^{+}$ LMC-like motor neurons in matured mitotically inhibited cultures might reveal ALS dependent differences in motor neuron survival. Indeed, a strong motivation for studying ALS in human cells in the first place is the potential that the

human genetic background of the cells may reveal aspects not mimicked by mouse cells or animal models.

In summary much work remains to be done to leverage the specificity of ES-and iPS-derived motor neuron subtypes into a useful tool for modeling ALS. The challenge of defining screenable phenotypes for an adult onset disease like ALS is considerable and is outside the scope of these studies and discussion. However the ability to define human motor neuron subtypes and control their rostrocaudal identities are first steps towards building more specific and targeted models of disease. It is our hope that in the future these cell types will show differential responses to ALS in vitro as they do in vivo. In turn these differential responses should be manipulated into screenable phenotypes which could identify therapeutic compounds and illuminate novel mechanisms of disease vulnerability and resistance, leading to new therapies and new hope for this untreatable disease.

Chapter 7. Experimental Procedures

Embryos

Anonymized postmortem embryos from voluntary terminations were obtained with informed consent and in accordance with IRB guidelines within 10 minutes after clinical procedures, and staged by collaborating physicians using last menstrual period and or crown rump length ultrasound. Post-mortem analysis of embryological features was used to confirm and adjust a developmental stage for embryos using Carnegie categories. Spinal cords were dissected intact and then fixed.

ES and iPS cell culture.

ES cell lines used: RUES1(James, Noggle et al. 2006), HBG1 (plasmid HB9:GFP motor neuron reporter) (Di Giorgio, Carrasco et al. 2007)); HBG47 (BAC-HB9:GFP motor neuron reporter) (Placantonakis, Tomishima et al. 2009). iPS and ES cell lines for used for iPS comparison study: see Table 4.1. All stem cell lines grown under standard pluripotency maintenance conditions: on irradiated CF-1 mouse embryonic fibroblast feeder cells (0.015 M cells/cm^2, Globalstem) on gelatinized (Millipore) TC plastic, fed daily with DMEM/F:12 (Invitrogen) with 20% KSR (Invitrogen), 110 uM BME (Sigma), L-Glutamine and NEAA (Invitrogen), and 20ng/ml bFGF (Invitrogen) added to medium just prior to feeding. Cultures were passaged weekly using dispase 50 ug/ml for 20 min (Invitrogen) followed by manual trituration. Parallel passages of ES cells were karyotyped at passage number subsequent to passages used for experiments and found normal, with the exception of abnormal karyotypes reported for iPS lines (Chapter 4). ES and iPS cells and motor neurons were cryopreserved by gradual dilution (dropwise addition of 1:1 volume, with gentle agitation, over 1-2 minutes) of single cell suspensions or colonies with ice cold 2x freezing medium for ES cells (Millipore), cryotubes were placed in isopropanol freezing

chambers, stored overnight at -80ºC, then transferred to liquid nitrogen. All cells were thawed by immersion in 37ºC water bath until only a few crystals remained, then immediate dropwise dilution with ES-medium for ES cells, or Neurobasal+B27 for ES/iPS-MNs over the course of ~2 minutes, with gentle agitation until 10mls was reached. Cells were pelleted at 400G for MNs, or settled for intact ES colonies. ES colonies were washed 3x with ES-medium, then plated. ES-MNs were resuspended in 1ml fresh Neurobasal+B27, then brought to 11mls, underlaid with a 4% BSA cushion, and spun at 400G for 5 minutes with no brake, to float cell debris.

Standard Protocol motor neuron differentiation

After a normal passage, washed ES or iPS cell colonies were incubated for 1 hour in ES medium with 10-30 µM ROCK inhibitor (Y-27632, Sigma), then washed with $Ca^{2+}Mg^{2+}$-free PBS trypsinized (0.5% trypsin with EDTA) to a single cell suspension and seeded in suspension at 0.4 M cells/ml in human ES medium with 20 ng/ml bFGF, 10 µM ROCK inhibitor, and 300 ng/ml recombinant mouse Noggin (R&D) to inhibit non-neural differentiation. Fresh ROCK inhibitor, FGF, and Noggin were added daily for 6 days. EBs were pelleted at 100 G on day 4 and resuspended in Neural Induction Medium (NIM: DMEM/F12 plus N2 supplement(Invitrogen), NEAA, L-Glutamine, 2 µg/ml Heparin (Sigma)) with ROCK inhibitor, FGF, and Noggin. EBs were pelleted and fed with fresh medium every other day, and ROCK inhibitor was discontinued after day 6. FGF was discontinued at day10, and 1:100 dilution of Wnt3a-Lcells conditioned medium (ATCC, source and protocol), all-trans retinoic acid (RA, 100 nM in DMSO, Sigma), Ascorbic Acid (0.4 µg/ml, Sigma), db-cAMP (1 µM, Sigma), and 100 ng/ml active-mutant recombinant mouse SHH protein (SHH-C25II, R&D) and 100 ng/ml recombinant human FGF-4 (R&D) were added. On Day 18, Wnt3a conditioned medium was removed, SHH increased to 200 ng/ml, and recombinant human BDNF (10 ng/ml R&D) was added. At day 25 base medium

was switch to Neural Differentiation Medium (Neurobasal with N2 and B27 (Invitrogen), L-Glutamine, NEAA, Ascorbic Acid, db-cAMP, with 10 ng/ml each recombinant human BDNF, GDNF, IGF-1, and CNTF (R&D), 200 ng/ml SHH, and 100 nM RA).

EB's were dissociated using trypsin on day 31, and cryopreserved using 2x freezing medium (Millipore, for ES cells) for future analysis. Separate vials were thawed for electrophysiology and immunocytochemistry time series in Neurobasal with B27 and seeded on Poly-ornithine/laminin coated glass coverslips, in complete day 25 Neural Differentiation medium, as above, with the addition of 1 µg/ml mouse laminin (Invitrogen), Beta-Mercaptoethanol (25 µM, Sigma), Glutamate (25 uM, Sigma), Forskolin (20 uM, Sigma) IBMX (100 µM, Fisher) at 0.25 M cells per 35 mm coverslip or 0.046 M cells per 15 mm coverslip and ½ medium was changed every 4 days. For labeling of dividing cells and inhibition of cell division, ClickIt EdU (0.5 µM, Invitrogen) was included in culture medium for morphometry studies after seeding, and refreshed with media changes. EdU was processed for immunocytochemistry following manufacturer's instructions (Invitrogen)

Accelerated Protocol MN differentiations

Performed according to Standard Protocol with the following modifications. ES/iPS colonies were not trypsinized at passage, rather trituration with a p1000 tip, 8 passes until colony fragments were just below visible size. Then seeded by eye at density comparable to single cell motor neuron seeding density (0.4 M cells/ml) in the same medium described above with all supplements except noggin, instead LDN-193189, (0.2 µM) and SB-431542 (10 µM) were used. FGF and ROCK inhibitor were refreshed at day 2 and more medium was added if medium was yellow. EBs were spun at 100 G for 2 minutes on day two and EBs were replated in NIM with

all previous supplements. At day 4 Rock inhibitor was not added nor subsequently. At day 5 patterning factors were added (Wnt3a-CM 1:10, RA, +/-FGF-4), this was the last day of LDN-193189/SB-431542 and FGF2 was not added, and 200ng/ml SHH protein was added. Medium was changed every other day and patterning treatments were last added on day 11. BDNF was added at day 13, and on day 15 culture were switched to NDM with all supplements as described above. EBs were dissociated at day 21 and fixed for acute analysis at day 23, or cultured longer for maturational analyses.

Trituration

All triturations were performed in complete trituration wash medium (CTWM: 1xPBS, $Ca^{2+}Mg^{2+}$-free plus 25mM Glucose, 0.1% dialyzed BSA, $MgCl^2$ 2mM, EDTA 2mM, 2.5% FBS, and N2 and B27 supplements for day 31 or day 23 EB dissociation) with a p1000 tip (12 passes, at 1 Hz for EBs, ~6 passes for ES colonies), plus freshly added DNAse (1:50-1:500 from 100mg/ml stock in 0.1%dialyzed BSA in 1xPBS stock).

4% dialyzed BSA

Fraction V BSA was dissolved at 4% weight/volume in was dissolved in and dialyzed against L15 with phenol red, using Pierce Slide-a-lyzer 10,000MW cutoff large volume dialysis cassettes, over 4-5 days with stirring at 4 degrees, with daily medium changes, until solution was claret colored and pH~7.5, filtered, then frozen for future use.

Fetal spinal cord astrocytes were purchased from ScienCel Research Laboratories and cultured with manufacturers medium and supplements on gelatin, passaged every 5 days at confluence and cryopreserved as described above. For motor neuron co-cultures they were seeded at 0.02 M cells/12mm coverslip 3-4 days before seeding ES-MN. ES-MNs were FACS sorted at low

pressure 20PSI using a large 100 µM nozzle under single cell mode with purity mask, at either the Herbert Irving Cancer Center Flow Cytometry Facility by Kristi Gordon, or New York Stem Cell Foundation by David J Kahler.

Fixation Cryosectioning and Immunocytochemistry

Spinal Cords and EBs

Spinal cords were fixed for 1.25 hrs on ice (for GW7), or 2.5hrs at room temperature (for one GW8 sample), and 1 hour for EBs in 4% PFA in 1x PBS, washed several times with PBS then incubated overnight at 4°C. Cords were then photographed and divided into sections <6 mm to facilitate sectioning. 4%PFA was prepared by dilution of sealed ampules of 32% liquid PFA (Electron Microscopy Sciences) with filtered water and 10x PBS, to 8%PFA, 2x PBS stock. 8% PFA was stored light protected at 4°C for one week, and dilution to 4% was performed immediately before use.

Cords and EBs were cyroprotected by equilibration with 30% sucrose, embedded in OCT. and serially sectioned at 12µM on a Hacker cryostat. Slides were stored at -80ºC for subsequent analysis.

Fixation of motor neuron cultures

Culture medium was removed from coverslips and multiwell chambers, replaced with cold 4% PFA and incubated for 30 minutes on ice (or 4 ºC), washed 3x in PBS then handled as per Post-fixation and Immunostaining section below

Motor neurons cultures were seeded on Poly-lysine/laminin pre-coated 8-well glass chamberslides (Invitrogen) or on German glass (Fisher) coverslips coated with 1mg/ml poly-ornithine in 0.1M boric acid coated, washed 3x with water, then coated overnight with laminin 10ug/ml in L-15 with bicarbonate.

Post-fixation and Immunostaining

All samples were permeabilized for 15 minutes at room temperature (RT) with Wash (PBS+0.1%Triton-X) + 100mM Glycine, incubated with Block (Wash+10% normal donkey serum +0.1%NaAzide for 0.5hr at room temperature, then with primary antibody (diluted in Block) for 2 hours at RT, or overnight at 4°C, washed, incubated with secondary antibodies for one hour at RT, washed, counterstained with DAPI and coverslipped using Fluoromount-G. Primary antibodies are described in Table 7.1. All secondary antibodies used were highly cross adsorbed Donkey anti-species whole IgG coupled to DyLight 488, 549, or 647 (Jackson ImmunoResearch). Samples were counterstained with DAPI (Invitrogen)

RNA, cDNA, qPCR

Dissociated day 31 motor neurons, or various timepoints of EBs, or dispase passaged ES colonies were lysed in Trizol or Trizol LS (Invitrogen), homogenized and sheared with a 21 gauge needle, and RNA was purified using RNEasy columns (Qiagen) following manufacturers' instructions. Superscript III RT was used to prepare cDNA following manufacturer's instructions (Invitrogen). qPCR primers were designed to produce 50-100 bp intron-spanning amplicons using Primer3 software, or were used from previous publications. All thermal cycling reactions used the following parameters: 10min, 95°; (30sec, 95°;1min, 55°; 45sec, 72°)x45 ;1min, 95°; 30sec 55°; 30sec, 95°. qPCR reactions were performed with Brilliant II Syber Green

2x Master Mix following manufacturer's instructions on a MX300 Light Cycler (Stratagene). PCR products were checked for single melting curve peaks; where ambiguous, reaction products were separated on an agarose gel, evaluated for appropriate size, and sequenced using amplification primers, confirming amplification of target sequence.

Southern Blot

Genomic DNA was prepared using Qiagen genomic DNA kit, followed by separation on agarose gel, denaturation, and neutral capillary transfer. Easy Hyb DIG labeled probes were synthesized and detected as described in (Boulting, Kiskinis et al. 2011).

Microscopy

Images were acquired using a Zeiss AxioObserver with14-bit Coolsnap HQ2 grayscale camera at 10x, 20x, or 40x. For quantitative experiments, 8-12 randomly placed fields were acquired manually per sample at 10x or 20x or by using an automated stage with fixed positions/well and autofocus on DAPI. Representative photos were acquired at 4x, 10x, 20x, or 40x, using Apotome structured illumination for optical sectioning where indicated. Image intensity look up tables were adjusted to accentuate salient signal to noise details and some images were brightened in Photoshop for better signal visibility in print.

Image analysis

14bit grayscale images were analyzed in Metamorph (Molecular Devices) using Multiwavelength Cell Scoring or Neurite Outgrowth modules. Threshold fluorescent intensities were determined and adjusted for each staining (>~2000-16000 grey levels over local background) and then applied to all images from each condition. ~2000 cells were counted per

field for day 33 MN phenotype analysis. Coexpression was automatically scored based on above threshold staining intensities for DAPI and up to 3 other stains simultaneously.

Statistical Analyses

Statistical analyses were performed using SigmaPlot 11, or Excel as indicated in text and figure legends. Paired 2-tailed T-tests were used where two conditions were compared. ANOVA was used for comparisons of more than 2 groups, or ANOVA on ranks where unequal variance was found with appropriate post hoc comparisons as indicated in text. Population histograms were constructed in Excel or Sigmaplot.

Figures were prepared in Adobe InDesign or Powerpoint.

Experiments reported and not performed by myself:

Electrophysiological studies of GFP human ES-MNs (Chapter 2) were performed by Tomonori Takazawa (Amy B. MacDermott laboratory) following standard practices for patch clamp recording.

See methods from (Dimos, Rodolfa et al. 2008; Bock, Kiskinis et al. 2011; Boulting, Kiskinis et al. 2011) for experiments not performed by myself, as described in general Statement of contributions and those pertaining to each chapter.

Table 7.1 Antibodies

Number	Target	Host Species	Name	Additional identifiers (clone or cu#)	Dilution	Human in vivo	Human ES/ iPS in vitro	supplier
1	HB9	m IgG1	HB9	MNR2/815.c10	1:100	Y	Y	DSHB
2	HB9	rb	HB9	affiinity purified plycolonal	1:64K	Y (weak)	Y (weak)	Jessell
3	HB9	gp	HB9	CU#695	1:32K	N	N	Jessell
4	HB9	rb	HB9	CU#1421, 1422, 1423, 1424	1:40K-80K	Y	Y	Jessell
5	HB9	gp	HB9	Cu#1633, CU#1634	1:32K both	Y	Y	PALS
6	ISL1	m	ISL1	49.4D5	1:100-200	Y	Y	DSHB
7	ISL1	gp	ISL1	CU#405, and CU#1248	1:16K	Y	Y	Jessell
8	ISL1	rb	ISL1	ab20670	1:2K	NT	Y	Abcam
9	ISL1/2	rb	ISL1/2	Santa Cruz: sc30200	1:500	NT	Y	DSHB
10	ISL2	rb	ISL2	Cu#321	1:16K	Y	Y	Jessell
11	ChAT	ch	ChAT	MO20019	1:5K	Y		Neuromics
12	ChAT	gt	ChAT	AB144P	1:1K	Y	N	Chemicon
13	FOXP1	gp	FOXP1	CU #1635, CU#1936	1:32K	Y	Y	Jessell
14	FOXP1	gp	FOXP1	CU1492, 1493	1:32K	Y	Y	PALS
15	FOXP1	rb	FOXP1	CU#1025	1:64K	Y	Y	Jessell
16	LHX3	m	LHX3	67.4E12-s	1:100	Y	Y	DSHB
17	LHX1+2	m	LHX1	F42	1:100	Y	Y	DSHB
18	p-SMAD	rb	p-SMAD	CU503 AB		Y	N	Jessell
19	RALDH2	rb	RALDH2	CU#1028	1:16K	Y	N	Jessell
20	HOXA5	gp	HOXA5	CU#571	1:16K	Y	Y	Jessell
21	HOXC8	m	HOXC8	Covance: MMS-266R	1:1K	Y	Y	Covance
22	HOXD9	rb	HOXD9	Santa Cruz: sc8320	1:500	Y	Y	Sant Cruz
23	HOXC6	gp	HOXC6	ab41587	1:1K	Y (scattered pools only)	N	Abcam
24	HOXC10	gp	HOXC10	H1041-25UL	nt	NT	NT	Sigma
25	HOXC9	m	HOXC9	5B5-2	1:1K	PAN SPINAL	NT	DSHB
26	B-III tubulin	m	TuJ1	MO15013 (Neuromics); ab14545 (Abcam)	1:2K	NT	Y	Neuromics, Abcam
27	B-III tubulin	rb	TuJ1	MRB-435P	1:1K	NT	Y	Covance
28	B-III tubulin	ch	TuJ1	CH23005	1:2K-5K	NT	Y	Neuromics
29	neurofilament H	ch	NF-H	CH22104-50	1:2K-5K	NT	Y	Neuromics
30	non-phosphorylated neurofilaments	m	NP-NF, SMI32	sc58554	1:2-5K	Y	Y	Santa Cruz
31	NESTIN	rb	NESTIN	AB5922	1:500	NT	Y	Chemicon
32	NESTIN	m, IgG1	NESTIN	MAB5326	1:500	NT	Y	Millipore
33	GFP	ch	GFP	A10262	1:2K	NA	Y	Invitrogen
34	GFP	rb	GFP	A11122 (Invitrogen); ab290 (Abcam)	1:2K (invitrogen) 1:5K (Abcam)	NA	Y	Abcam, Invitrogen
35	GFP	m, IgG2a	GFP	3E6 (A11120)	1:2K	NA	Y	Invitrogen
36	human NCAM	m, IgM	ERIC-1	sc106	1:1K	NT	Y	Sant Cruz
37	human nuclear antigen	m, IgG1		MAB4383, MAB1281	1:1K	NT	Y	Chemicon
38	phosphorylated neurofilaments		NF, SMI31			NT	Y	
39	NF-160	m			1:1K	NT	Y	Sigma
40	NKX2.1	m		F55A10-s	1:100	NT	Y	DSHB
41	GFAP	rb	GFAP	AB5804	1:250	NT	Y	Millpore
42	CD-44	m	CD44 variant v6	AHS4464	1:500	NT	Y	Invitrogen
43	OCT4	m		MAB4419MI	1:500	NT	Y	Millipore
44	OLIG2	rb, IgG		AB9610MI	1:2500	NT	Y	Millipore
45	PAX6	m, IgG1		PAX6	1:100	NT	Y	DSHB
45	PEA3	rb	affinity purified	CU#-1395	1:32K	Y	N	Jessell

Table 7.2 qPCR primers. Primers for qPCR were designed in house for qPCR with the exception of PAX6 (Li, Du et al. 2005)

OLIG2	F	GTTCTCCCCTGAGGCTTTTC
	R	GATAGTCGTCGCAGCTTTC
ISL1	F	CGCCTTGCAGAGTGACATAG
	R	GGACTGGCTACCATGCTGTT
HB9	F	GCACCAGTTCAAGCTCAACA
	R	CTTTTTGCTGCGTTTCCATT
HOXA5	F	CAGCACCCACATCAGCAG
	R	CGGAGAGGCAAAGAGCAT
HOXC6	F	CCAGGACCAGAAAGCCAGTA
	R	GTTAGGTAGCGATTGAAGTGAAA
HOXC8	F	CTTCGCTGTTTGATTTCTATTCTG
	R	TACGCTGGAGGTTTCTTTCTTT
HOXD9	F	TCGCTGAAGGAGGAGGAGA
	R	CAAACACCCACAAAGGAAAAC
HOXC10	F	GACTCCAGCCCAGACACCT
	R	TCTTCTTCCTTCCGCTCTTT
OCT4	F	GAGAACCGAGTGAGAGGCAACC
	R	CATAGTCGCTGCTTGATCGCTTG
PAX6*	F	GGCAACCTACGCAAGATGGC
	R	TGAGGGCTGTGTCTGTTCGG
SOX1	F	CCCTGTGTGTACCCTGGAGT
	R	GGCCCACATCCTAATCTTGA

Chapter 8. References

Altman, J. and S. A. Bayer (2001). Development of the human spinal cord : an interpretation based on experimental studies in animals. Oxford ; New York, Oxford University Press.

Arber, S., B. Han, et al. (1999). "Requirement for the homeobox gene Hb9 in the consolidation of motor neuron identity." Neuron **23**(4): 659-74.

Arber, S., D. R. Ladle, et al. (2000). "ETS gene Er81 controls the formation of functional connections between group Ia sensory afferents and motor neurons." Cell **101**(5): 485-98.

Armstrong, L., K. Tilgner, et al. (2010). "Human induced pluripotent stem cell lines show stress defense mechanisms and mitochondrial regulation similar to those of human embryonic stem cells." Stem Cells **28**(4): 661-73.

Bayer, S. A. and J. Altman (2002). Atlas of human central nervous system development. Boca Raton, CRC Press.

Bel-Vialar, S., N. Itasaki, et al. (2002). "Initiating Hox gene expression: in the early chick neural tube differential sensitivity to FGF and RA signaling subdivides the HoxB genes in two distinct groups." Development **129**(22): 5103-15.

Bock, C., E. Kiskinis, et al. (2011). "Reference Maps of Human ES and iPS Cell Variation Enable High-Throughput Characterization of Pluripotent Cell Lines." Cell **144**(3): 439-52.

Boillee, S., C. Vande Velde, et al. (2006). "ALS: a disease of motor neurons and their nonneuronal neighbors." Neuron **52**(1): 39-59.

Boillee, S., K. Yamanaka, et al. (2006). "Onset and progression in inherited ALS determined by motor neurons and microglia." Science **312**(5778): 1389-92.

Boulting, G. L., E. Kiskinis, et al. (2011). "A functionally characterized test set of human induced pluripotent stem cells." Nat Biotechnol.

Boyer, L. A., T. I. Lee, et al. (2005). "Core transcriptional regulatory circuitry in human embryonic stem cells." Cell **122**(6): 947-56.

Bradley, A., M. Evans, et al. (1984). "Formation of germ-line chimaeras from embryo-derived teratocarcinoma cell lines." Nature **309**(5965): 255-6.

Byrne, J. A., D. A. Pedersen, et al. (2007). "Producing primate embryonic stem cells by somatic cell nuclear transfer." Nature **450**(7169): 497-502.

Chambers, S. M., C. A. Fasano, et al. (2009). "Highly efficient neural conversion of human ES and iPS cells by dual inhibition of SMAD signaling." Nat Biotechnol **27**(3): 275-80.

Charcot, J. M. and A. Joffroy (1869). "Deux cas d'atrophie musculaire progressive avec lesion de la substance grise et des faisceaux antero-lateraux de la moelle epiniere." Arch. Physiol. Neurol. Path. **2**: 744–754.

Chin, M. H., M. J. Mason, et al. (2009). "Induced pluripotent stem cells and embryonic stem cells are distinguished by gene expression signatures." Cell Stem Cell **5**(1): 111-23.

Clement, A. M., M. D. Nguyen, et al. (2003). "Wild-type nonneuronal cells extend survival of SOD1 mutant motor neurons in ALS mice." Science **302**(5642): 113-7.

Clowry, G. J., J. A. Moss, et al. (2005). "An immunohistochemical study of the development of sensorimotor components of the early fetal human spinal cord." J Anat **207**(4): 313-24.

Cowan, C. A., I. Klimanskaya, et al. (2004). "Derivation of embryonic stem-cell lines from human blastocysts." N Engl J Med **350**(13): 1353-6.

Dalla Torre di Sanguinetto, S. A., J. S. Dasen, et al. (2008). "Transcriptional mechanisms controlling motor neuron diversity and connectivity." Curr Opin Neurobiol **18**(1): 36-43.

Dasen, J. S., A. De Camilli, et al. (2008). "Hox repertoires for motor neuron diversity and connectivity gated by a single accessory factor, FoxP1." Cell **134**(2): 304-16.

Dasen, J. S. and T. M. Jessell (2009). "Hox networks and the origins of motor neuron diversity." Curr Top Dev Biol **88**: 169-200.

Dasen, J. S., J. P. Liu, et al. (2003). "Motor neuron columnar fate imposed by sequential phases of Hox-c activity." Nature **425**(6961): 926-33.

Dasen, J. S., B. C. Tice, et al. (2005). "A Hox regulatory network establishes motor neuron pool identity and target-muscle connectivity." Cell **123**(3): 477-91.

de Carvalho, M. A., S. Pinto, et al. (2008). "Paraspinal and limb motor neuron involvement within homologous spinal segments in ALS." Clin Neurophysiol **119**(7): 1607-13.

Dengler, R., A. Konstanzer, et al. (1990). "Amyotrophic lateral sclerosis: macro-EMG and twitch forces of single motor units." Muscle Nerve **13**(6): 545-50.

Deschamps, J. and J. van Nes (2005). "Developmental regulation of the Hox genes during axial morphogenesis in the mouse." Development **132**(13): 2931-42.

Di Giorgio, F. P., G. L. Boulting, et al. (2008). "Human embryonic stem cell-derived motor neurons are sensitive to the toxic effect of glial cells carrying an ALS-causing mutation." Cell Stem Cell **3**(6): 637-48.

Di Giorgio, F. P., M. A. Carrasco, et al. (2007). "Non-cell autonomous effect of glia on motor neurons in an embryonic stem cell-based ALS model." Nat Neurosci **10**(5): 608-14.

Dimos, J. T., K. T. Rodolfa, et al. (2008). "Induced pluripotent stem cells generated from patients with ALS can be differentiated into motor neurons." Science **321**(5893): 1218-21.

Doi, A., I. H. Park, et al. (2009). "Differential methylation of tissue- and cancer-specific CpG island shores distinguishes human induced pluripotent stem cells, embryonic stem cells and fibroblasts." Nat Genet **41**(12): 1350-3.

Ebert, A. D., J. Yu, et al. (2009). "Induced pluripotent stem cells from a spinal muscular atrophy patient." Nature **457**(7227): 277-80.

Eggan, K. and R. Jaenisch (2003). "Micromanipulating dosage compensation: understanding X-chromosome inactivation through nuclear transplantation." Semin Cell Dev Biol **14**(6): 349-58.

Elkabetz, Y., G. Panagiotakos, et al. (2008). "Human ES cell-derived neural rosettes reveal a functionally distinct early neural stem cell stage." Genes Dev **22**(2): 152-65.

Ensini, M., T. N. Tsuchida, et al. (1998). "The control of rostrocaudal pattern in the developing spinal cord: specification of motor neuron subtype identity is initiated by signals from paraxial mesoderm." Development **125**(6): 969-82.

Erceg, S., S. Lainez, et al. (2008). "Differentiation of human embryonic stem cells to regional specific neural precursors in chemically defined medium conditions." PLoS One **3**(5): e2122.

Ericson, J., S. Thor, et al. (1992). "Early stages of motor neuron differentiation revealed by expression of homeobox gene Islet-1." Science **256**(5063): 1555-60.

Evans, M. J. and M. H. Kaufman (1981). "Establishment in culture of pluripotential cells from mouse embryos." Nature **292**(5819): 154-6.

Ferrucci, M., A. Spalloni, et al. (2010). "A systematic study of brainstem motor nuclei in a mouse model of ALS, the effects of lithium." Neurobiol Dis **37**(2): 370-83.

Fetcho, J. R. (1987). "A review of the organization and evolution of motoneurons innervating the axial musculature of vertebrates." Brain Res **434**(3): 243-80.

Fischer, L. R., D. G. Culver, et al. (2004). "Amyotrophic lateral sclerosis is a distal axonopathy: evidence in mice and man." Exp Neurol **185**(2): 232-40.

Frey, D., C. Schneider, et al. (2000). "Early and selective loss of neuromuscular synapse subtypes with low sprouting competence in motoneuron diseases." J Neurosci **20**(7): 2534-42.

Gao, B. X. and L. Ziskind-Conhaim (1998). "Development of ionic currents underlying changes in action potential waveforms in rat spinal motoneurons." J Neurophysiol **80**(6): 3047-61.

Ghosh, Z., K. D. Wilson, et al. (2010). "Persistent donor cell gene expression among human induced pluripotent stem cells contributes to differences with human embryonic stem cells." PLoS One **5**(2): e8975.

Gitcho, M. A., R. H. Baloh, et al. (2008). "TDP-43 A315T mutation in familial motor neuron disease." Ann Neurol **63**(4): 535-8.

Gizzi, M., A. DiRocco, et al. (1992). "Ocular motor function in motor neuron disease." Neurology **42**(5): 1037-46.

Grigoriadis, A. E., M. Kennedy, et al. (2010). "Directed differentiation of hematopoietic precursors and functional osteoclasts from human ES and iPS cells." Blood **115**(14): 2769-76.

Gutman, C. R., M. K. Ajmera, et al. (1993). "Organization of motor pools supplying axial muscles in the chicken." Brain Res **609**(1-2): 129-36.

Haase, G., E. Dessaud, et al. (2002). "GDNF acts through PEA3 to regulate cell body positioning and muscle innervation of specific motor neuron pools." Neuron **35**(5): 893-905.

Hagan, D. M., A. J. Ross, et al. (2000). "Mutation analysis and embryonic expression of the HLXB9 Currarino syndrome gene." Am J Hum Genet **66**(5): 1504-15.

Hanna, J., M. Wernig, et al. (2007). "Treatment of sickle cell anemia mouse model with iPS cells generated from autologous skin." Science **318**(5858): 1920-3.

Hollyday, M. (1980). "Organization of motor pools in the chick lumbar lateral motor column." J Comp Neurol **194**(1): 143-70.

Hu, B. Y., J. P. Weick, et al. (2010). "Neural differentiation of human induced pluripotent stem cells follows developmental principles but with variable potency." Proc Natl Acad Sci U S A **107**(9): 4335-40.

Hu, B. Y. and S. C. Zhang (2009). "Differentiation of spinal motor neurons from pluripotent human stem cells." Nat Protoc **4**(9): 1295-304.

Inman, G. J., F. J. Nicolas, et al. (2002). "SB-431542 is a potent and specific inhibitor of transforming growth factor-beta superfamily type I activin receptor-like kinase (ALK) receptors ALK4, ALK5, and ALK7." Mol Pharmacol **62**(1): 65-74.

Itoh, T., G. Sobue, et al. (1992). "Phosphorylated high molecular weight neurofilament protein in the peripheral motor, sensory and sympathetic neuronal perikarya: system-dependent normal variations and changes in amyotrophic lateral sclerosis and multiple system atrophy." Acta Neuropathol **83**(3): 240-5.

James, D., S. A. Noggle, et al. (2006). "Contribution of human embryonic stem cells to mouse blastocysts." Dev Biol **295**(1): 90-102.

Jessell, T. M. (2000). "Neuronal specification in the spinal cord: inductive signals and transcriptional codes." Nat Rev Genet **1**(1): 20-9.

Jung, H., J. Lacombe, et al. (2010). "Global control of motor neuron topography mediated by the repressive actions of a single hox gene." Neuron **67**(5): 781-96.

Kabashi, E., P. N. Valdmanis, et al. (2008). "TARDBP mutations in individuals with sporadic and familial amyotrophic lateral sclerosis." Nat Genet **40**(5): 572-4.

Kaminski, H. J., C. R. Richmonds, et al. (2002). "Differential susceptibility of the ocular motor system to disease." Ann N Y Acad Sci **956**: 42-54.

Kanning, K. C., A. Kaplan, et al. (2010). "Motor neuron diversity in development and disease." Annu Rev Neurosci **33**: 409-40.

Karumbayaram, S., T. K. Kelly, et al. (2009). "Human embryonic stem cell-derived motor neurons expressing SOD1 mutants exhibit typical signs of motor neuron degeneration linked to ALS." Dis Model Mech **2**(3-4): 189-95.

Karumbayaram, S., B. G. Novitch, et al. (2009). "Directed differentiation of human-induced pluripotent stem cells generates active motor neurons." Stem Cells **27**(4): 806-11.

Kong, J. and Z. Xu (1998). "Massive mitochondrial degeneration in motor neurons triggers the onset of amyotrophic lateral sclerosis in mice expressing a mutant SOD1." J Neurosci **18**(9): 3241-50.

Landmesser, L. (1978). "The development of motor projection patterns in the chick hind limb." J Physiol **284**: 391-414.

Landmesser, L. (1978). "The distribution of motoneurones supplying chick hind limb muscles." J Physiol **284**: 371-89.

Lee, G., E. P. Papapetrou, et al. (2009). "Modelling pathogenesis and treatment of familial dysautonomia using patient-specific iPSCs." Nature **461**(7262): 402-6.

Lee, H., G. A. Shamy, et al. (2007). "Directed differentiation and transplantation of human embryonic stem cell-derived motoneurons." Stem Cells **25**(8): 1931-9.

Li, X.-J., Z.-W. Du, et al. (2005). "Specification of motoneurons from human embryonic stem cells." Nat Biotech **23**(2): 215-221.

Li, X. J., Z. W. Du, et al. (2005). "Specification of motoneurons from human embryonic stem cells." Nat Biotechnol **23**(2): 215-21.

Li, X. J., B. Y. Hu, et al. (2008). "Directed differentiation of ventral spinal progenitors and motor neurons from human embryonic stem cells by small molecules." Stem Cells **26**(4): 886-93.

Lin, J. H., T. Saito, et al. (1998). "Functionally related motor neuron pool and muscle sensory afferent subtypes defined by coordinate ETS gene expression." Cell **95**(3): 393-407.

Liu, J. P., E. Laufer, et al. (2001). "Assigning the positional identity of spinal motor neurons: rostrocaudal patterning of Hox-c expression by FGFs, Gdf11, and retinoids." Neuron **32**(6): 997-1012.

Livet, J., M. Sigrist, et al. (2002). "ETS gene Pea3 controls the central position and terminal arborization of specific motor neuron pools." Neuron **35**(5): 877-92.

Loh, Y. H., Q. Wu, et al. (2006). "The Oct4 and Nanog transcription network regulates pluripotency in mouse embryonic stem cells." Nat Genet **38**(4): 431-40.

Lombardo, A., P. Genovese, et al. (2007). "Gene editing in human stem cells using zinc finger nucleases and integrase-defective lentiviral vector delivery." Nat Biotechnol **25**(11): 1298-306.

Mannen, T. (2000). "Neuropathological findings of Onuf's nucleus and its significance." Neuropathology **20 Suppl**: S30-3.

Mannen, T., M. Iwata, et al. (1977). "Preservation of a certain motoneurone group of the sacral cord in amyotrophic lateral sclerosis: its clinical significance." J Neurol Neurosurg Psychiatry **40**(5): 464-9.

Marchetto, M. C., A. R. Muotri, et al. (2008). "Non-cell-autonomous effect of human SOD1 G37R astrocytes on motor neurons derived from human embryonic stem cells." Cell Stem Cell **3**(6): 649-57.

Martin, G. R. (1981). "Isolation of a pluripotent cell line from early mouse embryos cultured in medium conditioned by teratocarcinoma stem cells." Proc Natl Acad Sci U S A **78**(12): 7634-8.

Miles, G. B., D. C. Yohn, et al. (2004). "Functional properties of motoneurons derived from mouse embryonic stem cells." J Neurosci **24**(36): 7848-58.

Mitsumoto, H., S. Przedborski, et al. (2006). Amyotrophic Lateral Sclerosis. New York, NY, Taylor and Francis**:** 830.

Moretti, A., M. Bellin, et al. (2010). "Patient-specific induced pluripotent stem-cell models for long-QT syndrome." N Engl J Med **363**(15): 1397-409.

Muhr, J., E. Graziano, et al. (1999). "Convergent inductive signals specify midbrain, hindbrain, and spinal cord identity in gastrula stage chick embryos." Neuron **23**(4): 689-702.

Munoz-Sanjuan, I. and A. H. Brivanlou (2002). "Neural induction, the default model and embryonic stem cells." Nat Rev Neurosci **3**(4): 271-80.

Nagai, M., D. B. Re, et al. (2007). "Astrocytes expressing ALS-linked mutated SOD1 release factors selectively toxic to motor neurons." Nat Neurosci **10**(5): 615-22.

Nakagawa, M., M. Koyanagi, et al. (2008). "Generation of induced pluripotent stem cells without Myc from mouse and human fibroblasts." Nat Biotechnol **26**(1): 101-6.

Nichols, J., B. Zevnik, et al. (1998). "Formation of pluripotent stem cells in the mammalian embryo depends on the POU transcription factor Oct4." Cell **95**(3): 379-91.

Nordstrom, U., T. M. Jessell, et al. (2002). "Progressive induction of caudal neural character by graded Wnt signaling." Nat Neurosci **5**(6): 525-32.

Nordstrom, U., E. Maier, et al. (2006). "An early role for WNT signaling in specifying neural patterns of Cdx and Hox gene expression and motor neuron subtype identity." PLoS Biol **4**(8): e252.

Oey, P. L., P. E. Vos, et al. (2002). "Subtle involvement of the sympathetic nervous system in amyotrophic lateral sclerosis." Muscle Nerve **25**(3): 402-8.

Ohi, Y., H. Qin, et al. (2011). "Incomplete DNA methylation underlies a transcriptional memory of somatic cells in human iPS cells." Nat Cell Biol **13**(5): 541-9.

Okita, K., M. Nakagawa, et al. (2008). "Generation of mouse induced pluripotent stem cells without viral vectors." Science **322**(5903): 949-53.

Osafune, K., L. Caron, et al. (2008). "Marked differences in differentiation propensity among human embryonic stem cell lines." Nat Biotechnol **26**(3): 313-5.

Papapetrou, E. P., G. Lee, et al. (2011). "Genomic safe harbors permit high beta-globin transgene expression in thalassemia induced pluripotent stem cells." Nat Biotechnol **29**(1): 73-8.

Park, I. H., N. Arora, et al. (2008). "Disease-specific induced pluripotent stem cells." Cell **134**(5): 877-86.

Park, I. H., R. Zhao, et al. (2008). "Reprogramming of human somatic cells to pluripotency with defined factors." Nature **451**(7175): 141-6.

Patani, R., A. J. Hollins, et al. (2011). "Retinoid-independent motor neurogenesis from human embryonic stem cells reveals a medial columnar ground state." Nat Commun **2**: 214.

Peljto, M., J. S. Dasen, et al. (2010). "Functional diversity of ESC-derived motor neuron subtypes revealed through intraspinal transplantation." Cell Stem Cell **7**(3): 355-66.

Placantonakis, D. G., M. J. Tomishima, et al. (2009). "Enriched motor neuron populations derived from bacterial artificial chromosome-transgenic human embryonic stem cells." Clin Neurosurg **56**: 125-32.

Prasad, A. and M. Hollyday (1991). "Development and migration of avian sympathetic preganglionic neurons." J Comp Neurol **307**(2): 237-58.

Pun, S., A. F. Santos, et al. (2006). "Selective vulnerability and pruning of phasic motoneuron axons in motoneuron disease alleviated by CNTF." Nat Neurosci **9**(3): 408-19.

Rath, G., G. Gopinath, et al. (1982). "Prenatal development of the human spinal cord. I. Ventral motor neurons." J Neurosci Res **7**(4): 437-41.

Ravits, J., P. Paul, et al. (2007). "Focality of upper and lower motor neuron degeneration at the clinical onset of ALS." Neurology **68**(19): 1571-5.

Ravits, J. M. and A. R. La Spada (2009). "ALS motor phenotype heterogeneity, focality, and spread: deconstructing motor neuron degeneration." Neurology **73**(10): 805-11.

Roelink, H., J. A. Porter, et al. (1995). "Floor plate and motor neuron induction by different concentrations of the amino-terminal cleavage product of sonic hedgehog autoproteolysis." Cell **81**(3): 445-55.

Romanes, G. J. (1942). "The spinal cord in a case of congenital absence of the right limb below the knee." J Anat **77**(Pt 1): 1-5.

Romanes, G. J. (1964). "The Motor Pools of the Spinal Cord." Prog Brain Res **11**: 93-119.

Rosen, D. R., T. Siddique, et al. (1993). "Mutations in Cu/Zn superoxide dismutase gene are associated with familial amyotrophic lateral sclerosis." Nature **362**(6415): 59-62.

Ross, A. J., V. Ruiz-Perez, et al. (1998). "A homeobox gene, HLXB9, is the major locus for dominantly inherited sacral agenesis." Nat Genet **20**(4): 358-61.

Schroder, H. D. and E. Reske-Nielsen (1984). "Preservation of the nucleus X-pelvic floor motosystem in amyotrophic lateral sclerosis." Clin Neuropathol **3**(5): 210-6.

Sharrard, W. J. (1955). "The distribution of the permanent paralysis in the lower limb in poliomyelitis; a clinical and pathological study." J Bone Joint Surg Br **37-B**(4): 540-58.

Shin, S., S. Dalton, et al. (2005). "Human motor neuron differentiation from human embryonic stem cells." Stem Cells Dev **14**(3): 266-9.

Singh Roy, N., T. Nakano, et al. (2005). "Enhancer-specified GFP-based FACS purification of human spinal motor neurons from embryonic stem cells." Exp Neurol **196**(2): 224-34.

Smith, A. G., J. K. Heath, et al. (1988). "Inhibition of pluripotential embryonic stem cell differentiation by purified polypeptides." Nature **336**(6200): 688-90.

Soldner, F., D. Hockemeyer, et al. (2009). "Parkinson's disease patient-derived induced pluripotent stem cells free of viral reprogramming factors." Cell **136**(5): 964-77.

Soundararajan, P., G. B. Miles, et al. (2006). "Motoneurons derived from embryonic stem cells express transcription factors and develop phenotypes characteristic of medial motor column neurons." J Neurosci **26**(12): 3256-68.

Sreedharan, J., I. P. Blair, et al. (2008). "TDP-43 mutations in familial and sporadic amyotrophic lateral sclerosis." Science **319**(5870): 1668-72.

Stadtfeld, M., E. Apostolou, et al. (2010). "Aberrant silencing of imprinted genes on chromosome 12qF1 in mouse induced pluripotent stem cells." Nature **465**(7295): 175-81.

Takahashi, H., K. Oyanagi, et al. (1993). "The intermediolateral nucleus in sporadic amyotrophic lateral sclerosis." Acta Neuropathol **86**(2): 190-2.

Takahashi, K. and S. Yamanaka (2006). "Induction of pluripotent stem cells from mouse embryonic and adult fibroblast cultures by defined factors." Cell **126**(4): 663-76.

Tanabe, Y., C. William, et al. (1998). "Specification of motor neuron identity by the MNR2 homeodomain protein." Cell **95**(1): 67-80.

Taura, D., M. Noguchi, et al. (2009). "Adipogenic differentiation of human induced pluripotent stem cells: comparison with that of human embryonic stem cells." FEBS Lett **583**(6): 1029-33.

Thomson, J. A., J. Itskovitz-Eldor, et al. (1998). "Embryonic stem cell lines derived from human blastocysts." Science **282**(5391): 1145-7.

Tokumoto, Y., S. Ogawa, et al. (2010). "Comparison of efficiency of terminal differentiation of oligodendrocytes from induced pluripotent stem cells versus embryonic stem cells in vitro." J Biosci Bioeng **109**(6): 622-8.

Urbach, A., M. Schuldiner, et al. (2004). "Modeling for Lesch-Nyhan disease by gene targeting in human embryonic stem cells." Stem Cells **22**(4): 635-41.

Van Deerlin, V. M., J. B. Leverenz, et al. (2008). "TARDBP mutations in amyotrophic lateral sclerosis with TDP-43 neuropathology: a genetic and histopathological analysis." Lancet Neurol **7**(5): 409-16.

Vierbuchen, T., A. Ostermeier, et al. (2010). "Direct conversion of fibroblasts to functional neurons by defined factors." Nature **463**(7284): 1035-41.

Vrieseling, E. and S. Arber (2006). "Target-induced transcriptional control of dendritic patterning and connectivity in motor neurons by the ETS gene Pea3." Cell **127**(7): 1439-52.

Wada, T., M. Honda, et al. (2009). "Highly efficient differentiation and enrichment of spinal motor neurons derived from human and monkey embryonic stem cells." PLoS One **4**(8): e6722.

Warren, L., P. D. Manos, et al. (2010). "Highly efficient reprogramming to pluripotency and directed differentiation of human cells with synthetic modified mRNA." Cell Stem Cell **7**(5): 618-30.

Watanabe, K., M. Ueno, et al. (2007). "A ROCK inhibitor permits survival of dissociated human embryonic stem cells." Nat Biotechnol **25**(6): 681-6.

Wernig, M., A. Meissner, et al. (2008). "c-Myc is dispensable for direct reprogramming of mouse fibroblasts." Cell Stem Cell **2**(1): 10-2.

Wernig, M., A. Meissner, et al. (2007). "In vitro reprogramming of fibroblasts into a pluripotent ES-cell-like state." Nature **448**(7151): 318-24.

Wichterle, H., I. Lieberam, et al. (2002). "Directed differentiation of embryonic stem cells into motor neurons." Cell **110**(3): 385-97.

Wichterle, H., M. Peljto, et al. (2009). "Xenotransplantation of embryonic stem cell-derived motor neurons into the developing chick spinal cord." Methods Mol Biol **482**: 171-83.

Willert, K., J. D. Brown, et al. (2003). "Wnt proteins are lipid-modified and can act as stem cell growth factors." Nature **423**(6938): 448-52.

Wilmut, I., A. E. Schnieke, et al. (1997). "Viable offspring derived from fetal and adult mammalian cells." Nature **385**(6619): 810-3.

Xi, J., M. Khalil, et al. (2010). "Comparison of contractile behavior of native murine ventricular tissue and cardiomyocytes derived from embryonic or induced pluripotent stem cells." FASEB J **24**(8): 2739-51.

Yohn, D. C., G. B. Miles, et al. (2008). "Transplanted mouse embryonic stem-cell-derived motoneurons form functional motor units and reduce muscle atrophy." J Neurosci **28**(47): 12409-18.

Yu, J., M. A. Vodyanik, et al. (2007). "Induced pluripotent stem cell lines derived from human somatic cells." Science **318**(5858): 1917-20.

Yu, P. B., D. Y. Deng, et al. (2008). "BMP type I receptor inhibition reduces heterotopic [corrected] ossification." Nat Med **14**(12): 1363-9.

Zhang, X., C. T. Huang, et al. (2010). "Pax6 is a human neuroectoderm cell fate determinant." Cell Stem Cell **7**(1): 90-100.

Zhao, T., Z. N. Zhang, et al. (2011). "Immunogenicity of induced pluripotent stem cells." Nature **474**(7350): 212-5.

Zwaka, T. P. and J. A. Thomson (2003). "Homologous recombination in human embryonic stem cells." Nat Biotechnol **21**(3): 319-21.